THE ROLE OF THE GROUP ENVIRONMENT IN THE EVOLUTION OF GALAXIES: INVESTIGATING GROUP DYNAMICS AND PRE-PROCESSING

THE ROLE OF THE GROUP ENVIRONMENT IN THE EVOLUTION OF GALAXIES: INVESTIGATING GROUP DYNAMICS AND PRE-PROCESSING

By

ANNIE HOU, B.Sc., M.Sc.

A Thesis
Submitted to the School of Graduate Studies
in Partial Fulfillment of the Requirements
for the Degree of

Doctor of Philosophy

McMaster University

DOCTOR OF PHILOSOPHY (August 2013) McMaster University
Hamilton, Ontario

TITLE: The role of the group environment in the evolution of galaxies: Investigating group dynamics and pre-processing

AUTHOR: Annie Hou, B.Sc., M.Sc.(University of Toronto, McMaster University)

SUPERVISORS: Dr. L. C. Parker, Dr. W. E. Harris

NUMBER OF PAGES: xx, 250

Abstract

The influence of environment in galaxy evolution has been observed in a wide range of environments, where in general red quiescent early-type galaxies preferentially reside in high-density regions. The aim of this thesis is to understand the role that galaxy groups, and in particular group dynamics, play in galaxy evolution.

We examine substructure in rich groups at intermediate redshifts and find that 4/15 groups contain substructure, which is preferentially found on the group outskirts. Galaxies in groups with substructure have properties similar to the field, while the galaxies in groups with no substructure are similar to cluster populations. These results indicate that substructure galaxies do not feel the effects of the environment until well inside the group potential.

We then study the evolution of group dynamics to $z \sim 1$ and find that the fraction of non-Gaussian groups increases with redshift, while the fraction of groups with substructure remains constant. Additionally, we find that the quiescent fraction correlates with galaxy stellar mass, but has little or no dependence on group dynamical mass or state. However, we do observe some correlation between substructure and quiescent fraction for low mass galaxies.

Finally, we investigate infalling subhalo galaxies to probe the importance of pre-processing in galaxy evolution. At $r_{200} \gtrsim 2$, galaxies in subhaloes show enhanced quenching, when compared to non-subhalo galaxies. At these radii, the infall population dominates, indicating that enhanced quenching is due to the infalling subhalo population. Additionally, the fraction of groups with subhaloes is a function of halo mass, where more massive systems have a higher fraction of subhaloes. We conclude that for groups, pre-processing is insignificant; however, for the most massive clusters a significant fraction ($\sim 25\%$) of the member galaxies have been pre-processed.

To Mom, Dad and Andrew

Co-Authorship

Chapters 3, 4 and 5 are original papers written by me, Annie Hou, and have been re-formatted to conform to the specifications of the McMaster thesis style.

Chapter 3 has been published in the journal *Monthly Notices of the Royal Astronomical Society* (*MNRAS*) with reference Hou, A.; Parker, L.C.; Wilman, D.J.; McGee, S.L.; Harris, W.E.; Connelly, J.L.; Balogh, M.L.; Mulchaey, J.S.; and, Bower, R.G., Volume 421, Issue 4, pp. 3594-361, Bib. Code: 2012MNRAS.421.3594H, DOI: 10.1111/j.1365-2966.2012.20586.x. My contribution to this article includes complete analysis of all of the work presented, as well as full authorship, both of which were done under the supervision of L.C. Parker and W.E. Harris. The group catalogue used in this work was defined by D.J. Wilman with follow-up data taken by D.J. Wilman, S.L. McGee, M.L. Balogh and J.S. Mulchaey. The stellar masses and star formation rates were obtained from spectral energy distribution fits carried out by S.L. McGee. J.S. Mulchaey and R.G. Bower are also members of the Group Environment and Evolution Collaboration (GEEC).

Chapter 4 has been accepted for publication in the journal *MNRAS* and is currently *in press.*. The listed authors are Hou, A.; Parker, L.C.; Balogh, M.L.; McGee, S.l.; Wilman, D.J.; Connelly, J.L.; Harris, W.E.; Mok, A.; Mulchaey, J.S.; Bower, R.G.; and, Finoguenov, A. The arXiv reference number is 1308.1406. My contribution to this article includes complete analysis of all of the work presented, as well as full authorship, both of which were done under the supervision of L.C. Parker and W.E. Harris. The group catalogues used in this work were defined by D.J. Wilman, S.L. McGee, M.L. Balogh and A. Finoguenov. GEEC data was collected by L.C. Parker, D.J. Wilman, S.L. McGee, J.L. Connelly, M.L. Balogh and A. Finoguenov. A. Mok, J.S. Mulchaey and R.G. Bower are also members of the Group Environment and Evolution Collaboration (GEEC).

Chapter 5 was submitted to *MNRAS* on July 4^{th} 2013 and includes revisions based on the referee's comments, which were received on August 9th,

2013. The listed authors are Hou, A.; Parker, L.C.; and, Harris, W.E. My contribution to this article includes complete analysis of all of the work presented, as well as full authorship, both of which were done under the supervision of L.C. Parker and W.E. Harris. The data and group catalogue are publicly available.

Chapters 1 and 2 (the introduction) include figures that are either free of copyright or figures for which I have obtained permission from both the author and the corresponding journal to reproduce in this thesis.

Acknowledgements

Firstly, I would like to thank my supervisors, Dr. Laura C. Parker and Dr. William E. Harris. They have both been a constant source of guidance and support over the years, allowing me to grow and develop as a researcher. Their scientific input and general advice has improved this thesis by an immeasurable amount. Also, their enthusiasm for science has been unbelievably refreshing and has helped motivate me throughout my degree, especially at times when I needed it the most. I am very lucky to have had two strong role models to try to emulate throughout my own career. I would also like to thank the members of the GEEC collaboration for many useful discussions and ideas, as well as other members of my committee Dr. Alison Sills and Dr. Doug Welch.

The Department of Physics and Astronomy at McMaster has also been incredible through the past six years. The strong sense of community and friendship within the department has helped me keep my sanity and even made graduate life fun. There are so many people to list, so I will just say thank you to you all for the chats, hangouts and homework times. A special thanks to Kate and Sandy, life would not have been the same with you two. Thank you for being such amazing friends.

Andrew, thank you for being the most patient, supportive and loving partner I could have ever hoped for. He has helped me through the rough times and kept me smiling (and sane) throughout it all. I would also like to thank my family for all the love, support and tolerance over the years. Above all, I would like to thank my mom and dad. They have always been there to love, nurture, guide and support me throughout my life. I would not be where, and more importantly who I am, without them. Mom, dad and Andrew, I dedicate this thesis to you.

List of Acronyms

2dFGRS	Two-degree-Field Galaxy Redshift Survey
3D-MF	Three Dimensional-Matched-Filter
ΛCDM	Λ Cold Dark Matter
AD	Anderson-Darling
ACT	Atacama Cosmology Telescope
AGN	Active Galactic Nuclei
BO	Butcher-Oemler
CFHTLS	Canada-France-Hawaii Telescope Legacy Survey
CFHTLS-SL2S	CFHTLS-Strong Lensing Legacy Survey
CNOC2	Canadian Network for Observational Cosmology Galaxy Redshift Survey
CRS	Cluster Red Sequence
CG	Compact Group
CMB	Cosmic Microwave Background
COBE	Cosmic Microwave Background Explorer
CMD	Colour-Magnitude Diagram
CDF	Cumulative Distribution Function
DES	Dark Energy Survey
DEEP2	Deep Evolutionary Exploratory Probe 2 Galaxy Redshift Survey
DS	Dressler-Shectman
EDF	Empirical Distribution Function
EGS	Extended Groth Strip
FoF	Friends-of-Friends
GEEC	Group Environment and Evolution Collaboration
HCG	Hickson Compact Group
HST	Hubble Space Telescope
IR	Infrared
IMF	Initial Mass Function
ISM	Interstellar Medium
ICM	Intracluster Medium

KS	Kolmogorov-Smirnov
IGM	Intragroup Medium
LSS	Large-scale-structure
LOS	Line-of-sight
MDR	Morphology-density Relation
NFW	Navarro-Frenk-White
Pan-STARRS	Panoramic Survey Telescope and Rapid Response System
PSB	Post Starburst
PS	Press-Schecter
pFoF	probability Friend-of-Friends
RCS	Red sequence Cluster Survey
SAMs	Semi-analytic Models
SDSS	Sloan Digital Sky Survey
SPH	Smoothed-particle Hydrodynamics
SPT	South Pole Telescope
SSFR	Specific Star Formation Rate
SED	Spectral Energy Distribution
SpARCS	Spitzer Adaptation of the Red sequence Clusters Survey
SFH	Star Formation History
SFR	Star Formation Rate
SARCS	Strong Lensing Legacy Survey-ARCS sample
SZ	Sunyaev-Zeldovich
SMBH	Supermassive Black Hole
SBP	Surface Brightness Profile
ULIRGS	Ultra Luminous Infrared Galaxies
UV	Ultraviolet
VDP	Velocity Dispersion Profile
VDM	The Voronoi-Delaunay Method
WMAP	Wilkinson Microwave Anisotropy Map
zCOSMOS	spectroscopic-Cosmic Evolution Survey

Contents

List of Figures

List of Tables

Chapter 1

An Overview of Galaxy Evolution

The field of Astronomy has been an active area of scientific enquiry for over three millennia; however, our current understanding of the Universe only began to really take shape in the 20th century. The past ∼100 years have arguably seen the most important discoveries in Astronomy, some of which have resulted in major paradigm shifts. Examples of these seminal discoveries, both observational and theoretical, include: the Milky Way Galaxy as just one of many galaxies in our Universe (Opik, 1922; Hubble, 1925, 1926), the expansion of the Universe (i.e. Hubble's Law: Hubble, 1929), the cosmic microwave background (Penzias & Wilson, 1965), nucleosynthesis (Alpher et al., 1948), and dark matter (e.g. Oort, 1932; Zwicky, 1937) and energy (Riess et al., 1998; Perlmutter et al., 1999).

One of the open debates in Astronomy concerns the evolution of galaxies and investigating when, where and how, galaxies form and evolve. In the last few decades, photometric and spectroscopic surveys of galaxies, spanning a wide range of redshifts and environments, have provided a vast amount of information about the observable properties of galaxies. The results of some of these studies have shown that galaxy properties, such as colour and morphology, vary as a function of both environment and a galaxy's stellar mass. Variations with a galaxy's environment, such as the morphology-density relation (MDR: Dressler, 1980), indicate that external processes, related to the properties of the host group or cluster halo, govern evolution. However, strong correlations between observed galaxy properties and galaxy stellar mass sug-

gest that internal processes, related to the galaxy itself, dominate. These seemingly contradictory results have sparked the so-called 'nature versus nurture' debate.

It is the goal of this thesis to understand the role of the environment, and in particular the intermediate density environment of galaxy groups, in galaxy evolution. In order to provide context and motivation for this work, the first chapter will include a discussion of the current theory of the growth of structure and a more detailed examination of the 'nature versus nurture' debate. I will then give an overview of the most relevant galaxy transformation processes, as well as discuss observational methods of probing galaxy evolution. In the following chapter, I will focus on the importance of the group environment and in particular group dynamics on galaxy evolution.

1.1 Hierarchical Structure Formation

One of the most important discoveries in modern Astronomy was that of the Cosmic Microwave Background (CMB: Penzias & Wilson, 1965), which confirmed the Big Bang model and is a key observational probe of the current standard model of cosmology, the Λ Cold Dark Matter (ΛCDM) model. Since its discovery, numerous surveys have been carried out to study the CMB in greater detail, including three all-sky surveys: the Cosmic Background Explorer (COBE: Smoot et al., 1992), the Wilkinson Microwave Anisotropy Probe (WMAP: Bennett et al., 2003) satellite, and the Planck satellite (Planck Collaboration et al., 2013). The results of the aforementioned missions have provided increasingly precise information about cosmological parameters from the temperature perturbations observed in the CMB.

In the ΛCDM concordance model, the primordial perturbations (seeded in the early Universe) observed in the CMB, which are on the order of 10^{-5} with respect to the background temperature level, are amplified over time by gravity to form the large-scale structure (LSS) we see today. The number density of dark matter haloes, or the halo mass distribution, formed via this process is generally well described by the analytic Press-Schecter (PS) formalism, which was developed from the work presented in Press & Schechter (1974). PS theory suggests that haloes correlate with the peaks in the Gaussian random density

field of dark matter in the early Universe. The basic idea of PS formalism is that once a region attains a density above some critical threshold, it will condense and form a dark matter halo. Additionally, as the PS formalism is self-similar, the theory allows for the development of an analytical theory for the group and cluster halo distributions (Bower, 1991) and also merger rates in a hierarchical Universe (Lacey & Cole, 1993). These latter theories are often referred to as extended-PS formalisms.

While the PS and extended-PS formalisms have provided great insight into the growth of structure, much of our current understanding has come from N-body simulations. In particular, dark matter-only simulations (in which gravity is the only acting force) have confirmed that structure does in fact grow hierarchically. In addition, these simulations have shown that galaxies preferentially reside in filaments (Bond et al., 1996; Kravtsov & Borgani, 2012), which mimic the pattern of the initial density perturbations observed in the CMB (Bond et al., 1996). Galaxy clusters and superclusters form at the intersection of these filaments and it is believed that galaxies accrete on to the highest-density regions, either individually from the field or in smaller groups of galaxies, along filaments.

In this model of structure formation, objects grow from the 'bottom-up' starting with single haloes that accrete and merge continuously to eventually form the LSS we see today. The constant accretion and mergers of galaxies has implications for galaxy evolution, as will be discussed in the remainder of this chapter and in the following chapter.

1.2 The "Nature versus Nurture" Debate

Broadly speaking, galaxies fall into two categories: early- and late-type. Early-type galaxies tend to be red in colour, have little or no on-going star formation and have elliptical or lenticular morphologies; while late-type galaxies are generally star-forming blue galaxies and are classified as either spiral or irregular. Despite the evolutionary progress suggested by this nomenclature, early-type galaxies do not evolve into late-type galaxies. In fact, observational and theoretical studies indicate that galaxy evolution typically follows the opposite direction, with late-type evolving into early-type galaxies (to be discussed in

more detail in Section 1.4). While the 'directionality' of this evolution may be known, the exact processes that drive it are still a source of debate.

Early simulations showed that the remnant of a major merger (i.e. merger of similar mass galaxies) between two late-type galaxies generally resembles the morphology of an elliptical or early-type galaxy (Toomre & Toomre, 1972; Barnes, 1988, 1992; Hernquist, 1993). However, more recent work has shown that the major merger of two spiral galaxies does not always result in an elliptical galaxy. Parameters such as the amount of gas in the disk galaxy, interactions with the surrounding interstellar medium (ISM), and the orbits of the merging galaxies can result in either the survival or reformation of a disk (Barnes, 2002; Robertson et al., 2006; Springel & Hernquist, 2005; Hopkins et al., 2009). Additionally, mergers may not always be necessary to form an early-type galaxy, as it has been suggested that lenticular or S0 galaxies may be the remnant of a 'faded spiral' galaxy (Aragón-Salamanca et al., 2006; Bedregal et al., 2006). Thus, the evolution from late- to early-type galaxy appears to be more complicated than originally thought and it is still unclear if there is one dominant evolutionary path or if a combination of multiple mechanisms result in the observed properties.

Early- and late-type galaxies appear to preferentially reside in different environments. Studies of galaxies in the cores of clusters showed that early-type galaxies were preferentially found in the high-density regions, while late-type galaxies were found in low-density regions, such as the field (Oemler, 1974; Dressler, 1980). This observation, now commonly referred to as the morphology-density relation (MDR), was one of the first indications that the environment can affect the observed properties of galaxies, sparking the 'nature versus nurture' debate. Since then, the MDR has been extended to lower density environments, such as the infall region of clusters and galaxy groups, which also show enhanced star formation quenching with respect to the field (Wilman et al., 2005a; Holden et al., 2007; van der Wel et al., 2010). Additionally, correlations between the environment and other galaxy properties have also been observed, including: the colour-density (Blanton et al., 2003; Baldry et al., 2006), star formation-density (Poggianti et al., 2008; Vulcani et al., 2010; McGee et al., 2011; Patel et al., 2011; Sobral et al., 2011) and gas-density (Kauffmann et al., 2004) relations. In addition, numerous studies

have shown that the fraction of either star-forming or quiescent galaxies is strongly dependent on the environment (Kauffmann et al., 2004; Balogh et al., 2004; Wilman et al., 2005a; Peng et al., 2010, 2012; Muzzin et al., 2012; Wetzel et al., 2012).

While these relations appear to suggest that the environment plays a dominant role in the evolution of galaxies, we now know that the situation is much more complex. Although the fraction of quiescent galaxies has been observed to be higher in groups and clusters, studies have shown that the observed properties of actively star-forming galaxies depend only weakly or do not depend at all on environment (Balogh et al., 2004; Rines et al., 2005; Wilman et al., 2005a; Cooper et al., 2008; Wolf et al., 2009; Peng et al., 2010; Grützbauch et al., 2011; Tyler et al., 2011; Muzzin et al., 2012). Additionally, studies have also shown that galaxy properties, such as morphology and colour, correlate more strongly with galaxy stellar mass (Allen et al., 2006; Bamford et al., 2009; Balogh et al., 2009; McGee et al., 2011). Based on these results, it would seem that nature is in fact the primary driver of galaxy evolution.

A third option is that neither nature nor nurture is dominant, and rather both factors contribute equally to the observed galaxy properties. In a study of galaxies in the local Universe, Kimm et al. (2009) showed that star formation quenching in satellite galaxies correlated strongly with both stellar mass *and* halo mass and to a similar degree. These authors concluded that the observed properties of satellite galaxies, at least equally depended on nature and nurture. Similar analysis presented by Woo et al. (2013) also indicated that the quiescent fraction ($f_{\rm q}$), defined as the fraction of galaxies with neglible star formation, depended on both stellar and halo mass, though they found a slightly stronger dependence with halo mass.

To further complicate matters, galaxy stellar mass, which is believed to trace internal processes, correlates with environment where higher mass galaxies are preferentially found in high-density regions. This correlation renders it difficult, if not impossible, to truly isolate the effects of 'nature' from those of 'nurture'. In addition, since hierarchical structure formation states that structure grows via the accretion and merger of smaller haloes, each galaxy has what De Lucia et al. (2012) refer to as a 'history bias', which these authors sum up by stating:

> *As structure grows, galaxies join more and more massive systems, therefore experiencing a variety of environments during their lifetimes. In this context, the nature-nurture debate appears to be ill-posed, as these two elements of galaxy evolution are inevitably and heavily intertwined.*

Despite the observed correlation between stellar mass and environment and the presence of a history bias, several authors still argue that it is possible to disentangle galaxy transformation processes related to 'nature' from those due to 'nurture' (Tasca et al., 2009; Peng et al., 2010, 2012; Sobral et al., 2011; Muzzin et al., 2012). In particular, it has been suggested that whether galaxy evolution is dictated by either internal or external processes is entirely dependent on the mass of a galaxy. The observed properties of high mass galaxies with $M_{\rm star} \gtrsim 10^{10.5} M_{\odot}$ show almost no dependence on environment, indicating a 'nature' evolutionary scenario; while the properties of low mass galaxies show correlations with environment, suggesting a 'nurture' evolutionary scenario (Tasca et al., 2009; Peng et al., 2010, 2012). Thus, the recent claims that the environment plays a secondary role in the evolution of galaxies may be a result of observational limits, as low mass galaxies are more difficult to observe at higher redshifts.

Although there has been much effort to settle the 'nature versus nurture' debate, the issue is far from resolved as various studies have resulted in different, and sometimes contradictory, conclusions. What is clear from these studies is that in order to properly probe environmental effects on galaxy evolution, one must try to take into account the accretion history of a galaxy and also isolate or disentangle correlations with galaxy stellar mass.

1.3 Observable Probes of Galaxy Evolution

Although there are numerous ways in which galaxies can be transformed, the general trend for evolution, at least out to $z \sim 1$, is to transform a blue, star-forming spiral or disk galaxies into red, passively-evolving elliptical galaxies. Thus, galaxy evolution studies typically use one or a combination of the following observables: colour, morphology and star formation rate (star formationR).

1.3.1 Colour

Arguably the simplest observable galaxy properties are the apparent magnitude and colour, defined as the difference between two magnitude bands (e.g. the SDSS $(g-r)$ colour with g-band at 8391 Å and r-band at 3551 Å). Since the colour of a galaxy is determined mainly by the stellar population, colour can provide vital information about star formation and the star formation history (star formationH) of a galaxy.

In all environments, the distribution of galaxy colours is bimodal, with galaxies either falling on the 'red sequence' or 'blue cloud' (Strateva et al., 2001; Blanton et al., 2003; Baldry et al., 2004; Balogh et al., 2004). In general, red galaxies have a stellar population that is dominated by cooler (3700 - 5200 K) and lower mass ($\sim 0.4 - 0.8 M_{\odot}$) K-stars and blue galaxies typically have a high fraction of hotter ($6000 - 10000$ K) and more massive ($\sim 1 - 2 M_{\odot}$) A and/or F stars. However, metallicity can also affect the observed colour of a galaxy, where higher metallicity galaxies have redder colours. Additionally, the presence of dust also alters the observed colour of galaxy, causing blue star-forming galaxies to appear red as dust absorbs more short wavelength radiation and re-emits it in the thermal infrared (IR).

For illustration, in Figure 1.1 I have plotted the $(g-r)$ colours for low redshift $(0 < z < 0.05)$ group galaxies observed in the Sloan Digital Sky Survey (SDSS - left: Yang et al., 2007; Abazajian et al., 2009) and for intermediate redshift $(0.15 < z < 0.55)$ group galaxies observed in the Group Environment and Evolution Collaboration (GEEC - right: Wilman et al., 2005b) survey. The colours shown in Figure 1.1 have been k-corrected (i.e. adjusting all of the magnitudes to the same rest-frame redshift) to redshifts of $z = 0$ for SDSS and to $z = 0.4$ for GEEC. The colour distributions for both the SDSS and GEEC samples show the expected bimodal distribution. Although the $(g-r)$ colour distributions are shown in Figure 1.1, the bimodal feature is present in numerous other filter combinations, e.g. $(u-r)$ in the low redshift Universe (Strateva et al., 2001; Balogh et al., 2004) and $(V-z)$ in the high redshift $(z \sim 1)$ Universe (Balogh et al., 2009)

In general, the colour distribution of galaxies can be fit with a double-Gaussian (Strateva et al., 2001). Since the properties of blue galaxies are more

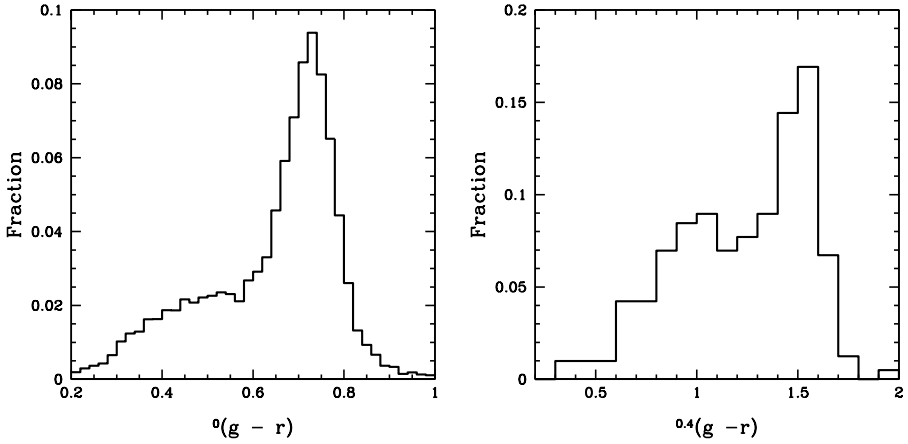

Figure 1.1: Left: ${}^{0}(g-r)$ colour distribution (k-corrected to a redshift of $z = 0$) for galaxies in the Yang et al. (2007) SDSS group catalogue with $z \leq 0.05$. Right: ${}^{0.4}(g-r)$ colour distribution (k-corrected to a redshift of $z = 0.4$) for galaxies in the Wilman et al. (2005b) GEEC group catalogue with $0.15 < z < 0.55$.

varied than those of red galaxies, the width of the Gaussian corresponding to the blue cloud is typically wider than that of the red sequence. Although the colour distribution is well fit by two Gaussian distributions, there is significant overlap, as can be seen in Figure 1.1, and there is usually no clear minimum value that easily divides red and blue galaxies. The overlapping region is often referred to the green valley and is thought to represent a transitional phase between the traditional blue and red galaxy populations. In a study of high redshift ($z \sim 1$) galaxies, Balogh et al. (2011) found that $\sim 30\%$ of the population resided in the green valley, defined by a range in $(V - z)$ colour; however, most galaxy studies do not show a significant population of green galaxies with colour distributions well fit by a double Gaussian (e.g. Strateva et al., 2001).

With a colour distribution it is possible to roughly distinguish between red and blue galaxies. However, in addition to the lack of a clear minimum, the red sequence itself shows a strong colour-magnitude correlation where brighter galaxies have redder colours. In Figure 1.2, I plot a ${}^{0}(g-r)$ versus ${}^{0}r$ colour-magnitude diagram (CMD) for galaxies in the Yang et al. (2007) SDSS group catalogue with $z < 0.05$. From this CMD, it is clear that the red galaxies form a relatively tight sequence that shows a strong relationship between colour

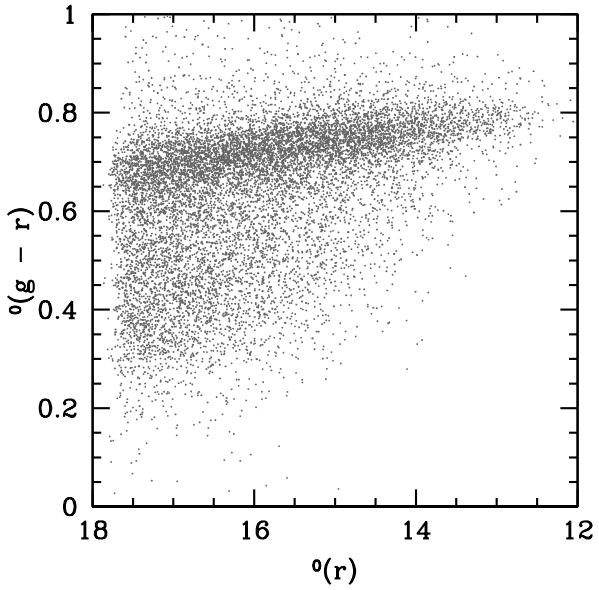

Figure 1.2: ${}^0(g-r)$ versus ${}^0r$ (k-corrected to a redshift of $z=0$) for galaxies in the Yang et al. (2007) SDSS group catalogue with $z \leq 0.05$.

and magnitude. A common method of distinguishing between red and blue galaxies is to make a cut in colour-magnitude space, often defined as a linear fit to the red sequence shifted down by, for example, one sigma in ${}^0(g-r)$.

With the ability to distinguish between blue and red galaxies, it is possible to determine the fraction of galaxies that reside in the red sequence ($f_{\rm red}$) and in the blue cloud ($f_{\rm blue} = 1 - f_{\rm red}$). The red/blue fraction is an important, and arguably the most common, probe of galaxy evolution and shows correlations with galaxy stellar mass, redshift and environment. In the following, I will highlight some observed colour and red fraction trends.

Correlations with Stellar mass

The general trend between red fraction and galaxy stellar mass is that higher mass galaxies typically have a higher red fraction (Baldry et al., 2006; Kimm et al., 2009; Prescott et al., 2011). Semi-analytic models (SAMs) provide insight into the physical processes behind this observed trend. In particular, it appears that feedback from the central active galactic nuclei (AGN) is needed in order to reproduce the observed fraction of red galaxies, at least for galaxies with $M_{\rm star} \gtrsim 10^{10} h^{-1} M_\odot$ (Bower et al., 2006; Somerville et al., 2008; Kimm

et al., 2009). The mass of a supermassive black hole (SMBH) correlates with the mass or velocity dispersion of the galaxy (i.e. the $M-\sigma$ relation: Ferrarese & Merritt, 2000) where more massive galaxies typically have more massive SMBHs. Since AGN feedback suppresses star formation, it follows that if more massive SMBHs output more energy, then quenching should be more efficient in higher mass galaxies, which would reproduce the observed trend. Additionally, SMBH growth can occur via a major merger. Since more massive galaxies have also likely experienced one or multiple major mergers in their assembly history, star formation quenching can occur as a result of a starburst phase and/or higher AGN feedback due to a more massive SMBH.

Correlations with Environment

The red fraction of galaxies also shows correlations with environment both in the local Universe and at $z \sim 1$, where higher density environments have a higher fraction of red galaxies (Baldry et al., 2006; Kimm et al., 2009; Woo et al., 2013). The colour-density trend holds for various probes of the environment, including: projected local density (Σ), defined as the number density of galaxies within some fixed distance on the sky and along the line-of-sight (LOS: e.g. Balogh et al., 2004); distance from group or cluster centre, where the density decreases with increasing radius (e.g. Prescott et al., 2011); and host group or cluster halo mass (e.g. Kimm et al., 2009).

The transformation from blue to red galaxy is a direct consequence of star formation quenching and may be due to processes related to either nature or nurture. In general, SAMs are able to reproduce the observed $f_{\rm red} - M_{\rm halo}$ trend for central galaxies and massive ($> 10^{10} M_{\odot}$) satellites; however, for galaxies with $M_{\rm star} \lesssim 10^{10} M_{\odot}$ most SAMs produce too many red galaxies at all halo masses. The overquenching of low mass galaxies in SAMs has been attributed to 'aggressive' satellite star formation quenching in the group and cluster environments. In many earlier models, star formation in a satellite galaxy was immediately quenched upon accretion. Font et al. (2008) claimed to have resolved this issue with more realistic models of stripping, where satellites retain a higher fraction of their hot gas halo after infall, allowing for continued star formation and resulting in a higher (lower) fraction of blue (red) galaxies.

Although it has been suggested that the correlation between red fraction

and environment is secondary to the $f_{\rm red}$-stellar mass trend (e.g. Grützbauch et al., 2011), both Baldry et al. (2006) and Kimm et al. (2009) found that at fixed stellar mass $f_{\rm red}$ still increased with increasing density. These authors concluded that the environment was at least as important as galaxy stellar mass in determining the fraction of red galaxies.

Redshift Evolution

In addition to correlations with stellar mass and environment, the fraction of blue and red galaxies also evolves with redshift. This was first observed by Butcher & Oemler (1984), who found that the fraction of blue galaxies in clusters increased from $f_{\rm blue} \sim 0.03$ for clusters at $z \leq 0.1$ to $f_{\rm blue} \sim 0.25$ for clusters at $z = 0.5$. This trend is now commonly referred to as the Butcher-Oemler (BO) effect. Since its discovery, numerous studies have confirmed the BO effect in clusters (Dressler & Gunn, 1982; Ellingson et al., 2001; Kodama & Bower, 2001; Margoniner et al., 2001) and have also found that the relation extends to higher redshift ($z \sim 1$: De Propris et al., 2003).

The observed BO effect appears to be the result of a combination of phenomena. Studies of the cosmic SFR density ($\rho_{\rm SFR}$ =SFR per unit volume) as a function of redshift, which showed that $\rho_{\rm SFR}$ rises steadily from $z = 0$ to a peak value at $z \sim 1-2$ and then turns over and declines to $z \sim 6$ (Lilly et al., 1996; Madau et al., 1996; Wall et al., 2005; Hopkins & Beacom, 2006; Dunne et al., 2009). Consequently, in the redshift range examined by most cluster studies (i.e. $z < 2$), the SFR is higher at higher redshift, which would explain the observed increase of blue galaxies with redshift. Additionally, the cluster environment itself may evolve with redshift. For example, Ellingson et al. (2001) observed the BO effect in clusters between $0.18 < z < 0.55$ but only when galaxies at large radii ($> 0.5r_{200}$, where r_{200} is taken to be the radius at which the density is 200 times the critical density and is often referred to as the virial radius) were included in their cluster sample. Galaxies within the cluster core showed no evolution in blue fraction with redshift. Based on this result, these authors concluded that the BO effect was not driven by galaxies in the cluster core, but by infalling blue galaxies from the field and thus, the increased fraction of blue galaxies indicated an increase in the infall rate onto the cluster. In particular, Ellingson et al. (2001) claimed that the rate of infall decreased

by a factor of ~ 3 between $z > 0.8$ and $z \sim 0.5$. Kodama & Bower (2001) reached a similar conclusion for lower redshift clusters ($0.23 \lesssim z \lesssim 0.43$).

The strength of the BO effect may depend on galaxy stellar mass. In a comparison of massive cluster galaxies ($M_\star \geq 1.34 \times 10^{11} M_\odot$) at $z \sim 2.2$ to similar cluster galaxies in the local Universe, Raichoor & Andreon (2012) found no evolution in the fraction of blue galaxies. I present a similar result in a published paper reproduced in Chapter 4 of this thesis.

1.3.2 Morphological Classification

The first morphological classification scheme for galaxies was developed by Edwin Hubble in 1926, who found that in general the observable shapes of galaxies were either elliptical or showed spiral features (Hubble, 1926). Elliptical galaxies have smooth light distributions in the shape of an ellipse and typically show no distinct visible features. In contrast, spiral galaxies contain a central 'bulge' or nucleus of stars that is surrounded by a flattened disk, which shows spiral features or 'arms'. In addition, more than half of the observed spiral population also contain a central bar (Eskridge & Frogel, 1999).

The Hubble classification scheme itself consists of two sequences, one for each morphological class. The spiral sequence also contains two sub-sequences, normal and barred spirals. Together the sequences intersect one another forming a 'fork-like' shape, hence the so-called 'Hubble's Tuning Fork Diagram'. In Figure 1.3, I show a schematic diagram of Hubble's classification scheme. The elliptical galaxies are classified as E0-E7, where the numerical suffix corresponds to the ellipticity with '0' being a nearly circular galaxy and '7' being a highly flattened galaxy. The normal spiral (S) and barred spiral (SB) sequences consists of subclasses that correspond to the tightness of the spiral arms and the brightness of the central bulge. The properties of the spiral subclasses, as defined by Hubble (1926), are listed below:

- Sa and SBa galaxies are defined as having tightly-wound spirals and a bright central bulge;
- Sb and SBb galaxies typically have spiral arms that are less tightly-wound and a fainter bulge, in comparison to Sa's and SBa's;

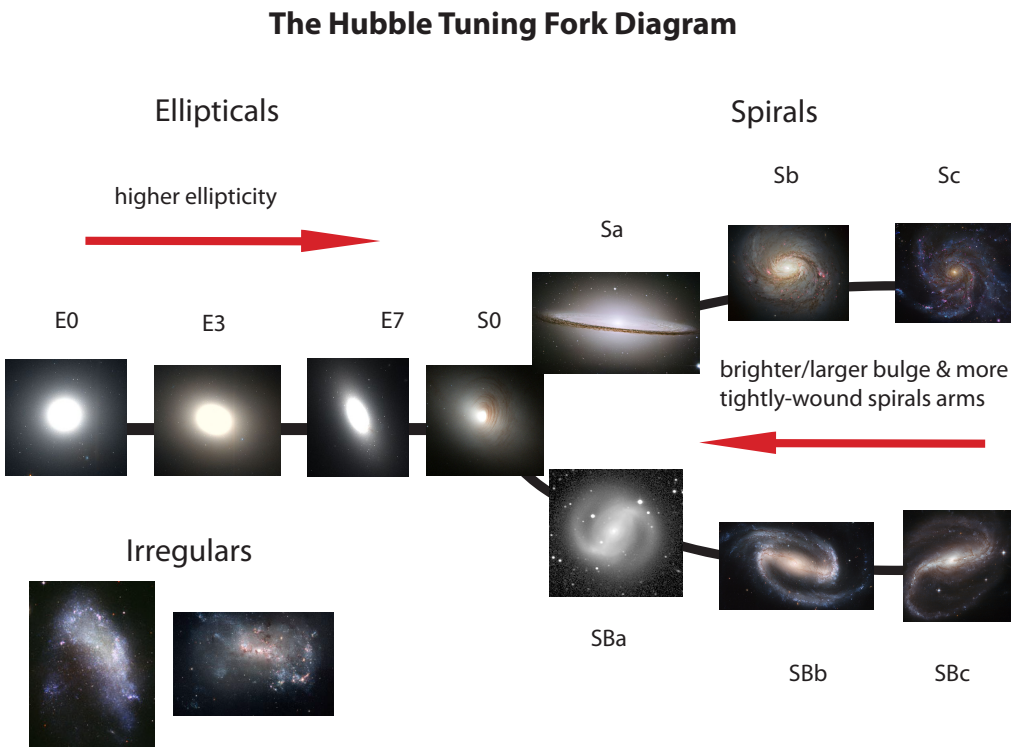

Figure 1.3: Schematic diagram for the Hubble morphological classification scheme (i.e. the Hubble Tuning Fork Diagam). Image Credits: NASA/ESA/STSci.

- Sc and SBc galaxies have loosely wound arms that are highly resolved, such that individual stellar clusters are visible. They also have a smaller and fainter bulge.

A fourth subclass (Sd and SBd) was added to this classification scheme by de Vaucouleurs (1959). These spirals have very loosely-wound spiral arms that are typically fragmented with most of the luminosity in the arms as opposed to the central nucleus. de Vaucouleurs (1959) also observed rings around some spiral galaxies and therefore added an additional suffix to the classification scheme, where 'r' denotes spirals with a ring and 's' for spirals with no ring.

The intersection point of the diagram represents a separate morphological category known as lenticular or S0 galaxies, which have a bright central bulge (similar to an elliptical galaxy) but is also surrounded by an extended

disk (similar to a spiral galaxy), though with no spiral features. Since lenticular galaxies have observable properties of both ellipticals and spirals, it is thought that these galaxies represent a transitory phase between the two main morphological classes.

A class of galaxies not included on the Hubble Tuning Fork Diagram are irregular galaxies (Figure 1.3: bottom-left). These galaxies were initially thought to only make up a few percent of the total population (Hubble, 1926); however, it is now thought that the fraction of irregulars is comparable to that of ellipticals and spirals, although they are typically lower mass (Gallagher & Hunter, 1984). Irregular galaxies fall into two subcategories: type I and type II. Type I irregulars show some structure, typically resembling spiral features (i.e. disk and central bulge) though significantly less organized, preventing their placement on the Hubble sequence. Type II irregular galaxies have no distinct features.

Although visual classification of galaxy morphologies on the Hubble Sequence is still a common practice, there are drawbacks with this methodology. In particular, since the Hubble sequence is a qualitative classification scheme, the same galaxy may be identified as different morphological types depending on the person performing the analysis. Additionally, visual classification is not feasible for large data sets. In order to overcome these issues, several quantitative morphological classification methods have been developed. In the following, I will list and briefly describe some of the more commonly used techniques.

- **The Sérsic Index:** First developed by Sérsic (1963), the Sérsic index (n) parametrizes the slope of the surface brightness profile (hereafter SBP) of a galaxy, that is the intensity of light from a galaxy as a function of radius ($I(R)$). In other words, the Sérsic index measures the concentration of a galaxy's flux. In general, the SBP follows the form $I(R) \propto \exp(-R^{1/n})$ where n can take on any value between $1/2 < n < 10$. Smaller values of n correspond to less centrally concentrated profiles. Spiral galaxies have a typical value of $n = 1$, corresponding to an exponential profile, and elliptical galaxies typically have $n = 4$, often referred to as the $R^{1/4}$ law.

- **Two-component SBP Fits:** The Sérsic index assumes that the SBP is well fit by a single-component model. However, spiral and lenticular galaxies have both a central bulge and an extended disk, which are better fit by a two-component model of the SBP. Currently, there are two commonly used, publicly available, automated programs that perform detailed bulge+disk decomposition analysis of galaxy SBPs, Galaxy IM 2D (GIM2D) (Simard et al., 2002) and GALFIT (Peng et al., 2002). Both programs compute properties such as: bulge effective radius (i.e. the radius within which one half of the total luminosity of the galaxy is emitted), disk scale length, bulge fraction (B/T = ratio of bulge luminosity to total luminosity) and bulge ellipticity, each of which can be used to classify galaxies. In particular, the B/T value can distinguish between elliptical and spiral galaxies relatively well, where ellipticals typically have high B/T values and spirals have lower values.

- **Concentration, Asymmetry and Clumpiness (CAS):** The CAS classification scheme combines the use of galaxy concentration (C: Abraham et al., 1994, 1996), asymmetry (A: Conselice et al., 2000) and clumpiness (S: Conselice, 2003). The concentration parameter is essentially a measure of the bulge-to-disk light ratio and is often defined as the ratio of the amount of light within 80% over 20% of the galaxy's radius. Ellipticals typically have $C > 4$ and disk galaxies generally have $4 < C < 3$ (Conselice, 2003). The asymmetry index is a comparison of an image rotated by 180° to the original (unrotated) image. The intensity of the residuals can be quantified by either a summation (Abraham et al., 1996) or comparison to the flux of the original image (Conselice, 2003). Higher values of A indicate a more asymmetrical galaxy. The final parameter, clumpiness, is meant to quantify the 'patchiness' of the galaxy light distribution, which can occur due to concentrated regions or knots of star formation, such as those seen in spiral arms. The S parameter is measured by comparing an original image to a smoothed or blurred image. Similar to asymmetry, the intensity of the residuals of the original image subtracted by the blurred image can be quantified to measure the 'clumpiness' of a galaxy. Each of these parameters encom-

passes different aspect of galaxy morphology (i.e. shape, SBP, rotational symmetry, and star formation) and combined provides a classification scheme that takes into account many of the features one would detect via visual classification.

- **The Gini Coefficient** The use of the Gini Coefficient in Astronomy was first proposed by Abraham et al. (2003). Initially developed for economics, the Gini coefficient is a measure of the distribution of wealth in a population. Applied to astronomical data, it becomes a measure of the distribution of light amongst the image pixels of a galaxy. A Gini coefficient of 0 indicates uniform surface brightness and a value of 1 means that all of the flux is within a single pixel. Therefore, higher values of the Gini coefficient correspond to elliptical galaxies, while lower values correspond to spirals. Additionally, Lotz et al. (2004) found that ellipticals, spirals and ultra luminous infrared galaxies (ULIRGS) occupied relatively distinct regions in the Gini Coefficient - $M20$ plane, where $M20$ is the second order moment of light of the brightest 20% of the galaxy, or in other words the flux in each pixel multiplied by the squared distance to the centre of the galaxy of the brightest 20% of the pixels over the summed total for the whole galaxy. The $M20$ values typically range between $-3 < M20 < 0$, where lower values correspond to more compact galaxies (ellipticals) and values closer to 0 correspond to more spatially extended galaxies (spirals).

Both qualitative and quantitative measures of morphology show that galaxies can be separated into two broad classes, early-type galaxies (ellipticals and lenticulars) and late-type galaxies (spirals and irregulars). In the following, I will discuss how morphology and the fraction of either early- or late-type galaxies correlate with galaxy stellar mass, environment and redshift. Many of the trends mirror those observed with colour (Bamford et al., 2009), as ellipticals are typically red and spirals are typically blue.

Correlations with Stellar Mass

In general, elliptical and S0 galaxies dominate at high galaxy stellar mass, while spirals make up the majority of low stellar mass galaxies (Bamford et al., 2009; Nair & Abraham, 2010; Vulcani et al., 2011; Wilman et al., 2013). Conse-

quently, the fraction of elliptical galaxies (f_e) increases strongly with increasing stellar mass (Bamford et al., 2009; Wilman et al., 2013). The observed morphology-stellar mass trends strongly favour the major merger formation scenario for ellipticals, as mergers are the most efficient way to gain a significant amount of stellar mass (Wilman & Erwin, 2012; Wilman et al., 2013).

Correlations with Environment

As previously mentioned, the MDR was one of the first observations to show that the properties of galaxies correlate with environment (Dressler, 1980; Postman & Geller, 1984; Bamford et al., 2009; Wilman et al., 2009; Wilman & Erwin, 2012). In general, early-type galaxies are preferentially found in high-density environments, such as rich groups and clusters, while late-type galaxies are preferentially found in the field or on the group or cluster outskirts. Thus, the fraction of ellipticals is also strongly correlated with local overdensity with values of $\sim 20\%$ in the lowest density environment and $\sim 60\%$ in the highest densities (Bamford et al., 2009). Additionally, in a study of galaxy morphologies in the redshift range of $0 < z < 1.2$, Capak et al. (2007) found that the fraction of elliptical (f_e) and SO galaxies increased with increasing local overdensity at all redshifts indicating that the MDR was in place since at least $z \sim 1.2$. While f_e is strongly correlated with the *local* overdensity, Wilman & Erwin (2012) and Wilman et al. (2013) found that only the fraction of central (i.e. brightest or most massive galaxy in the group or cluster) ellipticals correlated with the host halo mass. The satellite ellipticals showed no halo mass dependence.

Although the MDR is now a well established relation, recent studies have suggested that the correlation between morphology and environment are much weaker than the correlation between colour and environment (Bamford et al., 2009; Skibba et al., 2009). Additionally, Skibba et al. (2009) found that morphological changes were accompanied by a change in colour, that is a galaxy transformation from late- to early-type resulted in star formation quenching, but not vice versa. Based on these, and similar results, it has been suggested that the MDR is in fact driven by the colour-density relation (Blanton et al., 2005; Skibba et al., 2009). Alternatively, since both colour and morphology depend strongly on stellar mass, which also correlates with environment, much of the MDR ($\sim 40\%$) is actually a result of the varying stellar mass distributions

with environment (Bamford et al., 2009).

Redshift Evolution

Analogous to the redshift evolution of red and blue galaxies, the fraction of elliptical (spiral) galaxies decreases (increases) with increasing redshift, at least out to $z \sim 1.2$ (Lotz et al., 2008). Between $0.3 \lesssim z \lesssim 1.1$ the spiral fraction decreases from 64% at high-z to 47% at low-z and the elliptical fraction increases from 21% at high-z to 44% at low-z (Lotz et al., 2008).

1.3.3 Star formation Rates

Although galaxy colour is a probe of star formation, the correlation between colour and star formationR is not always one-to-one. This is mainly due to the fact that dust causes the reddening of light in star forming galaxies. Since all galaxy transformation mechanisms either trigger and/or quench star formation (to be discussed in more detail in the following section), it is important to be able to directly probe star formation in galaxies and investigate correlations between SFR and specific star formation rate (SFR normalized by galaxy stellar mass: SSFR $\equiv$ SFR/$M_{\rm star}$) with stellar mass and environment.

Similar to colour and morphology, the distribution of SSFRs is bimodal. In Figure 1.4, I plot the SSFR distribution for low redshift ($z < 0.05$) SDSS galaxies observed in the Yang et al. (2007) group catalogue. The SSFR distribution is visibly bimodal and unlike the colour distribution shown in Figure 1.1, which is plotted from the same data set, there is a clear minimum at $\log_{10}$(SSFR) = -10.7. Galaxies with $\log_{10}(\mathrm{SSFR}) < -10.7$ form the passive population and galaxies with $\log_{10}(\mathrm{SSFR}) > -10.7$ form the actively star-forming population.

There are numerous methods to probe star formation in galaxies and I will briefly outline some of the more commonly used star formation indicators, as well as discuss some of their drawbacks.

- **The Ultraviolet (UV) Stellar Continuum:** The bulk of the galaxy's emission in the UV regime originates from young massive stars. Therefore, the UV continuum is a direct probe of star formation in a galaxy

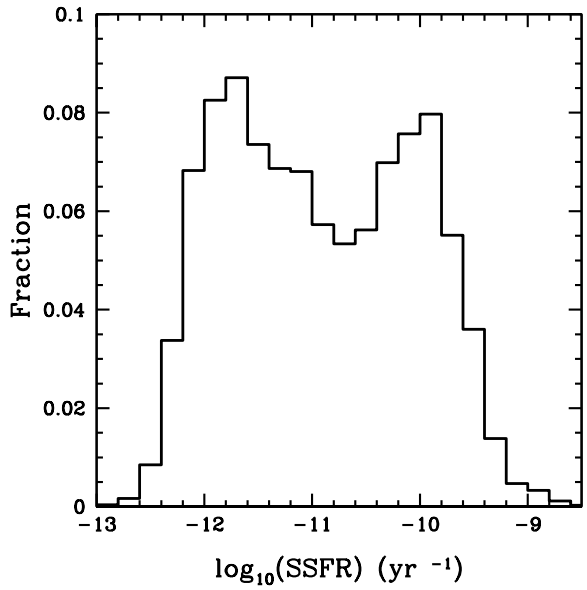

Figure 1.4: $\log_{10}$(SSFR) (yr^{-1}) distribution for all group galaxies in the Yang et al. (2007) SDSS group catalogue with $z \leq 0.05$, where the SSFR values are from the most recent release of the spectral reductions of Brinchmann et al. (2004).

and the star formationR scales linearly with UV luminosity as

$$SFR(M_\odot\ \mathrm{yr}^{-1}) = \text{constant} \times L_\nu(\text{ergs s}^{-1}\ \text{Hz}^{-1}), \qquad (1.1)$$

where L_ν is the UV luminosity, constant $\sim 1.3-1.4\times10^{-28}$ for a Salpeter initial mass function (IMF: the distribution of stellar mass on the zero-age main sequence). Equation 1.1 is valid in the wavelength region between 1500 -2800 Å and assumes solar metallicities and continuous star formation over timescales of 10^8 yrs or longer (Kennicutt, 1998; Madau et al., 1998). For younger stellar populations and starburst galaxies the SFR/L_ν ratio will be lower than quoted in Equation 1.1. The optimal wavelength regime for this star formation indicator is between 1250 - 2500 Å, which avoids emission from both the Lyman-alpha forest and older stellar populations (Kennicutt, 1998). For high redshift galaxies ($z \sim 1-5$) the UV continuum gets redshifted to optical wavelengths, rendering this technique optimal for high-z studies. A drawback of UV continuum derived SFRs is that this technique is very sensitive to ex-

tinction due to dust and therefore underestimates the SFR of dusty star formation galaxies (Kennicutt, 1998).

- **The Infrared (IR) Continuum:** One way to overcome the sensitivity of UV derived SFRs to dust is to take complementary observations in the IR. The effect of dust in a galaxy is to absorb the UV emission from stars and re-radiate it in the IR, at wavelengths beyond a few microns. Thus, the IR luminosity provides information about dust-obscured star formation and together with the UV luminosity, can measure the total star formation in a galaxy. Rieke et al. (2009) found that the SFR could be determined from the Sptizer Space Telescope Multiband Imaging Photometer (MIPS) 24 μm band with the following relation

$$SFR(M_\odot \text{ yr}^{-1}) = 7.8 \times 10^{-10} L(24\mu\text{m}, L_\odot), \tag{1.2}$$

for galaxies with total IR luminosities (L(TIR)) between $5\times10^9 - 10^{11} L_\odot$, and

$$SFR(M_\odot \text{ yr}^{-1}) = 7.8\times10^{-10} L(24\mu\text{m}, L_\odot)\times(7.76\times10^{-11} L(24\mu\text{m}, L_\odot))^{0.048}, \tag{1.3}$$

for galaxies with higher L(TIR)'s. A more general relation for all far-IR wavelengths (i.e. not just MIPS 24 μm data) goes as

$$SFR(M_\odot \text{ yr}^{-1}) = 4.5 \times 10^{-44} L_{FIR}(\text{erg s}^{-1}), \tag{1.4}$$

where L_{FIR} is the luminosity integrated over the full mid- and far-IR wavelengths (8 - 1000 μm: Kennicutt, 1998). These authors claim that other published IR derived SFRs are within $\pm$30% of Equation 1.4. A disadvantage of this methodology is that it is not a direct measure of SFR. Since it is based on re-emitted light, the IR wavelengths can contain emission from the old stellar population, which would lead to an overestimated SFR.

- **Recombination Lines:** An alternative method of measuring SFRs is from the strength or intensity of certain emission lines in the spectra of a star-forming galaxy. One such set of observed features are recombina-

tion lines, the most common of which is the Balmer series: Hα (6563 Å), Hβ (4861 Å), Hγ (4341 Å), Hδ (4102 Å) and so on. The UV emission from young massive stars ionizes the surrounding gas. Eventually, the free electrons recombine with the atoms, which are initially in highly excited states. As the electrons jump down to lower energy levels, they emit energy in the form of an emission line. Thus, recombination lines are a direct and sensitive probe of the young massive stellar population (Kennicutt, 1998). Since the Balmer lines lie in the optical wavelength regime, they are the most commonly used SFR indicators. In particular, the Hα line is quite strong and is therefore one of the easier spectral lines to identify and measure. SFRs derived from Hα measure the 'instantaneous' SFR, as only young massive (i.e. $M_{\rm star} > 10\ M_{\odot}$ and lifetimes $<$ 20 Myrs) contribute to the ionizing flux and therefore this measure does not probe the old stellar population. An example calibration between Hα luminosity ($L_{H\alpha}$) and SFR is

$$SFR(M_{\odot}\ \mathrm{yr}^{-1}) = 7.9 \times 10^{-42} L_{H\alpha}(\mathrm{erg\ s}^{-1}), \tag{1.5}$$

assuming a Salpeter IMF and solar abundances (Kennicutt et al., 1994; Kennicutt, 1998; Madau et al., 1998). However, it should be noted that there is approximately a 30% range in the published values of the calibration constant given in Equation 1.5. Similar to SFRs derived from the UV continuum, this methodology is sensitive to extinction and the IMF used for calibration (Kennicutt, 1998). Additionally, $H\alpha$ is redshifted out of the optical wavelengths at $z \sim 0.5$, which limits the use of this technique for studies of high-z galaxies.

- **Forbidden Lines:** Another set of emission lines often used to measure SFRs are forbidden lines, which occur when an electron in an excited, but relatively stable energy level, transitions to a lower energy. The probability of such an occurrence is extremely unlikely and requires very long timescales; however, the densities in the gas surrounding star forming regions are low enough such that atomic collisions are unlikely, providing the timescales needed for such transitions to occur (Kennicutt, 1998). The strongest forbidden-line feature in a galaxy's spectrum is the oxygen

double ([OII] at 3727 Å). However, unlike recombination lines, forbidden emission lines are not directly coupled to the ionizing UV luminosity and are sensitive to the electron temperature and the abundance and distribution of the gas (Kennicutt, 1998). SFRs derived from the [OII] emission line are calibrated empirically through Hα and an average of these calibrations go as

$$SFR(M_\odot \text{ yr}^{-1}) = 1.4 \pm 0.4 \times 10^{-41} L_{[OII]}(\text{erg s}^{-1}), \tag{1.6}$$

where $L_{[OII]}$ is the luminosity of the [OII] line (Kennicutt, 1998). Since the [OII]/Hα ratio varies significantly between galaxies, SFRs derived from [OII] are less precise than those derived from Hα (Kennicutt, 1998). The main advantage of this technique is that the [OII] doublet is observable in optical wavelengths out to redshifts of $z \sim 1.6$, and can therefore probe star formation in higher-z galaxies. Though at $z \sim 1$ Gilbank et al. (2010) found that the SFR-$L_{[OII]}$ relation differed for high and low mass galaxies and required a mass-dependent conversion to obtain more accurate SFRs.

- **The 4000 Å Break (D4000):** Another probe of star formation that makes use of features in a galaxy's spectra is the break strength at 4000 Å, or the D4000 value, defined as the flux ratio in the red continuum (4000 - 4100 Å) to that in the blue continuum (3850 - 3950 Å: Balogh et al., 1999). Galaxies with recent or on-going star formation (typically late-types) emit in the UV, which raises the level of the blue continuum resulting in a relatively level continuum from blue to red. In contrast, galaxies with only old stellar populations and no recent star formation (typically early-types) have little flux in the UV and show a clear break in the continuum at 4000 Å. Since D4000 measures the strength of the break, high values correspond to galaxies with no recent star formation and low values correspond to recent or on-going star formation. While this technique does not directly measure the SFR, it does probe the star formation history (SFH) of a galaxy. Additionally, galaxies tend to occupy two separate regions in the D4000-stellar mass plane (Blanton & Moustakas, 2009), analogous to the red sequence and blue cloud regions

in a CMD.

- **Spectral Energy Distribution (SED) Fitting:** With all of the aforementioned star formation indicators only a specific, and usually narrow, wavelength region of the galaxy's spectra is considered when deriving SFRs. In order to get a more complete picture of the total star formation and the SFH of a galaxy, it is important to try to incorporate as much of the spectral energy distribution (SED = brightness/flux as a function of wavelength or frequency) as possible. Theoretically, detailed analysis of a galaxy's full SED should provide complete information about the properties of the observed galaxy (e.g. stellar mass, SFR, dust properties, etc.). The UV to IR wavelength regimes of the SED provide information about the star forming properties of the galaxy, since the emission is dominated by stellar light at these wavelengths. With observations in multiple filters between the UV to the IR, it is possible to fit an SED with models that depend on, for example: the SFH, the IMF, the stellar population and the amount of dust. The basic idea of SED fitting is that the spectrum of a galaxy is the total sum of the spectra of the stars within that galaxy, a process known as stellar population synthesis initially developed by Tinsley (1972), Searle et al. (1973) and Larson & Tinsley (1978). The basic goal of stellar population synthesis codes is to determine the right combination of stars to produce the observed galaxy SED. For stars of a given age this requires an input IMF and large grids of stellar evolutionary tracks to obtain the final stellar mass distribution, as well a library of corresponding stellar spectra (either empirical or computed: Walcher et al., 2011). Observed galaxies are typically not composed of stars with a single age and metallicity, thus stellar population synthesis codes typically integrate the spectra of stars with a wide range of ages and metallicities. In order to determine the ages of the stars in the final population, a model of the SFH of the galaxy is required. An example of such a model SFH is an exponentially declining SFR with additional bursts of star formation (Salim et al., 2007). In addition to stars, SED fitting also requires models of the gas and dust within a galaxy, as these components absorb and re-radiate the emission from stars. SED fitting

combines all of these models and input parameters and finds the best fitting combination that produces the observed SED. While this method can provide a wealth of information regarding galaxy properties, SED fitting is very sensitive to the amount of available photometry and input parameters (e.g. IMF). SED fits that include UV, optical and IR bands provide more accurate fits and better estimates of the SFR.

Each of the aforementioned measures of SFR has its advantages and drawbacks. The choice of indicator used depends strongly on the available data, the desired redshift range of study and the science goals.

In the following, I discuss general trends in the observed SFR , SSFR and quiescent or quenched fraction ($f_{\rm q} \equiv$ the number of passive galaxies over the total number of galaxies) with stellar mass, environment and redshift.

Correlations with Stellar mass

Actively star-forming galaxies (i.e. $\log_{10}(\mathrm{SSFR}) \gtrsim -11$) in the local Universe and at higher redshift ($z \sim 0.8$), show a negative correlation in the SSFR-stellar mass plane, where higher mass galaxies have lower SSFRs (Brinchmann et al., 2004; Vulcani et al., 2010; McGee et al., 2011). This relation is often referred to as the 'main sequence' of star formation. Quiescent galaxies with $\log_{10}(\mathrm{SSFR}) \lesssim -11$ do not show an obvious trend with stellar mass (McGee et al., 2011). However, it should be noted that it is very difficult to obtain an accurate measure of SFR, and therefore SSFR, in galaxies with little or no recent star formation. Thus, SSFR values for quiescent galaxies are less certain than those measured for star forming galaxies (McGee et al., 2011).

The main-sequence of star formation itself shows a trend with stellar mass, where galaxies with $M_{\rm star} < 10^{10.5} M_{\odot}$ show more scatter in SSFR than in high mass galaxies (Vulcani et al., 2010). The dependency of SSFR on stellar mass has also been observed in the quiescent fraction of galaxies. Wetzel et al. (2012) found that for low mass galaxies ($M_{\rm star} \sim 10^{9.8} M_{\odot}$) $f_{\rm q}$ varied significantly (between $30 - 60\%$) depending on halo mass, where higher-mass haloes had a higher quiescent fraction. In contrast, for high-mass galaxies ($M_{\rm star} \sim 10^{11} M_{\odot}$) $f_{\rm q} \sim 0.9$, independent of halo mass.

Correlations with Environment

In a study of SDSS galaxies, Kauffmann et al. (2004) found that of all the observed galaxy properties in their sample (including stellar mass, effective stellar mass surface density, SSFR, D4000, concentration and colour) the SSFR correlated most strongly with environment. These authors defined the environment as the number of neighbours within a given volume and found that the $f_{\rm q}$ increased with an increasing number of neighbours. The quiescent fraction also appeared to correlate with other probes of the environment, such as cluster-centric radius, where $f_{\rm q}$ increases from the outskirts/infall region toward the cluster core (Rines et al., 2005), and halo mass, where more massive haloes have higher $f_{\rm q}$ (Kimm et al., 2009; Wetzel et al., 2012). Although it should be noted that for massive galaxies $M_{\rm star} > 10^{11} M_{\odot}$ $f_{\rm q}$ showed no dependence on halo mass (Kimm et al., 2009; Wetzel et al., 2012).

The enhanced quenching in clusters has also been observed in the high redshift Universe ($0.4 \leq z \leq 0.8$) where Vulcani et al. (2010) found that while the field and cluster galaxies showed similar trends in the SSFR-stellar mass plane, at a given stellar mass galaxies in clusters had lower values of SSFR, indicating enhanced quenching. Woo et al. (2013) also found that the quiescent fraction correlated well with halo for galaxies at $z \sim 1$.

Theoretically, many SAMs predict that the quiescent fraction should correlate with halo mass; however, most models are only able to reproduce the observed $f_{\rm q}$ -$M_{\rm halo}$ trend for central galaxies (Kimm et al., 2009). For satellite galaxies, most models severely overestimate $f_{\rm q}$, especially for low-mass galaxies (Kimm et al., 2009). As previously discussed in Section 1.3.1, the high $f_{\rm q}$ values in satellites are a result of overly efficient stripping in group and cluster haloes. Thus, while SAMs can reproduce the effects of 'nature' on the observed quenched fraction, more work is needed to properly model environmental star formation quenching.

Additionally, while SAMs and some observations show correlations between $f_{\rm q}$ and environment, several studies show that the properties of actively star forming galaxies are independent of environment (Rines et al., 2005; Bai et al., 2009; Wolf et al., 2009; Tyler et al., 2011). In particular, Rines et al. (2005) found that for galaxies with on-going star formation, the distribution of Hα equivalent widths are the same for galaxies within and beyond the virial radius of a host halo. Similarly, Wolf et al. (2009) found that the SSFRs of blue

galaxies were similar in the field, infall regions and cores of clusters. Therefore, while groups and clusters may quench star formation, these high density environments do not appear to affect galaxies that are actively star-forming.

Redshift Evolution

The evolution of star formation with redshift is well described by the SFR density ($\rho_{\rm SFR}$ in units of $M_\odot$ yr^{-1} mpc^{-3}) versus redshift plot, often referred to as the 'Lilly-Madau' plot, which shows that $\rho_{\rm SFR}$ increases from $z = 0$ to $z \sim 1-2$, where it reaches a peak and then turns over and decreases with increasing redshift (Lilly et al., 1996; Madau et al., 1996; Wall et al., 2005; Hopkins & Beacom, 2006; Dunne et al., 2009). Hopkins & Beacom (2006) found that the 'Lilly-Madau' plot puts strong constraints on the cosmic SFH and in particular, evolution in the stellar and metal mass densities, supernova rate densities and the IMF. With regards to the IMF, Hopkins & Beacom (2006) found that shallower or more 'top-heavy' IMFs (e.g. Baldry & Glazebrook, 2003) provide a better fit to the data than the more commonly used Salpeter IMF. Additionally, the SSFRs of actively star-forming galaxies also increase with redshift, for all stellar masses (Bauer et al., 2005; Damen et al., 2009; Dunne et al., 2009; Bouché et al., 2010; Cen, 2011). Since the inverse of the SSFR is the timescale for a galaxy to double in mass, assuming a constant and continuous SFR, an increasing SSFR with redshift indicates that galaxies at higher redshift were able to gain stellar mass in a shorter amount of time.

1.3.4 The Relationship Between Colour, Morphology and SFR

In the previous sections, I discussed colour, morphology and star formation separately; here, I will discuss how these observed properties correlate with each other. Based on the aforementioned correlations, it would appear that the general trends are that high-mass galaxies are typically red, quiescent, have early-type morphologies and preferentially reside in high-density environments, while low mass galaxies are blue, actively star-forming, have late-type morphologies and typically reside in low-density environments. Although these trends are on average representative of the galaxy population, colour,

morphology and star formation do not always correlate as expected.

In general, both qualitative and quantitative measures of morphology tend to correlate well with colour, where ellipticals are usually red and spirals are for the most part blue. However, several studies have observed a population of red spiral galaxies, which suggests either the presence of a significant amount of dust or that SF quenching has occurred with no obvious morphological changes (Bamford et al., 2009; Skibba et al., 2009). The latter suggests that the transformation from a blue to red galaxy occurs on a shorter timescale than the transformation from spiral to early-type (Bamford et al., 2009). Additionally, while the fraction of elliptical galaxies as a function of environment mirrors the $f_{\rm red}$ trend, the fraction of red galaxies is consistently higher by approximately 20% (Bamford et al., 2009), which further verifies that morphology and colour are not always directly linked. As a function of redshift, Lotz et al. (2008) found that the morphological make-up of the red sequence evolved with redshift. At $z \sim 1.1$ Sb and Irregular galaxies make up 29% of the red sequence, while at $z \sim 0.3$ almost all ($\sim 90\%$) of red sequence galaxies either have elliptical, S0 or Sa morphologies. Therefore, the correlation between colour and morphology also appears to evolve with redshift.

Since colour is, in essence, a probe of the stellar population of a galaxy, one would expect red galaxies to be quiescent and blue galaxies to be actively star-forming. In Figure 1.5, I plot ${}^0(g-r)$ versus SSFR for SDSS galaxies in the Yang et al. (2007) group catalogue, where the red dashed vertical line indicates the division between quiescent ($\log_{10}(\mathrm{SSFR}) \lesssim -10.6$) and actively star-forming ($\log_{10}(\mathrm{SSFR}) \gtrsim -10.6$) galaxies and the red solid horizontal line roughly corresponds to the division between red (${}^0(g-r) \gtrsim 0.6$) and blue (${}^0(g-r) \lesssim 0.6$) galaxies. In Figure 1.5, there are two visible sequences; one that corresponds to 'red & quiescent' galaxies (top-left region) and the other to 'blue & actively star-forming' galaxies (bottom-right region). For galaxies in these sequences, the correlation between colour and SSFR goes as expected. Very few ($\sim 2\%$) of the galaxies occupy the 'blue & quiescent' region of Figure 1.5. However, $\sim 10\%$ of the galaxy population reside in the 'red & actively star-forming' region and it is the presence of this population that renders colour a sometimes unreliable measure of star formation. It is thought that the majority of these galaxies contain significant amounts of dust, which reddens the UV

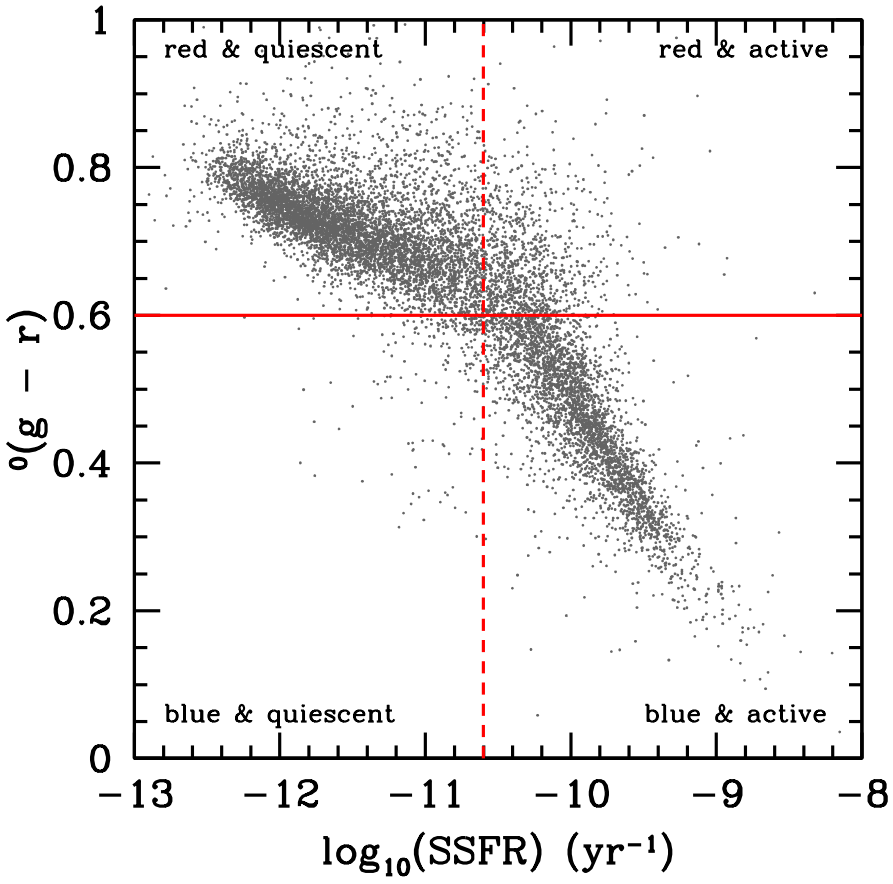

Figure 1.5: $^0(g-r)$ (k-corrected to a redshift of $z=0$) versus $\log_{10}(SSFR)$ for all group galaxies in the Yang et al. (2007) SDSS group catalogue with $z \leq 0.05$.

emission from star forming regions. Observations in the IR wavelengths can provide information about dust-obscured SF. However, in a study of 'dusty red galaxies', Wolf et al. (2009) found that at fixed stellar mass the SFRs in 'red & actively star-forming' galaxies were ~ 4 times lower than in blue star forming spirals. As a result, these authors claimed that dusty red galaxies were actually a transitory phase between red and blue galaxies, as opposed to 'normal' star forming galaxies with significant amounts of dust.

1.4 Galaxy Transformation Processes

One of the main goals of pursuing the 'nature versus nurture' issue is that it can provide insight into the physical processes responsible for galaxy transformation. These mechanisms are often divided into two categories: internal or secular processes that occur due to changes within the galaxy itself (i.e. nature) and external processes that relate to either the local environment or properties of the host group or cluster dark matter halo (i.e. nurture). While there are numerous theoretical galaxy transformation mechanisms, I will focus on those that are most probable and also relevant to this work.

1.4.1 Internal Processes

Internal processes refer to galaxy transformation mechanisms that occur within the galaxy itself, such as supernova feedback. While some of these processes may correlate with the external environment (for example galaxy-galaxy interactions are thought to fuel active galactic nuclei (AGN)) it believed that these processes more strongly correlate with galaxy stellar mass. Thus, these mechanisms are considered as part of the 'nature' scenario.

1.4.1.1 Feedback

A longstanding issue in the theory of galaxy formation is the overcooling problem, which essentially states that the gas in dark matter haloes cools far too efficiently and produces galaxies that are much more massive than observed (White & Rees, 1978; White & Frenk, 1991; Cole, 1991; Balogh et al., 2001). The favoured solution to this problem is to include processes that heat up

the gas and prevent cooling and therefore star formation, such as supernovae feedback or feedback from active galactic nuclei (AGN) (White & Frenk, 1991; Cole, 1991; Cole et al., 2000; Benson et al., 2003; Bower et al., 2006). Both Benson et al. (2003) and Bower et al. (2006) showed that supernovae feedback alone provided insufficient energy to overcome the overcooling problem in the most massive haloes. Since AGN can provide anywhere between 20-50 times more energy for heating, these authors claimed that AGN feedback is necessary to prevent overcooling; though the method by which the energy from the AGN heats the gas is still unknown (Benson, 2010). There are two proposed general methods of delivery, radiative and mechanical feedback (Benson, 2010). The radiative mode is straightforward, in that the AGN radiatively heats up the surrounding cold gas. For the mechanical feedback mode, AGN winds or highly collimated, powerful jets physically remove the cold gas from the galaxy.

Although supernovae feedback may not be efficient in the most massive galaxies, the energy output from supernovae can suppress star formation in lower mass galaxies (Cole et al., 2000; Bower et al., 2006; Stinson et al., 2006). Supernovae heat the surrounding cold gas such that it becomes part of the hot gas halo. If the hot gas is not able to re-settle into a cold phase, either due to long radiative cooling times or escape of the gas from the galaxy's potential well, then star formation is effectively quenched.

1.4.1.2 Secular Galaxy Evolution

Although galaxy-galaxy interactions and mergers are a natural consequence of hierarchical structure formation, observations of galaxies with an extremely thin disk and no bright central bulge (Goad & Roberts, 1981; Matthews et al., 1999; Kautsch et al., 2006) and pseudobulges, that is predominantly rotationally- rather than dispersion- supported bulges, indicate that at least some galaxies have not experienced a major merger since the onset of star formation. These galaxies have therefore evolved with no external influences, a process known as 'secular evolution', which refers to changes that arise from interactions between the various sub-components of a galaxy, i.e. bars, spiral structure and the triaxial dark matter halo (Toth & Ostriker, 1992). While there are many theoretical secular evolution processes, I will only briefly discuss the main mechanisms in order to emphasize the fact that morphological

changes can occur *in situ*. For a more detailed summary of secular galaxy evolution see Kormendy & Kennicutt (2004) and references therein.

Observations of spiral galaxies show that a large fraction, anywhere between $\sim 30 - 65\%$, contain a central bar (Eskridge & Frogel, 1999; Sheth et al., 2008; Masters et al., 2011). Additionally, bars appear to occur naturally in N-body simulations of spiral galaxies (Sellwood, 1981; Sparke & Sellwood, 1987; Athanassoula, 2003), arising as a connection between the end-points of a disk instability. Analytic and numerical investigations of bars show that they grow via the transfer of angular momentum to the outer disk (Lynden-Bell, 1979; Sellwood, 1981; Binney & Tremaine, 1987; Sparke & Sellwood, 1987; Athanassoula, 2003), which either drives gas inwards, forming a pseudobulge, or outwards, forming a ring.

Unbarred galaxies can undergo similar secular evolution to barred galaxies, if the galaxy contains global-pattern spirals (Kormendy & Kennicutt, 2004). Since spiral patterns are thought to be density waves that propagate through the disk, the 'spiral arms' are not made of the same continuous material. Instead, gas and old stars pass through the arms as they rotate around. SF is triggered as gas passes through the arms resulting in a concentration of young and bright stars, which are often observed in the spiral arms (Kormendy & Kennicutt, 2004). Additionally, shocks form in regions where gas piles up and generally mimics the shape of the spiral density wave. Further interaction between these shocks and gas results in a loss of energy. The gas then flows toward the centre of the galaxy, forming a pseudobulge. This process is slower than bar instability, but qualitatively produces the same morphological change.

1.4.2 External Processes

External processes involve interactions with the gas in the host group/cluster halo, i.e. intragroup or intracluster medium (IGM or ICM), or gravitational interactions between the galaxies themselves.

1.4.2.1 Ram Pressure-Stripping

Some of the first discovered extragalactic X-ray sources were associated with the nearby Virgo, Coma and Perseus clusters (Byram et al., 1966; Cavaliere

et al., 1971; Fritz et al., 1971; Gursky et al., 1971). Observations of the X-ray emission from these clusters showed that it was bright ($10^{43} - 10^{45}$ erg s^{-1}), did not vary temporally (Elvis, 1976) and was extended, roughly following the spatial distribution of galaxies (Forman et al., 1972; Kellogg et al., 1972). Further investigation of the X-ray emission, and in particular an emission feature at 7 keV, showed that it formed via thermal bremsstrahlung or free-free emission (i.e. scattering of free elections off ions) in hot ionized gas within the cluster (Mitchell et al., 1976). As gas falls into a potential well, it gets compressed and its kinetic energy is converted into thermal energy resulting in temperatures following

$$\frac{3kT_{\rm gas}}{2\mu m_p} \approx \frac{3}{2}\sigma_r^2, \tag{1.7}$$

where $T_{\rm gas}$ is the temperature of the IGM or ICM, μ is the mean molecular weight in unit of amu, m_p is the proton mass, and σ_r is the line-of-sight (LOS) velocity dispersion of the cluster (Sarazin, 1986). In the case of rich clusters with $\sigma_r \sim 1000$km s^{-1}, the temperature derived from Equation 1.7 is on the order of $\sim 10^8$ K and the baryonic matter remains in a dense gaseous state forming the intracluster medium (ICM).

The density and temperature of the ICM not only produces strong extended X-ray emission, but also acts as 'fluid' within the cluster. As a result, infalling galaxies experience a strong drag force in a process known as ram pressure stripping (Gunn & Gott, 1972). The drag pressure is given by

$$P_{\rm ram} = \rho_{\rm gas} v_{\rm rel}^2, \tag{1.8}$$

where $\rho_{\rm gas}$ is the density of the ICM and $v_{\rm rel}$ is the relative velocity between the infalling galaxy and the ICM. Stripping occurs if $P_{\rm ram}$ is greater than the restoring gravitational force per unit area of the infalling disk, which is given by

$$\frac{F_{\rm restoring}}{A} = 2\pi G \Sigma_{\rm disk} \Sigma_{\rm ISM}, \tag{1.9}$$

where $\Sigma_{\rm disk}$ is the surface density of the stars in the disk and $\Sigma_{\rm ISM}$ is the surface density of the hot gas in the ISM (Sarazin, 1986).

Combining Equations 1.8 and 1.9, taking $v_{\rm rel}^2 = 3\sigma_r^2$ and assuming a disk with radius $r_{\rm disk}$, mass $M_{\rm disk}$ and uniform surface density, Sarazin (1986) showed that the condition for ram pressure-stripping becomes

$$\left(\frac{n_{\rm gas}}{10^{-3}{\rm cm}^{-3}}\right)\left(\frac{\sigma_r}{10^3{\rm km\ s}^{-1}}\right)^2 \gtrsim 3\left(\frac{M_{\rm disk}}{10^{11}M_\odot}\right)^2\left(\frac{r_{\rm disk}}{10{\rm kpc}}\right)^{-4}\left(\frac{M_{\rm ISM}}{0.1M_{\rm disk}}\right), \tag{1.10}$$

where $n_{\rm gas}$ in the number density of atoms in the ISM and $M_{\rm ISM}$ is the mass of the ISM.

From Equation 1.10, we see that an infalling galaxy is more easily stripped in a massive cluster (large σ_r), if the infalling disk has low mass ($M_{\rm disk}$) or an extended disk ($r_{\rm disk}$). When ram pressure-stripping does occur, the gas, rather than the stars, in the infalling galaxy is much more easily removed. Using Smoothed-particle hydrodynamics (SPH) N-body simulations, Abadi et al. (1999) showed that the analytic predictions of Gunn & Gott (1972) provided a good approximation for the effects of ram pressure-stripping. These authors showed that a spiral galaxy falling onto a Coma-like cluster would lose $\sim 80\%$ of its diffuse gas in only ~ 10 Myr resulting in a truncated disk. However, in less massive clusters or in galaxy groups, Abadi et al. (1999) found that the infalling galaxies lost significantly less gas. Thus, ram pressure-stripping is only efficient in the most massive clusters.

The effect of ram pressure-stripping on galaxy evolution is to remove the supply of the cold gas used to form stars (Gunn & Gott, 1972). Subsequently, star formation is quenched in the infalling galaxy. Although the process does not directly result in morphological change, star formation quenching can lead to disk-fading which is one possible formation mechanism for SO or lenticular galaxies.

Observational evidence of ram pressure-stripping can be seen in galaxies on the outskirts of nearby clusters (e.g. Coma and Virgo). Examples include galaxies with: truncated or deficient HI disks (Haynes & Giovanelli, 1986; Cayatte et al., 1994; Vollmer et al., 2001), extended UV, HI or Hα tails (Sun et al., 2007; Smith et al., 2010; Abramson et al., 2011), and bent radio lobes (Blanton et al., 2001; Wing & Blanton, 2011). Thus, while it is clear that ram pressure-stripping does affect cluster galaxies, it is far less efficient in

galaxy groups, where both $n_{\rm gas}$ and σ_r in Equation 1.10 are reduced. Since, environmental trends are seen even in poor or low mass groups, ram pressure-stripping is unlikely to be the main mechanism of galaxy transformation in the group environment.

1.4.2.2 Strangulation

Ram pressure-stripping is only effective in massive haloes with $\sigma_r \sim 1000$km s^{-1}. In lower mass systems, such as galaxy groups, ram pressure-stripping is inefficient; however, the IGM still imparts a drag force on infalling galaxies. Although this drag force cannot directly remove cold gas, it is able to remove the hot gas from the infalling galaxy, a process that is often referred to as 'strangulation' (Larson et al., 1980; Balogh et al., 2000; Kawata & Mulchaey, 2008).

Using cosmological simulations, Kawata & Mulchaey (2008) studied the effects of the group environment ($M_{\rm halo} \sim 8 \times 10^{12} M_{\odot}$) on an infalling disk galaxy with $V_{\rm rot} \sim 150$km s^{-1}. Their simulations showed that ram pressure could not strip the cold gas, but that after roughly 1 Gyr the majority of hot gas in the galaxy was stripped. The removal of the hot gas halo does not 'instantly' quench star formation, as in the case of ram pressure-stripping, but instead effectively cuts off the supply of gas for any future star formation. In a study of 210 nearby spiral and irregular galaxies, Kennicutt et al. (1994) found that a spiral galaxy would convert the majority of its disk gas into stars within $\sim$3 Gyr; however, the additional supply of gas from the surrounding hot halo could extend the star formation lifetime by factors of 1.5-4. Thus, the effect of strangulation is to limit the duration of star formation in late-type galaxies.

Recent results suggest that strangulation may be the preferred galaxy transformation mechanism. Evidence in favour of this process includes the fact that strangulation is efficient in the low-mass galaxy groups, where environmental trends begin to take place, and the long timescale over which the mechanism acts. In particular, SAMs have shown that environmental processes begin in haloes with masses between $10^{12} - 10^{13}$ $M_{\odot}$ (McGee et al., 2009) and that complete star formation quenching requires timescales on the order of $\sim 2 - 7$ Gyrs (McGee et al., 2009; De Lucia et al., 2012). Both of these conditions appear to rule out ram pressure-stripping, which again acts

Figure 1.6: Left: Interacting galaxies NGC 4038 and NGC 4039 (the Antennae Galaxies). Right: Interacting galaxies Arp 87. Both Image credits: NASA, ESA and the Hubble Heritage Team (STSci/AURA).

on very short timescales and is only efficient is massive clusters. While the results of these SAMs suggest that strangulation is the preferred mechanism for galaxy evolution, it cannot directly induce any morphological changes, which is necessary to explain the MDR.

1.4.2.3 Galaxy Mergers and Interactions

In the 1950s and 1960s, astronomers began to observe galaxies with peculiar features, such as extended tails and filamentary structures (i.e. bridges) connecting pairs or multiples of galaxies (Zwicky, 1956; Vorontsov-Velyaminov, 1959; Arp, 1966). In Figure 1.6, we show examples of interacting galaxies, taken with the Hubble Space Telescope (HST); the image on the left is of the Antennae Galaxies (NGC 4038 and 4039) and the image on the right is of Arp 87.

While observations showed that these peculiar galaxies were interacting with each other, it would take numerical simulations to show that the driving force of the interaction was purely gravity. With a simulation of two equal mass disk galaxies, each with just 120 test particles, Toomre & Toomre (1972) demonstrated that through gravitational forces alone one could reproduce the tails and bridges observed in peculiar pairs of galaxies. Toomre (1977) later suggested that such an interaction would eventually lead to a merger and the formation of a single galaxy with an early-type morphology.

Advancements in computer technology and numerical techniques have since provided a wealth of information regarding gravitational interactions. In particular, we now know that frequent galaxy-galaxy interactions and mergers are a direct consequence of hierarchical structure formation. Additionally, numerical studies have shown that there are numerous sub-categories of mergers (e.g. minor, major, wet, dry, etc.), each of which has a different influence on galaxy evolution. Major mergers, defined as an interaction of two similar mass galaxies, were originally thought to produce an early-type galaxy (Toomre, 1977; Barnes & Hernquist, 1992); however, simulations have since shown that major mergers can also result in the remnants with late-type morphologies (Barnes, 2002; Springel & Hernquist, 2005; Robertson et al., 2006; Hopkins et al., 2009). For the most part the stars within the galaxies are thought to be collisionless, but the gas within galaxies is not. Major mergers between gas-rich galaxies, so-called 'wet mergers', can have very different results in comparison to mergers between galaxies with little or no gas, so-called 'dry mergers'. The latter are thought to mainly produce early-type galaxies, while the former can result in the survival of the disk (Springel & Hernquist, 2005; Hopkins et al., 2009). The addition of interactions between the merging galaxies and the surrounding ISM can further aide in a surviving or newly-formed disk, depending on the orbital parameters (Barnes, 2002). Robertson et al. (2006) showed that during a merger, pressurization from the ISM prevented star formation and allowed the gas to settle into a rotationally-supported disk that can eventually form stars and spiral features.

In addition, the gaseous component of galaxies undergoing a major merger experiences strong shocks and loses both energy and angular momentum. The gas is then funnelled toward the centre of the remnant galaxy and then quickly cools, resulting in a burst of star formation (Mihos & Hernquist, 1996; Cox et al., 2006). Major mergers are therefore believed to be the cause of the high star formation rates (SFRs) seen in starburst galaxies (Barnes & Hernquist, 1991; Mihos & Hernquist, 1996; Elbaz & Cesarsky, 2003; Cox et al., 2006; Hopkins et al., 2006; Teyssier et al., 2010). Indeed, many of the observed post-starburst (PSB) galaxies show signs of galaxy-galaxy interactions and mergers (Zabludoff et al., 1996; Yang et al., 2004, 2008; Goto, 2005). Simulations show that the majority of the gas is consumed during the starburst phase, and

assuming there is no additional supply of gas, star formation is subsequently quenched in the remnant galaxy. As the starburst phase is relatively short, ∼150 Myr (Mihos & Hernquist, 1996), the transition from blue cloud to red sequence for the merger remnant is relatively quick.

Although major mergers have the ability to drastically alter the star forming and morphological properties of galaxies, it appears that the majority of mergers occur between galaxies with mass ratios greater than 1:4, so-called minor mergers or accretion. Observational studies have shown that the minor merger rate is roughly 3 times higher than the major merger rate, at least to $z \sim 0.7$ (Lotz et al., 2011). N-body simulations show similar results to redshifts as high as $z = 3$ (Hopkins et al., 2010). While these interactions are much less violent than major mergers, minor mergers can still result in morphological change, e.g. a warped or thickened disk (Quinn & Goodman, 1986; Huang & Carlberg, 1997). Also, a fraction of the gas can still accrete onto the inner region of the remnant galaxy (Hernquist & Mihos, 1995), which could lead to a starburst scenario similar to that observed in major mergers.

Based on these results, it is evident the galaxy-galaxy interactions and mergers play an important role in the evolution of galaxies. The questions that remain are: how much of a contribution does this process play and is there a correlation between mergers and environment? SAMs have provided insight into the environmental dependence of mergers. For example, Jian et al. (2012) found that the correlation between merger rate and environment differed depending on the definition of environment. These authors found the merger rate showed a strong dependence on environment when defined either by the local overdensity or the 6th nearest neighbour. However, when the environment is defined by the host group or cluster halo mass, Jian et al. (2012) showed that merger rate did not monotonically increase, as with the other estimators of environment, but rather peaked at halo masses between $10^{12} - 10^{13}\ h^{-1}M_{\odot}$, which corresponds to group scales. While it is difficult to observationally determine the galaxy merger rates as a function of radius, it is possible to study correlations between dynamical state, observable signs of interactions (e.g. asymmetries, PSB) and environment. We will discuss our method of investigating this topic in a letter section.

1.4.2.4 Galaxy Harassment

The effects of gravitational forces on galaxy evolution are not limited to mergers and direct interactions, which only occur if the galaxies are moving slowly enough for dynamical friction to reduce the orbital energies of the galaxies. When galaxies are moving at high speeds, relative to each other, there is insufficient time for a merger to take place. In the rich galaxy cluster environment, where $\sigma \sim 1000$ km s^{-1}, galaxies are moving too quickly for direct interactions to take place; instead galaxies experience multiple high-speed encounters with other cluster members with a frequency of one per Gyr in high density regions (Moore et al., 1996). These repeated gravitational encounters, often referred to as 'galaxy harassment', can cause impulsive gravitational heating, which can lead to morphological distortions and the ejection of gas and stars beyond the galaxy's tidal radii (Moore et al., 1996, 1998). These authors found that harassment could lead to the morphological transformation of a late-type galaxy into a spheroidal one in approximately 5 Gyrs. Additionally, Moore et al. (1996, 1998) suggested that galaxy harassment could explain the observation of disturbed blue spirals, dwarf ellipticals or the enhanced star formationRs seen in cluster galaxies at all radii. Many of these galaxies did not appear to have any neighbouring or 'close' galaxies; thus, direct interactions could not be the cause of the distorted features or higher rate of star formation (Moore et al., 1996, 1998).

Another feature of galaxy harassment is that its efficiency is thought to be independent of cluster radius. According to the impulse approximation, the amount of energy transferred during harassment scales as the square of the opposing galaxy's mass ($M^2_{\rm opp}$: Spitzer, 1958), assuming that mass scales linearly with cluster-centric radius ($M_{\rm opp} \propto r_{\rm cluster}$). The efficiency of harassment ($\epsilon_{\rm harassment}$) also depends on the density of galaxies (ρ), which scales as $r^{-2}_{\rm cluster}$. Putting these together, we see that the efficiency is independent of $r_{\rm cluster}$,

$$\epsilon_{\rm harassment} \quad \propto \quad M^2_{\rm opp} \times \rho \quad \propto \quad r^2_{\rm cluster} \times r^{-2}_{\rm cluster}. \tag{1.11}$$

Thus, harassment differs from other galaxy transformation processes, such as ram pressure-stripping, since it is equally efficient at all radii.

1.5 Conclusions

In this chapter I have presented some of the basic properties of galaxy evolution, including observed correlations between galaxy properties and the main galaxy transformation processes that may drive these observed relations. In the following chapter I will discuss the specifics of galaxy evolution in the group environment, which serves as motivation for the three papers presented in Chapters 3, 4 and 5.

Bibliography

Abadi, M. G., Moore, B., & Bower, R. G. 1999, MNRAS, 308, 947

Abazajian, K. N., Adelman-McCarthy, J. K., Agüeros, M. A., Allam, S. S., Allende Prieto, C., An, D., Anderson, K. S. J., Anderson, S. F., Annis, J., Bahcall, N. A., & et al. 2009, ApJS, 182, 543

Abraham, R. G., Valdes, F., Yee, H. K. C., & van den Bergh, S. 1994, ApJ, 432, 75

Abraham, R. G., van den Bergh, S., Glazebrook, K., Ellis, R. S., Santiago, B. X., Surma, P., & Griffiths, R. E. 1996, ApJS, 107, 1

Abraham, R. G., van den Bergh, S., & Nair, P. 2003, ApJ, 588, 218

Abramson, A., Kenney, J. D. P., Crowl, H. H., Chung, A., van Gorkom, J. H., Vollmer, B., & Schiminovich, D. 2011, AJ, 141, 164

Allen, P. D., Driver, S. P., Graham, A. W., Cameron, E., Liske, J., & de Propris, R. 2006, MNRAS, 371, 2

Alpher, R. A., Bethe, H., & Gamow, G. 1948, Physical Review, 73, 803

Aragón-Salamanca, A., Bedregal, A. G., & Merrifield, M. R. 2006, A&A, 458, 101

Arp, H. 1966, Atlas of peculiar galaxies

Athanassoula, E. 2003, MNRAS, 341, 1179

Bai, L., Rieke, G. H., Rieke, M. J., Christlein, D., & Zabludoff, A. I. 2009, ApJ, 693, 1840

Baldry, I. K., Balogh, M. L., Bower, R. G., Glazebrook, K., Nichol, R. C., Bamford, S. P., & Budavari, T. 2006, MNRAS, 373, 469

Baldry, I. K. & Glazebrook, K. 2003, ApJ, 593, 258

Baldry, I. K., Glazebrook, K., Brinkmann, J., Ivezić, Ž., Lupton, R. H., Nichol, R. C., & Szalay, A. S. 2004, ApJ, 600, 681

Balogh, M. L., Baldry, I. K., Nichol, R., Miller, C., Bower, R., & Glazebrook, K. 2004, ApJ, 615, L101

Balogh, M. L., McGee, S. L., Wilman, D., Bower, R. G., Hau, G., Morris, S. L., Mulchaey, J. S., Oemler, Jr., A., Parker, L., & Gwyn, S. 2009, MNRAS, 398, 754

Balogh, M. L., McGee, S. L., Wilman, D. J., Finoguenov, A., Parker, L. C., Connelly, J. L., Mulchaey, J. S., Bower, R. G., Tanaka, M., & Giodini, S. 2011, MNRAS, 412, 2303

Balogh, M. L., Morris, S. L., Yee, H. K. C., Carlberg, R. G., & Ellingson, E. 1999, ApJ, 527, 54

Balogh, M. L., Navarro, J. F., & Morris, S. L. 2000, ApJ, 540, 113

Balogh, M. L., Pearce, F. R., Bower, R. G., & Kay, S. T. 2001, MNRAS, 326, 1228

Bamford, S. P., Nichol, R. C., Baldry, I. K., Land, K., Lintott, C. J., Schawinski, K., Slosar, A., Szalay, A. S., Thomas, D., Torki, M., & et al. 2009, MNRAS, 393, 1324

Barnes, J. 1988, ApJ, 331, 699

—. 1992, ApJ, 393, 484

—. 2002, MNRAS, 333, 481

Barnes, J. E. & Hernquist, L. 1992, ARA&A, 30, 705

Barnes, J. E. & Hernquist, L. E. 1991, ApJ, 370, L65

Bauer, A. E., Drory, N., Hill, G. J., & Feulner, G. 2005, ApJ, 621, L89

Bedregal, A. G., Aragón-Salamanca, A., & Merrifield, M. R. 2006, MNRAS, 373, 1125

Bennett, C., Halpern, M., Hinshaw, G., Jarosik, N., Kogut, A., Limon, M., Meyer, S., Page, L., Spergel, D., Tucker, G., & et al. 2003, ApJS, 148, 1

Benson, A. J. 2010, Phys. Rep., 495, 33

Benson, A. J., Bower, R. G., Frenk, C. S., Lacey, C. G., Baugh, C. M., & Cole, S. 2003, ApJ, 599, 38

Binney, J. & Tremaine, S. 1987, Galactic dynamics

Blanton, E. L., Gregg, M. D., Helfand, D. J., Becker, R. H., & Leighly, K. M. 2001, AJ, 121, 2915

Blanton, M. R., Eisenstein, D., Hogg, D. W., Schlegel, D. J., & Brinkmann, J. 2005, ApJ, 629, 143

Blanton, M. R., Hogg, D. W., Bahcall, N. A., Baldry, I. K., Brinkmann, J., Csabai, I., Eisenstein, D., Fukugita, M., Gunn, J. E., Ivezić, Ž., & et al.,. 2003, ApJ, 594, 186

Blanton, M. R. & Moustakas, J. 2009, ARA&A, 47, 159

Bond, J., Kofman, L., & Pogosyan, D. 1996, Nature, 380, 603

Bouché, N., Dekel, A., Genzel, R., Genel, S., Cresci, G., Förster Schreiber, N. M., Shapiro, K. L., Davies, R. I., & Tacconi, L. 2010, ApJ, 718, 1001

Bower, R. G. 1991, MNRAS, 248, 332

Bower, R. G., Benson, A. J., Malbon, R., Helly, J. C., Frenk, C. S., Baugh, C. M., Cole, S., & Lacey, C. G. 2006, MNRAS, 370, 645

Brinchmann, J., Charlot, S., White, S. D. M., Tremonti, C., Kauffmann, G., Heckman, T., & Brinkmann, J. 2004, MNRAS, 351, 1151

Butcher, H. & Oemler, Jr., A. 1984, ApJ, 285, 426

Byram, E. T., Chubb, T. A., & Friedman, H. 1966, Science, 152, 66

Capak, P., Abraham, R. G., Ellis, R. S., Mobasher, B., Scoville, N., Sheth, K., & Koekemoer, A. 2007, ApJS, 172, 284

Cavaliere, A. G., Gursky, H., & Tucker, W. H. 1971, Nature, 231, 437

Cayatte, V., Kotanyi, C., Balkowski, C., & van Gorkom, J. H. 1994, AJ, 107, 1003

Cen, R. 2011, ApJ, 741, 99

Cole, S. 1991, ApJ, 367, 45

Cole, S., Lacey, C. G., Baugh, C. M., & Frenk, C. S. 2000, MNRAS, 319, 168

Conselice, C. J. 2003, ApJS, 147, 1

Conselice, C. J., Bershady, M. A., & Jangren, A. 2000, ApJ, 529, 886

Cooper, M. C., Newman, J. A., Weiner, B. J., Yan, R., Willmer, C. N. A., Bundy, K., Coil, A. L., Conselice, C. J., Davis, M., Faber, S. M., Gerke, B. F., Guhathakurta, P., Koo, D. C., & Noeske, K. G. 2008, MNRAS, 383, 1058

Cox, T. J., Jonsson, P., Primack, J. R., & Somerville, R. S. 2006, MNRAS, 373, 1013

Damen, M., Labbé, I., Franx, M., van Dokkum, P. G., Taylor, E. N., & Gawiser, E. J. 2009, ApJ, 690, 937

De Lucia, G., Weinmann, S., Poggianti, B., Aragón-Salamanca, A., & Zaritsky, D. 2012, MNRAS, 423, 1277

De Propris, R., Stanford, S. A., Eisenhardt, P. R., & Dickinson, M. 2003, ApJ, 598, 20

de Vaucouleurs, G. 1959, Handbuch der Physik, 53, 275

Dressler, A. 1980, ApJ, 236, 351

Dressler, A. & Gunn, J. E. 1982, ApJ, 263, 533

Dunne, L., Ivison, R. J., Maddox, S., Cirasuolo, M., Mortier, A. M., Foucaud, S., Ibar, E., Almaini, O., Simpson, C., & McLure, R. 2009, MNRAS, 394, 3

Elbaz, D. & Cesarsky, C. J. 2003, Science, 300, 270

Ellingson, E., Lin, H., Yee, H. K. C., & Carlberg, R. G. 2001, ApJ, 547, 609

Elvis, M. 1976, MNRAS, 177, 7P

Eskridge, P. B. & Frogel, J. A. 1999, Ap&SS, 269, 427

Ferrarese, L. & Merritt, D. 2000, ApJ, 539, L9

Font, A. S., Bower, R. G., McCarthy, I. G., Benson, A. J., Frenk, C. S., Helly, J. C., Lacey, C. G., Baugh, C. M., & Cole, S. 2008, MNRAS, 389, 1619

Forman, W., Kellogg, E., Gursky, H., Tananbaum, H., & Giacconi, R. 1972, ApJ, 178, 309

Fritz, G., Davidsen, A., Meekins, J. F., & Friedman, H. 1971, ApJ, 164, L81

Gallagher, III, J. S. & Hunter, D. A. 1984, ARA&A, 22, 37

Gilbank, D. G., Baldry, I. K., Balogh, M. L., Glazebrook, K., & Bower, R. G. 2010, MNRAS, 405, 2594

Goad, J. W. & Roberts, M. S. 1981, ApJ, 250, 79

Goto, T. 2005, MNRAS, 357, 937

Grützbauch, R., Conselice, C. J., Varela, J., Bundy, K., Cooper, M. C., Skibba, R., & Willmer, C. N. A. 2011, MNRAS, 411, 929

Gunn, J. E. & Gott, III, J. R. 1972, ApJ, 176, 1

Gursky, H., Kellogg, E., Murray, S., Leong, C., Tananbaum, H., & Giacconi, R. 1971, ApJ, 167, L81

Haynes, M. P. & Giovanelli, R. 1986, ApJ, 306, 466

Hernquist, L. 1993, ApJ, 409, 548

Hernquist, L. & Mihos, J. C. 1995, ApJ, 448, 41

Holden, B. P., Illingworth, G. D., Franx, M., Blakeslee, J. P., Postman, M., Kelson, D. D., van der Wel, A., Demarco, R., Magee, D. K., Tran, K.-V., Zirm, A., Ford, H., Rosati, P., & Homeier, N. 2007, ApJ, 670, 190

Hopkins, A. M. & Beacom, J. F. 2006, ApJ, 651, 142

Hopkins, P., Somerville, R., Cox, T., Hernquist, L., Jogee, S., Kereš, D., Ma, C., Robertson, B., & Stewart, K. 2009, MNRAS, 397, 802

Hopkins, P. F., Bundy, K., Croton, D., Hernquist, L., Keres, D., Khochfar, S., Stewart, K., Wetzel, A., & Younger, J. D. 2010, ApJ, 715, 202

Hopkins, P. F., Somerville, R. S., Hernquist, L., Cox, T. J., Robertson, B., & Li, Y. 2006, ApJ, 652, 864

Huang, S. & Carlberg, R. G. 1997, ApJ, 480, 503

Hubble, E. 1929, Proceedings of the National Academy of Science, 15, 168

Hubble, E. P. 1925, ApJ, 62, 409

—. 1926, ApJ, 64, 321

Jian, H.-Y., Lin, L., & Chiueh, T. 2012, ApJ, 754, 26

Kauffmann, G., White, S. D. M., Heckman, T. M., Ménard, B., Brinchmann, J., Charlot, S., Tremonti, C., & Brinkmann, J. 2004, MNRAS, 353, 713

Kautsch, S. J., Grebel, E. K., Barazza, F. D., & Gallagher, III, J. S. 2006, A&A, 445, 765

Kawata, D. & Mulchaey, J. S. 2008, ApJ, 672, L103

Kellogg, E., Gursky, H., Tananbaum, H., Giacconi, R., & Pounds, K. 1972, ApJ, 174, L65

Kennicutt, Jr., R. C. 1998, ARA&A, 36, 189

Kennicutt, Jr., R. C., Tamblyn, P., & Congdon, C. E. 1994, ApJ, 435, 22

Kimm, T., Somerville, R. S., Yi, S. K., van den Bosch, F. C., Salim, S., Fontanot, F., Monaco, P., Mo, H., Pasquali, A., Rich, R. M., & Yang, X. 2009, MNRAS, 394, 1131

Kodama, T. & Bower, R. G. 2001, MNRAS, 321, 18

Kormendy, J. & Kennicutt, Jr., R. C. 2004, ARA&A, 42, 603

Kravtsov, A. & Borgani, S. 2012, ARAA, 50, 353

Lacey, C. & Cole, S. 1993, MNRAS, 262, 627

Larson, R. B. & Tinsley, B. M. 1978, ApJ, 219, 46

Larson, R. B., Tinsley, B. M., & Caldwell, C. N. 1980, ApJ, 237, 692

Lilly, S. J., Le Fevre, O., Hammer, F., & Crampton, D. 1996, ApJ, 460, L1

Lotz, J. M., Davis, M., Faber, S. M., Guhathakurta, P., Gwyn, S., Huang, J., Koo, D. C., Le Floc'h, E., Lin, L., Newman, J., Noeske, K., Papovich, C., Willmer, C. N. A., Coil, A., Conselice, C. J., Cooper, M., Hopkins, A. M., Metevier, A., Primack, J., Rieke, G., & Weiner, B. J. 2008, ApJ, 672, 177

Lotz, J. M., Jonsson, P., Cox, T. J., Croton, D., Primack, J. R., Somerville, R. S., & Stewart, K. 2011, ApJ, 742, 103

Lotz, J. M., Primack, J., & Madau, P. 2004, AJ, 128, 163

Lynden-Bell, D. 1979, MNRAS, 187, 101

Madau, P., Ferguson, H. C., Dickinson, M. E., Giavalisco, M., Steidel, C. C., & Fruchter, A. 1996, MNRAS, 283, 1388

Madau, P., Pozzetti, L., & Dickinson, M. 1998, ApJ, 498, 106

Margoniner, V. E., de Carvalho, R. R., Gal, R. R., & Djorgovski, S. G. 2001, ApJ, 548, L143

Masters, K. L., Nichol, R. C., Hoyle, B., Lintott, C., Bamford, S. P., Edmondson, E. M., Fortson, L., Keel, W. C., Schawinski, K., Smith, A. M., & Thomas, D. 2011, MNRAS, 411, 2026

Matthews, L. D., Gallagher, III, J. S., & van Driel, W. 1999, AJ, 118, 2751

McGee, S. L., Balogh, M. L., Bower, R. G., Font, A. S., & McCarthy, I. G. 2009, MNRAS, 400, 937

McGee, S. L., Balogh, M. L., Wilman, D. J., Bower, R. G., Mulchaey, J. S., Parker, L. C., & Oemler, A. 2011, MNRAS, 413, 996

Mihos, J. C. & Hernquist, L. 1996, ApJ, 464, 641

Mitchell, R. J., Culhane, J. L., Davison, P. J. N., & Ives, J. C. 1976, MNRAS, 175, 29P

Moore, B., Katz, N., & Lake, G. 1996, ApJ, 457, 455

Moore, B., Lake, G., & Katz, N. 1998, ApJ, 495, 139

Muzzin, A., Wilson, G., Yee, H. K. C., Gilbank, D., Hoekstra, H., Demarco, R., Balogh, M., van Dokkum, P., Franx, M., Ellingson, E., & et al. 2012, ApJ, 746, 188

Nair, P. B. & Abraham, R. G. 2010, ApJS, 186, 427

Oemler, Jr., A. 1974, ApJ, 194, 1

Oort, J. H. 1932, Bull. Astron. Inst. Netherlands, 6, 249

Opik, E. 1922, ApJ, 55, 406

Patel, S. G., Kelson, D. D., Holden, B. P., Franx, M., & Illingworth, G. D. 2011, ApJ, 735, 53

Peng, C. Y., Ho, L. C., Impey, C. D., & Rix, H.-W. 2002, AJ, 124, 266

Peng, Y.-j., Lilly, S. J., Kovač, K., Bolzonella, M., Pozzetti, L., Renzini, A., Zamorani, G., Ilbert, O., Knobel, C., Iovino, A., & et al. 2010, ApJ, 721, 193

Peng, Y.-j., Lilly, S. J., Renzini, A., & Carollo, M. 2012, ApJ, 757, 4

Penzias, A. A. & Wilson, R. W. 1965, ApJ, 142, 419

Perlmutter, S., Aldering, G., Goldhaber, G., Knop, R. A., Nugent, P., Castro, P. G., Deustua, S., Fabbro, S., Goobar, A., Groom, D. E., & Supernova Cosmology Project. 1999, ApJ, 517, 565

Planck Collaboration, Ade, P., Aghanim, N., Armitage-Caplan, C., Arnaud, M., Ashdown, M., Atrio-Barandela, F., Aumont, J., Baccigalupi, C., Banday, A., & et al. 2013, ArXiv e-prints

Poggianti, B. M., Desai, V., Finn, R., Bamford, S., De Lucia, G., Varela, J., Aragón-Salamanca, A., Halliday, C., Noll, S., Saglia, R., & et al. 2008, ApJ, 684, 888

Postman, M. & Geller, M. J. 1984, ApJ, 281, 95

Prescott, M., Baldry, I. K., James, P. A., Bamford, S. P., Bland-Hawthorn, J., Brough, S., Brown, M. J. I., Cameron, E., Conselice, C. J., Croom, S. M., & et al. 2011, MNRAS, 417, 1374

Press, W. & Schechter, P. 1974, ApJ, 187, 425

Quinn, P. J. & Goodman, J. 1986, ApJ, 309, 472

Raichoor, A. & Andreon, S. 2012, A&A, 537, A88

Rieke, G. H., Alonso-Herrero, A., Weiner, B. J., Pérez-González, P. G., Blaylock, M., Donley, J. L., & Marcillac, D. 2009, ApJ, 692, 556

Riess, A. G., Filippenko, A. V., Challis, P., Clocchiatti, A., Diercks, A., Garnavich, P. M., Gilliland, R. L., Hogan, C. J., Jha, S., Kirshner, R. P., Leibundgut, B., Phillips, M. M., Reiss, D., Schmidt, B. P., Schommer, R. A., Smith, R. C., Spyromilio, J., Stubbs, C., Suntzeff, N. B., & Tonry, J. 1998, AJ, 116, 1009

Rines, K., Geller, M. J., Kurtz, M. J., & Diaferio, A. 2005, AJ, 130, 1482

Robertson, B., Bullock, J., Cox, T., Di Matteo, T., Hernquist, L., Springel, V., & Yoshida, N. 2006, ApJ, 645, 986

Salim, S., Rich, R. M., Charlot, S., Brinchmann, J., Johnson, B. D., Schiminovich, D., Seibert, M., Mallery, R., Heckman, T. M., Forster, K., & et al. 2007, ApJS, 173, 267

Sarazin, C. L. 1986, Reviews of Modern Physics, 58, 1

Searle, L., Sargent, W. L. W., & Bagnuolo, W. G. 1973, ApJ, 179, 427

Sellwood, J. A. 1981, A&A, 99, 362

Sérsic, J. L. 1963, Boletin de la Asociacion Argentina de Astronomia La Plata Argentina, 6, 41

Sheth, K., Elmegreen, D. M., Elmegreen, B. G., Capak, P., Abraham, R. G., Athanassoula, E., Ellis, R. S., Mobasher, B., Salvato, M., Schinnerer, E., & et al. 2008, ApJ, 675, 1141

Simard, L., Willmer, C. N. A., Vogt, N. P., Sarajedini, V. L., Phillips, A. C., Weiner, B. J., Koo, D. C., Im, M., Illingworth, G. D., & Faber, S. M. 2002, ApJS, 142, 1

Skibba, R. A., Bamford, S. P., Nichol, R. C., Lintott, C. J., Andreescu, D., Edmondson, E. M., Murray, P., Raddick, M. J., Schawinski, K., Slosar, A., Szalay, A. S., Thomas, D., & Vandenberg, J. 2009, MNRAS, 399, 966

Smith, R. J., Lucey, J. R., Hammer, D., Hornschemeier, A. E., Carter, D., Hudson, M. J., Marzke, R. O., Mouhcine, M., Eftekharzadeh, S., James, P., Khosroshahi, H., Kourkchi, E., & Karick, A. 2010, MNRAS, 408, 1417

Smoot, G., Bennett, C., Kogut, A., Wright, E., Aymon, J., Boggess, N., Cheng, E., de Amici, G., Gulkis, S., Hauser, M., & et al. 1992, ApJ, 396, L1

Sobral, D., Best, P. N., Smail, I., Geach, J. E., Cirasuolo, M., Garn, T., & Dalton, G. B. 2011, MNRAS, 411, 675

Somerville, R. S., Hopkins, P. F., Cox, T. J., Robertson, B. E., & Hernquist, L. 2008, MNRAS, 391, 481

Sparke, L. S. & Sellwood, J. A. 1987, MNRAS, 225, 653

Spitzer, Jr., L. 1958, ApJ, 127, 17

Springel, V. & Hernquist, L. 2005, ApJ, 622, L9

Stinson, G., Seth, A., Katz, N., Wadsley, J., Governato, F., & Quinn, T. 2006, MNRAS, 373, 1074

Strateva, I., Ivezić, Ž., Knapp, G. R., Narayanan, V. K., Strauss, M. A., Gunn, J. E., Lupton, R. H., Schlegel, D., Bahcall, N. A., Brinkmann, J., & et al. 2001, AJ, 122, 1861

Sun, M., Donahue, M., & Voit, G. M. 2007, ApJ, 671, 190

Tasca, L. A. M., Kneib, J.-P., Iovino, A., Le Fèvre, O., Kovač, K., Bolzonella, M., Lilly, S. J., Abraham, R. G., Cassata, P., Cucciati, O., & et al. 2009, A&A, 503, 379

Teyssier, R., Chapon, D., & Bournaud, F. 2010, ApJ, 720, L149

Tinsley, B. M. 1972, A&A, 20, 383

Toomre, A. 1977, in Evolution of Galaxies and Stellar Populations, ed. B. M. Tinsley & R. B. G. Larson, D. Campbell, 401

Toomre, A. & Toomre, J. 1972, ApJ, 178, 623

Toth, G. & Ostriker, J. P. 1992, ApJ, 389, 5

Tyler, K. D., Rieke, G. H., Wilman, D. J., McGee, S. L., Bower, R. G., Bai, L., Mulchaey, J. S., Parker, L. C., Shi, Y., & Pierini, D. 2011, ApJ, 738, 56

van der Wel, A., Bell, E. F., Holden, B. P., Skibba, R. A., & Rix, H.-W. 2010, ApJ, 714, 1779

Vollmer, B., Cayatte, V., Balkowski, C., & Duschl, W. J. 2001, ApJ, 561, 708

Vorontsov-Velyaminov, B. A. 1959, in Atlas and catalog of interacting galaxies (1959), 0

Vulcani, B., Poggianti, B. M., Aragón-Salamanca, A., Fasano, G., Rudnick, G., Valentinuzzi, T., Dressler, A., Bettoni, D., Cava, A., D'Onofrio, M., Fritz, J., Moretti, A., Omizzolo, A., & Varela, J. 2011, MNRAS, 412, 246

Vulcani, B., Poggianti, B. M., Finn, R. A., Rudnick, G., Desai, V., & Bamford, S. 2010, ApJ, 710, L1

Walcher, J., Groves, B., Budavári, T., & Dale, D. 2011, Ap&SS, 331, 1

Wall, J. V., Jackson, C. A., Shaver, P. A., Hook, I. M., & Kellermann, K. I. 2005, A&A, 434, 133

Wetzel, A. R., Tinker, J. L., & Conroy, C. 2012, MNRAS, 424, 232

White, S. D. M. & Frenk, C. S. 1991, ApJ, 379, 52

White, S. D. M. & Rees, M. J. 1978, MNRAS, 183, 341

Wilman, D. J., Balogh, M. L., Bower, R. G., Mulchaey, J. S., Oemler, A., Carlberg, R. G., Eke, V. R., Lewis, I., Morris, S. L., & Whitaker, R. J. 2005a, MNRAS, 358, 88

Wilman, D. J., Balogh, M. L., Bower, R. G., Mulchaey, J. S., Oemler, A., Carlberg, R. G., Morris, S. L., & Whitaker, R. J. 2005b, MNRAS, 358, 71

Wilman, D. J. & Erwin, P. 2012, ApJ, 746, 160

Wilman, D. J., Fontanot, F., De Lucia, G., Erwin, P., & Monaco, P. 2013, ArXiv e-prints

Wilman, D. J., Oemler, Jr., A., Mulchaey, J. S., McGee, S. L., Balogh, M. L., & Bower, R. G. 2009, ApJ, 692, 298

Wing, J. D. & Blanton, E. L. 2011, AJ, 141, 88

Wolf, C., Aragón-Salamanca, A., Balogh, M., Barden, M., Bell, E. F., Gray, M. E., Peng, C. Y., Bacon, D., Barazza, F. D., Böhm, A., & et al. 2009, MNRAS, 393, 1302

Woo, J., Dekel, A., Faber, S. M., Noeske, K., Koo, D. C., Gerke, B. F., Cooper, M. C., Salim, S., Dutton, A. A., Newman, J., & et al. 2013, MNRAS, 428, 3306

Yang, X., Mo, H. J., van den Bosch, F. C., Pasquali, A., Li, C., & Barden, M. 2007, ApJ, 671, 153

Yang, Y., Zabludoff, A. I., Zaritsky, D., Lauer, T. R., & Mihos, J. C. 2004, ApJ, 607, 258

Yang, Y., Zabludoff, A. I., Zaritsky, D., & Mihos, J. C. 2008, ApJ, 688, 945

Zabludoff, A. I., Zaritsky, D., Lin, H., Tucker, D., Hashimoto, Y., Shectman, S. A., Oemler, A., & Kirshner, R. P. 1996, ApJ, 466, 104

Zwicky, F. 1937, ApJ, 86, 217

—. 1956, Ergebnisse der exakten Naturwissenschaften, 29, 344

Chapter 2

Galaxy Evolution in the Group Environment

Although the 'nature versus nurture' debate emerged from trends observed in the rich cluster environment ($M_{\rm halo} \gtrsim 10^{14} M_{\odot}$), it now appears that the lower-mass group environment ($10^{12.5} \lesssim M_{\rm halo} \lesssim 10^{14} M_{\odot}$) may be equally, and possibly even more, important in shaping the observed properties of galaxies. The importance of the group environment arises from the following observational and theoretical results:

- Galaxy groups are the most common environment in the local Universe (Geller & Huchra, 1983; Eke et al., 2004, 2005; Berlind et al., 2006; Knobel et al., 2009), and the fraction of galaxies in groups has tripled since $z \sim 1$ (Knobel et al., 2009);

- Environmental effects on galaxy evolution have been observed even in poor or low-mass groups, where, for example, groups have a higher fraction of galaxies with high D4000 values with respect to the field (Blanton & Moustakas, 2009);

- SAMs indicate that anywhere between $\sim 25-45\%$ of galaxies in present-day simulated clusters fell in as members of a group with $M_{\rm halo} \geq 10^{13} M_{\odot}$, which suggests that 'pre-processing', that is galaxies that have had their star formation quenched in the group environment, may be significant (McGee et al., 2009; De Lucia et al., 2012);

- Results from SAMs suggest that the timescale for star formation quenching is on the order of a few Gyrs (McGee et al., 2009; De Lucia et al., 2012) pointing to a slow transformation process, such as strangulation, which is most efficient in the group environment;
- Galaxy-galaxy interactions and mergers are currently the only transformation mechanism known that can explain the formation of classical ellipticals and this process is thought to be most efficient in galaxy groups (Barnes, 1985; Zabludoff & Mulchaey, 1998b; Brough et al., 2006).

Therefore, in order to better understand the role of the environment in the evolution of galaxies, it is important to study the intermediate density environment of groups. In particular, correlations between group dynamical state and member galaxy properties can probe the importance of gravitational interactions in both morphological transformations and star formation quenching.

2.1 The Group Environment

Galaxy groups represent an intermediate environment between isolated field galaxies and massive galaxy clusters. The group environment itself can be subdivided into two categories, loose and compact groups.

2.1.1 Loose Groups

Most references to 'groups', including those presented in this thesis, almost exclusively refer to studies of loose groups of galaxies, as opposed to compact groups. There is no one set definition for a loose galaxy group, in part because group membership is typically defined by the parameters of the group-finding algorithm (to be discussed in more detail in the following section). The same is also true of richer galaxy clusters, although the discrepancy between different cluster-finding techniques is not as significant, as the density contrast between a cluster and the field is much greater. Additionally, the properties of groups and their members, are much more varied than those of galaxy clusters. However, there are general criteria that loose groups follow. Broadly speaking, groups are typically defined as having:

- Between $3 \sim 50$ member galaxies, though the upper limit is somewhat arbitrary;
- Halo masses ranging from $\sim 10^{12.5} - 10^{14} M_{\odot}$ (Huchra & Geller, 1982; Mamon, 2007);
- Virial radii or r_{200}, defined as the radius at which the density is 200 times the critical overdensity, between $0.3 \sim 1$ Mpc (Mamon, 2007), and;
- Velocity dispersions between $\sim 100 - 450$ km s^{-1} (Mamon, 2007).

Additionally, some groups emit extended X-ray emission (e.g. Mulchaey & Zabludoff, 1998; Zabludoff & Mulchaey, 1998b; Osmond & Ponman, 2004; Connelly et al., 2012; Erfanianfar et al., 2013), with typical X-ray temperatures between 0.2 - 2 keV (Mamon, 2007), while others show no detectable X-ray emission. All of the work presented in this thesis focuses on the loose group subcategory of the group environment.

2.1.2 Compact Groups (CGs)

Unlike loose groups, there are specific criteria for what defines a CG. Following Hickson (1982), CGs, often referred to as Hickson compact groups (HCGs) are defined as having:

- More than four members ($N \geq 4$) within 3 mags of brightness of each other;
- The mean surface brightness of the member galaxies ($\overline{\mu}_G$ per arcsec squared), averaged over the smallest angular diameter than contains the geometric centres of all HCG member galaxies (Θ_G), must have $\overline{\mu}_G < 26$;
- The largest angular diameter (Θ_N) that contains no other external galaxy must have $\Theta_N \geq 3\Theta_G$.

The first criteria ensures that the system is not composed of a single bright galaxy surrounded by many significantly smaller and less luminous satellite galaxies. The second criteria requires that the galaxies are in close proximity to one another (i.e. compact), typically having mean intergalactic separations

similar to the scale of the galaxies themselves. The final criterion ensures that the system is isolated, which excludes clusters from the sample.

Recently, McConnachie et al. (2009) identified 2297 CGs, down to a limiting magnitude of $r = 18$, in the SDSS-DR6 sample with the aforementioned HCG criteria. Their sample contained CGs with as many as 10 members, velocity dispersions between $\sim 50 - 400$ km s^{-1}, maximum group radial extent $\lesssim 200$ kpc and typical intergalactic separations between 50-100 kpc.

The size of the member galaxies and the compactness of CGs provide the ideal environment for galaxy-galaxy interactions and mergers, even more so than in loose groups. Most CG galaxies show signs of interactions and have morphological or kinematic distortions, starburst or PSB galaxies and/or AGN activity (Hickson, 1997, and references therein). Figure 2.1 is an image of the first CG discovered, referred to as Stephen's Quintet. This CG contains five member galaxies that show signs of interactions, such as disrupted spiral features and bright star forming regions.

CGs have been also observed to be associated or embedded in loose groups (Ramella et al., 1994), and it has been suggested HCGs form from the collapse of loose groups (Mamon, 1987; Diaferio et al., 1994; Ramella et al., 1994). Thus, loose groups provide a continuous source for the formation of CGs, which provides an explanation for how these systems can be observed in such abundance despite the fact that strong gravitational interaction should render CGs relatively short-lived (Diaferio et al., 1994).

Figure 2.1: An image of Stephen's Quintet, which includes five interacting CG galaxies. Image credits: X-ray- NASA/CXC/CfA/E and optical- Canada-France-Hawaii-Telescope/Coelum

2.2 Defining a group sample

Unlike galaxy clusters, groups are not as massive, do not always have evolved stellar populations or have pronounced density contrast over the background. Therefore, techniques typically used to identify clusters are not able to detect the full range of group systems, and tend to only identify rich, massive and typically dynamically relaxed galaxy groups. In order to study groups that may still be in the process of assembling (i.e. dynamically young), different methods must be employed. The ability to detect both poor and rich groups, that span a wide range of dynamical states, is particularly important for the work presented in this thesis, as one of the main goals is to investigate the role of group dynamics in galaxy evolution. In the following, I will describe the most commonly used group-finding algorithms, as well as their limitations.

2.2.1 Extended X-ray Emission

As previously discussed in Section 1.4, as gas falls onto the group potential it gets shock heated to the virial temperature of the host halo. If the IGM is hot enough, roughly $10^7 - 10^8$ K, then the gas will produce extended X-ray emission due to thermal bremsstrahlung radiation. However, obtaining such high gas temperatures requires a large velocity dispersion ($\sim$ 1000 km s^{-1}), and therefore mass (Equation 1.7). Thus, surveys that search for extended X-ray emission tend to identify massive groups, which are on average more evolved and dynamically relaxed.

An additional obstacle in employing this method to identify groups is that the X-ray emission from groups is not as bright as in more massive clusters, with $L_{\rm x,\ group} \sim 10^{41} - 10^{42}$erg s^{-1} compared to $L_{\rm x,\ cluster} \sim 10^{43} - 10^{45}$erg s^{-1}. The fainter X-ray luminosities not only render groups more difficult to observe in general, especially at higher redshifts, but also make it difficult to determine if the emission is from the group or an individual galaxy, which can also produce extended X-ray emission of comparable brightness ($L_{\rm x,\ galaxy} \sim 10^{38} - 10^{42}$erg s^{-1}). In some cases, X-ray groups exhibit a two-component surface brightness profile (SBP) with a broad central peak corresponding to either the brightest or most massive group galaxy and an extended component corresponding to the group emission (Mulchaey & Zabludoff, 1998). However, it is not always possible to fit a two-component SBP, especially if there are insufficient statistics (i.e. low X-ray counts). Fortunately, Osmond & Ponman (2004) found that they could still identify groups from a single-component SBP fit, if they applied a minimum threshold for the radial extent of the group emission, such that $r_{\rm ext,\ group} > 60$ kpc.

Furthermore, since X-ray emission can only be observed from space-based observatories, it can be quite costly to obtain large-scale, blind surveys with sufficient depth to detect galaxy groups. Only recently has it been possible to acquire unbiased catalogues with as many as $\sim 40 - 60$ X-ray selected groups (Osmond & Ponman, 2004; Connelly et al., 2012; Erfanianfar et al., 2013).

While this method of detecting groups has its disadvantages, X-ray selected catalogues are necessary to gain a complete understanding of the group environment. In particular, it is important to understand why some groups

are X-ray bright, while others are X-ray faint. In a study comparing optically-selected (X-ray faint) and X-ray selected (X-ray bright) groups, Connelly et al. (2012) showed that both samples covered a similar range in velocity dispersion, indicating that mass or the depth of the potential well alone is not the factor that separates X-ray bright and faint systems. Clearly, more work needs to be done to understand what drives X-ray emission in the IGM.

2.2.2 Gravitational Lensing

A consequence of Einstein's theory of General Relativity is that matter bends or warps space-time (Einstein, 1915). Since light travels along geodesics, which are locally the shortest path between two points, these space-time distortions cause light to appear to bend near massive objects, such as galaxy clusters or black holes. The distorted distribution of light from a background galaxy can manifest itself in two ways: strong and weak gravitational lensing.

In strong lensing the light from a background source is highly distorted and split into multiple images. Einstein rings occur when the source, lens and observer are aligned and if the lens is symmetrical. For a point source, the size of the ring (in radians) is given by

$$\Theta_E = \sqrt{\frac{4GMd_{LS}}{c^2 d_L d_S}}, \tag{2.1}$$

where G is the gravitational constant, M is the mass of the lens, d_{LS} is the angular diameter distance between the lens and the source, d_L is the angular diameter distance between the observer and the lens and d_S is the angular diameter distance between the observer and the source.

If the alignment is not perfect or the lens is not symmetrical, then a background source is mapped into multiple images on the sky. The radius at which the arc is observed can be expressed approximately by Equation 2.1. Thus, if the angle of deflection of an arc ($\sim \Theta_E$) and the distances to the lens and sources (i.e. d_{LS}, d_L and d_S) are known, then it is possible to reconstruct the mass distribution of the lens. Though, in reality this process is much more difficult to carry out and involves sophisticated ray-tracing techniques to re-create the lensed image. However, strong lensing does provide vital information

about dark matter, which dominates the lens mass distribution.

Observationally, perfect Einstein rings (both complete and partial) are very rare. On the other hand, arcs, which do not require a symmetrical lens mass distribution, are much more common. In fact, strong lensing arcs have been used to identify galaxy clusters in photometric surveys (e.g. Cabanac et al., 2007; Postman et al., 2012; Furlanetto et al., 2013). Strong lensing typically identifies rich galaxy clusters, as more massive systems are more likely to produce visible arcs; however, it is possible to detect lower-mass groups using this technique. Additionally, since group-sized haloes are more common than cluster-sized haloes, there should theoretically be a relatively high probability of finding group-scale lenses (More et al., 2012). Recently, the Canada-France-Hawaii Telescope Legacy Survey (CFHTLS) Strong Lensing Legacy Survey (SL2S) detected strong lenses from galaxy groups with typical halo masses of $10^{13}h^{-1}M_{\odot}$ (Cabanac et al., 2007). The group-scale lenses of CFHTSLS-SL2S were presented in Limousin et al. (2009), which included 13 strong lensing systems with Einstein radii consistent with group-sized dark matter haloes ($\sim 3-8''$) and in More et al. (2012), which included 54 good group-scale lens candidates in the Strong Lensing Legacy Survey-ARCS (SARCS) sample.

Gravitationally-distorted light from a source object can also manifest in the form of weak lensing, where the image of a background galaxy can be magnified and/or stretched tangentially with respect to the lensing mass (Kristian, 1967; Brainerd et al., 1996). Observationally, it is extremely difficult to detect magnification; though it is possible with large scale surveys such as SDSS (e.g. Scranton et al., 2005; Ménard et al., 2010). A shear can also be difficult to detect, in particular because galaxies themselves are elliptical in shape; however, since the shear is tangential to lensing mass, it is possible to obtain a weak lensing signal by analyzing the shapes of galaxies in a large statistical sample. The tangential component of the measured shear vector is directly proportional to the lens mass distribution, providing another probe of the dark matter distribution of the lensing object. However, it should be noted that source galaxies can be weakly lensed by any mass distribution along the LOS. Therefore, projection effects may result in a false detection of a group-scale weak-lensing signal.

While individual galaxy clusters have been discovered via weak-lensing

(Wittman et al., 2001, 2003; Gavazzi & Soucail, 2007; Abate et al., 2009), extending this methodology down to group-scales is challenging. In general, weak-lensing signals from groups can only be detected by stacking groups (Hoekstra et al., 2001; Parker et al., 2005), which provides information about the average group properties and not individual systems. However, Limousin et al. (2009) recently presented weak-lensing masses for 13 galaxy groups which are in good agreement with masses measured from photometric catalogues (Coupon et al., 2009). So while weak-lensing can be used to study a population of previously determined groups, it cannot be used to blindly search for new group systems, as the signal is just too weak.

2.2.3 The Sunyaev-Zel'dovich Effect

The Sunyaev-Zel'dovich (SZ) Effect is the result of interactions between photons from the CMB and high-energy electrons, where the photons gain energy from the electrons via inverse-Compton scattering (Sunyaev & Zeldovich, 1972). The thermal SZ effect refers to interactions between photons and high-energy electrons in the hot gas in group and clusters; while, the kinetic SZ effect, or alternatively the Ostriker-Vishniac Effect (Ostriker & Vishniac, 1986), refers to interactions with electrons that gain their high energies due to their bulk motion. Astrophysical observations, at least the ones discussed here, are almost exclusively a result of the thermal SZ effect.

The increase in energy from the SZ effect results in an overall shift of the CMB spectrum to higher frequencies. Observationally, this results in a decrease in the intensity of the CMB at frequencies $\lesssim 218$ GHz and an increase in the intensity at frequencies $\gtrsim 218$ GHz. At low frequencies, Sunyaev & Zeldovich (1972) showed that the change in temperature due to inverse-Compton scattering is given by

$$\frac{\Delta T_{\rm CMB}}{T_{\rm CMB}} = -2\frac{k_B T_e}{m_e c^2}\sigma_T N_e l, \tag{2.2}$$

where T_{CMB} is the temperature of the CMB, k_B is the Boltzmann constant, T_e is the temperature of the electron, $m_e c^2$ is the rest mass energy of the electron, σ_T is the Thomson scattering cross-section, N_e is the number density of electrons and l is the LOS dimension of the source in units of inverse volume.

Sunyaev & Zeldovich (1972) showed that for a cluster with $T_e \sim 7 \times 10^7$ K, $N_e \sim 10^{-3}\text{cm}^{-3}$ and $l \sim 10^{25}\text{cm}^{-3}$, the temperature variations due to inverse-Compton scattering were on the order of $\Delta T_{\text{CMB}}/T_{\text{CMB}} \sim 2 \times 10^{-4}$. While this is a small deviation in temperature, it is detectable with modern submillimeter and millimeter telescopes, such as the South Pole Telescope (SPT) or the Atacama Cosmology Telescope (ACT). From Equation 2.2, it is clear that higher electron densities and temperatures will result in larger temperature variations. These conditions are normally met in more massive galaxy clusters with $M_{\text{halo}} \gtrsim 10^{14} M_\odot$. There are currently several ongoing SZ-cluster surveys, including a catalogue of 224 cluster candidates observed with SPT (Reichardt et al., 2013) and a catalogue of 68 spectroscopically confirmed clusters observed with ACT (Menanteau et al., 2013). For both catalogues, the cluster masses are typically greater than $5 \times 10^{14} M_\odot$ and contains clusters with redshifts as high as $z \sim 1.3$. While it is theoretically possible to detect lower-mass galaxy groups in SZ surveys, the predicted temperature variation is even smaller assuming lower IGM temperatures and densities (Equation 2.2). Additionally, Holder et al. (2007) found that the confusion limit between the SZ background, which is the superposition of numerous weak SZ signals from unresolved clusters spanning a range of masses along the LOS, and a true SZ cluster signal occurs at $\sim 10^{14} h^{-1} M_\odot$, which is the approximate mass boundary between groups and clusters. Thus, it may only be possible to detect massive groups with this technique.

There are several advantages to employing the SZ effect to search for massive groups and clusters. In particular, the SZ effect is redshift independent, as shown in Equation 2.2, and can therefore detect systems at (theoretically) any redshift with equal probability. Thus, the SZ effect is likely the best method to detect high-redshift clusters. Additionally, it provides an independent measure of the properties of hot gas in the ICM, and in conjunction with X-ray observations can provide vital information about the ICM.

2.2.4 Photometric Surveys

The strong morphology- and colour-density relations observed in rich galaxy clusters, with red early-type galaxies preferentially found in the dense cluster

environment, provides a method of detecting clusters based on photometric data alone. First proposed by Gladders & Yee (2000), these authors developed a cluster-finding algorithm that makes use of the fact that all rich clusters appear to have a large, coeval population of passively-evolving elliptical galaxies that formed at high redshifts. As discussed in Chapter 1, red galaxies form a tight sequence with relatively little scatter on a CMD, often referred to as the red sequence. Gladders & Yee (2000) showed that with the appropriate filters, the red sequence cluster galaxies would have redder observed colours than non-cluster galaxies at lower redshifts. Therefore, cluster members could be identified with a simple cut in a CMD with extremely low contamination, that is false positive rates $< 5\%$ where the false positive rate is the fraction of systems falsely identified as clusters (Gladders & Yee, 2005). Since the cluster red sequence (CRS) method only relies on the presence of a dominant red sequence, it is possible to detect both low- and high-redshift clusters. With this methodology Gladders & Yee (2005) have identified 429 group and cluster candidates, including 67 cluster candidates in the redshift range of $0.9 < z < 1.4$ in the Red sequence Cluster Survey (RCS). The follow-up survey to RCS, RCS2 contains between $\sim$20 000 - 30 000 group and cluster candidates in the redshift range of $0.1 < z < 1$ (Gilbank et al., 2011). Muzzin et al. (2009) have also used the CRS method to identify two spectroscopically-confirmed $z \sim 1.2$ clusters in the Spitzer Adaptation of the Red sequence Clusters Survey (SpARCS).

Although Gladders & Yee (2000) claim that the CRS method can detect group-sized systems with $\sigma \sim 300\text{km s}^{-1}$, it is likely that only concentrated groups with a high fraction of bright red elliptical galaxies can be identified with this methodology. Additionally, while the false-positive rate for the CRS method is low, the false-negative rate (i.e. the rate that a true group or cluster member is *not* identified) may not be. Since the galaxy population of groups is more varied than in clusters, it is likely that the CRS method will either miss a significant fraction of faint and/or blue group members or only identify old, concentrated and dynamically evolved systems. Both scenarios would lead to a biased view of the role of the group environment in galaxy evolution.

While the CRS method is arguably the most commonly used photometric group- and cluster-finding algorithm, there are other algorithms that only require photometric data, including the 3D-Matched-Filter (3D-MF) galaxy

cluster finder (Milkeraitis et al., 2010). The 3D-MF algorithm uses galaxy cluster radial profiles, luminosity functions and photometric redshifts to detect clusters in photometric surveys. For a given luminosity function and cluster radial distribution, the 3D-MF algorithm searches within a single wavelength band and photo-z redshift slice for regions that 'maximally and simultaneously' match both the luminosity function and radial distribution, essentially 'filtering' out clusters. Likelihood values are then computed for each candidate cluster and systems above some threshold value are then identified as clusters. Based on performance tests with simulated mock catalogues, Milkeraitis et al. (2010) found that for clusters with $M_{200} \geq 3 \times 10^{14} M_{\odot}$ the 3D-MF algorithm has 100% completeness, which is defined as the fraction of true group members identified by the algorithm. However, for groups sized haloes ($M_{200} \sim 10^{13} M_{\odot}$) the completeness drops significantly to 72% and the false detection rate is also quite high at 24%. Thus, the 3D-MF algorithm is not a reliable *group*-finding technique.

It should be noted that there is another group-finding algorithm that uses only photometric data (i.e. the probability friends-of-friends algorithm); however, it is based on the same principles as the spectroscopic friends-of-friends group-finding algorithm, so I will discuss this technique in the following section.

2.2.5 Spectroscopic Surveys

Although all of the aforementioned methods can identify group-sized haloes, most of them are technically cluster-finding algorithms and as a result typically only detect old, massive and/or dynamically relaxed galaxy groups. Additionally, since the galaxy overdensity, with respect to the background, is much lower for groups, reliable group membership cannot be assigned with photometric data alone, at least not without significant contamination from interloping background or foreground galaxies (i.e. low purity). In order to maximize the purity of an identified group, *group*-finding algorithms require velocity information to ensure that the galaxies are also associated along the LOS.

The necessity to have costly spectroscopic redshifts to accurately assign

group membership is part of the reason why, historically, the group environment has not been as actively investigated as individual galaxies or rich clusters. However, recent large-scale spectroscopic surveys have made it possible to study statistical samples of galaxy groups. The most notable of these surveys is the SDSS (York et al., 2000), which with the seventh data release (DR7) has an imaging footprint of 11 663 square degrees, a spectroscopic footprint of 9380 square degrees of the sky and obtained a total of 1 640 960 spectra (Abazajian et al., 2009). Other examples of large spectroscopic surveys include: the Two-degree-Field Galaxy Redshift Survey (2dFGRS: Colless et al., 2001), the second Canadian Network for Observational Cosmology Galaxy Redshift Survey (CNOC2: Yee et al., 2000), the Deep Evolutionary Exploratory Probe 2 Galaxy Redshift Survey (DEEP2: Gerke et al., 2005, 2012) and the spectroscopic follow-up of the Cosmic Evolution Survey (zCOSMOS: Lilly et al., 2007). Numerous galaxy group and cluster catalogues have been identified from these surveys and in the following I will discuss some of the current group-finding algorithms.

2.2.5.1 The Friends-of-Friends (FoF) group-finding algorithm

The FoF group-finding algorithm is one of the most commonly used methods of identifying groups and clusters, in both redshift surveys and in N-body simulations. First developed by Huchra & Geller (1982), the FoF algorithm searches for groups, which they defined as '...an association of galaxies which are likely to be physically (and dynamically) associated: more precisely, they are density enhancements in redshift space', by linking together galaxies that are close in projection on the sky and also along the LOS. For each galaxy in the catalogue, not already assigned to a group, the FoF algorithm calculates the distance to neighbouring galaxies, first in projected space on the sky and then in redshift space, and links the galaxies together as 'friends' if the projected distance between them follows

$$D_{12} = \frac{2\sin(\theta/2)\,V}{H_0} \leq D_L(V_1, V_2, m_1, m_2), \tag{2.3}$$

where $V = (V_1 + V_2)/2$, V_1 and V_2 are the redshifts of the initial galaxy and its friend, m_1 and m_2 are their magnitudes, θ is their angular separations, and

D_L is the spatial linking-length parameter. Additionally, the LOS velocities between the two galaxies must follow

$$V_{12} = |V_1 - V_2| \leq V_L(V_1, V_2, m_1, m_2), \tag{2.4}$$

where V_L is the redshift linking-length parameter. The algorithm repeats this process for each neighbouring galaxy until no more 'friends' can be added to the group.

From Equations 2.3 and 2.4, it is clear that assigning group membership is entirely dependent on the linking lengths, D_L and V_L. As these values are free parameters, the type of groups identified can vary widely between different catalogues. With short linking lengths the FoF algorithm typically identifies more compact groups that are likely already virialized. Catalogues from FoF algorithms with small linking lengths are limited in the available mass and dynamical range, which could potentially bias evolutionary studies. On the other hand, groups identified with large values of D_L and V_L tend to have a high fraction of interloping field and neighbouring group galaxies, which again could affect studies of environmental effects on galaxy evolution.

There are methods of determining so-called 'optimal linking lengths' by testing the FoF algorithm on mock catalogues generated from N-body simulations in which true group membership is already known. However, even with an 'optimized' FoF group-finder, membership can differ significantly between group catalogues derived from the same data set. For example, multiple groups defined in Berlind et al. (2006) can be identified as a single group in Yang et al. (2007), or vice versa, even though both catalogues were defined based on the same SDSS sample. The reason for this likely lies in the fact that what is being 'optimized' differs between authors, with some aiming for low contamination (i.e. purity) and others aiming to recover 100% membership within the same dark matter halo (i.e. completeness). In fact in their abstract Berlind et al. (2006) state

> *Extensive tests with these mock catalogues show that no combination of perpendicular and line-of-sight linking lengths is able to yield groups and clusters that simultaneously recover the true halo multiplicity function, projected size distribution, and velocity*

dispersion.

Since there is no universal value for the FoF linking lengths, it is extremely important to understand how a particular value may affect the types of groups selected, especially when comparing groups from different catalogues.

In recent years, there has been an adaptation to the FoF algorithm where photometric redshifts are used in place of spectroscopic ones and is referred to as the probability-FoF algorithm (pFoF: Li & Yee, 2008; Liu et al., 2008; Jian et al., 2013). While the precise algorithm and selection parameters for the Li & Yee (2008) and Liu et al. (2008) pFoF group-finders may differ, the underlying methodologies are similar in that groups are defined using photometric data alone. Although, it should be noted that the Liu et al. (2008) pFOF algorithm does utilize spectroscopically-determined groups as a training set to optimize the group-finder.

The success of the pFoF algorithm is almost entirely dependent on the error associated with photometric redshifts, which are typically 50-100 times larger than spectroscopic redshift errors. A direct consequence of this increase in redshift uncertainly is an increase in the percentage of contamination from foreground and background interloping galaxies. In a performance study of the pFoF group-finder, Jian et al. (2013) found that the purity of a group, which they define as the fraction of pFoF members that are true group members in an N-body simulation, ranges between $\sim 40 - 65\%$ depending on the redshift uncertainty. While this recovery rate is much lower than with a spectroscopic FoF group-finder, improvements in photometric redshift determination will undoubtedly increase the accuracy of the pFOF algorithm. Additionally, it is advantageous to further test and develop group-finding methods that only require photometric data as they can be applied to much wider and deeper surveys. In particular, large scale photometric surveys, such as the Panoramic Survey Telescope and Rapid Response System (Pan-STARRS: Kaiser et al., 2002) and the Dark Energy Survey (DES: Flaugher, 2005) may not have complementary spectroscopic data, at least not with sufficient completeness, and therefore algorithms like pFoF will be necessary to study the group environment.

2.2.5.2 The halo-based group-finding algorithm

The main goal of the halo-based group-finding algorithm, developed by Yang et al. (2005), is to identify groups of galaxies that share the same host dark matter halo in order to better compare observed results with theoretical predictions. While this is likely the goal of all group-finding algorithms, Yang et al. (2005) claim that most algorithms define groups as a local overdensity of galaxies that do not necessarily have to share a common dark matter halo. Since the distribution of dark matter haloes is not directly observable, Yang et al. (2005) use the results of N-body simulations and SAMs to relate the properties of the dark matter distribution to the expected galaxy distribution to design their group-finder.

The halo-based group-finder, as presented in Yang et al. (2005), consists of five steps which can be applied to any galaxy redshift survey. The initial step is to identify a potential group and group center with a traditional FoF algorithm. As the main goal of this step is to identify a group center, the projected (D_L) and LOS (V_L) linking lengths are chosen to be very short. The geometric center is then taken to be the group centroid. The second step of the algorithm is to estimate the total luminosity of the group ($L_{\rm total}$) from the summed luminosity of all the potential group members, corrected for spectroscopic incompleteness and 'missed' galaxies resulting from the magnitude limit of the survey. Next, the halo mass is estimated from $L_{\rm total}$ and a model for the mass-to-light ratio. The virial radius, virial velocity and LOS velocity dispersion are then computed from the halo mass. The fourth step involves assigning group membership, where galaxies are added and removed as group members based on the mass, size and velocity dispersion computed in step three, and assuming that the projected galaxy distribution follows an Navarro-Frenk & White (NFW) dark matter distribution (Navarro et al., 1996) and a LOS Gaussian distribution. The final step involves re-computing the group centroid and then going back to step 2. The algorithm continues iteratively until no further members can be added to the group.

Testing this algorithm on mock catalogues, (Yang et al., 2005) found that on average the halo-based group-finder had a completeness of $\sim 90\%$, where the completeness is defined as the percentage of true host halo member galaxies

recovered with the algorithm, and a contamination between $0 - 50\%$ from interloping galaxies for haloes between $\sim 10^{12} - 10^{15} M_{\odot}$. Also, in contrast with many of the aforementioned group-finding techniques, the halo-based algorithm appears to better detect group-, rather than cluster-, sized haloes in volume-limited surveys, as groups tend to have higher completeness values (Yang et al., 2005).

Thus far, the halo-based group finder has been applied to 2dFGRS (Yang et al., 2005) and SDSS (Yang et al., 2007) and the group catalogues have been made publicly available. Numerous works, including the final paper presented in this thesis, have made use of the Yang group catalogues to investigate various aspects of the group environment. The wide-spread use of the same catalogue allows for fair comparison of results from different studies.

2.2.5.3 The Voronoi-Delaunay Method (VDM)

The application of the Voronoi-Delaunay Method (VDM) to detect overdensities in redshift-space was first presented in Marinoni et al. (2002). Unlike the FoF or halo-based group finders, the Voronoi-Delaunay Method (VDM) is a geometric and nonparametric method that makes use of Voronoi diagrams and its complementary Delaunay triangulation to identify groups and clusters. A Voronoi diagram divides the data into regions, referred to as Voronoi cells, where the size of each cell depends on the local density of nearest neighbours. Large cells correspond to low-density regions, such as isolated galaxies or voids, and small cells represent high-density regions, such as groups or clusters. The mean galaxy density is then computed by taking the number of galaxies within each cell divided by the volume of the cell. The centres of the Voronoi cells are joined together by the Delaunay complexes, which are triangular in shape. The Delaunay complexes provide information about the distances to neighbouring cells, where high density regions will be connected by Delaunay complexes with small areas, while voids will be connected to neighbouring cells with Delaunay complexes that have large areas.

Once the VDM is applied to a redshift catalogue, groups and clusters are found by identifying peaks in the galaxy density field, which is done by sorting all of the galaxies in the catalogue by their inverse Voronoi cell volume. As previously stated, the smallest cells correspond to the densest regions and

these are identified as potential group 'seeds'. Each group seed is then linked to its nearest neighbours via the Delaunay complexes. Galaxies within some fixed distance ($R_{\rm min}$), typically $1h^{-1}$ Mpc, of the group seed are referred to as *first-order Delaunay neighbours* and are then used to compute the potential group's center of mass (CoM). To account for the peculiar velocities introduced by the group potential, which causes groups to appear elongated along the LOS, Marinoni et al. (2002) define a cylinder in redshift space centered on the potential groups CoM with radius $R_{\rm II} \geq R_{\rm min}$ and length $L_{\rm II} = 20h^{-1}$ Mpc along the LOS. All of the galaxies within this cylinder are referred to as *second-order Delaunay neighbours*.

Final group membership is then assigned based on the richness (N_{II}) of the potential groups, which is taken to be the sum of the *first-* and *second-order Delaunay neighbours*. From the group richness, a new cylindrical window with

$$R = max[rN_{\rm II}, R_{\rm II}], \tag{2.5}$$

$$L = max[vN_{\rm II}, L_{\rm min}], \tag{2.6}$$

where R is the radius of the cylinder, L is the length of the cylinder, r and v are coefficients that fix the scale of the cylinder and $L_{\rm min}$ is a minimum cutoff filter that takes into account redshift distortions due to peculiar velocities within the group potential. Galaxies are added as members if they fall within this cylinder and are connected via the Delaunay complexes. Thus, in contrast to the FoF algorithm, group membership via VDM is not assigned by linking 'friends' but rather by searching for members that fall within some window of the central group seed position.

With the VDM Gerke et al. (2012) has identified 1165 groups, with more than two members, in the Extended Groth Strip (EGS) spanning a redshift range of $0 < z < 1.5$ and 1295 in the rest of the DEEP2 fields with $z > 0.6$. Testing the VDM on mock catalogues made to mimic the DEEP2 survey, Gerke et al. (2005) found that $\sim 78\%$ of all real groups were identified with $\sim 72-79\%$ completeness and $\sim 46\%$ contamination from interloping galaxies. While the completeness rates for this group-finding algorithm are comparable to other methods, the contamination from interlopers is significantly higher than other algorithms that require redshift information and similar to the

pFoF group-finder, which only requires photometric data.

2.3 Environmental Trends in Galaxy Groups

Much of our knowledge regarding environmental effects on galaxy evolution comes from studies of rich and massive galaxy clusters, which typically have hundreds of member galaxies and halo masses $> 10^{14}\ M_{\odot}$. However, the cluster environment represents the extreme end of the galaxy density scale, and in order to get a more complete picture of the role of the environment in galaxy evolution, it is essential to examine group-sized haloes. The difficulty with studying this intermediate density regime is that current methods of defining group samples that span the full range of group properties (i.e. membership, halo mass, dynamical state and galaxy population) require spectroscopic redshifts. Thus, defining a group catalogue can be a costly endeavour. Fortunately, recent large-scale spectroscopic surveys, such as SDSS (York et al., 2000; Abazajian et al., 2003), have made it possible to study statistical samples of galaxy groups. With these surveys and the group finding algorithms described in Section 2.2.5, numerous authors have published group catalogues that span a wide range of redshifts and group properties. In Table 2.1, we list examples of well-studied group catalogues identified in spectroscopic surveys. These catalogues contain large samples of groups and clusters, allowing for in-depth studies of the environment.

Table 2.1: Examples of group catalogues.

Group Catalogue	Redshift Survey	Redshift Range	Number of Groups Identified	Halo Mass or Dispersion Range	Group Finding Algorithm
Eke et al. (2004)	2dFGRS-2PIGG	$0 < z < 0.3$	> 7000	$\sim 10^{11.5} - 10^{15.5} M_{\odot}$	FoF
Berlind et al. (2006)	SDSS	$0.01 \leq z \leq 0.2$	132	$\sim 200 - 1000$ km s^{-1}	FoF
Yang et al. (2007)	SDSS	$0.01 \leq z \leq 0.2$	> 5000	$10^{12.5} - 10^{15} M_{\odot}$	halo-based
Carlberg et al. (2001)	CNOC2	$0.1 < z < 0.6$	> 200	$\sim 50 - 1000$ km s^{-1}	FoF
Wilman et al. (2005)	GEEC	$0.3 < z < 0.55$	26	$\sim 100 - 800$ km s^{-1}	FoF
Knobel et al. (2009)	zCOSMOS	$0.1 \lesssim z \lesssim 1$	102	$\sim 10^{12.5} - 10^{14.5} M_{\odot}$	FoF
Gerke et al. (2012)	EGS	$0 < z < 1.5$	1165	$\sim 10 - 1000$ km s^{-1}	VDM
Gerke et al. (2012)	DEEP2	$0.6 < z < 1.4$	1295	$\sim 10 - 1000$ km s^{-1}	VDM

2.3.1 Group Scaling Relations

Studies of rich galaxy clusters have shown that many of the cluster properties follow scaling relations that describe how important physical properties of the cluster, such as mass, luminosity and richness ($n_{\rm members}$), correlate with one another. Examples of cluster scaling relations include: the $L_x - T_x$, the $L_x - \sigma$ and the σ - $n_{\rm members}$ relations. The parameters of most cluster scaling relations (e.g. L_x, T_x, σ, M_{200}) all probe the depth of the cluster potential. Since groups are essentially lower mass versions of clusters, one would expect the scaling relations to extend to the group regime. However, studies of scaling relations in the group environment have contradictory results. It is important to investigate and understand group scaling relations, as deviations from the cluster scaling relations can provide vital information about the physical differences between groups and clusters.

Theoretically, for a system in virial equilibrium, $L_x \propto \sigma^4$ (Navarro et al., 1995). Observations of the $L_x - \sigma$ relation in galaxy clusters are generally in good agreement with the theoretically predicted value, with power-law observed slopes of 4.29 ± 0.37 (Mulchaey & Zabludoff, 1998), $4.4^{+0.7}_{-0.3}$ (Mahdavi & Geller, 2001) and 3.7 ± 0.3 (Popesso et al., 2005). In the group regime, the $L_x - \sigma$ slope has been observed to either deviate from clusters, with observed values of 0.37 ± 0.3 (Mahdavi et al., 2000), 2.31 ± 0.12 (Xue & Wu, 2000) and 2.5 ± 0.4 (Osmond & Ponman, 2004), or follow the cluster scaling relation (Mulchaey & Zabludoff, 1998; Helsdon & Ponman, 2000; Rines & Diaferio, 2010). Theoretically, a shallower $L_x - \sigma$ slope is difficult to understand, as the most obvious scenarios (i.e. substructure or interloping galaxies) would result in an overestimation of the group velocity dispersion and therefore a steeper slope (Bird, 1994; Mahdavi et al., 2000; Rines & Diaferio, 2010). A possible explanation for the observed shallow $L_x - \sigma$ group slope, which is driven by systems with low velocity dispersions, is that for groups with $\sigma \lesssim 300$ km s^{-1} the velocity dispersion no longer appears to correlate with mass (Mahdavi et al., 2000). Therefore, the expected $L_x - \sigma$ relation cannot apply to these low dispersion systems as the relation between M and σ no longer holds.

Another commonly measured scaling relation is the $L_x - T_x$ relation. Since $L_x \propto \sigma^4$ and $T_x \propto \sigma^2$ (also as a result of the virial theorem), then $L_x \propto T_x^2$

(Navarro et al., 1995). Unlike the $L_x - \sigma$ relation, the observed slope of the cluster $L_x - T_x$ relation is steeper than theoretically predicted with an observed slope value of 2.64 ± 0.27 (Markevitch, 1998). Cavaliere et al. (1997) also found a steeper relation for clusters with $L_x \propto T_x^3$; however, for very hot clusters ($T_x \geq 8 \times 10^7 K$) the relation followed the expected slope of $L_x \propto T_x^2$. Similar to the $L_x - \sigma$ relation, there appears to be some debate regarding the $L_x - T_x$ relation in galaxy groups. Most studies find a steeper relation than observed in clusters with an average slope of ~ 5 (Cavaliere et al., 1997; Helsdon & Ponman, 2000; Xue & Wu, 2000). However, Osmond & Ponman (2004) observe a shallower slope of 2.75 ± 0.46 which is in agreement with the cluster relation. Osmond & Ponman (2004) suggested that differences in the measured $L_x - T_x$ slopes in groups resulted from differences in the group samples. In particular, these authors suggested that their group sample contained groups with a wider range of X-ray properties, including a larger sample of cool ($T_x < 0.7$ keV) systems, in comparison to the Helsdon & Ponman (2000) group sample, which only contained X-ray bright groups. However, given the results of Cavaliere et al. (1997), it is difficult to understand how cooler systems would result in a shallower slope.

Deviations from the expected scaling relations may also be due to the presence of dynamically young systems, as the derived scaling relations all assume that the systems are in dynamical equilibrium. In a study of X-ray- and optically-selected groups, Connelly et al. (2012) found that non-Gaussian groups and groups with significant substructure were often outliers in their best fit $L_x - \sigma$ relation. For illustration, I have included an adapted version of Figure 8 in Connelly et al. (2012), which shows the $L_x - \sigma$ relation for optically selected groups (Figure 2.2). For our purposes, the important features of Figure 2.2 are the black line and shaded region, which indicate the best fitting $L_x - \sigma$ relation for these data, and the filled diamonds and squares, which indicate non-Gaussian groups and groups with substructure. The majority of the dynamically complex systems in Figure 2.2 are outliers; though there appears to be no systematic offset. In a more recent study of X-ray groups, Erfanianfar et al. (2013) also found that groups with substructure were extreme outliers in the $L_x - \sigma$ relation, having significantly higher values of σ than expected. Thus, dynamical studies in both groups and clusters can provide vital informa-

tion about systems that both follow and stray from the theoretically expected scaling relations.

2.3.2 The Properties of Group Galaxies

As discussed in Chapter 1, galaxy-galaxy interactions and mergers, as well as strangulation are the most efficient galaxy transformation processes in the group environment. Therefore, similar to the more massive cluster environment, the main effect of the group environment is to quench star formation. In the local Universe ($z \sim 0$), group galaxies show a higher quiescent fraction than observed in the field, though lower than found in rich clusters (Kimm et al., 2009; McGee et al., 2011; Peng et al., 2012; Wetzel et al., 2012; Woo et al., 2013). Similar results have been observed when star formation is probed via the fraction of red galaxies (Kimm et al., 2009). Enhanced quenching in groups, with respect to the field, has also been observed at higher redshifts, out to $z \sim 1$ (Gerke et al., 2005; Iovino et al., 2010; George et al., 2011; McGee et al., 2011; Presotto et al., 2012; Mok et al., 2013).

As discussed in Section 1.3.1, the colour distribution of group and cluster galaxies is often observed to be bimodal, separating red and blue galaxies, in all environments and in a wide range of redshifts ($0 < z \lesssim 1$). While there are galaxies that reside in the 'green valley', that is galaxies with intermediate colours between the blue cloud and red sequence galaxies (e.g. Martin et al., 2007), the fraction of the green valley population is typically quite low. However, in a high-redshift group sample Balogh et al. (2011) recently showed that $\sim 30\%$ of group members were in the green valley. If green valley galaxies are a transient population between the blue cloud and red sequence then the number of galaxies in this population can tell us about the timescale of star formation quenching in groups.

In addition to colour and SFRs, the morphological composition of group galaxies has also provided vital insight about galaxy evolution. The MDR observed in clusters has also been shown to extend down to group-sized haloes to at least $z \sim 1$ (Postman & Geller, 1984; Ramella et al., 1999; Capak et al., 2007; Kovač et al., 2010). However, unlike the quiescent or red fractions, the the relative fractions of elliptical, S0 and late-type galaxies do not appear to

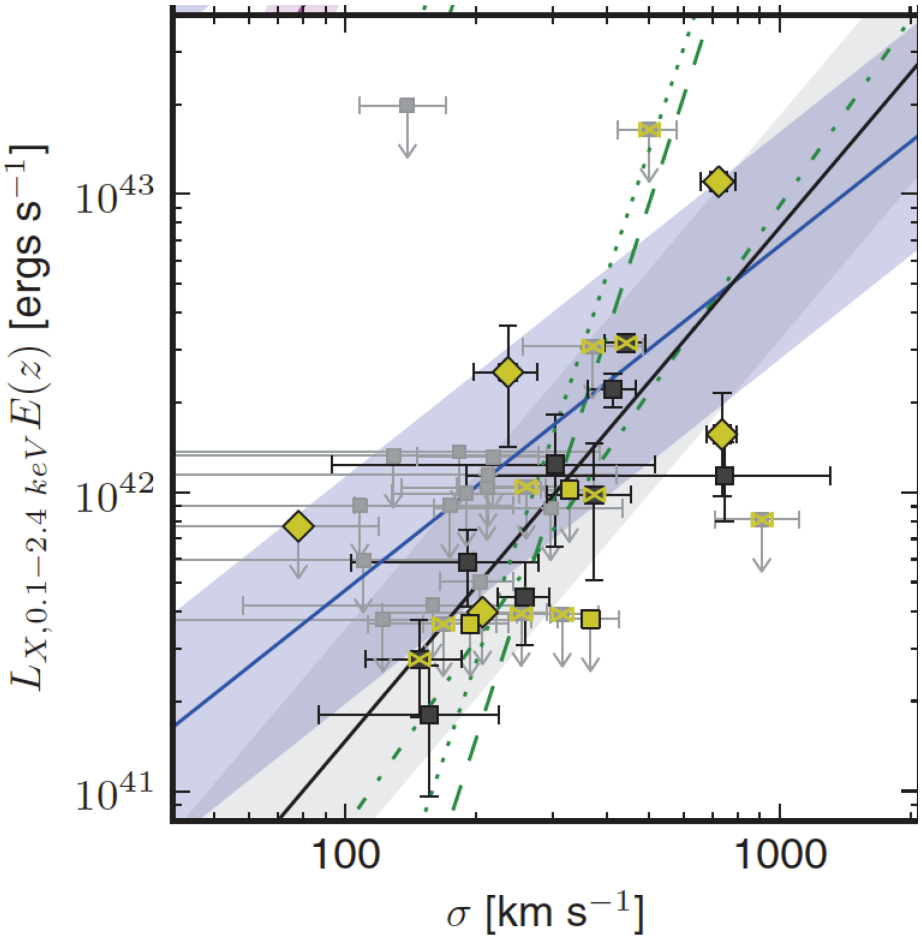

Figure 2.2: Adapted version of Connelly et al. (2012)'s figure 8 showing X-ray luminosity (L_x) versus group velocity dispersion (σ) for optically selected GEEC groups and including all members within 1 Mpc of the group centroid. Dashed and dot-dashed green lines show $z \sim 0$ sample fits (Mulchaey et al., 2003) while the dotted line is a $z \sim 0.25$ sample (Rykoff et al., 2008). Bayesian best fits for the X-ray (blue) and optical systems (black) are shown with filled region representing the scatter. Yellow bow-ties show systems tested for substructure. Filled yellow diamonds and squares indicate systems with substructure according to AD and DS tests, respectively.

smoothly increase (or decrease in the case of late-types) from the low density environment of the field to the highest density environment of rich clusters. Indeed, in a study of galaxies between $0 < z < 1.2$, Capak et al. (2007) found that the star formation-density relation showed strong evolution at all densities and at all redshifts, while the MDR of low density environments (< 100 galaxies Mpc^{-2}) show no evolution beyond $z = 0.4$. Based on these results, these authors concluded that the dominant transformation processes responsible for morphological change differed from those that resulted in star formation quenching. Thus, galaxy morphologies probe a different aspect of evolution.

Although the MDR has been observed in the group environment, there are deviations from the relations observed in clusters. For example, Zabludoff & Mulchaey (1998b) found that the fraction of ellipticals in groups varied significantly from one group to another, with values between $\lesssim 25\%$ to $\sim 55\%$. Additionally, Helsdon & Ponman (2003) found that X-ray bright groups had a *lower* fraction of spiral galaxies and a *higher* fraction of ellipticals than clusters. Based on the observed increased fraction of ellipticals in groups, Helsdon & Ponman (2003) concluded that morphological transformation was more efficient in X-ray bright groups than in clusters. The observed fraction of S0 galaxies also appears to deviate from the observed cluster MDR. Both Helsdon & Ponman (2003) and Wilman et al. (2009) found that the S0 fraction in groups was as least as high as in clusters, which indicates that the formation of S0 galaxies cannot depend only on cluster-related galaxy transformation mechanisms. Additionally, Wilman et al. (2009) found that the fraction of S0's was highest at radii $\geq 0.3h_{75}^{-1}$ Mpc from the group core, which also suggested that interactions with the IGM could not be responsible for the morphological change. Instead, Wilman et al. (2009) claimed that galaxy-galaxy interactions and mergers were responsible for S0 formation. Since interactions have been shown to be elevated in the group environment (Barnes, 1985; Zabludoff & Mulchaey, 1998b; Brough et al., 2006), (Wilman et al., 2009) concluded that galaxy groups are the 'site of S0 formation'.

2.4 The Role of Group Dynamics

A goal of current galaxy evolution studies is to not only determine whether nature or nurture dominates, but also to understand when and where galaxies do the majority of their evolution. In other words, does galaxy evolution occur primarily in the field, in which case nature would govern evolution, in group-sized haloes or in cluster-sized haloes? On the surface it would seem that this is simply a re-phrasing of the 'nature versus nurture' debate; however, the difference lies in the fact that groups and clusters are truly different environments. While there is no strict mass or density threshold that separates groups and clusters, the efficiency of the galaxy transformation mechanisms discussed in Section 1.4 differ in each environment. In particular, ram pressure-stripping and galaxy harassment are most efficient in rich clusters as a result of the hot ICM and high velocity dispersions. In the group environment, ram pressure-stripping is thought to be inefficient so strangulation begins to dominate and it is also thought that groups are the ideal environment for galaxy-galaxy interactions and mergers due to the relatively low observed velocity dispersions (Barnes, 1985; Zabludoff & Mulchaey, 1998b; Brough et al., 2006).

Strangulation is extremely difficult, if not impossible, to observe; however, it is possible to directly observe on-going interactions and post-merger galaxies by looking for features such as tidal tails and bridges (Toomre & Toomre, 1972), asymmetries (Conselice et al., 2000) or the distribution of pixel brightness (i.e. Gini coefficient: Abraham et al., 2003; Lotz et al., 2004). Although visually-disturbed galaxies provide the most convincing proof that an interaction or merger has occurred, the aforementioned techniques require deep and high resolution imaging for reliable classification, which limits searches for morphologically disturbed galaxies to either low redshift surveys or small area space-based surveys. It is therefore difficult to study correlations between mergers and the environment at higher redshifts, where mergers are more likely to occur.

Fortunately, in addition to morphological distortions, interactions are also thought to induce an intense burst of star formation resulting in a starburst galaxy, which can be identified by searching for galaxies with very high SFRs (Kennicutt & Evans, 2012). It is also possible to identify post-starburst (PSB)

galaxies, that is galaxies that have had their star formation shut off abruptly within the past Gyr, by looking for specific spectral features, such as the equivalent width of the Hα line (Dressler & Gunn, 1983). Due to their star formation history, PSB galaxies lack emission lines and show strong Balmer absorption lines, which is a result of the combined spectra of K- and A-stars (Dressler & Gunn, 1983). If the rate of mergers is truly higher in groups, then one might expect a correlation between starburst or PSB galaxies and the group environment. Indeed, in a study of starburst and PSB galaxies in the ESO Distant Cluster Survey ($0.4 \leq z \leq 0.8$), Poggianti et al. (2009) found that the fraction of dusty starburst galaxies, with strong Balmer and emission lines, was highest in the group environment and that post-starburst galaxies were preferentially found in groups with $200 \leq \sigma \leq 400$km s^{-1} and a low fraction of OII-emitting galaxies. Based on these results, Poggianti et al. (2009) concluded that starburst galaxies were triggered by mergers in groups.

Another way to probe galaxy-galaxy interactions and mergers is to look at the dynamical state of the host group. Theoretically, dynamically young or complex systems are still in the process of assembling and should have a higher rate of interactions and/or accretion. Therefore, the dynamical state of a group can be used as an indicator of 'age', where dynamically relaxed groups likely formed earlier. Additionally, there may be correlations between dynamical state and the properties of the group and its members. The aim of the work presented in this thesis is to first find reliable ways to classify group dynamics and then investigate possible correlations between the dynamical state and observed properties.

2.4.1 Determining the Dynamical State of a Group

Generally speaking, there are two ways to study the dynamical state of groups and clusters: X-ray emission and group member velocities. The observed X-ray luminosity (L_x) provides information about the group centroid, while the X-ray temperature (T_x) can provide information about the group or cluster velocity dispersion, assuming that the system is in virial equilibrium. In Equation 1.7, the virial theorem was used to derive a relationship between the temperature of the hot gas in the ICM to velocity dispersion of the halo, such that T_x goes

as σ^2. Further application of the virial theorem allows us relate the dispersion to the halo mass with the following relation

$$T_x \propto \sigma^2 \propto \frac{M}{R} \propto M^{2/3}, \tag{2.7}$$

where M is the mass of the group or cluster halo, R is the halo radius and the final relation assumes constant density (Osmond & Ponman, 2004). If the relations in Equation 2.7 hold, then the X-ray temperature is a probe of the halo mass and therefore the depth of the potential well.

Early studies of X-ray selected groups and clusters showed that these systems followed the $T_x - \sigma$ scaling relation, or alternatively the $L_x - \sigma$ relation as T_x and L_x are well correlated, shown in Equation 2.7. Since this relation only holds for systems in dynamical equilibrium, it was thought that all X-ray emitting groups and clusters were old and dynamically relaxed systems (Mulchaey & Zabludoff, 1998). However, recent work has shown that X-ray groups can be classified as dynamically young or complex if a more relaxed group radial cut is applied (Connelly et al., 2012). Additionally, in a study of 49 DEEP2 and DEEP3 X-ray bright groups Erfanianfar et al. (2013) found that groups with substructure, and therefore dynamically young, were significant outliers in the $L_x - \sigma$ plane having much higher velocity dispersions when compared to groups with similar X-ray luminosities. This result is not unexpected as the presence of substructure has been shown to boost the observed velocity dispersion (Bird, 1994).

An alternative method of probing group dynamics is to examine the velocities of the member galaxies with respect to the group centre. The shape of the overall group velocity distribution provides information about whether the system has reached dynamical equilibrium. Theoretically, the total three-dimensional (3-D) velocity distribution of a system of particles (either stars or galaxies) in or near dynamical equilibrium will take on the form of a Maxwell-Boltzmann distribution, similar to an ideal gas in thermodynamic equilibrium. However, observational astronomers are privy to only one component of the velocity distribution, i.e. the redshift or radial velocities. With only the radial velocities, the expected velocity distribution is Gaussian in shape, which results from the integration over two of the three velocity components. There-

fore, systems with non-Gaussian distributions are thought to be dynamically young or complex.

Studies of group dynamics require statistically reliable methods to determine if a velocity distribution deviates from Gaussian, i.e. is non-Gaussian. Statistical techniques that look for deviations from a Gaussian distribution can be divided in two categories: one-dimensional (1-D) and three-dimensional (3-D) tests[1]. 1-D probes of the dynamical state make use of the group velocity distribution, along the LOS, to determine if the shape of the distribution is non-Gaussian. Many statistical tests, often referred to as goodness-of-fit tests, have been developed to determine if two distributions come from the same underlying parent distribution (for a good review see D'Agostino & Stephens (1986) or Pinkney et al. (1996)). Unfortunately, most goodness-of-fit tests have been developed assuming large sample sizes (i.e. $n \sim 100-1000's$). Thus, while these techniques may be reliable for dynamical studies of clusters, they begin to break down at group scales. In Hou et al. (2009), we used Monte Carlo simulations to test the performance ability of two commonly used statistics, the Kolmogorov-Smirnov (KS) Test and the Pearson's χ^2 test, as well as the Anderson-Darling (AD) Test, to identify non-Gaussian velocity distributions for small sample sizes. The Pearson's χ^2 Test is computed as

$$\chi^2 = \sum_{i=1}^{n} \frac{(\text{observed}_i \text{ - } \text{expected}_i)^2}{\text{expected}_i}, \tag{2.8}$$

where the observed values correspond to binned data and the expected values correspond to the assumed underlying distribution (e.g. Gaussian). An observed distribution of data is considered to be statistically different from the expected distribution if the χ^2 value is above some critical value. For the Pearson's χ^2 Test, these critical values were developed for large sample sizes. Indeed, in Hou et al. (2009) we found that the statistic began to break down at $N = 30$ and severely overestimate the expected χ^2 value, resulting in almost a 100% false positive rate. Since most groups contain fewer than 30 members,

[1]It should be noted that two-dimensional (2-D) statistical tests also exist, but these typically deal with only positional data (i.e. *RA* and *DEC*). Since the focus of this work focuses in dynamical studies with LOS velocity information, I will not discuss any 2-D tests. For a detailed discussion on 1-D, 2-D and 3-D tests see Pinkney et al. (1996).

we concluded that the χ^2 would not be a reliable tool for classifying group dynamics.

In addition, we also conducted performance tests of the KS and AD Tests, both referred to as 'empirical distribution function (EDF) statistics', as they compare the EDF of observed data to the cumulative distribution function (CDF) of an assumed underlying distribution. For the KS Test, the statistic measures the maximum vertical distance between the EDF and CDF and is computed as

$$D = max(D^+, D^-) \tag{2.9}$$

$$D^+ = \text{supremum}|\frac{i}{n} - F_n(x)|, \tag{2.10}$$

$$D^- = \text{supremum}|F(x) - \frac{(i-1)}{n}|, \tag{2.11}$$

where $F_n(x) = \frac{i}{n}$ for D^+, $F_n(x) = \frac{(i-1)}{n}$ for D^-, x is the input data and $1 \leq i \leq n$ for n member galaxies. Systems with D values greater than some critical value, determined by the desired level of significance (i.e. 95 or 99 %), are then considered to be inconsistent with the assumed distribution.

The AD Test is also an EDF statistic, but it differs from the χ^2 and KS Tests in that it does not require any binning or graphical analysis. Instead, the AD Test makes use of a computing formula with the underlying principle that if the EDF and CDF come from the same underlying parent distribution, then the observed data can be transformed into a Uniform distribution. Deviations from uniformity indicate that the EDF and CDF are distinct for a given significance level. The AD statistic is calculated from ordered data x_i as

$$A^2 = -n - \frac{1}{n}\sum_{i=1}^{n}(2i-1)(\ln\Phi(x_i) + \ln(1 - \Phi(x_{n+1-i}))), \tag{2.12}$$

$$A^{2*} = A^2\left(1 + \frac{0.75}{n} + \frac{2.25}{n^2}\right), \tag{2.13}$$

where $x_i \leq x < x_{i+1}$, $\Phi(x_i)$ is the CDF of the hypothetical underlying distribution, which for dynamical studies in a Gaussian distribution and the x_i values are taken to be the group member velocities. The A^{2*} values are correction factors that are applied when the distribution parameters (e.g. mean

and velocity dispersion) are not known *a priori* and must be estimated from the x_i values.

With Monte Carlo simulations, we showed that both the KS and AD statistics were found to be reliable for systems with $N \geq 5$; however, we also found that the KS Test had a higher rate of false negatives (i.e. rate that a test fails to detect real deviations) when compared to the AD Test, especially for small sample sizes (Hou et al., 2009). As a result, we concluded that the AD Test was both a reliable and robust statistic for classifying group dynamics. Indeed, D'Agostino & Stephens (1986) also found that the AD Test was one of the most powerful statistics for detecting departures from a Gaussian distribution.

Another probe of group dynamics that makes use of the group member velocities is the group velocity dispersion profile (VDP), which shows the projected velocity dispersion as a function of group-centric radius. Studies of cluster VDPs have suggested that systems with rising profiles either indicate galaxy-galaxy interactions (Menci & Fusco-Femiano, 1996) or the presence of substructure or neighbouring systems (Girardi et al., 1996).

In addition to having non-Gaussian velocity distributions, dynamically young groups may also contain substructure, which is typically defined as a kinematically distinct subhalo within a large parent halo. Thus, the presence of substructure is thought to be an indication of the recent accretion of galaxies or smaller groups of galaxies and groups that contain substructure are still in the process of assembling (Lacey & Cole, 1993). Observational probes of substructure make use of the positions of the galaxies on the sky (i.e. RA and DEC), as well as the members velocities and are therefore referred to as 3-D tests (see Pinkney et al. (1996) for a good review of 3-D tests of substructure). Arguably the most common of the 3-D tests is the Dressler-Shectman (DS) Test for substructure (Dressler & Shectman, 1988), which was originally developed for clusters but has since been modified for application to group-size haloes (Silverman, 1986; Pinkney et al., 1996; Zabludoff & Mulchaey, 1998b). The main idea of this test is compare the kinematic properties (i.e. velocity dispersion and mean velocity) of a few neighbouring group members to the properties of the host group. The DS test identifies clumps of galaxies that have kinematic properties that differ from their host groups. A more in-depth discussion of the DS Test will be presented in the following chapters, as it is

used as the main method of studying group dynamics in this work.

2.4.2 Previous Work on Group Dynamics

Although group dynamics is an important probe of the role of interactions and mergers in the evolution of galaxies, there have been relatively few studies regarding the dynamical state of groups. The main reasons for this are that large statistical samples of groups have only recently become available (see Table 2.1) and reliable statistical tools to study group dynamics had not been developed or tested.

Much of the previous work on group dynamics has focused on identifying substructure in richer and more massive galaxy groups. Zabludoff & Mulchaey (1998a) examined six X-ray bright groups in the local Universe, each with more that 30 spectroscopically confirmed members, and found that group cores (i.e. galaxies within 0.1 h^{-1}Mpc of the group centre) were close to virialization. However, these authors found significant substructure on the group outskirts (between 0.3-0.4 h^{-1}Mpc of the group centre). Based on these results, Zabludoff & Mulchaey (1998a) concluded that like clusters, groups also form hierarchically through the merger and accretion of smaller systems. In a more recent study of substructure in groups, Firth et al. (2006) found that 3 of their 6 groups contained substructure. Additionally, these authors classified the dynamical state of the groups in their sample based on the computed relaxation times, where $\tau_{\rm relaxation} \propto N/\log(0.4N)$ (Aarseth & Saslaw, 1972) and found that three of the groups had not yet virialized. These same groups were also identified as having significant (> 95 % confidence level) substructure. We present our own substructure analysis of galaxy groups in Chapters 3, 4 and 5.

Even though there have been many published group catalogues within the last decade or so (see Table 2.1), most of the groups in these catalogues have fewer than 10 members. Previous studies of group dynamics via substructure have required a minimum of 30 member galaxies (Zabludoff & Mulchaey, 1998a). However, in Hou et al. (2009), we showed that the AD Test could reliably classify group dynamics for systems with as few as five members, reducing the minimum group membership required for dynamical studies by a factor of

six. With this methodology we were able to study a much larger sample of groups and classified the dynamical state of 106 intermediate redshift ($z \sim 0.4$) GEEC groups. We found that $\sim 32\%$ of the GEEC groups had non-Gaussian velocity distributions and were classified as dynamically young or complex. Additionally, we found that the shape of the velocity dispersion profiles for the richest GEEC groups ($N \geq 20$) correlated with dynamical state, where non-Gaussian groups had increasing profiles and Gaussian groups either had flat or decreasing profiles (shown in Figure 2.3, which is a reproduction of figure 9 of Hou et al. (2009)). Based on these results, we concluded that the AD Test was able to distinguish between systems in different dynamical states.

The study of group dynamics is currently an active field of research and the use of the AD Test to classify groups dynamics has since been applied to other group catalogues (Ribeiro et al., 2010; Martínez & Zandivarez, 2012). Ribeiro et al. (2010) examined 57 groups in the 2dFGRS-2PIGG survey (Table 2.1) and found that 16% of their groups had non-Gaussian velocity distributions. Comparison of the $(B - R)$ colours in Gaussian and non-Gaussian groups showed that the dynamically relaxed Gaussian systems has significantly redder colours, further supporting the idea that these systems are more evolved. Our methodology has also been applied to over $\sim$6000 groups identified in SDSS-DR7 by Martínez & Zandivarez (2012), who found that $\sim 9\%$ were identified as non-Gaussian. Having classified their group sample based on dynamical states, Martínez & Zandivarez (2012) then compared the luminosity functions of Gaussian and non-Gaussian groups. They found that the Gaussian groups had a brighter characteristic magnitude, by about 0.3 mag, and a steeper faint-end slope. Thus, Martínez & Zandivarez (2012) concluded that the dynamical state of a group was directly related to the luminosity of its member galaxies. Also, since non-Gaussian groups appear to be fainter, these authors claimed that these systems likely contain substructure that has yet to be influenced by processes related to the more massive host halo. As a result, non-Gaussian groups likely contain few, if any, bright ellipticals. We find a similar result for the same SDSS sample, though with a different group catalogue, which will be presented in Chapter 4 of this thesis.

In addition, other methods of distinguishing between Gaussian and non-Gaussian velocity distributions have been applied to groups. For example,

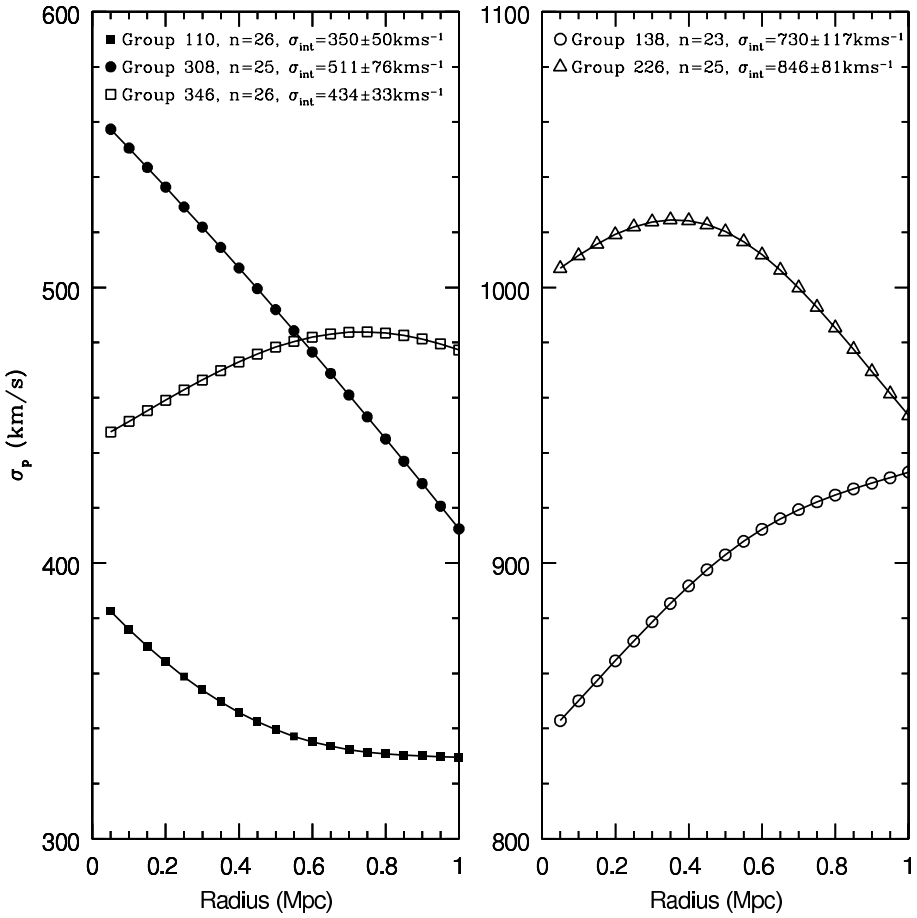

Figure 2.3: Reproduced figure 9 of Hou et al. (2009). Velocity Dispersion Profiles (VDPs)for the GEEC groups with $n > 20$ after a 1Mpc radius cut and using a constant window width of 0.35 Mpc. The open symbols indicate groups classified as non-Gaussian and the closed symbols indicate those classified as Gaussian.

both Ribeiro et al. (2011) and Krause et al. (2013) used the Cramér von Mises Test, which is sensitive to multi-modal distributions, to study group dynamics. Ribeiro et al. (2011) studied correlations between dynamical state and virial mass and found that non-Gaussian groups had significantly higher masses than Gaussian groups. Krause et al. (2013) also applied the Cramér von Mises Test to a sample of 40 galaxy groups within the Ursa Major supercluster and found that $\sim 32\%$ of their groups were consistent with having non-Gaussian velocity distributions. Since these groups had multi-modal distributions, Krause et al. (2013) concluded that their non-Gaussian groups contained substructure. Comparing Gaussian and non-Gaussian groups, Krause et al. (2013) found that Gaussian groups were preferentially found in the denser regions of the supercluster and also had smaller group-group pairwise separations. Based on these results, these authors concluded that dynamically relaxed (i.e. Gaussian) groups likely formed earlier and evolved faster in high-density regions.

2.5 Thesis Outline and Goals

Our current understanding of galaxy evolution indicates that several factors, related to both nature and nurture, play an important role in transforming galaxies. With regards to environmental effects, recent theoretical and observational results suggest that significant evolution occurs in the intermediate mass and density group environment. The main goal of this thesis is to understand the importance of group-related processes in the evolution of galaxies. In particular, this thesis aims to investigate correlations between group dynamical state, which probes the importance of galaxy-galaxy interactions and mergers, and galaxy member properties for a wide variety of systems, including previously unexplored low richness groups, with as few as five members, to the most massive clusters with hundreds of members and $M_{\rm halo} \sim 10^{15} M_{\odot}$.

The observational data used in this thesis come from three surveys and four group catalogues. Here, I will briefly introduce each catalogue, as more detailed discussion of these data are presented in the following Chapters. The group catalogues analyzed in this thesis are:

- The Group Environment and Evolution Collaboration (GEEC) group

catalogue (Wilman et al., 2005), which is based on a sample of over 200 groups initially identified in the second Canadian Network for Observational Cosmology (CNOC2) survey in the redshift range of $0.1 \leq z \leq 0.6$ (Yee et al., 2000; Carlberg et al., 2001). The GEEC survey includes extensive spectroscopic and multi-wavelength (UV-IR) follow-up on a subset of the CNOC2 groups that lie within a redshift range of $0.35 \leq z \leq 0.55$;

- The extended Group Environment and Evolution Collaboration (GEEC2) group catalogue currently includes a sample of 11 high redshift ($0.8 < z < 1$) X-ray bright groups (Balogh et al., 2011; Mok et al., 2013);

- The McGee et al. (2011) SDSS group catalogue identified using galaxies observed in SDSS-DR6 (Adelman-McCarthy et al., 2008). The observational constraints and group-find algorithm used by McGee et al. (2011) were made to mimic the GEEC survey and group catalogue;

- The Yang et al. (2007) SDSS group catalogue identified using a halo-based group finder and galaxies observed in SDSS-DR7 (Abazajian et al., 2009).

In Chapter 3, I test the reliability of the modified DS Test for low richness groups, identify substructure in the GEEC groups and then examine correlations between substructure, galaxy member properties and other probes of dynamical state. By searching for trends between group dynamical state and galaxy properties, we can probe the importance of group dynamics in galaxy evolution. In Chapter 4, the analysis presented in Chapter 3 is extended to a sample of groups in the local Universe and at high redshifts. This allows us to study the evolution of both group dynamics and the correlations between dynamical state and group properties for galaxies in the redshift range of $0 < z < 1$. In Chapter 5, I use a combination of techniques to investigate the role of pre-processing in SDSS groups and clusters. The methods presented in Chapter 5 allow us to directly compare the contribution of rich group- and cluster-related galaxy transformation processes to those that act primarily in lower-mass systems (i.e. pre-processing). Finally, in Chapter 6 I will summarize our results and discuss future work. Chapters 3, 4 and 5

represent unchanged versions of papers that were either published in (Chapter 2: Hou et al. (2012)), have been accepted for publication (Chapter 4) or have been submitted to (Chapter 5) the *Monthly Notices of the Royal Astronomical Society* (*MNRAS*), a refereed astronomical journal.

Bibliography

Aarseth, S. J. & Saslaw, W. C. 1972, ApJ, 172, 17

Abate, A., Wittman, D., Margoniner, V. E., Bridle, S. L., Gee, P., Tyson, J. A., & Dell'Antonio, I. P. 2009, ApJ, 702, 603

Abazajian, K., Adelman-McCarthy, J. K., Agüeros, M. A., Allam, S. S., Anderson, S. F., Annis, J., Bahcall, N. A., Baldry, I. K., Bastian, S., Berlind, A., & et al. 2003, AJ, 126, 2081

Abazajian, K. N., Adelman-McCarthy, J. K., Agüeros, M. A., Allam, S. S., Allende Prieto, C., An, D., Anderson, K. S. J., Anderson, S. F., Annis, J., Bahcall, N. A., & et al. 2009, ApJS, 182, 543

Abraham, R. G., van den Bergh, S., & Nair, P. 2003, ApJ, 588, 218

Adelman-McCarthy, J. K., Agüeros, M. A., Allam, S. S., Allende Prieto, C., Anderson, K. S. J., Anderson, S. F., Annis, J., Bahcall, N. A., Bailer-Jones, C. A. L., Baldry, I. K., & et al.,. 2008, ApJS, 175, 297

Balogh, M. L., McGee, S. L., Wilman, D. J., Finoguenov, A., Parker, L. C., Connelly, J. L., Mulchaey, J. S., Bower, R. G., Tanaka, M., & Giodini, S. 2011, MNRAS, 412, 2303

Barnes, J. 1985, MNRAS, 215, 517

Berlind, A. A., Frieman, J., Weinberg, D. H., Blanton, M. R., Warren, M. S., Abazajian, K., Scranton, R., Hogg, D. W., Scoccimarro, R., Bahcall, N. A., & SDSS Collaboration. 2006, ApJS, 167, 1

Bird, C. 1994, ApJ, 422, 480

Blanton, M. R. & Moustakas, J. 2009, ARA&A, 47, 159

Brainerd, T. G., Blandford, R. D., & Smail, I. 1996, ApJ, 466, 623

Brough, S., Forbes, D. A., Kilborn, V. A., & Couch, W. 2006, MNRAS, 370, 1223

Cabanac, R. A., Alard, C., Dantel-Fort, M., Fort, B., Gavazzi, R., Gomez, P., Kneib, J. P., Le Fèvre, O., Mellier, Y., Pello, R., Soucail, G., Sygnet, J. F., & Valls-Gabaud, D. 2007, A&A, 461, 813

Capak, P., Abraham, R. G., Ellis, R. S., Mobasher, B., Scoville, N., Sheth, K., & Koekemoer, A. 2007, ApJS, 172, 284

Carlberg, R. G., Yee, H. K. C., Morris, S. L., Lin, H., Hall, P. B., Patton, D. R., Sawicki, M., & Shepherd, C. W. 2001, ApJ, 552, 427

Cavaliere, A., Menci, N., & Tozzi, P. 1997, ApJ, 484, L21

Colless, M., Dalton, G., Maddox, S., Sutherland, W., Norberg, P., Cole, S., Bland-Hawthorn, J., Bridges, T., Cannon, R., Collins, C., & et al. 2001, MNRAS, 328, 1039

Connelly, J. L., Wilman, D. J., Finoguenov, A., Hou, A., Mulchaey, J. S., McGee, S. L., Balogh, M. L., Parker, L. C., Saglia, R., Henderson, R. D. E., & Bower, R. G. 2012, ApJ, 756, 139

Conselice, C. J., Bershady, M. A., & Jangren, A. 2000, ApJ, 529, 886

Coupon, J., Ilbert, O., Kilbinger, M., McCracken, H. J., Mellier, Y., Arnouts, S., Bertin, E., Hudelot, P., Schultheis, M., Le Fèvre, O., & et al. 2009, A&A, 500, 981

D'Agostino, R. & Stephens, M. 1986, Goodness-of-fit Techniques (Marcel Dekker Inc.)

De Lucia, G., Weinmann, S., Poggianti, B., Aragón-Salamanca, A., & Zaritsky, D. 2012, MNRAS, 423, 1277

Diaferio, A., Geller, M. J., & Ramella, M. 1994, AJ, 107, 868

Dressler, A. & Gunn, J. E. 1983, ApJ, 270, 7

Dressler, A. & Shectman, S. A. 1988, AJ, 95, 985

Einstein, A. 1915, Sitzungsberichte der Königlich Preußischen Akademie der Wissenschaften (Berlin), Seite 844-847., 844

Eke, V. R., Baugh, C. M., Cole, S., Frenk, C. S., King, H. M., & Peacock, J. A. 2005, MNRAS, 362, 1233

Eke, V. R., Baugh, C. M., Cole, S., Frenk, C. S., Norberg, P., Peacock, J. A., Baldry, I. K., Bland-Hawthorn, J., Bridges, T., Cannon, R., Colless, M., Collins, C., Couch, W., Dalton, G., de Propris, R., Driver, S. P., Efstathiou, G., Ellis, R. S., Glazebrook, K., Jackson, C., Lahav, O., Lewis, I., Lumsden, S., Maddox, S., Madgwick, D., Peterson, B. A., Sutherland, W., & Taylor, K. 2004, MNRAS, 348, 866

Erfanianfar, G., Finoguenov, A., Tanaka, M., Lerchster, M., Nandra, K., Laird, E., Connelly, J. L., Bielby, R., Mirkazemi, M., Faber, S. M., & et al. 2013, ApJ, 765, 117

Firth, P., Evstigneeva, E. A., Jones, J. B., Drinkwater, M. J., Phillipps, S., & Gregg, M. D. 2006, MNRAS, 372, 1856

Flaugher, B. 2005, International Journal of Modern Physics A, 20, 3121

Furlanetto, C., Santiago, B. X., Makler, M., Cypriano, E. S., Caminha, G. B., Pereira, M. E. S., Neto, A. F., Estrada, J., Lin, H., Hao, J., McKay, T. A., da Costa, L. N., & Maia, M. A. G. 2013, MNRAS, 432, 73

Gavazzi, R. & Soucail, G. 2007, A&A, 462, 459

Geller, M. J. & Huchra, J. P. 1983, ApJS, 52, 61

George, M. R., Leauthaud, A., Bundy, K., Finoguenov, A., Tinker, J., Lin, Y.-T., Mei, S., Kneib, J.-P., Aussel, H., Behroozi, P. S., & et al. 2011, ApJ, 742, 125

Gerke, B. F., Newman, J. A., Davis, M., Coil, A. L., Cooper, M. C., Dutton, A. A., Faber, S. M., Guhathakurta, P., Konidaris, N., Koo, D. C., Lin, L., Noeske, K., Phillips, A. C., Rosario, D. J., Weiner, B. J., Willmer, C. N. A., & Yan, R. 2012, ApJ, 751, 50

Gerke, B. F., Newman, J. A., Davis, M., Marinoni, C., Yan, R., Coil, A. L., Conroy, C., Cooper, M. C., Faber, S. M., Finkbeiner, D. P., & et al. 2005, ApJ, 625, 6

Gilbank, D. G., Gladders, M. D., Yee, H. K. C., & Hsieh, B. C. 2011, AJ, 141, 94

Girardi, M., Fadda, D., Giuricin, G., Mardirossian, F., Mezzetti, M., & Biviano, A. 1996, ApJ, 457, 61

Gladders, M. D. & Yee, H. K. C. 2000, AJ, 120, 2148

—. 2005, ApJS, 157, 1

Helsdon, S. F. & Ponman, T. J. 2000, MNRAS, 319, 933

—. 2003, MNRAS, 339, L29

Hickson, P. 1982, ApJ, 255, 382

—. 1997, ARA&A, 35, 357

Hoekstra, H., Franx, M., Kuijken, K., Carlberg, R. G., Yee, H. K. C., Lin, H., Morris, S. L., Hall, P. B., Patton, D. R., Sawicki, M., & Wirth, G. D. 2001, ApJ, 548, L5

Holder, G. P., McCarthy, I. G., & Babul, A. 2007, MNRAS, 382, 1697

Hou, A., Parker, L. C., Harris, W. E., & Wilman, D. J. 2009, ApJ, 702, 1199

Hou, A., Parker, L. C., Wilman, D. J., McGee, S. L., Harris, W. E., Connelly, J. L., Balogh, M. L., Mulchaey, J. S., & Bower, R. G. 2012, MNRAS, 421, 3594

Huchra, J. P. & Geller, M. J. 1982, ApJ, 257, 423

Iovino, A., Cucciati, O., Scodeggio, M., Knobel, C., Kovač, K., Lilly, S., Bolzonella, M., Tasca, L. A. M., Zamorani, G., Zucca, E., & et al. 2010, A&A, 509, A40

Jian, H.-Y., Lin, L., Chiueh, T., Lin, K.-Y., Liu, H. B., Merson, A., Baugh, C., Huang, J.-S., Chen, C.-W., Foucaud, S., Murphy, D. N. A., Cole, S., Burgett, W., & Kaiser, N. 2013, ArXiv e-prints

Kaiser, N., Aussel, H., Burke, B. E., Boesgaard, H., Chambers, K., Chun, M. R., Heasley, J. N., Hodapp, K.-W., Hunt, B., Jedicke, R., & et al. 2002, in Society of Photo-Optical Instrumentation Engineers (SPIE) Conference Series, Vol. 4836, Society of Photo-Optical Instrumentation Engineers (SPIE) Conference Series, ed. J. A. Tyson & S. Wolff, 154–164

Kennicutt, R. C. & Evans, N. J. 2012, ARA&A, 50, 531

Kimm, T., Somerville, R. S., Yi, S. K., van den Bosch, F. C., Salim, S., Fontanot, F., Monaco, P., Mo, H., Pasquali, A., Rich, R. M., & Yang, X. 2009, MNRAS, 394, 1131

Knobel, C., Lilly, S. J., Iovino, A., Porciani, C., Kovač, K., Cucciati, O., Finoguenov, A., Kitzbichler, M. G., Carollo, C. M., Contini, T., & et al. 2009, ApJ, 697, 1842

Kovač, K., Lilly, S. J., Knobel, C., Bolzonella, M., Iovino, A., Carollo, C. M., Scarlata, C., Sargent, M., Cucciati, O., Zamorani, G., & et al. 2010, ApJ, 718, 86

Krause, M. O., Ribeiro, A. L. B., & Lopes, P. A. A. 2013, A&A, 551, A143

Kristian, J. 1967, ApJ, 147, 864

Lacey, C. & Cole, S. 1993, MNRAS, 262, 627

Li, I. H. & Yee, H. K. C. 2008, AJ, 135, 809

Lilly, S. J., Le Fèvre, O., Renzini, A., Zamorani, G., Scodeggio, M., Contini, T., Carollo, C. M., Hasinger, G., Kneib, J.-P., Iovino, A., & et al. 2007, ApJS, 172, 70

Limousin, M., Cabanac, R., Gavazzi, R., Kneib, J.-P., Motta, V., Richard, J., Thanjavur, K., Foex, G., Pello, R., Crampton, D., & et al. 2009, A&A, 502, 445

Liu, H. B., Hsieh, B. C., Ho, P. T. P., Lin, L., & Yan, R. 2008, ApJ, 681, 1046

Lotz, J. M., Primack, J., & Madau, P. 2004, AJ, 128, 163

Mahdavi, A., Böhringer, H., Geller, M. J., & Ramella, M. 2000, ApJ, 534, 114

Mahdavi, A. & Geller, M. J. 2001, ApJ, 554, L129

Mamon, G. A. 1987, ApJ, 321, 622

Mamon, G. A. 2007, in Groups of Galaxies in the Nearby Universe, ed. I. Saviane, V. D. Ivanov, & J. Borissova, 203–+

Marinoni, C., Davis, M., Newman, J. A., & Coil, A. L. 2002, ApJ, 580, 122

Markevitch, M. 1998, ApJ, 504, 27

Martin, D. C., Wyder, T. K., Schiminovich, D., Barlow, T. A., Forster, K., Friedman, P. G., Morrissey, P., Neff, S. G., Seibert, M., Small, T., & et al. 2007, ApJS, 173, 342

Martínez, H. J. & Zandivarez, A. 2012, MNRAS, 419, L24

McConnachie, A. W., Patton, D. R., Ellison, S. L., & Simard, L. 2009, MNRAS, 395, 255

McGee, S. L., Balogh, M. L., Bower, R. G., Font, A. S., & McCarthy, I. G. 2009, MNRAS, 400, 937

McGee, S. L., Balogh, M. L., Wilman, D. J., Bower, R. G., Mulchaey, J. S., Parker, L. C., & Oemler, A. 2011, MNRAS, 413, 996

Menanteau, F., Sifón, C., Barrientos, L. F., Battaglia, N., Bond, J. R., Crichton, D., Das, S., Devlin, M. J., Dicker, S., Dünner, R., & et al. 2013, ApJ, 765, 67

Ménard, B., Scranton, R., Fukugita, M., & Richards, G. 2010, MNRAS, 405, 1025

Menci, N. & Fusco-Femiano, R. 1996, ApJ, 472, 46

Milkeraitis, M., van Waerbeke, L., Heymans, C., Hildebrandt, H., Dietrich, J. P., & Erben, T. 2010, MNRAS, 406, 673

Mok, A., Balogh, M. L., McGee, S. L., Wilman, D. J., Finoguenov, A., Tanaka, M., Giodini, S., Bower, R. G., Connelly, J. L., Hou, A., Mulchaey, J. S., & Parker, L. C. 2013, MNRAS, 431, 1090

More, A., Cabanac, R., More, S., Alard, C., Limousin, M., Kneib, J.-P., Gavazzi, R., & Motta, V. 2012, ApJ, 749, 38

Mulchaey, J. S., Davis, D. S., Mushotzky, R. F., & Burstein, D. 2003, ApJS, 145, 39

Mulchaey, J. S. & Zabludoff, A. I. 1998, ApJ, 496, 73

Muzzin, A., Wilson, G., Yee, H. K. C., Hoekstra, H., Gilbank, D., Surace, J., Lacy, M., Blindert, K., Majumdar, S., Demarco, R., Gardner, J. P., Gladders, M., & Lonsdale, C. 2009, ApJ, 698, 1934

Navarro, J. F., Frenk, C. S., & White, S. D. M. 1995, MNRAS, 275, 720

—. 1996, ApJ, 462, 563

Osmond, J. P. F. & Ponman, T. J. 2004, MNRAS, 350, 1511

Ostriker, J. P. & Vishniac, E. T. 1986, ApJ, 306, L51

Parker, L. C., Hudson, M. J., Carlberg, R. G., & Hoekstra, H. 2005, ApJ, 634, 806

Peng, Y.-j., Lilly, S. J., Renzini, A., & Carollo, M. 2012, ApJ, 757, 4

Pinkney, J., Roettiger, K., Burns, J. O., & Bird, C. M. 1996, ApJS, 104, 1

Poggianti, B. M., Aragón-Salamanca, A., Zaritsky, D., De Lucia, G., Milvang-Jensen, B., Desai, V., Jablonka, P., Halliday, C., Rudnick, G., Varela, J., Bamford, S., & et al. 2009, ApJ, 693, 112

Popesso, P., Biviano, A., Böhringer, H., Romaniello, M., & Voges, W. 2005, A&A, 433, 431

Postman, M., Coe, D., Benítez, N., Bradley, L., Broadhurst, T., Donahue, M., Ford, H., Graur, O., Graves, G., Jouvel, S., & et al. 2012, ApJS, 199, 25

Postman, M. & Geller, M. J. 1984, ApJ, 281, 95

Presotto, V., Iovino, A., Scodeggio, M., Cucciati, O., Knobel, C., Bolzonella, M., Oesch, P., Finoguenov, A., Tanaka, M., Kovač, K., & et al. 2012, A&A, 539, A55

Ramella, M., Diaferio, A., Geller, M. J., & Huchra, J. P. 1994, AJ, 107, 1623

Ramella, M., Zamorani, G., Zucca, E., Stirpe, G. M., Vettolani, G., Balkowski, C., Blanchard, A., Cappi, A., Cayatte, V., Chincarini, G., & et al. 1999, A&A, 342, 1

Reichardt, C. L., Stalder, B., Bleem, L. E., Montroy, T. E., Aird, K. A., Andersson, K., Armstrong, R., Ashby, M. L. N., Bautz, M., Bayliss, M., & et al. 2013, ApJ, 763, 127

Ribeiro, A. L. B., Lopes, P. A. A., & Trevisan, M. 2010, MNRAS, 409, L124

—. 2011, MNRAS, 413, L81

Rines, K. & Diaferio, A. 2010, AJ, 139, 580

Rykoff, E. S., Evrard, A. E., McKay, T. A., Becker, M. R., Johnston, D. E., Koester, B. P., Nord, B., Rozo, E., Sheldon, E. S., Stanek, R., & Wechsler, R. H. 2008, MNRAS, 387, L28

Scranton, R., Ménard, B., Richards, G. T., Nichol, R. C., Myers, A. D., Jain, B., Gray, A., Bartelmann, M., Brunner, R. J., Connolly, A. J., & et al. 2005, ApJ, 633, 589

Silverman, B. W. 1986, Density estimation for statistics and data analysis

Sunyaev, R. A. & Zeldovich, Y. B. 1972, Comments on Astrophysics and Space Physics, 4, 173

Toomre, A. & Toomre, J. 1972, ApJ, 178, 623

Wetzel, A. R., Tinker, J. L., & Conroy, C. 2012, MNRAS, 424, 232

Wilman, D. J., Balogh, M. L., Bower, R. G., Mulchaey, J. S., Oemler, A., Carlberg, R. G., Eke, V. R., Lewis, I., Morris, S. L., & Whitaker, R. J. 2005, MNRAS, 358, 88

Wilman, D. J., Oemler, Jr., A., Mulchaey, J. S., McGee, S. L., Balogh, M. L., & Bower, R. G. 2009, ApJ, 692, 298

Wittman, D., Margoniner, V. E., Tyson, J. A., Cohen, J. G., Becker, A. C., & Dell'Antonio, I. P. 2003, ApJ, 597, 218

Wittman, D., Tyson, J. A., Margoniner, V. E., Cohen, J. G., & Dell'Antonio, I. P. 2001, ApJ, 557, L89

Woo, J., Dekel, A., Faber, S. M., Noeske, K., Koo, D. C., Gerke, B. F., Cooper, M. C., Salim, S., Dutton, A. A., Newman, J., Weiner, B. J., Bundy, K., Willmer, C. N. A., Davis, M., & Yan, R. 2013, MNRAS, 428, 3306

Xue, Y.-J. & Wu, X.-P. 2000, ApJ, 538, 65

Yang, X., Mo, H. J., van den Bosch, F. C., & Jing, Y. P. 2005, MNRAS, 356, 1293

Yang, X., Mo, H. J., van den Bosch, F. C., Pasquali, A., Li, C., & Barden, M. 2007, ApJ, 671, 153

Yee, H. K. C., Morris, S. L., Lin, H., Carlberg, R. G., Hall, P. B., Sawicki, M., Patton, D. R., Wirth, G. D., Ellingson, E., & Shepherd, C. W. 2000, ApJS, 129, 475

York, D. G., Adelman, J., Anderson, Jr., J. E., Anderson, S. F., Annis, J., Bahcall, N. A., Bakken, J. A., Barkhouser, R., Bastian, S., Berman, E., & SDSS Collaboration. 2000, AJ, 120, 1579

Zabludoff, A. I. & Mulchaey, J. S. 1998a, ApJ, 498, L5

—. 1998b, ApJ, 496, 39

Chapter 3

Substructure in the Most Massive GEEC Groups: Field-like Populations in Dynamically Active Groups

This chapter incorporates the article *"Substructure in the Most Massive GEEC Groups: Field-like Populations in Dynamically Active Groups"*, which has been published in the *Monthly Notices of the Royal Astronomical Society.* The full reference is given below:

Annie Hou[1], Laura C. Parker[1], David J. Wilman[2], Sean L. McGee[3,4], William E. Harris[1], Jennifer L. Connelly[2], Michael L. Balogh[4], John S. Mulchaey[5], Richard G. Bower[3]. 2012. *MNRAS.* Volume 421, Issue 4, pp. 3594-3611.

[1] *Department of Physics & Astronomy, McMaster University, Hamilton ON L8S 4M1, Canada*
[2] *Max-Planck-Institut für Extraterrestrische Physik, Giessenbachstraße, D-85748 Garching, Germany*
[3] *Department Of Physics, University of Durham, Durham, UK DH1 3LE*
[4] *Department of Physics and Astronomy, Univeristy of Waterloo, Waterloo, Ontario, N2L 3G1, Canada*
[5] *Observatories of the Carnegie Institution, 813 Santa Barbara Street, Pasadena, California, USA*

Abstract

The presence of substructure in galaxy groups and clusters is believed to be a sign of recent galaxy accretion and can be used not only to probe the assembly history of these structures, but also the evolution of their member galaxies. Using the Dressler-Shectman (DS) Test, we study substructure in a sample of intermediate redshift ($z \sim 0.4$) galaxy groups from the Group Environment and Evolution Collaboration (GEEC) group catalog. We find that 4 of the 15 rich GEEC groups, with an average velocity dispersion of $\sim$525 km s^{-1}, are identified as having significant substructure. The identified regions of localized substructure lie on the group outskirts and in some cases appear to be infalling. In a comparison of galaxy properties for the members of groups with and without substructure, we find that the groups with substructure have a significantly higher fraction of blue and star-forming galaxies and a parent colour distribution that resembles that of the field population rather than the overall group population. In addition, we observe correlations between the detection of substructure and other dynamical measures, such as velocity distributions and velocity dispersion profiles. Based on this analysis, we conclude that some galaxy groups contain significant substructure and that these groups have properties and galaxy populations that differ from groups with no detected substructure. These results indicate that the substructure galaxies, which lie preferentially on the group outskirts and could be infalling, do not exhibit signs of environmental effects, since little or no star-formation quenching is observed in these systems.

3.1 Introduction

The current theory of structure formation in the Universe is based on the standard Λ cold dark matter (ΛCDM) cosmological model, in which objects grow hierarchically from the initial matter density perturbations through mergers and accretion (e.g., Press & Schechter, 1974; Lacey & Cole, 1993; Springel et al., 2005). In order to test the theory of hierarchical structure formation, one must investigate the assembly history of the large structures in the Universe, namely galaxy groups and clusters.

A natural consequence of a hierarchical Universe is the existence of substructure within larger systems. Traditionally, substructure has been defined as a kinematically distinct sub-halo within a larger parent halo. A broader, more observationally motivated definition, and one that we will assume here, also includes separate haloes that are either merging to form a larger halo; gravitationally bound and infalling onto a pre-existing halo; or in the nearby large-scale-structure, but not necessarily bound or infalling. In general, accreting structure does not have the same kinematic properties as the host, but whether or not substructure can be observed depends on how long it remains intact after infall. Early N-body simulations suggested that the assimilation of substructure into the host was rapid, providing no detectable long-lived features (Katz & White, 1993; Summers et al., 1995). However, later work has shown that the lack of observable substructure in these simulations was due to poor resolution (Moore et al., 1996). Indeed, high resolution N-body simulations (e.g., Diemand et al., 2008; Springel et al., 2008), demonstrate that several hundred thousand sub-haloes can exist in a Milky Way sized dark matter halo at a redshift of zero. Using semi-analytic models to study the substructure within individual galaxy to cluster-sized haloes, Taylor & Babul (2004) showed that accreting systems could survive within the host halo for many orbits, depending on the orbital parameters of the substructure upon infall.

These theoretical results suggest that substructure should be a detectable quantity and numerical dark matter simulations of galaxy groups and clusters in a ΛCDM Universe predict that approximately 30 per cent of all systems should contain substructure (Knebe & Müller, 2000). Studies of individual

clusters (e.g., Beers et al., 1982; Dressler & Shectman, 1988; West & Bothun, 1990; Bird, 1994a; Colless & Dunn, 1996; Burgett & et al., 2004; Böhringer et al., 2010) indicate that a large fraction of systems show evidence of significant sub-clustering. The predicted theoretical value of 30 per cent is in agreement with some substructure studies of groups and clusters (e.g., Zabludoff & Mulchaey, 1998a; Solanes et al., 1999), but several other results have demonstrated a much higher fraction of substructure; Bird (1994b) observed that 44 per cent[1] of their sample contained substructure, Dressler & Shectman (1988) observed 53 per cent and Ramella et al. (2007) find an extremely high substructure fraction of 73 per cent. Although the precise fraction of groups and clusters with substructure may still be a source of debate, the observed presence of any substructure strongly suggests that these systems grow in a hierarchical manner through the accretion of galaxies and smaller groups of galaxies.

Though galaxy clusters are amongst the largest structures in the local Universe, they do not represent the most common host environment for galaxies. Galaxy groups, which contain a few to tens of member galaxies, are the host environment of more than half of the present-day galaxy population (Geller & Huchra, 1983; Eke et al., 2005). Despite the importance of groups in the build up of large galaxy clusters, there have been few studies on the assembly history of groups themselves.

One method of probing group assembly histories is to look at the amount of substructure within these systems. The presence of such structure would indicate that the group has recently accreted galaxies (Lacey & Cole, 1993). Studies have been carried out for galaxy groups in the local Universe by Zabludoff & Mulchaey (1998a), who observed significant (> 99 per cent confidence level) substructure in two of their six local groups. An interesting result of their analysis showed that the substructure was located on the outskirts of the systems, that is $\sim$0.3-0.4 h^{-1} Mpc, where $h = H_0/(100$ km s^{-1} Mpc$^{-1})$, from the core of the group. Based on these results, Zabludoff & Mulchaey (1998a) concluded that like rich galaxy clusters, some galaxy groups assembled in a hierarchical manner through the accretion of smaller structures from the field.

[1] 11/25 galaxies in their sample have significant (> 95 per cent) substructure based on results of the Dressler-Shectman statistics.

A more recent study of local galaxy groups by Firth et al. (2006) found similar results, with roughly half of their sample showing significant substructure. Although, the findings of Zabludoff & Mulchaey (1998a) and Firth et al. (2006) provided an important first step in unveiling the assembly history of groups, their analysis was based on a small sample of very nearby systems. In order to gain a better understanding of the role of groups in the growth of structure, we must search for substructure in a larger sample of galaxy groups with highly complete spectroscopy that cover a wide range in redshift. Such studies have only become possible with recent deep spectroscopic surveys that have produced large group catalogues, such as the Sloan Digital Sky Survey (SDSS) (Berlind & et al., 2006; Yang et al., 2007), the Group Environment and Evolution Collaboration (GEEC) (Wilman et al., 2005; Carlberg et al., 2001), and the higher redshift extension of GEEC (GEEC2) (Balogh et al., 2011) optical group catalogs.

In addition to the role of the group environment in the growth of large scale structure in the Universe, studies of substructure within groups allows us to probe galaxy evolution. Since groups have fewer members than galaxy clusters, any substructure present will have a stronger effect on the observed group properties (i.e. colours, blue or active fractions). If substructure traces accreting galaxies, one might expect a correlation between observed galaxy properties and substructure. Possible correlations could exist between substructure and the colours of galaxies in groups, or with substructure and star formation rates. One of the main goals of this paper is to search for such correlations.

In this paper we search for substructure in a sample of intermediate redshift galaxy groups from the GEEC Group Catalog. In Section 3.2, we discuss the sensitivity and reliability of the Dressler-Shectman (DS) Test for group-sized systems using Monte Carlo simulations. In Section 3.3, we apply the DS Test to the GEEC groups and discuss the results of our analysis. In Section 3.4, we discuss the relationship between the presence of substructure and other indicators of dynamical state, such as the shape of the group velocity distribution. In Section 3.5, we look for correlations between substructure and the properties of members galaxies, such as colour and star formation rate, and discuss the possible implications of our findings. In Section 3.6 we present our

conclusions. Additionally, we include an Appendix, which provides detailed results of our Monte Carlo Simulations.

Throughout this paper we assume a ΛCDM cosmology with $\Omega_M = 0.3$, $\Omega_\Lambda = 0.7$, and $H_0 = 75$ km s^{-1} Mpc^{-1}.

3.2 Detecting Substructure in Groups

Numerous tests for substructure have been developed and carried out for cluster-sized systems (see Pinkney et al., 1996, for a thorough review). In a comparison of five 3-dimensional (3-D) tests, which use both velocity and spatial information, Pinkney et al. (1996) determined that the Dressler-Shectman (DS) Test (Dressler & Shectman, 1988) was the most sensitive test for substructure, for systems with as few as 30 members. In the following section we look at the DS Test, and determine its reliability and robustness for smaller group-sized systems.

3.2.1 The Dressler-Shectman (D-S) Test

Substructure manifests itself as detectable deviations in the spatial and/or velocity structure of a system. The aim of the DS Test is to compute *local* mean velocity and velocity dispersion values, for each individual galaxy and its nearest neighbours, and then compare these to the global group values. Following the notation of Dressler & Shectman (1988), we define $(\bar{\nu}, \sigma)$ as the mean velocity and velocity dispersion of the entire group, which is assumed to have $n_{\rm members}$ galaxies. Then for each galaxy i in the group, we select it plus a number of its nearest neighbours, $N_{\rm nn}$, and compute their mean velocity $\bar{\nu}^i_{\rm local}$ and velocity dispersion $\sigma^i_{\rm local}$. From these we compute the individual galaxy deviations, δ_i, given as

$$\delta_i^2 = \left(\frac{N_{\rm nn}+1}{\sigma^2}\right)\left[\left(\overline{\nu}^i_{\rm local} - \overline{\nu}\right)^2 + \left(\sigma^i_{\rm local} - \sigma\right)^2\right], \tag{3.1}$$

where $1 \leq i \leq n_{\rm members}$ (i.e. δ_i is computed for each galaxy in the system). Dressler & Shectman (1988) originally developed the test for cluster-sized systems and the number of nearest neighbours used to compute the δ_i values

was relatively high (i.e. $N_{\rm nn} = 11$). Since substructure in galaxy groups is likely to have fewer than 11 constituent galaxies, we take $N_{\rm nn}$ to be $\sqrt{n_{\rm members}}$ following the methodology of authors who have previously applied the DS Test to group-size systems (Silverman, 1986; Pinkney et al., 1996; Zabludoff & Mulchaey, 1998b). This ensures that large kinematic deviations of a few neighbouring galaxies do not get diluted by adding too many unassociated galaxies, and thereby lowering the computed $\overline{\nu}^i_{\rm local}$ and $\sigma^i_{\rm local}$ values in Equation 3.1.

The statistic used in the DS Test is the Δ-value, given by

$$\Delta = \sum_i \delta_i. \tag{3.2}$$

A system is then considered to have substructure if $\Delta/n_{\rm members} > 1.0$ (Dressler & Shectman, 1988). This method of using a threshold value to find substructure is referred to as the critical values method.

An alternative method of identifying substructure with the DS Test is to use probabilities (P-values) rather than critical values. The P-values for the DS Test are computed by comparing the observed Δ-value to 'shuffled' Δ-values, which are computed by randomly shuffling the observed velocities and re-assigning these values to the member positions, a procedure called 'MC shuffling'. The P-values are given by

$$P = \sum \left(\Delta_{\rm shuffled} > \Delta_{\rm observed}\right) / n_{\rm shuffle}. \tag{3.3}$$

where $\Delta_{\rm shuffled}$ and $\Delta_{\rm observed}$ are both computed using Equation 3.2 and $n_{\rm shuffle}$ is the number of 'MC shuffles', and therefore the number of $\Delta_{\rm shuffled}$-values, used to compute the probability . One can see from Equation 3.3 that systems with significant substructure will have low P-values, since it is unlikely to obtain the observed Δ-value randomly (Equation 3.2).

3.2.2 Monte Carlo Simulations

Although Pinkney et al. (1996) have carried out an extensive investigation of the DS Test, their analysis was performed on systems with a minimum of 30 members, and the majority of our intermediate redshift groups have fewer member galaxies (see Section 3.1). Therefore, we perform our own Monte Carlo

simulations in order to check the reliability, sensitivity and robustness of the DS Test, using both the critical value and probability (P-value) methods, for group-sized systems. It should be noted that we specifically model our host mock groups after the observed GEEC group sample.

3.2.2.1 Generating the Mock Groups

Mock galaxy groups, both with and without substructure, are generated using Monte Carlo methods to assign member galaxy positions. These mock groups are then used to compute the false negative and positive rates of the DS Test, and also determine the sensitivity of the test against a variety of input parameters.

The radial positions for the members of the mock groups are randomly drawn from fits to the projected group-centric radial distributions of the galaxies observed in the GEEC group catalog (Wilman et al., 2005). The groups are divided into four bins based on the number of members in each group (Fig. 3.1), and fits to each bin are used to populate the mock groups. Since the GEEC groups span such a wide range of masses and group membership, we elect not to use a single fit to the radial distribution of all the group galaxies in our sample. Instead, we divide our sample into bins of group membership ($5 \leq n_{\rm members} < 10$, $10 \leq n_{\rm members} < 15$, $15 \leq n_{\rm members} < 20$ and $n_{\rm members} \geq 20$) and fit each distribution separately. It should be noted that we bin our sample by group membership, rather than mass or velocity dispersion, as we aim to study the false positive and negative rates of the DS Test as a function of $n_{\rm members}$. However, the results are similar if we bin by σ rather than $n_{\rm members}$. The histograms and fits to the radial distributions of the binned groups are shown in Fig. 3.1. The general form of the radial distribution of member galaxies is given by

$$N \propto \exp\left(-\lambda R\right), \tag{3.4}$$

where R is the radial position of the given galaxy and $\lambda = 2.98$, 1.31, 0.902 and 0.606 Mpc^{-1} for the $5 \leq n_{\rm members} < 10$, $10 \leq n_{\rm members} < 15$, $15 \leq n_{\rm members} < 20$ and $n_{\rm members} \geq 20$ bins, respectively. From these results it is clear that groups with fewer members have steeper radial distributions and smaller maximum group centric radii (Fig. 3.1).

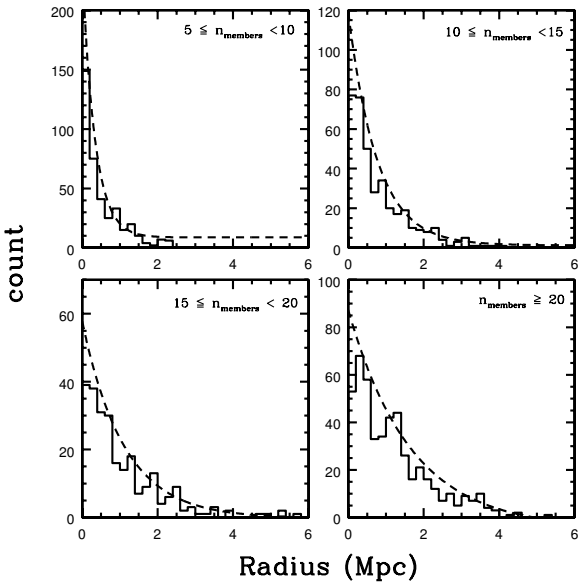

Figure 3.1: Histograms of the radial distribution of the galaxies in the GEEC Group Catalog stacked in bins of $n_{\rm members}$. The dashed line corresponds to an exponential fit to the distribution, which we use to generate the radial positions of galaxies in our mock groups.

The redshifts of the member galaxies in the mock groups are randomly drawn from Gaussian distributions. The dispersions of the input Gaussians are taken to be the average velocity dispersion of the aforementioned group membership bins, which are: 300, 350, 400 and 550 km s^{-1}. These dispersion values are chosen for the mocks groups in order to best mimic the systems in our GEEC sample. We also generate mock groups with the same input host velocity dispersion ($\sigma_{\rm host}$) for all values of $n_{\rm members}$ and find no significant difference in our results (see Appendix for further detail).

As will be shown in Section 3.2.2.2, in order to determine the false negative rates for the DS Test, we must include substructure within the host group. The positions and redshifts of the substructure galaxies are drawn from a Gaussian distribution[2]. The free parameters in our mock groups with substructure are: the velocity dispersion of the substructure ($\sigma_{\rm redshift}$), spatial dispersion of the substructure ($\sigma_{\rm position}$), location of the substructure, in both position ($\epsilon_{\rm position}$)

[2]Tests with non-Gaussian input substructure have also been carried out and for all reasonable distributions the results do not differ significantly from the results presented here.

and velocity ($\epsilon_{\rm redshift}$) space, the number of galaxies in the substructure ($n_{\rm sub}$), the number of galaxies in the host group ($n_{\rm members}$), and velocity dispersion of the host group ($\sigma_{\rm host}$). We briefly analyze the effects of each of these parameters on the robustness of the DS Test in the following sections, and give a more detailed discussion in the Appendix.

3.2.2.2 Testing for False Positives

Using the mock groups with no input substructure described in Section 3.2.2.1, we determine the false positive rates, or type I errors, which for the DS Test occur when substructure is identified when none exists. The only parameter we vary for these systems is the number of member galaxies ($n_{\rm members}$).

We first compute the false positive rates using the critical values method. For each value of $n_{\rm members}$ we compute the Δ-statistic, (Equations 3.1 and 3.2) and then classify a group as having substructure if $\Delta/n_{\rm members} > 1.0$. With this criterion, we find that for all relevant values of $n_{\rm members}$ the false positive rates are extremely high. For example for $n_{\rm members} = 20$, the false positive rate is $\sim$81 per cent and even for larger systems, $n_{\rm members} = 100$, we find that the rate is equally high. A similar result was observed by Knebe & Müller (2000) in a study of substructure in numerically simulated galaxy clusters. They found that for haloes with no substructure the $\Delta/n_{\rm members}$- values were often greater than 1.0, with values peaking closer to 1.4 for larger (i.e. $n_{\rm members}$ $\sim$80 -100) clusters. Although it is possible to better identify substructure in richer systems, such as clusters, with a higher value of $\Delta/n_{\rm members}$ $\sim$1.4 - 1.6 (e.g., Girardi et al., 2005; Knebe & Müller, 2000), we find that for group-sized systems this methodology could not simultaneously produce low false positive and false negative rates.

Alternatively, when P-values are used to identify substructure, we find that the false positive rates are much lower than with the critical values method and also remarkably stable for a wide range of group members (i.e. $5 \leq n_{\rm members} \leq 50$). From our mock groups we find that for significance levels of 0.01, 0.05 and 0.10, the false positive rates are 5, 10 and 15 per cent for all values of $n_{\rm members}$ tested. In other words, the DS Test will falsely identify roughly 5 per cent more substructure than the desired significance level. Although these rates are higher than the expected values for a given significance level, they

Table 3.1: Input parameter values for the 'base' mock groups described in Section 3.2.2.3; i.e. Monte Carlo groups with a zero false negative rate.

$n_{\rm members}$	$n_{\rm sub}$	$\sigma_{\rm host}$ km s^{-1}	$\sigma_{\rm position}$ Mpc	$\epsilon_{\rm position}$ Mpc	$\sigma_{\rm redshift}$ km s^{-1}	$\epsilon_{\rm redshift}$ km s^{-1}
10	4	350	0.01	0.5	100	1300
15	5	400	0.01	0.5	100	1300
20	5	550	0.01	0.5	100	1300
50	10	550	0.01	0.5	100	1300

are still substantially lower than the rates obtained using the critical values method. Also, as long as one chooses significance levels of 0.01 or 0.05, the rate of false identifications is acceptably low. Based on these results, we rule out the critical values method and only perform the following analysis using the probabilities, P-values, method.

3.2.2.3 Testing for False Negatives

Having determined the rate of false identifications obtained with the DS Test, we now test for the rate of false negatives, or type II errors. For this statistic the false negative rate measures how often the DS Test fails to detect substructure when indeed it exists. The purpose of conducting these false negative tests is twofold: first, they help determine the reliability of the statistic and second, by varying only one of the free input parameters (listed in Section 3.2.2.1) at a time, you can determine how sensitive the test is to each parameter. The latter places quantitative constraints on the maximum size and location of substructure that can be identified.

Before we begin looking at the input parameters, we first determine how reliable the test is at identifying 'obvious' substructure, that is to say galaxies that are tightly correlated and located far from the group centre, both in projection on the sky and along the line-of-sight (see Table 3.1 for input parameter values). For these mock groups, we find that substructure is correctly identified in almost all cases, using the P-value method and a significance level of 0.01, producing false negative rates of 0 or 1 per cent.

We then investigate the individual free parameters in more detail to determine how each alters the false negative rate. We briefly discuss the main

results here and leave the detailed quantitative analysis, as well as full tables of false negative rates, for the Appendix.

Of the five free parameters, we find that the DS Test is most sensitive to the number of galaxies in the substructure ($n_{\rm sub}$) and the location of the peak of the substructure's velocity distribution with respect to the peak of the host's ($\epsilon_{\rm redshift}$). Previous studies of substructure in galaxy clusters by Dressler & Shectman (1988) and Pinkney et al. (1996) showed that the DS Test was unable to find substructure that was 'superimposed' with the highest density regions of the hosts, since the galaxies were spatially mixed. Pinkney et al. (1996) even stated that in these cases, any type of 3-D test would not be able to accurately detect substructure. An important distinction, not made by these authors, is that two forms of 'superposition' can occur. Substructure can be superimposed with the host group either in projected angular position or in redshift space. Our analysis shows that the DS Test is significantly more sensitive to $\epsilon_{\rm redshift}$ than to $\epsilon_{\rm position}$. The test can usually identify substructure with superpositions as projected on the sky, but has a very difficult time with those along the line-of-sight. From Equation 3.1, it is clear that only collections of neighbouring galaxies with a different local mean velocity and velocity dispersion will produce high δ_i values, no matter their angular position.

In addition we also find that the level of sensitivity of the DS Test to $\epsilon_{\rm redshift}$, the distance between the substructure's and host's peak velocity distribution, is dependent on the number of members in the host group. We find that for small groups (i.e. $n_{\rm members} < 20$), the input substructure needs to be further than $2\sigma_{\rm host}$ from the group centre in order to be detected. On the other hand, the DS Test can identify substructure that is roughly $2\sigma_{\rm host}$ away from the peak of the host's Gaussian velocity distribution in groups with more than 20 members. For even larger systems, that is clusters with $n_{\rm members} \geq 50$, the input substructure can be located *within* $1\sigma_{\rm host}$ and still be identified.

Another result from this analysis is that the DS Test is sensitive to the number of galaxies that are part of the substructure ($n_{\rm sub}$). Our simulations show that no matter the membership of the host group, the test cannot identify substructure with fewer then four members. Also, the minimum required number of members within the substructure increases with $n_{\rm members}$. This is due to the fact that we set N_{nn} in Equation 3.1 to $\sqrt{n_{\rm members}}$. Therefore,

more members in the host group means that the velocity information of more 'neighbours' will be used to calculate $\overline{\nu}^i_{\rm local}$ and $\sigma^i_{\rm local}$. Thus, if there are too few galaxies in the substructure, their kinematic deviations can be washed out by other neighbouring host galaxies.

We find that for rich galaxy groups, with $n_{\rm members} \geq 20$, the DS Test can reliably identify true substructure, as has been shown by several other authors (e.g., Dressler & Shectman, 1988; Pinkney et al., 1996; Knebe & Müller, 2000). For systems with fewer member galaxies, such as poor groups with $n_{\rm members} < 20$, the false negative rates are very low (< 5 per cent) only for tightly correlated substructure galaxies with large kinematic deviations. In these poor groups, substructure that is more loosely associated with a velocity peak close to that of its host group is not as easily detected by the test.

Taking into account the results of both the false negative and positive tests, we conclude that for systems with $n_{\rm members} \geq 20$, the DS Test can reliably identify real substructure if the P-values method is employed using a confidence level of either 0.01 or 0.05. For groups with $n_{\rm members} < 20$, we find that the percentage of groups with substructure identified by the DS Test should be taken as a *lower limit*.

3.3 Substructure in the GEEC Groups

3.3.1 The GEEC Group Catalog

The Group Environment and Evolution Collaboration (GEEC) group catalog is based on a set of ∼200 intermediate redshift, $0.1 < z < 0.6$, galaxy groups initially identified in the second Canadian Network for Observational Cosmology (CNOC2) redshift survey (Yee et al., 2000; Carlberg et al., 2001). The CNOC2 survey observed ∼4 $\times 10^4$ galaxies covering four patches, totalling 1.5 deg^2 in area, in the $UBVR_CI_C$ bands down to a limiting magnitude of $R_C = 23.0$. Spectra of more than 6000 galaxies were obtained with the MOS spectrograph on the Canada-France-Hawaii Telescope (CFHT), with 48 per cent completeness at $R_C = 21.5$ (Yee et al., 2000). The GEEC group catalog includes extensive follow-up spectroscopy with the Inamori Magellan Areal Camera and Spectrograph (IMACS) (Connelly, J. et al., submitted) and Low

Dispersion Survey Spectrograph (LDSS2) on Magellan (Wilman et al., 2005), as well the Focal Reducer and low dispersion Spectrograph (FORS2) on the Very Large Telescope (VLT) (Connelly, J. et al., submitted). We have also obtained multi-wavelength imaging data, which includes: X-ray observations with the X-ray Multi-Mirror Mission-Newton (XMM-Newton) and Chandra X-ray Observatories (Finoguenov et al., 2009), ultraviolet observations with Galaxy Evolution Explorer (GALEX) (McGee et al., 2011), optical observations with the Advanced Camera for Surveys (ACS) on the Hubble Space Telescope (HST) (Wilman et al., 2009), infrared observations with the Multiband Imaging Photometer for Spitzer (MIPS) on the Spitzer Space Telescope (Tyler et al., 2011), and near-infrared observations with Isaac Newton Group Red Imaging Device (INGRID) on the William Herschel Telescope (Balogh et al., 2009), Infrared Array Camera (IRAC) on Spitzer (Wilman et al., 2008), and the Son of ISAAC (SOFI) on the New Technology Telescope (NTT) (Balogh et al., 2009). In addition, improved optical imaging was obtained in the $ugrizBVRI$ filters from the CFHT Megacam and CFH12K imagers (Balogh et al., 2009).

In addition to the follow-up observations of the CNOC2 fields, group membership has also been redefined by Wilman et al. (2005) using more relaxed algorithm parameters than those used by Carlberg et al. (2001). The original search parameters were optimized such that the group-finding algorithm would identify dense, virialized groups, while the Wilman et al. (2005) catalog includes looser group populations that cover a wider range of dynamical states. For this reason, the GEEC group catalog is ideal for the investigation of substructure within groups, since we are not restricted to dense group cores and are able to probe the surrounding large scale structure.

3.3.2 Analysis of the GEEC Groups

We apply the DS Test, as described in Section 3.2, to a subset of the GEEC groups. Although there are roughly 200 groups in the GEEC catalog, the majority of systems have fewer than 10 members. In Section 3.2.2.3, we determined that in order to obtain a reliable measure of substructure, the minimum number of member galaxies for the DS Test is $n_{\rm members} = 20$, which leaves us

with a subset of 15 groups. These groups are amongst the most massive GEEC groups with an average velocity dispersion of $\sim$525 km s^{-1}.

As previously mentioned, due to the relaxed membership allocation algorithm parameters, some of the GEEC groups have relatively large radial extents, and can be larger than the suggested maximum group virial radius (r_{200}) of 1.0 Mpc (Mamon, 2007), but for the purposes of detecting substructure we elect not to apply any radial cuts to our groups for our main analysis. Our definition of substructure is liberal, in that we include structure that may be infalling or structure that is in nearby large scale structure but not necessarily bound to the host group. Thus, to ensure that we do not eliminate any possible detection of substructure, we analyze all galaxies identified as group members by the FOF-algorithm applied in Wilman et al. (2005). Our decision not to apply radial cuts is further justified given that substructure is often in group and cluster outskirts (West & Bothun, 1990; Zabludoff & Mulchaey, 1998a).

For the distribution parameters we estimate $\overline{\nu}^i_{\rm local}$ and $\overline{\nu}$, from Equation 3.1, as the group and local (i.e. ith galaxy and its $\sqrt{n_{\rm members}}$ nearest neighbours) canonical mean velocity, and $\sigma^i_{\rm local}$ and σ, also from Equation 3.1, as the local and group intrinsic velocity dispersion, computed following the method outlined in Wilman et al. (2005). The dispersion uncertainties are computed using the jackknife method (Efron, 1982) and are given in Tables 3.2 and 3.3.

Table 3.2: Group properties and DS statistics for the GEEC groups with substructure

GEEC Group ID	$n_{\rm members}$	z_{group}	σ km s^{-1}	$\Delta/n_{\rm members}$	P value[a]	AD Test Classification	Shape of VDP
25	28	0.362	491±32	0.693	0	non-Gaussian	rising
208	22	0.269	530±45	0.841	0	non-Gaussian	rising
226	86	0.359	944±17	1.37	0	non-Gaussian	rising
320	29	0.245	463±33	0.751	0.00383	Gaussian	rising

[a]Using 100 000 'MC shuffles'. We identify groups with P values < 0.01 as having significant substructure.

Table 3.3: Group properties and DS statistics values for the GEEC groups with no substructure

GEEC Group ID	$n_{\rm members}$	z_{group}	σ km s^{-1}	$\Delta/n_{\rm members}$	P-value[a]	AD Test Classification	Shape of VDP
4	20	0.201	360±39	0.605	0.524	non-Gaussian	flat
38	34	0.511	739±21	0.910	0.0372	non-Gaussian	declining
104	27	0.145	365±25	0.659	0.0501	Gaussian	flat
110	33	0.156	338±22	0.599	0.413	Gaussian	declining
117	27	0.220	261±20	0.412	0.851	Gaussian	flat
138	53	0.438	743±29	0.983	0.354	non-Gaussian	flat
238	21	0.408	606±52	0.826	0.135	non-Gaussian	flat
308	26	0.224	511±35	0.854	0.610	Gaussian	declining
334	20	0.323	454±30	0.670	0.0563	Gaussian	flat
346	32	0.373	439±20	0.612	0.232	non-Gaussian	flat
362	24	0.460	666±43	0.861	0.0817	Gaussian	rising

[a]Using 100 000 'MC shuffles'. We only identify groups with P values < 0.01 as having significant substructure.

Of the 15 GEEC groups with $n_{\rm members} \geq 20$ we find that 4 groups, ($\sim$27 per cent) are identified as having substructure at the 99 per cent confidence level (c.l.). In Table 3.2, we list group properties, $\Delta/n_{\rm members}$-values, and P-values for the groups with substructure, identified as the systems that have P-values of less than 1 per cent. In Table 3.3 we list the same values, but for groups without substructure, that is systems that have P-values greater than 1 per cent. Also, it should be noted that although we list the $\Delta/n_{\rm members}$ critical values in Tables 3.2 and 3.3, we rely on the P-values to identify substructure in our groups. In addition, Tables 3.2 and 3.3 lists the dynamical properties of the groups to be discussed in Sections 3.4.1 and 3.4.2. In Fig. 3.2, we plot both the intrinsic velocity dispersion of the group (top) and the total number of group members (bottom) versus the mean group redshift. Groups with and without substructure both span a wide range of velocity dispersions and group membership indicating that there is no apparent redshift bias with regards to group velocity dispersions or $n_{\rm members}$ for the DS Test.

Although the minimum membership cut needed to determine a reliable percentage of groups that contain substructure is $n_{\rm members} = 20$, we can still apply the DS Test to systems with fewer members and establish a lower limit on this fraction. Including groups with as few as ten members increases our sample size to 63 systems. Applying the same methodology described above we find that 11 of our 63 groups ($\sim$17 per cent) are identified as having significant ($>$ 99 per cent c.l.) substructure.

3.3.3 GEEC Groups with Substructure

We examine the GEEC groups classified as having substructure by the DS Test in detail to determine if we can identify the regions of localized substructure. By examining the available position and velocity information, we can find collections of galaxies that are kinematically distinct from the host group.

In the following analysis, we focus on small subgroups of galaxies that may be part of some localized substructure. This is done by looking at the δ_i histogram (Figs. 3.3(a) - 3.6(a)), velocity histograms (Figs. 3.3(b) - 3.6(b)), 'bubble-plots' (i.e. position plots of the group members weighted by $\exp \delta_i$ (Dressler & Shectman, 1988) (Figs. 3.3(c) - 3.6(c)) and group-centric radial

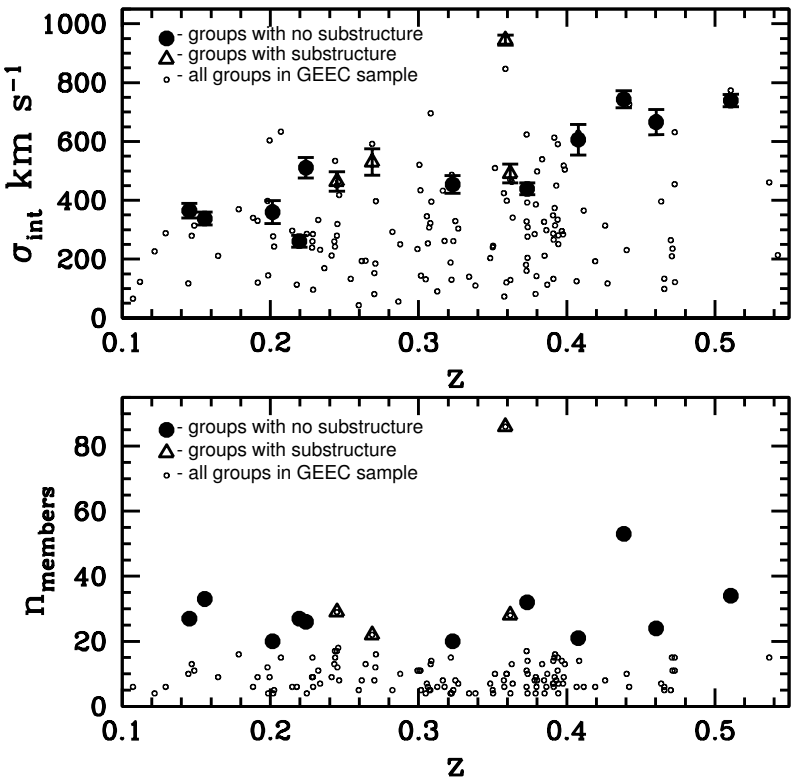

Figure 3.2: Top: Intrinsic velocity dispersion σ_{int} versus the group redshift for the galaxy groups in our sample. Solid circles indicate groups with no substructure and open triangles indicate groups with identified substructure according to the DS Test, at a 99 per cent confidence level. The smaller open circles represent the dispersions of all the groups in the GEEC catalogue, the majority of which are not used in this analysis. Our $n_{\rm members} \geq 20$ GEEC sample tend to have higher velocity dispersions. Bottom: $n_{\rm members}$ versus the group redshift for the galaxy groups in our sample. Symbols are the same as the plot above.

velocity (i.e. $cz_{\rm member} - cz_{\rm group}$) weighted position plots (Figs. 3.3(d) - 3.6(d)).

The δ_i and velocity histograms provide an estimate on the amount of substructure and the dynamical state of the groups. The δ_i histogram gives an overall view of the kinematic deviations and the velocity histogram can be used to identify non-Gaussian features, such as multiple peaks. In order to look for local regions of substructure, one must look at both the 'bubble-plot' and velocity weighted position plots in Figs. 3.3 - 3.6. The 'bubble-plots' allow for the visual identification of candidate regions of local substructure. Since the size of the symbols in the 'bubble-plot' scales with a galaxy's δ_i value, large symbols correspond to strong local kinematic deviations from the global values. Thus, a collection of neighbouring galaxies with similarly large symbols, such as region A in Fig. 3.5(c), could indicate a kinematically distinct system. In order to confirm that these candidate regions are truly distinct, one must check that the candidate substructure galaxies also have similar velocities, since the sign or direction of the galaxy velocity is not taken into account in the DS Test (Equation 3.1). To determine this, we look at the group-centric velocity weighted position plot to see if the candidate local substructure galaxies have similar velocities. In Figs. 3.3(d) to 3.6(d) the red symbols correspond to positive group-centric velocities (i.e. $cz_{\rm member} - cz_{\rm group} > 0$), blue symbols correspond to negative group-centric velocities (i.e. $cz_{\rm member} - cz_{\rm group} < 0$) and the symbol size scales with the magnitude of the velocity offset. We only identify galaxies as part of local substructure if neighbouring galaxies have similar large kinematic deviations, shown in the 'bubble-plots' *and* similar group-centric radial velocities, shown in the weighted position plots.

We will now discuss each of the four GEEC Groups with substructure in detail. Using the methodology described above, we search for candidate local regions of substructure in our sample. GEEC Group 25 (Fig. 3.3) has a collection of five galaxies, just south-east of the group centre, that all have high δ_i values and comparable velocities. Similarly in GEEC Group 208 there are seven galaxies that lie south-west of the group centre, with equally high δ_i values (Fig. 3.4(c)). Though, when we look at these same galaxies in the velocity weighted position plot (Fig. 3.4(d)), only five of these seven galaxies have comparable radial velocities. This result highlights the importance of looking at both the 'bubble-plot' and velocity weighted positions plots, as

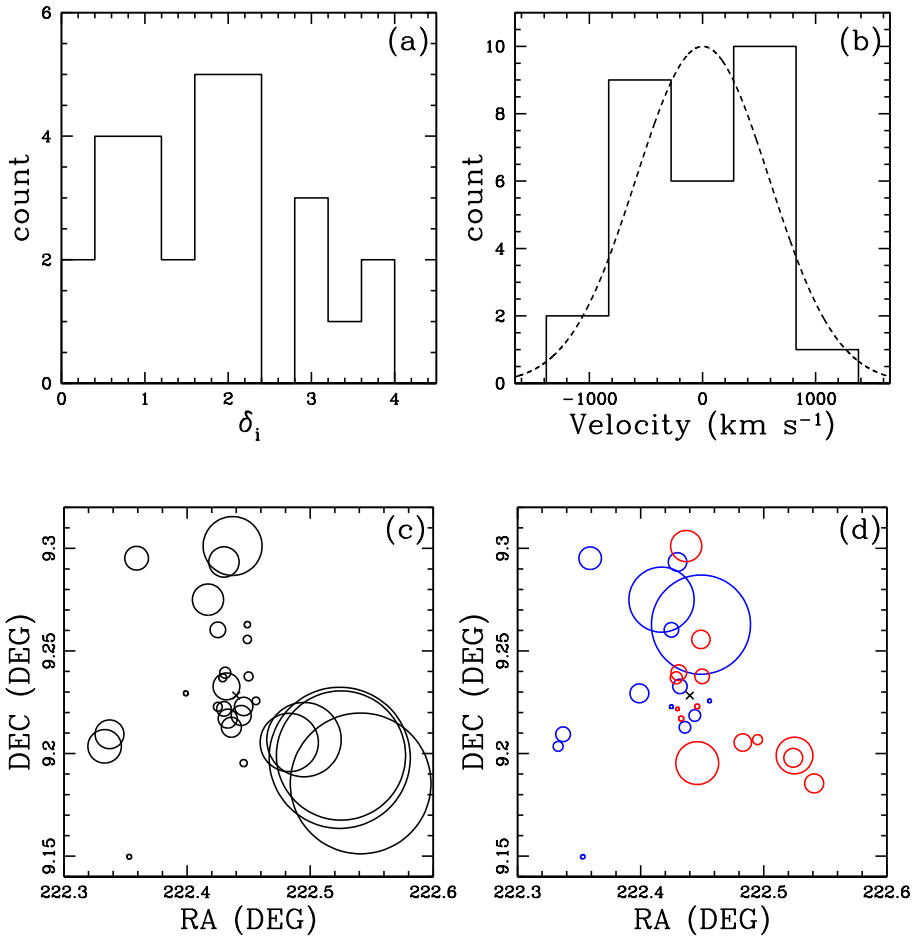

Figure 3.3: GEEC Group 25. (a): δ_i histogram. (b): Histogram of the velocity distribution, where the dashed-line indicates the best fitting Gaussian velocity dispersion. (c): Dressler & Shectman (1988) 'bubble-plot' where the galaxy symbols scale with $\exp(\delta_i)$. (d): Position plot where the galaxy symbols scale with group-centric velocity (i.e. $\exp\left(cz_{\rm member} - cz_{\rm group}\right)/350$), blue symbols correspond to galaxies with negative group-centric velocities (i.e. $cz_{\rm member} - cz_{\rm group} < 0$) and red symbols correspond to galaxies with positive group-centric velocities (i.e. $cz_{\rm member} - cz_{\rm group} > 0$).

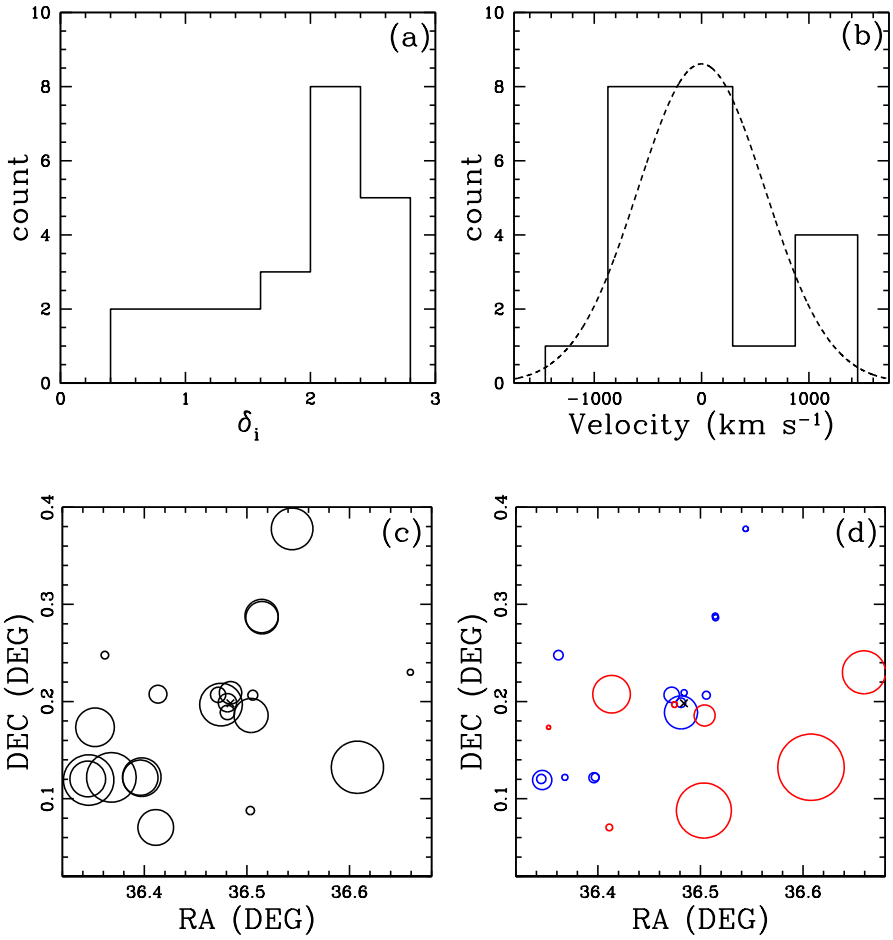

Figure 3.4: Same as Fig. 3.3 but for GEEC Group 208 and the velocity weighted plot now scales as $\exp\left(cz_{\rm member} - cz_{\rm group}\right)/400$.

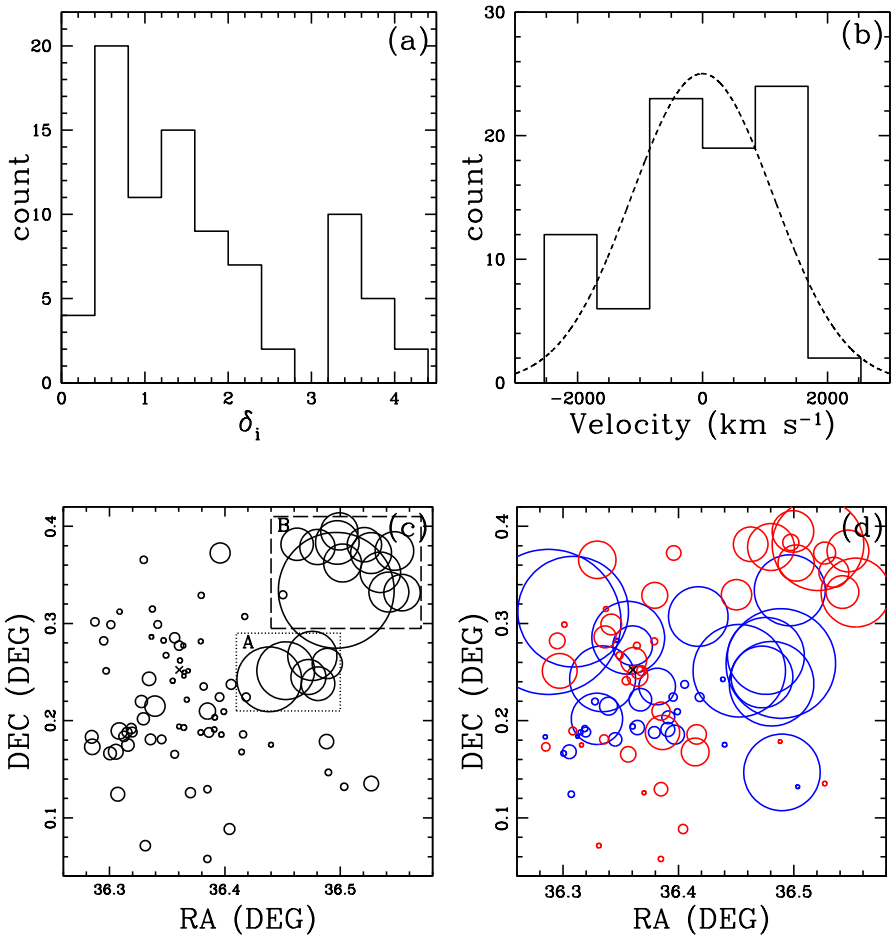

Figure 3.5: Same as Fig. 3.3 but for GEEC Group 226 and the velocity weighted plot now scales as $\exp\left(cz_{\rm member} - cz_{\rm group}\right)/600$. The dotted box encompasses the first identified region of local substructure (region A) and the long dashed box encompasses the second region of local substructure (region B).

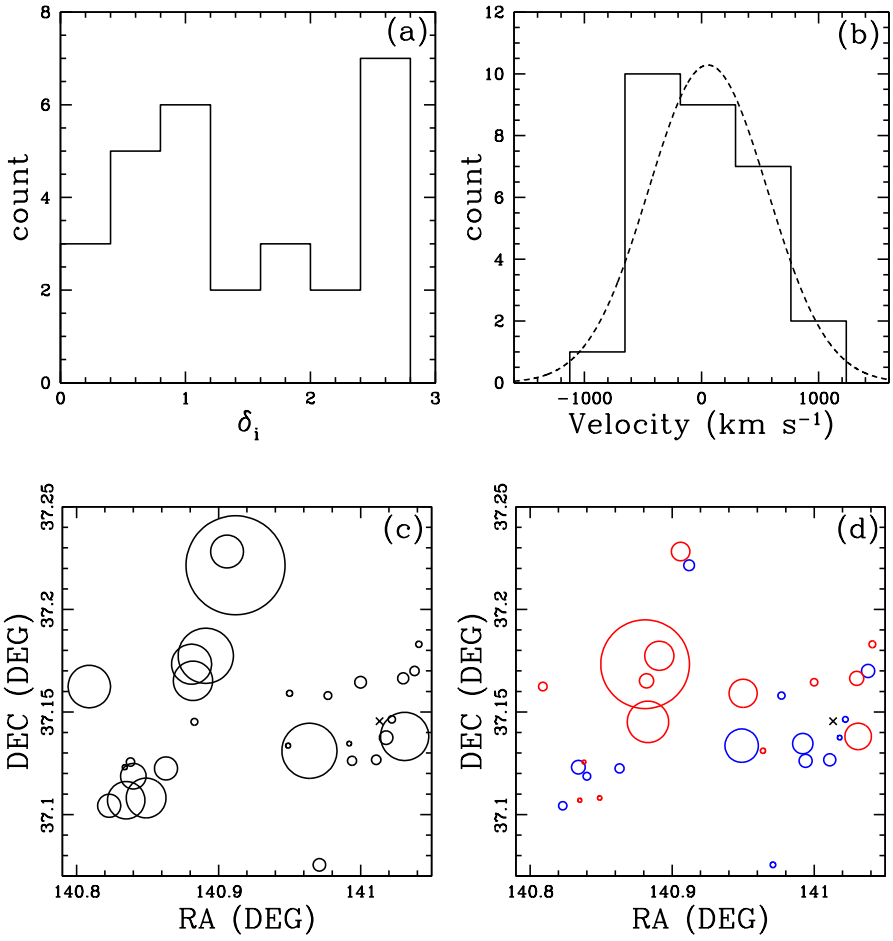

Figure 3.6: Same as Fig. 3.3 but for GEEC Group 320.

galaxies with large kinematic deviations may be correlated in position-space, but not in velocity-space.

In Fig. 3.5, we show the substructure analysis plots for GEEC Group 226 and from the 'bubble-plot' we see that there are two possibly distinct regions of localized substructure. The first region lies directly north-east of the group centre (region A in Fig. 3.5(c)) and includes the galaxy with the highest δ_i value. All of the members within this given substructure have similar radial velocities (Fig. 3.5(d)). The second region of interest contains eleven galaxies that lie in the very north-east corner of the 'bubble-plot' (region B in Fig. 3.5(c)). Again, all of the galaxies within this particular substructure have similar group-centric velocities, though in the opposite direction of the members in region A.

From the 'bubble-plot' of GEEC Group 320 (Fig. 3.6(c)), we see two possible regions of substructure; one just north-west of centre and another further south-west of centre. The structure near the group centre does not appear to be very localized, as the velocities, though in the same direction, have significantly different magnitudes (Fig. 3.6(d)). The second region of high δ_i values may actually be two separate structures. The velocity weighted position plot in Fig. 3.6(d) reveals that three of the galaxies in the structure have similar negative group-centric velocities (i.e. $cz_{\rm member} - cz_{\rm group} < 0$) and two have similar positive velocities (i.e. $cz_{\rm member} - cz_{\rm group} > 0$). Therefore, we identify the collection of three galaxies, with the negative group-centric radial velocities, as the best candidate of substructure within this system.

In each of the GEEC groups with substructure, it appears that our identified regions of localized substructure lie on the outskirts or edges of the group, and may either be infalling onto a pre-existing system or in the nearby large scale structure, but not necessarily bound or infalling. This result is in agreement with similar studies of substructure in local groups (Zabludoff & Mulchaey, 1998a) and clusters (West & Bothun, 1990).

It should also be noted that although the DS Test has been shown to be reliable for group-sized systems, the number of members within the substructure can affect the results of the statistic. As discussed in Section 3.2.2, and shown in more detail in the Appendix, fewer(more) true members of substructure can increase(decrease) the rate of false negatives. However, we also show that the

rate of false positives is consistently low for all of our mock groups (see Section 3.2.2). Thus, any detection of substructure in these systems is likely to be real.

3.3.4 Is the localized substructure gravitationally bound to the group?

The local regions of substructure we detect lie on the group outskirts and are possibly bound and infalling, or not bound, but close in large scale structure. In order to help distinguish between these two possibilities, we apply a simple bound test to estimate whether or not the regions of localized substructure are gravitationally bound to the host group. This is done by computing the limits for bound systems, using a variation of the virial theorem as discussed in Beers et al. (1982), and determining if the substructure falls within these limits. Beers et al. (1982) state that for a two-body system on a linear orbit, the Newtonian limit for gravitational binding, projected onto the sky is given by

$$V_r^2 R_p \leq 2GM \sin^2 \alpha \cos \alpha, \tag{3.5}$$

where,

$$V_r = V \sin \alpha, \quad R_p = R \cos \alpha, \tag{3.6}$$

and where α is the angle between the line joining the two-body system and the plane of the sky (see Fig. 7 of Beers et al., 1982), M is the *total* mass of the entire system (substructure plus host group), and R and V are the true (3-dimensional) positional and velocity separations between the two objects. V_r is the line-of-sight relative velocity between the two bodies and R_p is the projected separation, both of which are measurable quantities.

The unknown quantity in Equation 3.5 is the projection angle α. Thus, to compute the limit between bound and unbound systems, one must work in $\alpha - V_r$ space to determine the probability that the system is gravitationally bound for any given projection angle. This is achieved by setting $0° \leq \alpha \leq 90°$ and solving for V_r in Equation 3.5, producing a distinct line in $\alpha - V_r$ space that clearly separates bound and unbound solutions (Fig. 3.7). One can then compute the probability of a bound solution, for a given projection angle, using the $\alpha - V_r$ plot.

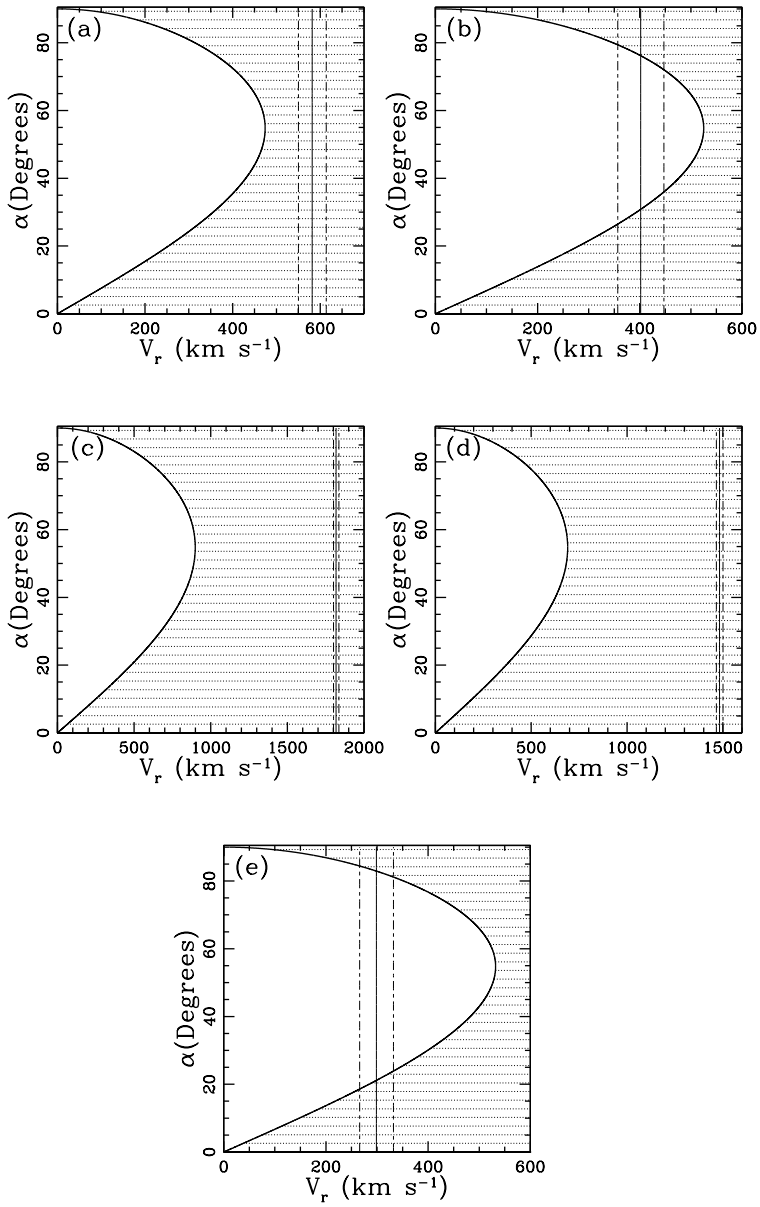

Figure 3.7: $\alpha - V_r$ plot for GEEC Groups (a) 25, (b) 208, (c) region A and the host group of 226, (d) region B and the host group of 226 (d) and (e) 320 . The unshaded regions correspond to bound solutions and shaded regions correspond to unbound solutions of the virial theorem given by Equation 3.5. The solid line corresponds to the measured value of V_r (i.e. the line-of-sight velocity difference between the substructure and host group centres). The dashed lines correspond to one-sigma deviations, taken to be the errors on the intrinsic velocity dispersion.

To apply this methodology to our group sample, we treat our identified regions of local substructure as one-body and the remaining galaxies as the second-body, which we refer to as the 'host' group. The total mass of the system is taken to be the virial mass, M_{200} (i.e. the total mass within a radius that encloses a mean density of 200 times the critical density of the Universe at the redshift of the galaxy), of the GEEC Groups as computed in Balogh et al. (2009) and given by

$$M_{200} = \frac{3^{3/2}\sigma^3}{G} \frac{1}{10H_0\,(1+z)^{1.5}}, \tag{3.7}$$

where σ is the measured intrinsic velocity dispersion. The measured V_r and R_p values are taken to be the distance between the R-band luminosity-weighted centres of the local substructure and the 'host' group centre, along the line-of-sight (V_r) and projected on the sky (R_p).

In Fig. 3.7, we plot the $\alpha - V_r$ plots for the five candidate regions of local substructure, as discussed in Section 3.3.3. The shaded regions indicate the areas spanned by unbound solutions, as given by Equation 3.5, the solid black vertical line is the measured value of V_r, and the long-short dashed vertical lines indicate one sigma deviations, taken to be the intrinsic velocity dispersion error.

Using the methodology described above and Fig. 3.7, we conclude that the identified local substructures in GEEC Groups 25 and 226 are not bound to the host group, while for GEEC Groups 208 and 320 the detected substructure is likely bound to the host group.

3.3.5 Substructure within 1 Mpc of the Group Centroid

In the previous section we analyzed a subset of 15 GEEC groups, with $n_{\rm members} \geq 20$, without applying any radial cuts. Here we apply a 1.0 Mpc cut, which is the suggested maximum virial radius for groups (Mamon, 2007), on the same subset of groups and re-apply the DS Test. Applying this radial cut, while still requiring a minimum number of 20 member galaxies, reduces our sample from 15 to 5 groups (GEEC Groups 110, 138, 226, 308 and 346). With this radial cut, we find that all 5 groups are identified as not having substructure

Table 3.4: Groups properties and DS statistics values for the GEEC Groups with a 1.0 Mpc radius cut

GEEC Group ID	$n^a_{\rm members}$	$\overline{\nu}$ km s^{-1}	σ_{int} km s^{-1}	P-value
110	26	-15.3	350	0.403
138	23	-226	730	0.792
226	25	-174	847	0.110
308	25	2.52	512	0.507
346	26	-80.4	434	0.128

[a]Group membership after the 1.0 Mpc radius cut

(see Table 3.4) according to the DS Test. The only group that was previously identified as having substructure, prior to the 1.0 Mpc cut, is GEEC Group 226. In Fig. 3.5, it is evident that although there are galaxies with relatively high δ_i values close to the group centre, the members with the highest δ_i values lie near the edge of the group. In fact the most significant feature in the 'bubble-plot' (Fig. 3.5) is on the top-right corner of the plot, far from the group centre.

If we include all of the groups with $n_{\rm members} \geq 10$ after a 1.0 Mpc radial cut, we find that 2 out 33 groups ($\sim$6 per cent) of our sample contains significant substructure. Again, we note that for systems with fewer than 20 members, the DS Test can only provide a lower limit on the amount of substructure present.

3.4 Correlations between Substructure and Other Indicators of Dynamical State

Having identified the GEEC groups that contain substructure, we can also look at other dynamical properties, i.e. the velocity distributions and velocity dispersion profiles (VDPs), to determine if there are any correlations with substructure.

3.4.1 Comparison with the Dynamical Classification of Velocity Distribution

If a correlation does exist between substructure and recent galaxy accretion, one would expect that the groups with substructure should also be dynamically complex, with perhaps non-Gaussian velocity distributions. In Hou et al. (2009), we established a classification scheme to distinguish between dynamically relaxed and complex groups. Using the Anderson-Darling (AD) goodness-of-fit test, we are able to determine how much a system's velocity distribution deviates from Gaussian. This is done by comparing the cumulative distribution function (CDF) of the ordered data, which in our case is the observed velocity distribution, to the model Gaussian empirical distribution function (EDF) using computing formulas given in D'Agostino & Stephens (1986). The AD statistic is then converted into a probability, or P-value, using results determined via Monte Carlo methods in Nelson (1998). A system is then considered to have a non-Gaussian velocity distribution if its computed P-value is less then 0.01 corresponding to a 99 per cent c.l.

We now apply this scheme to our sample of 15 GEEC groups, with $n_{\rm members} \geq 20$ and no radial cut, to compare the dynamical state with the detection of substructure[3]. The results of our dynamical classification scheme indicate that 8 of the 15 groups are classified as having non-Gaussian velocity distributions, at the 99 per cent c.l., and are thus dynamically complex (see Tables 3.2 and 3.3). Of the four GEEC groups with substructure only GEEC Group 320 shows a velocity distribution consistent with being Gaussian. Five groups, GEEC Groups 4, 38, 138, 238, and 346, are identified as being dynamically complex, but do not contain any substructure according to the DS Test.

Pinkney et al. (1996) found that different statistical tools (i.e. 1-D, 2-D and 3-D tests) probe the dynamical state of a system at varying epochs. Using N-body simulations, these authors determined that 1-D tests, such as the AD Test are most sensitive to scenarios when substructure passes through the core of the host group (i.e. core-crossing). During this time substructure can become spatially mixed within the host group, and if the substructure is loosely bound

[3]The dynamical classifications in this paper differ from those in Hou et al. (2009). The reason for this difference is that in Hou et al. (2009) we applied a 1.0 Mpc radius cut to the GEEC groups, whereas no radial cut is applied in this analysis.

then it may be difficult to detect with 3-D tests, such as the DS Test. Thus, groups with non-Gaussian velocity distributions may contain substructure that is missed by the DS Test.

3.4.2 Comparison with the Velocity Dispersion Profiles

In a study of the VDPs of galaxy clusters, Menci & Fusco-Femiano (1996) found a correlation between the efficiency of merger activity in the cluster core and the shape of the VDP, where actively interacting systems had strongly rising profiles. We presented a similar correlation for galaxy groups in Hou et al. (2009), where we found that groups classified as dynamically complex (i.e. non-Gaussian velocity distributions) also had rising VDPs. We now look at the VDPs of the current GEEC group sample to see if there is a similar relationship between the shape of the profile and the detection of substructure.

The VDPs are computed following the method outlined in Bergond et al. (2006). Unlike traditional methods of computing binned projected velocity dispersions this technique generates a smoothed VDP. This is done by using a 'moving window' prescription, which takes into account the contribution of every radial velocity measurement at each computed radius. The values are binned with an exponentially weighted moving window given by

$$w_i(R) = \frac{1}{\sigma_R} \exp\left[\frac{(R - R_i)^2}{2\sigma_R^2}\right] \tag{3.8}$$

where σ_R is the width of the window, which can be constant or a function of radius R, and the R_i's are the radial positions of the members of the system. The projected velocity dispersions are then defined as:

$$\sigma_p(R) = \sqrt{\frac{\sum_i w_i(R)(x_i - \bar{x})^2}{\sum_i w_i(R)}} \tag{3.9}$$

where the x_i's are the radial velocities and $\bar{x}$ is the mean velocity of the system.

We compute VDPs for our GEEC group sample and the profiles are shown in Fig. 3.8 using a widow width, σ_R, equal to one-third the maximum group radius. It should be noted that the projected velocity dispersions do not include any redshift or instrumental error corrections, so the intrinsic dispersion

values (Tables 3.2 and 3.3) are generally lower than the projected velocity dispersions.

Comparing the profiles of the groups with and without substructure, we find that all four GEEC groups identified as having substructure (Groups 25, 208, 226 and 320) also have strongly rising profiles. In contrast, almost all of the groups with no detected substructure, with the exception of GEEC Group 362, either have flat or generally decreasing VDPs, within the intrinsic velocity dispersion error. See Tables 3.2 and 3.3 for a description of the shape of the VDP for each GEEC group. Thus, we do indeed observe a correlation between detectable substructure and rising VDPs. As previously mentioned, studies of rich galaxy clusters suggest that a strongly increasing profile may be a signature of merger activity or galaxy interactions (Menci & Fusco-Femiano, 1996), but an alternative explanation of rising VDPs is the presence of subclumps with different mean velocities (Girardi et al., 1996; Barrena et al., 2007). In our case, it is likely that the increasing profile is being caused by the kinematically distinct substructure, which has a different mean velocity from the host group.

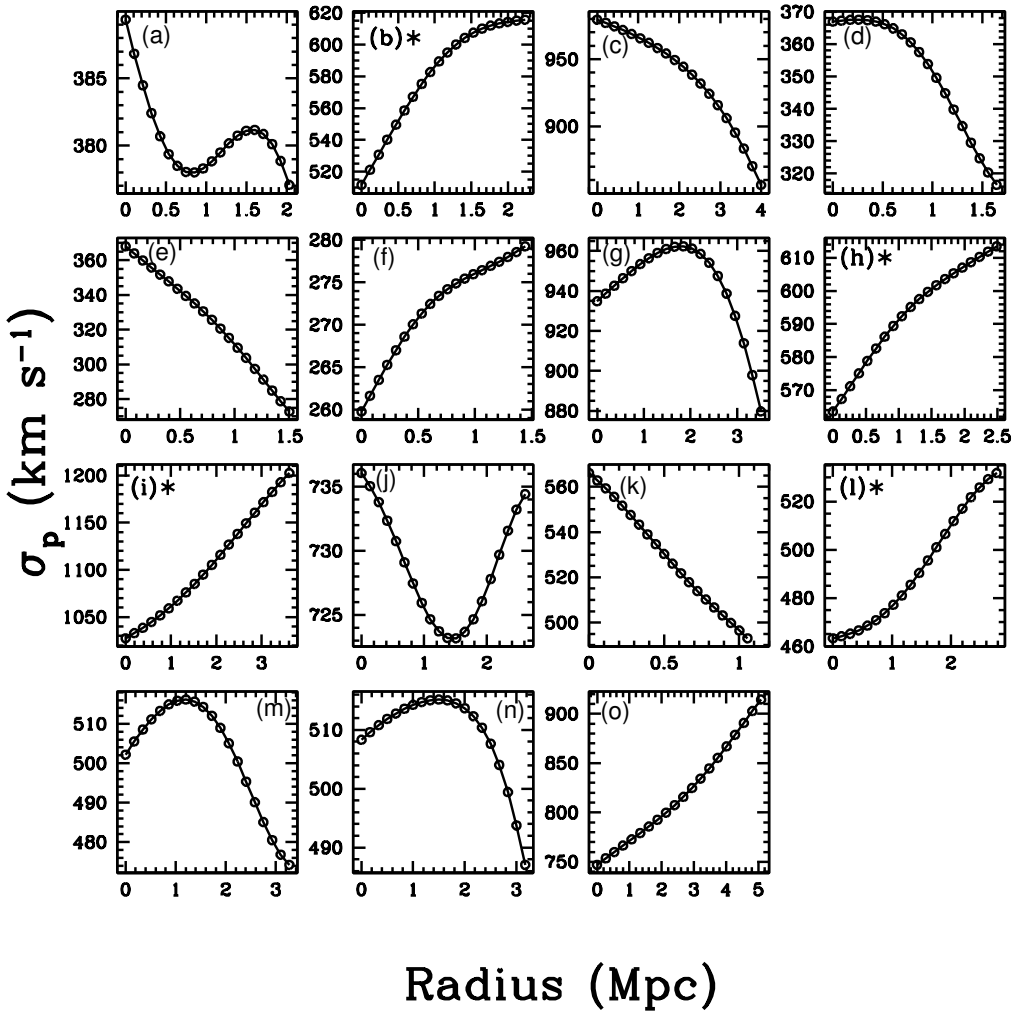

Figure 3.8: Velocity dispersion profiles (VDPs) for the GEEC Groups with $n \geq 20$: panel (a) Group 4, (b) Group 25, (c) Group 38, (d) Group 104, (e) Group 110, (f) Group 117, (g) Group 138, (h) Group 208, (i) Group 226, (j) Group 238, (k) Group 308, (l) Group 320, (m) Group 334, (n) Group 346 and (o) Group 362. The plots with asterisks in the top-left corner indicate groups that have been identified as having significant substructure. The intrinsic velocity dispersions, with errors, for each group can be found in Tables 3.2 and 3.3.

3.5 Correlations between Substructure and Galaxy Properties

Thus far, we have looked at possible correlations between substructure and other indicators of the dynamical state of a system. We now compare properties of the member galaxies to see if there are any differences between the galaxies in groups with and without substructure.

3.5.1 Substructure and Colour

In the following analysis we compare the ${}^{0.4}(g-r)$ colours, which have been corrected for galactic extinction and k-corrected to a redshift of $z = 0.4$ (Balogh et al., 2009), and blue fractions, f_b, for the groups with and without substructure.

In addition to extinction and k-corrections, we also apply a completeness correction to address the differing spectroscopic coverage. We apply magnitude weights that depend on whether the group had follow-up spectroscopy. The weights we apply are similar to those derived in Wilman et al. (2005), except we do not include any radial weights. We compute weights in r-band magnitude bins of 0.25, and up to a limit of $r = 22.0$, which is the limit of the unbiased Magellan spectroscopy. These weights are then applied to all of the member galaxies in our sample.

In Fig. 3.9 we show the completeness weighted ${}^{0.4}(g-r)$-histograms for the galaxies, with $r < 22.0$, in groups with substructure (solid line) and for those in groups with no detected substructure (dashed line). From this figure, it is clear that both histograms are bimodal with a distinct red sequence and blue cloud. Although both colour distributions have the expected bimodal shape, it is obvious that galaxies in the groups with and without substructure come from very different parent colour distributions. The groups with no identified substructure have a well populated red sequence, while the groups with substructure appear to have a much more dominant blue cloud. Results from a two-sample Kolmogorov-Smirnov (KS) Test on the unbinned ${}^{0.4}(g-r)$ distributions show that these two samples are distinct at the 99 per cent c.l.

We also plot colour distributions of the groups with and without substruc-

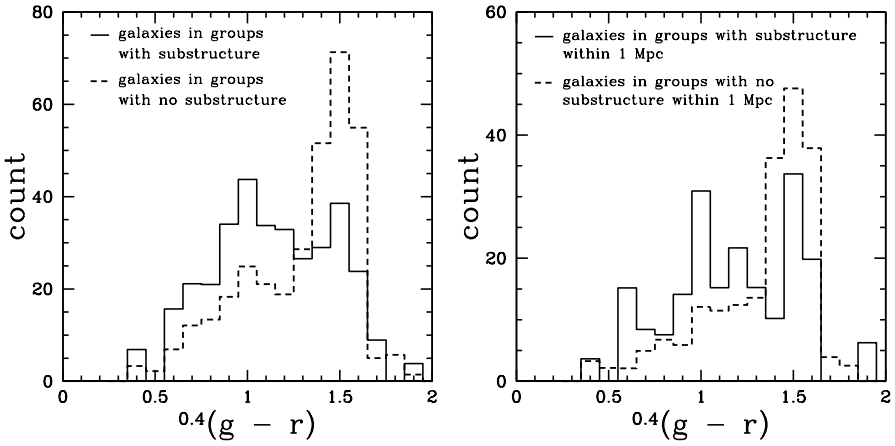

Figure 3.9: Left: $^{0.4}(g-r)$ colour histograms for the GEEC groups with substructure (solid line), which has be normalized to match the number count of the groups with no substructure and for the GEEC groups with no detectable substructure (dashed line). Both histograms have r-band magnitude based weights which have been computed to take into account the differing spectroscopic coverage between the original CNOC2 survey and the follow-up Magellan survey. Right: Same as figure on the left, expect a 1.0 Mpc radial cut has been applied to all groups in the sample.

ture with a 1.0 Mpc radial cut applied to all groups in our sample (Fig. 3.9: right). Although, the blue cloud for the groups with substructure in less populated when a radial cut is applied, it is still more populated than the groups without substructure and the two distributions are still statistically distinct. This result indicates that the increase in blue galaxies in the groups with substructure is not only coming from galaxies at radii greater than 1.0 Mpc. Our findings are similar to those of Ribeiro et al. (2010) who showed that there are many more red galaxies in dynamically evolved group systems, even out to 4 virial radii.

To obtain a more quantitative comparison we compute the fraction of blue galaxies within each sample. We take a multi-stage approach to determine the appropriate colour cut needed to distinguish between the red sequence and blue cloud. First, we apply an initial colour cut of $^{0.4}(g-r) = 1.2$, based on the minimum value in the colour distribution of all the member galaxies in our sample, shown in Fig. 3.10. We then determine a linear fit to all of the galaxies with $^{0.4}(g-r) > 1.2$ and set the colour cut to be one standard deviation below

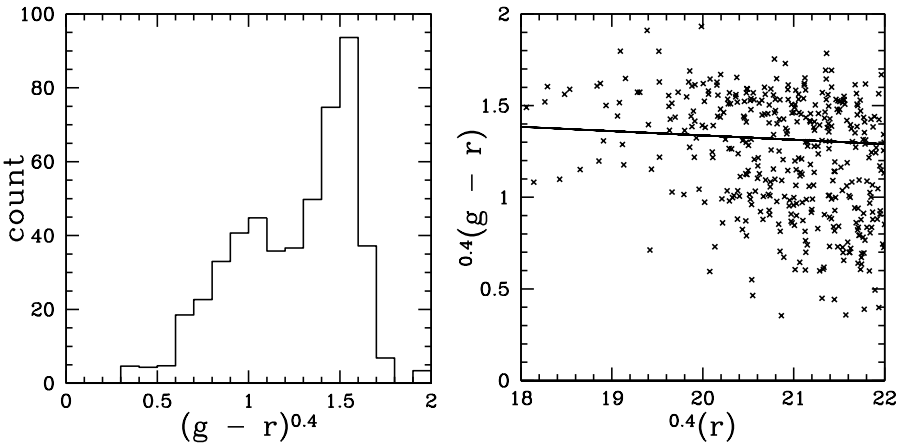

Figure 3.10: Left: Weighted ${}^{0.4}(g-r)$ histogram of all the member galaxies in our group sample. Right: ${}^{0.4}(g-r)$ versus r colour-magnitude diagram of all the galaxies in our sample, with no completeness correction. The solid line indicates the colour cut used to distinguish between the red sequence and the blue cloud.

the fit to the red sequence. The final colour cut is determined to be

$$ {}^{0.4}(g-r) = -0.0236({}^{0.4}r) + 1.810, \tag{3.10}$$

and is represented by the solid line in the colour-magnitude diagram shown in Fig. 3.10.

The blue fraction, f_b, is then computed as the ratio of galaxies with ${}^{0.4}(g-r)$ values that fall below Equation 3.10 to the total number of galaxies in the sample. The error in the blue fraction is computed using confidence intervals (CIs) derived from the beta distribution (Cameron, 2010). This method has been shown to more accurately determine CIs, especially for small samples, over traditional methods such as Poisson errors, which systematically underestimates the width of the CIs. We find that $f_b = 41\pm^{3}_{4}$ per cent for the groups without substructure and $f_b = 69\pm^{4}_{6}$ per cent for the groups with substructure. Thus, the groups with substructure have a significantly higher blue fraction, which is clear in the ${}^{0.4}(g-r)$-histograms of Fig. 3.9. We note that although these blue fractions are derived from weighted colour distributions, they are in agreement with the unweighted values,[4] suggesting that the applied magnitude

[4] $f_b = 44 \pm 4$ per cent for the groups without substructure and $f_b = 68\pm^{5}_{6}$ per cent for

weights do not affect the observed differences in colour.

In addition, we also compare the blue fractions of the individual galaxies identified as being part of the local substructure (see Section 3.3.3) to the other members of the group. We find that for the galaxies in the identified regions of localized substructure, $f_b \simeq 74\pm^{8}_{10}$ per cent, and for the galaxies not in the substructure, $f_b \simeq 50\pm^{3}_{4}$ per cent. This suggests that the observed increase in the blue fraction of groups with substructure is being enhanced by the galaxies in the identified regions of local substructure.

We now compare our groups with substructure sample to a sample of intermediate redshift field galaxies. In Fig. 3.11 we reproduce the ${}^{0.4}(g-r)$-histogram for the field galaxies in Fig. 6 of Balogh et al. (2009) (dashed line), summing up all of the counts in each of the quoted M_{K_s} bins in order to get the total colour distribution[5]. We also over-plot the colour histogram for the galaxies in groups with substructure, except we now apply an M_i magnitude cut in order to match the M_{K_s} range used in Balogh et al. (2009). Both the field galaxies in the Balogh et al. (2009) sample and the galaxies in our groups with substructure lack a prominent red sequence, and have well populated blue clouds. Despite subtle differences in the two colour histograms, a two-sample KS Test shows that the ${}^{0.4}(g-r)$ colours of the field galaxies and groups with substructure galaxies very likely come from the same parent distribution (P-value = 0.67).

Our blue fractions can be compared to those computed in the zCOSMOS survey, where Iovino & et al. (2010) determined the blue fractions of isolated and group galaxies at various redshifts in their sample. At a redshift of $z = 0.4$, Iovino & et al. (2010) found $f_b \sim 70$ per cent for isolated galaxies and $f_b \sim 45$ per cent for group galaxies[6]. From these results it is clear that our observed blue fraction of 69 per cent for the galaxies in groups with substructure is significantly higher than the observed zCOSMOS group sample, but is in agreement with their field sample. On other hand, the f_b values for our GEEC groups

the groups with substructure

[5]It should be noted that although only a fraction of our sample actually have measured M_{K_s} values, those that do span the entire range of magnitudes quoted in Fig. 6 of Balogh et al. (2009)

[6]We look at the Sample II of Iovino & et al. (2010), as this is the data-set that corresponds best to our GEEC sample.

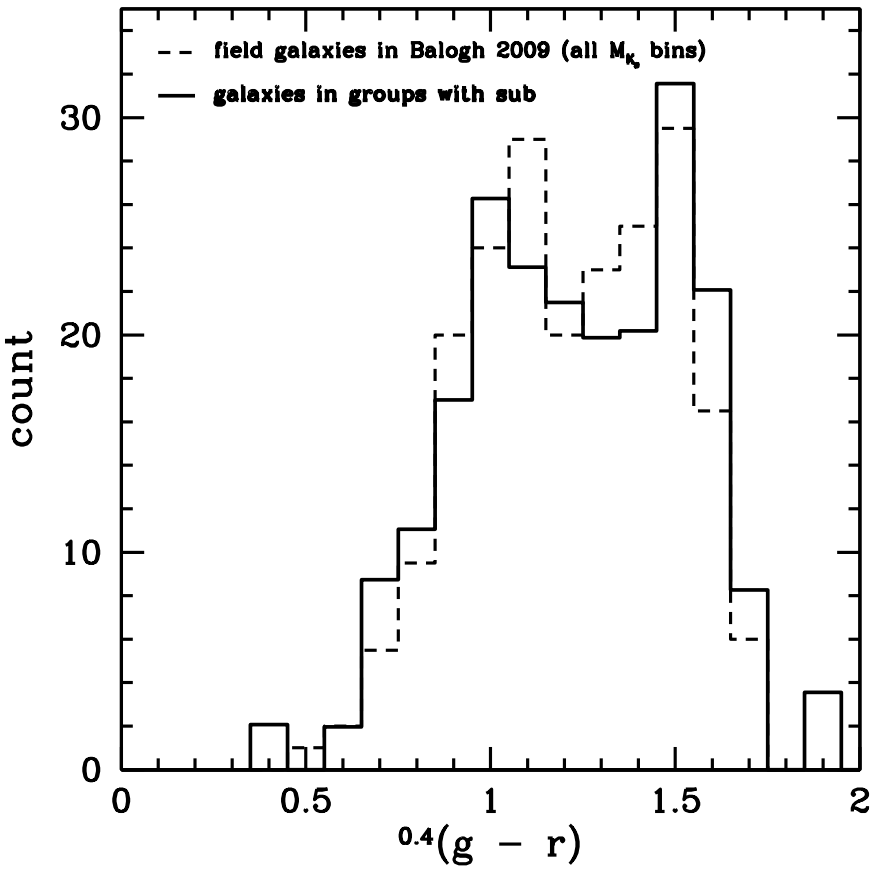

Figure 3.11: $^{0.4}(g-r)$ colour histograms for the GEEC groups with substructure (solid line) and for all of field galaxies in the GEEC groups found in Fig. 6 of Balogh et al. (2009) (dashed line). It should be noted that the colour distribution for the field galaxies is a sum of all the counts in each magnitude bin of Fig. 6 of Balogh et al. (2009), since our group galaxy sample covers the entire magnitude range. In addition, the group sample has been normalized to match the number count of the field sample.

with no substructure roughly agree with the zCOSMOS group sample.

3.5.2 Substructure as a Function of Colour, Stellar Mass and Star Formation Rates

In the previous sections we compared the $^{0.4}(g-r)$ colours of the galaxies in groups with substructure to those in groups with no detected substructure. Here we again compare the colours of the member galaxies but now as a function of stellar mass and specific star formation rate (defined as the ratio of the star formation rate to the stellar mass - SSFR). Additionally, we compare the SSFR distributions of the galaxies in groups with and without substructure. It should be noted that since only 3 of the 4 original CNOC2 fields were targeted with GALEX, the sample used in the following analysis contains fewer galaxies than used in the colour analysis of Section 3.4.3. In our sample of 15 ($n_{\rm members} \geq 20$) GEEC groups, 275 group galaxies have measured SFRs, stellar masses and colours, while 401 group members have well determined colours.

The stellar masses and star formation rates (SFRs) for the GEEC sample were obtained from spectral energy distribution (SED) template-fitting to all of the available photometry. Detailed discussion of the methodology is presented in McGee et al. (2011), but we give a brief summary here. The photometry used in the SED-fitting process typically included photometry in the K, i, r, g, u, NUV and FUV bands (see Balogh et al., 2009, for details of the GEEC photometry). The observed photometry was then compared to a large grid of model SEDs constructed using the Bruzual & Charlot (2003) stellar population synthesis code and assuming a Chabrier initial mass function. Following the methodology of Salim & et al. (2007), McGee et al. (2011) created a grid of models that uniformly sampled the allowed parameters of formation time, galaxy metallicity, and the two-component dust model of Charlot & Fall (2000). The star formation history was modelled as an exponentially declining base rate with random bursts of star formation of varying duration and relative strength. The model magnitudes were obtained by convolving these model SEDs with the observed photometric bandpasses at nine redshifts between 0.25 and 0.60. χ^2-minimization was then performed by summing over

all of the models and taking into account the observed uncertainty on each point. The one sigma uncertainties in stellar mass, when compared to both mock groups and other independent estimates, are on the order of 0.15 dex and the SFRs have been averaged over the last 100 Myr (McGee et al., 2011). It should be noted that there may be additional systematic uncertainties due to, for example, the Initial Mass Function assumed in the fitting procedure.

In Fig. 3.12 we show ${}^{0.4}(g-r)$ versus stellar mass for the field galaxies (black dots), galaxies in groups with substructure (closed blue circles), galaxies in groups with no identified substructure (closed magenta circles) and the galaxies identified as being part of local substructure (open green squares). The dotted red vertical line in Fig. 3.12 represents the stellar mass limit of $1.4 \times 10^{10} \mathrm{M}_{\odot}$ at the median redshift ($z \sim 0.3$) in the GEEC group sample (McGee et al., 2011). It should be noted that this stellar mass limit shifts to lower(higher) masses for groups at lower(higher) redshifts. From Fig. 3.12, it is clear that the galaxies in groups with substructure lie preferentially along the blue cloud, as discussed in Section 3.4.3, but we also see that these galaxies span a similar mass range as the galaxies in groups with no identified substructure. A two-sample KS Test of the stellar mass distributions of the galaxies with and without substructure shows that the two distributions likely come from the same parent distribution (P-value = 0.55). The similar stellar mass distribution of the two populations tells us that the DS Test does not simply detect substructure in groups which are probed further down the stellar mass function.

Now we examine the SSFRs for groups with and without substructure. Following McGee et al. (2011), we define actively star-forming galaxies to have $\log_{10}(\mathrm{SFFR}) > -11$ and the fraction of actively star-forming galaxies to be $f_{\mathrm{active}} = n_{\mathrm{actively\ star\text{-}forming\ galaxies}}/n_{\mathrm{total}}$. We find that for galaxies in groups with substructure $f_{\mathrm{active}} = 63 \pm 8$ per cent and for groups with no detected substructure $f_{\mathrm{active}} = 49^{+6}_{-5}$ per cent. These active fractions agree with the blue fractions found in Section 3.5.1.

Both blue and active fractions are used as independent indicators of quiescent versus actively star-forming galaxies. However, colour and SSFR probe significantly different timescales, and might be telling us something different about the star formation history of galaxies. For instance, a dust enshrouded star-forming galaxy would be classified as 'red', and therefore quiescent, based

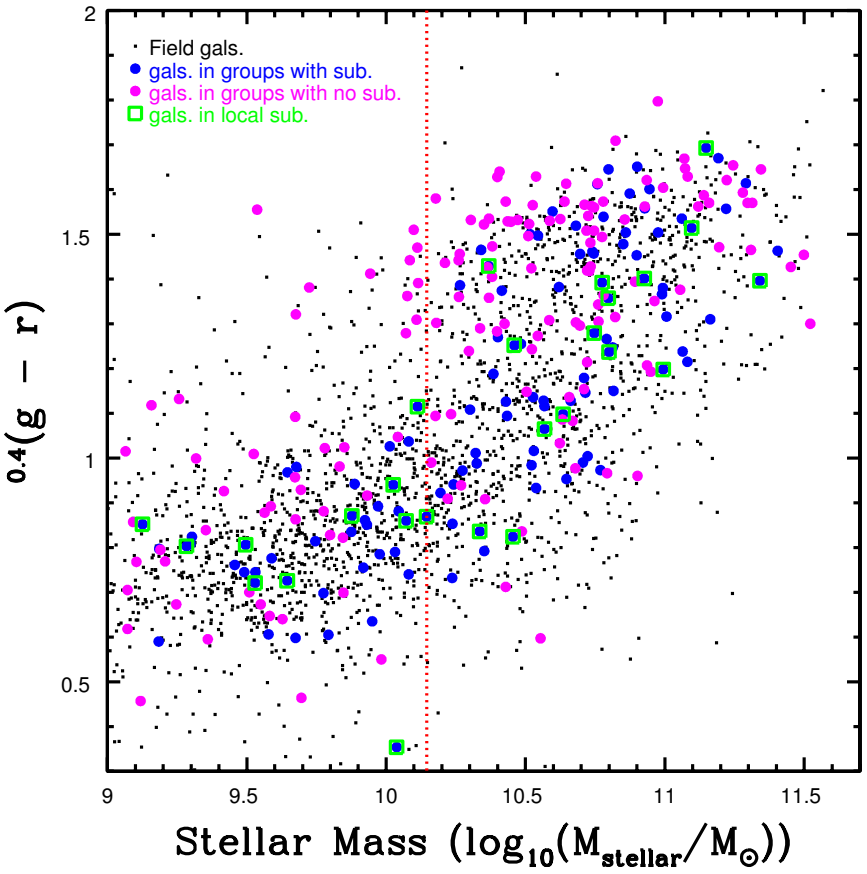

Figure 3.12: $^{0.4}(g-r)$ versus stellar mass for field galaxies (black dots), galaxies in groups with substructure (blue circles), galaxies in groups with no substructure (magenta circles) and galaxies identified as part of localized substructure (green squares). The red dotted line indicates the stellar mass limit ($M_{stellar} = 1.4 \times 10^{10} M_{\odot}$) at median redshift ($z \sim 0.3$) of the GEEC sample.

on colour but would be classified as actively star-forming based on SSFR. A better approach is to look at colour and SSFR simultaneously (Weinmann et al., 2006). We follow this approach in Fig. 3.13 where we plot $^{0.4}(g-r)$ versus SSFR for all the galaxies in our sample (top) and with a $M_{stellar} > 1.4\times10^{10}M_{\odot}$ cut applied to the sample (bottom). The colour scheme is the same as in Fig. 3.12, except the red dotted line now corresponds to the division between actively star-forming and quiescent/passive galaxies. From Fig. 3.13, we can see that there is a correlation between colour and SSFR with two well populated regions of the plot that correspond to 'red and passive' and 'blue and active' galaxies, where active refers strictly to actively star-forming galaxies. In Table 3.5, we list the percentage of all galaxies in our sample that populate each region of the colour-SSFR space in Fig. 3.13 with errors computed using the methodology described in Cameron (2010). Similarly, Table 3.6 lists the same information but for galaxies above the stellar mass completeness limit of $1.4 \times 10^{10}M_{\odot}$. From these tables we see that the galaxies in groups with substructure have significantly more blue and actively star-forming galaxies than groups with no substructure, though slightly less than the fraction observed in the field. This result indicates that environmentally driven mechanisms of star-formation quenching are not as efficient in groups with observed substructure. We note that although the percentages within each region of colour-SSFR space differ between the whole versus stellar mass limited sample, the general trends remain the same. Since the mass-selected sample only includes galaxies with the highest stellar masses, we expect a decrease in the 'blue and active' region due to stellar mass trends (i.e. higher mass galaxies are preferentially more red and passive: Iovino & et al., 2010; Peng & et al., 2010).

While the majority of galaxies are either 'red and passive' or 'blue and active', a non-negligible fraction appear to lie in the other two regions of Fig. 3.13. Even if we take into account the small uncertainties in colour (typically 0.02 mags) and the uncertainties in SSFR (McGee et al., 2011, quote one sigma errors on the order of 0.25 dex), a measurable fraction of galaxies still remain in these two regions. From Table 3.5, we see that $\sim$9 per cent of all galaxies in the field and group samples reside in the 'blue and passive' region. This value is higher than the $\sim$1.1 per cent observed by Weinmann et al. (2006), though appears similar to the results of Lara-López et al. (2010).

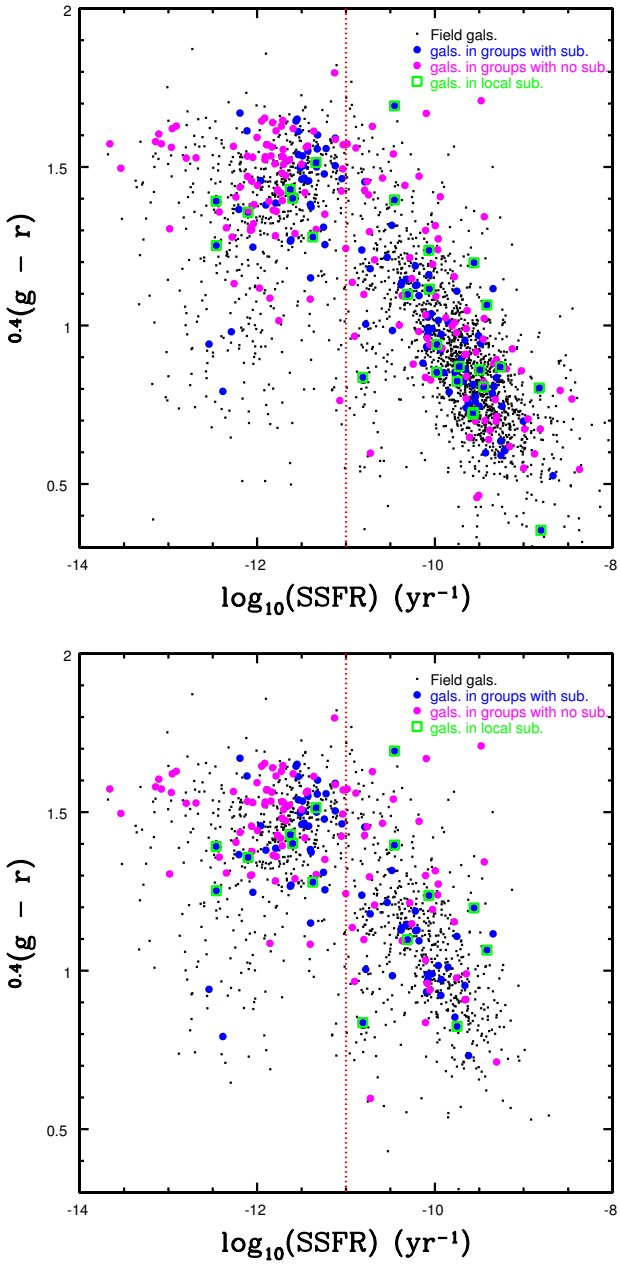

Figure 3.13: Top: $^{0.4}(g-r)$ versus specific star formation rate (SSFR) for field galaxies (black dots), galaxies in groups with substructure (blue circles), galaxies in groups with no substructure (magenta circles) and galaxies identified as part of localized substructure (green squares). The red dotted line at $\log_{10}(\mathrm{SFFR})$ yr^{-1} indicates the division between active ($\log_{10}(\mathrm{SFFR}) > -11$ yr^{-1}) and passive ($\log_{10}(\mathrm{SFFR}) < -11$ yr^{-1}) galaxies determined in McGee et al. (2011). Bottom: Same as figure on the left except with a $\mathrm{M_{stellar}} > 1.4 \times 10^{10}\mathrm{M_{\odot}}$ stellar mass cut applied.

Note that both these results are based on SDSS galaxies. Although we do observe a substantial population of 'blue and passive' galaxies in Fig. 3.13, we acknowledge that obtaining accurate measures of SSFR for galaxies with low SFRs is notoriously difficult. As discussed in McGee et al. (2011) the errors in the measured SSFRs increase for galaxies with lower values and some of these galaxies may have underestimated SSFRs.

The final region of the ${}^{0.4}(g-r)$-SSFR plot in Fig. 3.13 corresponds to 'red and active' galaxies. While this population is negligible for the groups with substructure sample and small for the field sample (see Table 3.5), it contains $\sim 11 \pm^{4}_{3}$ per cent of the galaxies in the groups with no detected substructure and $\sim 14 \pm^{6}_{4}$ for the stellar mass limited sample. Although this population may be a result of dusty star-forming galaxies or edge-on discs with strong extinction, it seems unlikely that these galaxies would preferentially be found in groups with no substructure. An alternative explanation is that this population could be the 'transition' galaxies observed by Wolf (2009). These galaxies are still star-forming but at a lower rate ($\sim$4 times) than the field and have more obscured star formation resulting in weak optical signatures (i.e. not blue). A population of 'transition' galaxies could explain why there are more 'red and active' galaxies in groups with no substructure, as a relaxed system could contain galaxies that are being quenched but have not had their star formation completely cut off.

3.5.3 Implications of the Observed Properties of Groups with Substructure

The field-like colour distribution of the groups with substructure and the fact that the substructure galaxies are found in the group outskirts may have implications for the nature of environmental effects in galaxy evolution. It is well known that the properties of galaxies depend, at least in some part, on their local environment (Postman & Geller, 1984; Dressler et al., 1997). Galaxies that reside in dense environments, such as groups or clusters, generally experience some form of star-formation attenuation due to processes such as ram pressure stripping (Gunn & Gott, 1972; Abadi et al., 1999; Quilis et al., 2000), strangulation (Larson et al., 1980; Balogh et al., 2000; Kawata & Mulchaey,

Table 3.5: Percentage of all galaxies in our sample within a given region of $^{0.4}(g-r)$ versus SSFR space

$^{0.4}(g-r)$-SSFR region	Galaxies in groups with substructure	Galaxies in groups with no substructure	Field galaxies
red and passive[a]	28 ± 6	$42\pm^{5}_{6}$	17 ± 1
red and active[b]	$3\pm^{3}_{2}$	$11\pm^{4}_{3}$	4 ± 1
blue and passive	$9\pm^{4}_{3}$	$9\pm^{4}_{3}$	$9\pm^{2}_{1}$
blue and active	$60\pm^{7}_{6}$	$38\pm^{6}_{5}$	$70\pm^{2}_{1}$

[a]Passive denotes quiescent galaxies with $\log_{10}(\mathrm{SFFR}) < -11$ yr^{-1}

[b]Active refers to actively star-forming galaxies with $\log_{10}(\mathrm{SFFR}) > -11$ yr^{-1}

Table 3.6: Same as Table 3.5 except for galaxies above the stellar mass completeness limit of $\mathrm{M_{stellar}} > 1.4 \times 10^{10}\mathrm{M_{\odot}}$

$^{0.4}(g-r)$-SSFR region	Galaxies in groups with substructure	Galaxies in groups with no substructure	Field galaxies
red and passive	42 ± 8	57 ± 7	33 ± 2
red and active	$4\pm^{5}_{2}$	$14\pm^{6}_{4}$	8 ± 1
blue and passive	$13\pm^{7}_{4}$	$8\pm^{5}_{3}$	11 ± 1
blue and active	$41\pm^{8}_{7}$	$21\pm^{6}_{5}$	48 ± 2

2008) or mergers and interactions (Toomre & Toomre, 1972; Brough et al., 2006). However, the precise details of the galaxy transformation process (i.e. exactly when and where quenching occurs, which mechanisms dominate in the different environment, etc.) are still unclear.

Our substructure analysis in the GEEC groups suggests that the identified local substructure in our sample, which in some cases appears to be infalling, do not feel any strong environmental effects from the host group. The observed colours and SSFR's of the galaxies in groups with substructure are significantly more blue, active and remarkably field-like when compared to galaxies in groups with no substructure. This suggests that an enhanced fraction of red galaxies - either/both via the suppression of star formation or/and dust obscuration - only happens in relaxed groups with no detected substructure. Thus, any environmental effects felt by infalling substructure galaxies do not likely occur until well inside the group potential.

Recent studies of star-formation as a function of group- or cluster-centric radius have produced conflicting results with regards to the radius at which

environmental effects become observable. Similar to our results, Wetzel et al. (2011) conclude that galaxies do not show suppressed star formation outside the virial radius. In contrast, von der Linden et al. (2010) state that suppressed star formation could be detected in SDSS clusters out to $\sim$ several virial radii. Such differences are likely sensitive to group or cluster finding algorithms as well as membership assignment.

In a study of the effects of environment on the colours of galaxies in the SDSS survey, Wilman et al. (2010) take a different approach to classifying environment. Rather than using a catalog derived from a group-finding algorithm, these authors parametrize the environment using non-overlapping annular measurements of density on independent scales, allowing for comparison of environmental effects at various radii. Based on their analysis, Wilman et al. (2010) concluded that the fraction of red galaxies correlated with local density only up to scales of $\sim$1 Mpc, which is similar to our results, as well as those of Wetzel et al. (2011). Though numerous and independent analyses of environmental effects on galaxy evolution seem to indicate that star-formation truncation does not occur until galaxies are well-inside the group/cluster potential, there are studies that suggest the contrary. Clearly more work, both observational and theoretical, is needed to better understand when and where environmental effects become observable.

3.6 Conclusions

We have studied the Dressler-Shectman Test for substructure to determine the sensitivity and reliability of this test for group-sized systems. Using mock groups with and without substructure, generated using Monte Carlo methods, we find that the DS Test can reliably be applied to groups with more than 20 members, *if* the probabilities, or P-value, method is used with a high confidence level of 99 or 95 per cent. We also find that for groups with $10 \leq n_{\rm members} < 20$, the DS Test cannot detect all of the substructure within a system, but it can be used to determine a reliable *lower limit* on the amount of substructure.

Of the 15 rich GEEC groups, with a velocity dispersion range of $\sim$260-950 km s^{-1} and $20 < n_{\rm members} < 90$, we find that 4 groups are identified

as having significant substructure. Further analysis indicates that 2 of these systems, GEEC Groups 208 and 320, likely have gravitationally bound local substructure that lies on the group outskirts and could be accreting onto the system.

We then looked at various dynamical and galaxy properties to search for correlations with the presence of substructure. The main results of this analysis are;

1. The majority of groups with detected substructure also have non-Gaussian velocity distributions;

2. The shape of a group's velocity dispersion profile (VDP) correlates with the detection of substructure, where GEEC groups with substructure have rising profiles;

3. The ${}^{0.4}(g-r)$ colour distributions of the groups with and without substructure are found to be significantly different, and the colour distribution for the galaxies in groups with substructure is similar to the field distribution;

4. Groups with substructure have a significantly higher fraction of blue galaxies, as do the galaxies within identified regions of localized substructure;

5. Groups with substructure have a larger fraction of actively star-forming galaxies ($\log_{10}(\mathrm{SFFR}) > -11$ yr^{-1}), when compared to groups with no identified substructure;

6. There is a measurable fraction of galaxies that populate the 'red and active' region of ${}^{0.4}(g-r)$-SSFR space and we find that this fraction is significantly higher in groups with no substructure for both the whole and stellar mass limited samples.

In conclusion, we find that a considerable fraction of intermediate redshift galaxy groups contain significant substructure, which suggests that like massive clusters, groups grow hierarchically through the accretion of smaller structures. The field-like colour distribution and measured SSFRs of the galaxies

in groups with substructure, combined with the location of the substructure, suggests that these galaxies are not experiencing any form of environment-related star-formation quenching. To fully understand the results presented here within the context of galaxy evolution will require the use of sophisticated modelling. To this end we plan to duplicate this analysis on a sample of semi-analytic groups obtained from GALFORM simulations (Bower et al., 2006) and compare these with our observational results. With this we hope to be able to better understand the nature of substructure identified by the DS Test.

3.7 Acknowledgments

We would like to thank the CNOC2 team for the use of unpublished redshifts. A.H, L.C.P, and W.E.H would like to thank the National Science and Engineering Research Council of Canada (NSERC) for funding.

Bibliography

Abadi, M. G., Moore, B., & Bower, R. G. 1999, MNRAS, 308, 947

Balogh, M. L., McGee, S. L., Wilman, D., Bower, R. G., Hau, G., Morris, S. L., Mulchaey, J. S., Oemler, Jr., A., Parker, L., & Gwyn, S. 2009, MNRAS, 398, 754

Balogh, M. L., McGee, S. L., Wilman, D. J., Finoguenov, A., Parker, L. C., Connelly, J. L., Mulchaey, J. S., Bower, R. G., Tanaka, M., & Giodini, S. 2011, MNRAS, 412, 2303

Balogh, M. L., Navarro, J. F., & Morris, S. L. 2000, ApJ, 540, 113

Barrena, R., Boschin, W., Girardi, M., & Spolaor, M. 2007, A&A, 469, 861

Beers, T. C., Geller, M. J., & Huchra, J. P. 1982, ApJ, 257, 23

Bergond, G., Zepf, S. E., Romanowsky, A. J., Sharples, R. M., & Rhode, K. L. 2006, A&A, 448, 155

Berlind, A. A. & et al. 2006, ApJS, 167, 1

Bird, C. 1994a, ApJ, 422, 480

Bird, C. M. 1994b, AJ, 107, 1637

Böhringer, H., Pratt, G. W., Arnaud, M., Borgani, S., Croston, J. H., Ponman, T. J., Ameglio, S., Temple, R. F., & Dolag, K. 2010, A&A, 514, A32+

Bower, R. G., Benson, A. J., Malbon, R., Helly, J. C., Frenk, C. S., Baugh, C. M., Cole, S., & Lacey, C. G. 2006, MNRAS, 370, 645

Brough, S., Forbes, D. A., Kilborn, V. A., & Couch, W. 2006, MNRAS, 370, 1223

Bruzual, G. & Charlot, S. 2003, MNRAS, 344, 1000

Burgett, W. S. & et al. 2004, MNRAS, 352, 605

Cameron, E. 2010, ArXiv e-prints

Carlberg, R. G., Yee, H. K. C., Morris, S. L., Lin, H., Hall, P. B., Patton, D. R., Sawicki, M., & Shepherd, C. W. 2001, ApJ, 552, 427

Charlot, S. & Fall, S. M. 2000, ApJ, 539, 718

Colless, M. & Dunn, A. M. 1996, ApJ, 458, 435

D'Agostino, R. & Stephens, M. 1986, Goodness-of-fit Techniques (Marcel Dekker Inc.)

Diemand, J., Kuhlen, M., Madau, P., Zemp, M., Moore, B., Potter, D., & Stadel, J. 2008, Nature, 454, 735

Dressler, A., Oemler, Jr., A., Couch, W. J., Smail, I., Ellis, R. S., Barger, A., Butcher, H., Poggianti, B. M., & Sharples, R. M. 1997, ApJ, 490, 577

Dressler, A. & Shectman, S. A. 1988, AJ, 95, 985

Efron, B. 1982, The Jackknife, the Bootstrap and other resampling plans

Eke, V. R., Baugh, C. M., Cole, S., Frenk, C. S., King, H. M., & Peacock, J. A. 2005, MNRAS, 362, 1233

Finoguenov, A., Connelly, J. L., Parker, L. C., Wilman, D. J., Mulchaey, J. S., Saglia, R. P., Balogh, M. L., Bower, R. G., & McGee, S. L. 2009, ApJ, 704, 564

Firth, P., Evstigneeva, E. A., Jones, J. B., Drinkwater, M. J., Phillipps, S., & Gregg, M. D. 2006, MNRAS, 372, 1856

Geller, M. J. & Huchra, J. P. 1983, ApJS, 52, 61

Girardi, M., Demarco, R., Rosati, P., & Borgani, S. 2005, A&A, 442, 29

Girardi, M., Fadda, D., Giuricin, G., Mardirossian, F., Mezzetti, M., & Biviano, A. 1996, ApJ, 457, 61

Gunn, J. E. & Gott, III, J. R. 1972, ApJ, 176, 1

Hou, A., Parker, L. C., Harris, W. E., & Wilman, D. J. 2009, ApJ, 702, 1199

Iovino, A. & et al. 2010, A&A, 509, A40+

Katz, N. & White, S. D. M. 1993, ApJ, 412, 455

Kawata, D. & Mulchaey, J. S. 2008, ApJ, 672, L103

Knebe, A. & Müller, V. 2000, A&A, 354, 761

Lacey, C. & Cole, S. 1993, MNRAS, 262, 627

Lara-López, M. A., Bongiovanni, A., Cepa, J., Pérez García, A. M., Sánchez-Portal, M., Castañeda, H. O., Fernández Lorenzo, M., & Pović, M. 2010, A&A, 519, A31+

Larson, R. B., Tinsley, B. M., & Caldwell, C. N. 1980, ApJ, 237, 692

Mamon, G. A. 2007, in Groups of Galaxies in the Nearby Universe, ed. I. Saviane, V. D. Ivanov, & J. Borissova, 203–+

McGee, S. L., Balogh, M. L., Wilman, D. J., Bower, R. G., Mulchaey, J. S., Parker, L. C., & Oemler, A. 2011, MNRAS, 413, 996

Menci, N. & Fusco-Femiano, R. 1996, ApJ, 472, 46

Moore, B., Katz, N., & Lake, G. 1996, ApJ, 457, 455

Nelson, L. 1998, Journal of Quality Technology, 30, 298

Peng, Y.-j. & et al. 2010, ApJ, 721, 193

Pinkney, J., Roettiger, K., Burns, J. O., & Bird, C. M. 1996, ApJS, 104, 1

Postman, M. & Geller, M. J. 1984, ApJ, 281, 95

Press, W. H. & Schechter, P. 1974, ApJ, 187, 425

Quilis, V., Moore, B., & Bower, R. 2000, Science, 288, 1617

Ramella, M., Biviano, A., Pisani, A., Varela, J., Bettoni, D., Couch, W. J., D'Onofrio, M., Dressler, A., Fasano, G., Kjørgaard, P., Moles, M., Pignatelli, E., & Poggianti, B. M. 2007, A&A, 470, 39

Ribeiro, A. L. B., Lopes, P. A. A., & Trevisan, M. 2010, MNRAS, 409, L124

Salim, S. & et al. 2007, ApJS, 173, 267

Silverman, B. W. 1986, Density estimation for statistics and data analysis

Solanes, J. M., Salvador-Solé, E., & González-Casado, G. 1999, A&A, 343, 733

Springel, V., Wang, J., Vogelsberger, M., Ludlow, A., Jenkins, A., Helmi, A., Navarro, J. F., Frenk, C. S., & White, S. D. M. 2008, MNRAS, 391, 1685

Springel, V., White, S. D. M., Jenkins, A., Frenk, C. S., Yoshida, N., Gao, L., Navarro, J., Thacker, R., Croton, D., Helly, J., Peacock, J. A., Cole, S., Thomas, P., Couchman, H., Evrard, A., Colberg, J., & Pearce, F. 2005, Nature, 435, 629

Summers, F. J., Davis, M., & Evrard, A. E. 1995, ApJ, 454, 1

Taylor, J. E. & Babul, A. 2004, MNRAS, 348, 811

Toomre, A. & Toomre, J. 1972, ApJ, 178, 623

Tyler, K. D., Rieke, G. H., Wilman, D. J., McGee, S. L., Bower, R. G., Bai, L., Mulchaey, J. S., Parker, L. C., Shi, Y., & Pierini, D. 2011, ApJ, 738, 56

von der Linden, A., Wild, V., Kauffmann, G., White, S. D. M., & Weinmann, S. 2010, MNRAS, 404, 1231

Weinmann, S. M., van den Bosch, F. C., Yang, X., & Mo, H. J. 2006, MNRAS, 366, 2

West, M. J. & Bothun, G. D. 1990, ApJ, 350, 36

Wetzel, A. R., Tinker, J. L., & Conroy, C. 2011, ArXiv e-prints

Wilman, D. J., Balogh, M. L., Bower, R. G., Mulchaey, J. S., Oemler, A., Carlberg, R. G., Morris, S. L., & Whitaker, R. J. 2005, MNRAS, 358, 71

Wilman, D. J., Oemler, A., Mulchaey, J. S., McGee, S. L., Balogh, M. L., & Bower, R. G. 2009, ApJ, 692, 298

Wilman, D. J., Pierini, D., Tyler, K., McGee, S. L., Oemler, Jr., A., Morris, S. L., Balogh, M. L., Bower, R. G., & Mulchaey, J. S. 2008, ApJ, 680, 1009

Wilman, D. J., Zibetti, S., & Budavári, T. 2010, MNRAS, 406, 1701

Wolf, C. e. a. 2009, MNRAS, 393, 1302

Yang, X., Mo, H. J., van den Bosch, F. C., Pasquali, A., Li, C., & Barden, M. 2007, ApJ, 671, 153

Yee, H. K. C., Morris, S. L., Lin, H., Carlberg, R. G., Hall, P. B., Sawicki, M., Patton, D. R., Wirth, G. D., Ellingson, E., & Shepherd, C. W. 2000, ApJS, 129, 475

Zabludoff, A. I. & Mulchaey, J. S. 1998a, ApJ, 498, L5+

—. 1998b, ApJ, 496, 39

3.8 Appendices

3.8.1 False Negative Rates in More Detail

In Section 3.2.2.3, we presented the main results of the effects of changing various input parameters in our mock groups. Here we present tables detailing the specific false negative rates obtained and also discuss each free parameter in detail. As discussed in Section 3.2.2.3, we determine the sensitivity of the DS Test to each of the free parameters in our mock groups ($\sigma_{\rm position}$, $\epsilon_{\rm position}$, $\sigma_{\rm redshift}$, $\epsilon_{\rm redshift}$, $n_{\rm sub}$ and $\sigma_{\rm host}$) by beginning with a 'base' mock group (Table

Table 3.7: False Negative Rates: Dependency on the Angular Size of the Input Substructure ($\sigma_{\rm position}$)

$\sigma_{\rm position}$ Mpc	$n_{\rm members} = 10$	$n_{\rm members} = 15$	$n_{\rm members} = 20$	$n_{\rm members} = 50$
0.01[a]	1[b]	0	0	0
0.05	3	1	0	0
0.09	4	1	3	0
0.1	11	3	2	0
0.2	48	26	20	1
0.5	83	74	73	27

[a]These mock groups have the following input parameters; $\epsilon_{\rm position} = 0.5$ Mpc, $\sigma_{\rm redshift} = 100$ km s^{-1}, $\epsilon_{\rm redshift} = 1300$ km s^{-1} and $\sigma_{\rm host}$ values listed in Table 3.1. Only the $\sigma_{\rm position}$ parameter is varied for these trials.

[b]Values quoted are the false negative rates, given as a percentage, obtained for 100 trials with each set of inputs, using 100 000 mc shuffles.

3.1), which has a false negative rate of zero per cent. We then change only one parameter at a time to ensure that any change in the false negative rate can be directly attributed to the altered free parameter.

3.8.1.1 Angular Size of the Substructure ($\sigma_{\rm position}$)

In Table 3.7 we present the false negative rates (listed as a percentage) for mock groups with n_{member} values of 10, 15, 20 and 50 as a function of projected angular size on the sky ($\sigma_{\rm position}$). The first line in the table indicate the results for our 'base' groups, which have P-values of either 0 or 1 per cent. We then increase the value of $\sigma_{\rm position}$ and from Table 3.7, we can see that the DS Test reliably identifies substructure with a projected dispersion of *up to* 0.1 Mpc for groups with 10 members, and as large as 0.1 Mpc for groups with more then 15 members. If we increase $\sigma_{\rm position}$ to 0.2 Mpc, we find that for groups with roughly 20 members or less, the false negative rates increases dramatically, but still remain very low (1 per cent) for richer groups with 50 members. The general conclusion from Table 3.7 is that the DS Test is not very sensitive to the size of the substructure and that even for small groups it can identify real substructure that is relatively large (~ 0.1 Mpc).

Table 3.8: False Negative Rates: Dependency on the Location of the Input Substructure in Position Space ($\epsilon_{\rm position}$)

$\epsilon_{\rm position}$ Mpc	$n_{\rm members} = 10$	$n_{\rm members} = 15$	$n_{\rm members} = 20$	$n_{\rm members} = 50$
0.001[a]	7[b]	2	0	0
0.01	11	2	3	0
0.1	6	0	0	0
0.2	0	1	0	0
0.3	2	0	0	0
0.4	1	0	0	0
0.5	3	0	0	0
1.0	0	1	0	0

[a]These mock groups have the following input parameters; $\sigma_{\rm position} = 0.01$ Mpc, $\sigma_{\rm redshift} = 100$ km s^{-1}, $\epsilon_{\rm redshift} = 1300$ km s^{-1} and $\sigma_{\rm host}$ values listed in Table 3.1. Only the $\epsilon_{\rm position}$ parameter is varied for these trials.
[b]Values quoted are the false negative rates, given as a percentage, obtained for 100 trials with each set of inputs, using 100 000 mc shuffles.

3.8.1.2 Location of Substructure in Position Space ($\epsilon_{\rm position}$)

In Table 3.8 we list the false negative rates for mock groups with n_{member} values of 10, 15, 20 and 50 as a function of the projected radial distance of the substructure with respect to the group centroid ($\epsilon_{\rm position}$). It is clear from this Table that the DS Test is quite insensitive to $\epsilon_{\rm position}$. In other words, the test can reliably identify substructure that is 'close' to the projected group centre, and easily detects structure that lies on the group outskirts.

3.8.1.3 Velocity Dispersion of the Input Substructure ($\sigma_{\rm redshift}$)

In Table 3.9 we list the false negative rates for mock groups with n_{member} values of 10, 15, 20 and 50 as a function of the velocity dispersion of the input substructure ($\sigma_{\rm redshift}$). From Table 3.9 it is evident that the DS Test is also insensitive to this parameter and can reliably detect substructure with a wide range of velocity dispersions for all values of $n_{\rm members}$. Only for groups with a fewer than 20 members and a very large dispersion value of 450 km s^{-1} do the false negative rates go above 5 per cent.

Table 3.9: False Negative Rates: Dependency on the Velocity Dispersion of the Input Substructure ($\sigma_{\rm redshift}$)

$\sigma_{\rm redshift}$ km s^{-1}	$n_{\rm members} = 10$	$n_{\rm members} = 15$	$n_{\rm members} = 20$	$n_{\rm members} = 50$
50[a]	0[b]	0	0	0
100	0	0	1	0
150	1	1	0	0
200	0	0	0	0
250	4	2	0	0
300	3	4	0	0
350	3	2	0	0
400	3	4	1	0
450	13	13	3	0

[a]These mock groups have the following input parameters; $\sigma_{\rm position} = 0.01$ Mpc, $\epsilon_{\rm position} = 0.5$ Mpc, $\epsilon_{\rm redshift} = 1300$ km s^{-1} and $\sigma_{\rm host}$ values listed in Table 3.1. Only the $\sigma_{\rm redshift}$ parameter is varied for these trials.

[b]Values quoted are the false negative rates, given as a percentage, obtained for 100 trials with each set of inputs, using 100 000 mc shuffles.

3.8.1.4 Location of Substructure Along the Line-of-Sight ($\epsilon_{\rm redshift}$)

In Table 3.9 we list the false negative rates for mock groups with n_{member} values of 10, 15, 20 and 50 as a function of the location of the substructure along the line-of-sight ($\epsilon_{\rm redshift}$). This parameter is taken to be a displacement (in km s^{-1}) of the peak in the velocity distribution of the substructure with respect to the peak of the host's distribution. Unlike the previously discussed parameters, the DS Test appears to be extremely sensitive to the location of the substructure along the line-of-sight, or more specifically the separation between the main groups velocity distribution and the substructure velocity distributionty.

The first set of entries in Table 3.9 are the false negative rates from mock groups with $\sigma_{\rm host}$ values set to the average dispersion of observed GEEC groups with similar group membership (Table 3.1). It is clear that if the peaks of the host and substructure velocity distributions are close (< 300 km s^{-1}), then the DS Test cannot always identify real substructure. For groups with fewer than ~ 20 members, the peaks must be at least 900 km s^{-1} apart in order for the false negative rates to fall below 5 per cent.

We also find that not only is the DS Test sensitive to the $\epsilon_{\rm redshift}$ parameter, but that the level of sensitivity is dependent on the number of members in the host group. This is best seen by looking at the false negative rates listed in the second set of values listed in Table 3.10, where we use a constant value of $\sigma_{\rm host} = 500$ km s^{-1} for all values of $n_{\rm members}$. From this section of the table we see that when the velocity distribution of the substructure is located at $1\sigma_{\rm host}$, the false negative rates are 43, 49, 34 and 4 per cent for mock groups with 10, 15, 20 and 50 members. At $2\sigma_{\rm host}$ the rates are 10 per cent for groups with 10 and 15 members and 0 per cent for groups with 20 and 50 members. This results indicates that for groups with fewer member galaxies, the velocity distributions of the host and substructure must be very distinct in order for the DS Test to detect substructure. Alternatively, groups with more than 20 members can have substructure galaxies with a velocity distribution embedded within the host distribution and still be identified by the test.

3.8.1.5 Number of Members in the Input Substructure ($n_{\rm sub}$)

In Table 3.9 we list the false negative rates for mock groups with n_{member} values of 10, 15, 20 and 50 as a function of the number of members in the input substructure ($n_{\rm sub}$) (see Section 3.2.2.3 for discussion).

3.8.1.6 Velocity Dispersion of the Host Group ($\sigma_{\rm host}$)

In addition to the above tests, we also check to see if changing the velocity dispersion, and therefore mass, of the host group ($\sigma_{\rm host}$) affects the observed false negative rates. We present the results in Table 3.12, where we see that for groups with more that 20 members the dispersion of the host group does not significantly increase the rate of false negatives. However, for systems with fewer members and larger values of $\sigma_{\rm host}$ (> 700 km s^{-1}), the DS Test is more likely to miss true substructure. Fortunately, observed groups with 10 or so members do not generally have such high dispersion values.

Table 3.10: False Negative Rates: Dependency on the Location of the Input Substructure Along the Line-of-Sight (i.e. redshift space) ($\epsilon_{\rm redshift}$) .

$\epsilon_{\rm redshift}$ km s^{-1}	$n_{\rm members} = 10$	$n_{\rm members} = 15$	$n_{\rm members} = 20$	$n_{\rm members} = 50$
100[a]	91[b]	94	80	43
200	85	81	74	39
300	62	71	72	21
400	53	49	54	7
500	32	42	39	0
600	25	25	18	0
700	10	19	7	0
800	7	9	9	0
900	3	5	4	0
1000	3	2	4	0
1100	2	0	0	0
1200	1	1	0	0
1300	1	0	0	0
100[c]	84	94	87	51
200	83	87	67	43
300	80	81	69	21
400	63	66	48	4
500	43	49	34	4
600	37	43	21	0
700	35	26	13	0
800	21	22	3	0
900	17	8	1	0
1000	10	10	0	0
1100	5	15	0	0
1200	5	2	0	0
1300	2	5	0	0

[a]These mock groups have the following input parameters; $\sigma_{\rm position} = 0.01$ Mpc, $\epsilon_{\rm position} = 0.5$ Mpc, $\epsilon_{\rm redshift} = 1300$ km s^{-1} and $\sigma_{\rm host}$ values listed in Table 3.1. Only the $\sigma_{\rm redshift}$ parameter is varied for these trials.

[b]Values quoted are the false negative rates, given as a percentage, obtained for 100 trials with each set of inputs, using 100 000 mc shuffles.

[c]These mock groups have the following input parameters; $\sigma_{\rm position} = 0.01$ Mpc, $\epsilon_{\rm position} = 0.5$ Mpc, $\epsilon_{\rm redshift} = 1300$ km s^{-1} and a *constant* $\sigma_{\rm host}$ value of 500 km s^{-1} for all values of $n_{\rm members}$. Again, only the $\sigma_{\rm redshift}$ parameter is varied for these trials.

Table 3.11: False Negative Rates: Dependency on the Number of Members in the Input Substructure ($n_{\rm sub}$)

$n_{\rm sub}$	$n_{\rm members} = 10$	$n_{\rm members} = 15$	$n_{\rm members} = 20$	$n_{\rm members} = 50$
3[a]	43[b]	39	54	51
4	1	2	9	16
5		0	0	3
6				0
7				0
8				0
9				0

[a]These mock groups have the following input parameters; $\sigma_{\rm position} = 0.01$ Mpc, $\epsilon_{\rm position} = 0.5$ Mpc, $\sigma_{\rm redshift} = 100$ km s^{-1}, $\epsilon_{\rm redshift} = 1300$ km s^{-1} and $\sigma_{\rm host}$ values given in Table 3.1. For these simulations we only change the number of members in the substructure ($n_{\rm sub}$).

[b]Values quoted are the false negative rates, given as a percentage, obtained for 100 trials with each set of inputs, using 100 000 mc shuffles. A null entry indicates that no trials were run with the associated $n_{\rm sub}$ value.

Table 3.12: False Negative Rates: Dependency on the Velocity Dispersion of the Host Group ($\sigma_{\rm host}$) .

$\sigma_{\rm host}$ km s^{-1}	$n_{\rm members} = 10$	$n_{\rm members} = 15$	$n_{\rm members} = 20$	$n_{\rm members} = 50$
100[a]	0[b]	0	0	0
200	1	0	0	0
300	0	0	0	0
400	1	0	0	0
500	2	2	0	0
600	10	3	1	0
700	9	10	3	0
800	21	20	3	0
900	22	28	3	0

[a]These mock groups have the following input parameters; $\sigma_{\rm position} = 0.01$ Mpc, $\epsilon_{\rm position} = 0.5$ Mpc, $\sigma_{\rm redshift} = 100$ km s^{-1} and $\epsilon_{\rm redshift} = 1300$ km s^{-1}. For these simulations we keep the values of the input substructure constant, but change the velocity dispersion of the host group ($\sigma_{\rm host}$).

[b]Values quoted are the false negative rates, given as a percentage, obtained for 100 trials with each set of inputs, using 100 000 mc shuffles.

Chapter 4

Do group dynamics play a role in the evolution of member galaxies?

This chapter incorporates the article *"Do group dynamics play a role in the evolution of member galaxies?"*, which has been accepted to the *Monthly Notices of the Royal Astronomical Society* and is currently in press.

Annie Hou[1], Laura C. Parker[1], Michael L. Balogh[2], Sean L. McGee[3,4], David J. Wilman[5], Jennifer L. Connelly[5], William E. Harris[1], Angus Mok[2], John S. Mulchaey[6], Richard G. Bower[3] & Alexis Finoguenov[7,8]

[1] *Department of Physics & Astronomy, McMaster University, Hamilton ON L8S 4M1, Canada*
[2] *Department of Physics and Astronomy, Univeristy of Waterloo, Waterloo, Ontario, N2L 3G1, Canada*
[3] *Department Of Physics, University of Durham, Durham, DH1 3LE, United Kingdom*
[4] *Leiden Observatory, Leiden University, PO Box 9513, 2300 RA Leiden, the Netherlands*
[5] *Max-Planck-Institut für Extraterrestrische Physik, Giessenbachstraße, D-85748 Garching, Germany*
[6] *Observatories of the Carnegie Institution, 813 Santa Barbara Street, Pasadena, California, USA*
[7] *Department of Physics, University of Helsinki, Gustaf Hallstromin katu 2a, FI-00014 Helsinki, Finlanda*
[8] *CSST, University of Maryland, Baltimore County, 1000 Hilltop Circle, Baltimore, MD 21250, USA*

Abstract

We examine galaxy groups from the present epoch to $z \sim 1$ to explore the impact of group dynamics on galaxy evolution. We use group catalogues from the Sloan Digital Sky Survey (SDSS), the Group Environment and Evolution Collaboration (GEEC) and the high redshift GEEC2 sample to study how the observed member properties depend on galaxy stellar mass, group dynamical mass and dynamical state of the host group. We find a strong correlation between the fraction of non-star-forming (quiescent) galaxies and galaxy stellar mass, but do not detect a significant difference in the quiescent fraction with group dynamical mass, within our sample halo mass range of $\sim 10^{13}-10^{14.5} M_{\odot}$, or with dynamical state. However, at $z \sim 0.4$ we do see some evidence that the quiescent fraction in low mass galaxies ($\log_{10}(M_{\rm star}/M_{\odot}) \lesssim 10.5$) is lower in groups with substructure. Additionally, our results show that the fraction of groups with non-Gaussian velocity distributions increases with redshift to $z \sim 0.4$, while the amount of detected substructure remains constant to $z \sim 1$. Based on these results, we conclude that for massive galaxies ($\log_{10}(M_{\rm star}/M_{\odot}) \gtrsim 10.5$), evolution is most strongly correlated to the stellar mass of a galaxy with little or no additional effect related to either the group dynamical mass or dynamical state. For low mass galaxies, we do see some evidence of a correlation between quiescent fraction and the amount of detected substructure, highlighting the need to probe further down the stellar mass function to elucidate the role of environment in galaxy evolution.

4.1 Introduction

A long-standing debate is whether the evolution of galaxies is governed primarily by internal processes (e.g. feedback) or those related to the external environment (e.g. stripping). The morphology-density relation seen in the cores of clusters (Oemler, 1974; Dressler, 1980) was one of the first observations to show that the environment may influence the properties of galaxies, where elliptical and S0 (early-type) galaxies were found preferentially in high-density regions and spiral and irregular (late-type) galaxies in low-density regions. Since then, numerous correlations between galaxy properties and environment have been observed. For example, differences in the distributions of colours (Blanton et al., 2003; Baldry et al., 2006; Hou et al., 2009), the fraction of either star-forming or quiescent galaxies (Kauffmann et al., 2004; Balogh et al., 2004; Wilman et al., 2005a; Peng et al., 2010; McGee et al., 2011; Patel et al., 2011; Sobral et al., 2011; Muzzin et al., 2012), and the amount of observed dust (Kauffmann et al., 2004). Correlations between environment and galaxy properties appear to have been in place since at least $z \sim 1$, as the observed star formation rate (SFR)-density and specific star formation rate (SSFR = SFR/stellar mass)-density relations show variations with environment at this redshift (Cooper et al., 2008; Patel et al., 2011).

Although there have been numerous observations of correlations between environment and galaxy properties, where red and quiescent galaxies are preferentially found in higher density regions, recent studies have suggested that internal or secular processes, traced by the mass of the galaxy, may actually be the dominant factor in galaxy evolution. In particular, several studies have found that the properties of actively star-forming galaxies only weakly depend on the environment (Balogh et al., 2004; Wilman et al., 2005a; Poggianti et al., 2008; Peng et al., 2010; Tyler et al., 2011). Similarly, Muzzin et al. (2012) found that although the environment does determine the fraction of galaxies that remain actively star-forming, the stellar populations of both actively star-forming and quiescent galaxies are most strongly correlated to the stellar mass of a galaxy.

The emerging picture appears to suggest that *both* internal and external processes contribute to the evolution of galaxies. Although observations have

shown that stellar mass correlates well with environment, both in the local Universe (Hogg et al., 2003; Kauffmann et al., 2004; Blanton et al., 2005; Baldry et al., 2006) and at $z \sim 1$ (Bolzonella et al., 2010; Sobral et al., 2011), recent studies have claimed that the effects due to the environment can still be disentangled from transformation processes traced by galaxy stellar mass (Peng et al., 2010; Sobral et al., 2011; Muzzin et al., 2012). In an empirically driven picture of galaxy evolution, Peng et al. (2010) claimed that the evolution of low mass galaxies ($\log_{10}(M_{\rm star}/M_{\odot}) \lesssim 10.5$) is dominated by environmentally driven star-formation quenching whereas high mass galaxy evolution ($\log_{10}(M_{\rm star}/M_{\odot}) \gtrsim 10.5$) is governed by processes which are traced by galaxy stellar mass.

Galaxy groups are ideal for studies of the role of the environment in the evolution of galaxies. Not only are groups the most common environment in the local Universe (Geller & Huchra, 1983; Eke et al., 2005), but it is also believed that as many as 40 per cent of galaxies, especially low mass galaxies, that live in rich groups or clusters were pre-processed (i.e. had their star formation quenched) in haloes with $M_{\rm halo} \gtrsim 10^{13} h^{-1} M_{\odot}$ before infall (McGee et al., 2009; De Lucia et al., 2012).

The pre-processing of galaxies in low mass groups may be driven by galaxy-galaxy interactions and mergers. As a result of the relatively low velocity dispersion observed in groups, it has been shown that the rate of mergers is higher in the group environment with respect to both the field and richer galaxy clusters (Barnes, 1985; Zabludoff & Mulchaey, 1998b; Brough et al., 2006; De Lucia et al., 2011). Interactions are thought to initially trigger an intense burst of star formation (Sanders et al., 1988; Elbaz & Cesarsky, 2003; Cox et al., 2006; Teyssier et al., 2010), which can use up the supply of cold gas and lead to the quenching of star formation, if no further gas accretes onto galaxy. Thus, mergers and interactions can either enhance or quench star formation depending on the evolutionary stage at which the galaxy is observed. In addition, star formation quenching in galaxies may occur as a satellite falls into a larger dark matter halo due to processes such as strangulation (Larson et al., 1980; Balogh et al., 2000; Kawata & Mulchaey, 2008) and ram-pressure stripping (Gunn & Gott, 1972; Abadi et al., 1999). Thus, galaxy evolution appears to be related to the accretion history of the galaxy and with the

number of interactions a galaxy has experienced. By looking for correlations between group dynamics and member properties, it is possible to probe the importance of accretion history and dynamical interactions on the evolution of galaxies.

In this paper we study the dependance of galaxy evolution on galaxy stellar mass, group dynamical mass and group dynamics. The paper is structured as follows: in Section 4.2 we describe the data and group catalogues, as well as discuss the methods for determining stellar mass and SFR. In Section 4.3, we look for correlations of galaxy properties with galaxy stellar mass and group dynamical mass. In Section 4.4, we classify the dynamical state of our groups and compare the properties of galaxies in dynamically young and dynamically evolved systems. We discuss our results in Section 4.5 and finally present our conclusions in Section 4.6.

Throughout this paper we assume a ΛCDM cosmology with $\Omega_{m,0} = 0.27$, $\Omega_{\Lambda,0} = 0.73$ and $H_0 = 71$ km s^{-1} Mpc^{-1}.

4.2 Data

In order to investigate the role of group dynamics in galaxy evolution, we look at three highly complete group catalogues that span a redshift range of $0 \lesssim z \lesssim 1$. This allows us to probe not only how the properties of the member galaxies depend on the properties of the host group, but also how these correlations evolve with redshift. The low redshift ($0 < z < 0.12$) group sample is from the Sloan Digital Sky Survey (SDSS), the intermediate redshift ($0.15 < z < 0.55$) sample is from the Group Environment and Evolution Collaboration (GEEC) survey, and the high redshift ($0.8 < z < 1$) groups are from the GEEC2 survey (to be discussed in detail in Sections 4.2.1-4.2.3).

4.2.1 The SDSS group catalogue

Although there are many publicly available SDSS group catalogues (e.g., Berlind et al., 2006; Yang et al., 2007), we elect to use the groups defined in McGee et al. (2011), who applied a multi-stage approach to mimic both the observing conditions and group-finding algorithm used to identify our intermediate redshift

GEEC groups (see Section 4.2.2). This selection allows for a better comparison of the group and galaxy properties by reducing possible effects introduced by differences in the spectroscopic completeness, limiting magnitude or in the group-finding algorithm. A full description of our SDSS group catalogue is given in McGee et al. (2011), but we give a brief summary here. Groups were identified using galaxies observed in the SDSS Data Release 6 (DR6), which contains over 790 000 spectra in an area of $\sim$7425 deg^2 (Adelman-McCarthy et al., 2008). In addition to the SDSS *ugriz* photometry, McGee et al. (2011) made use of the overlapping GALEX Medium Imaging Survey (MIS), which covered an area of $\sim$1000 deg^2 of the SDSS (Martin et al., 2005; Morrissey et al., 2007). The inclusion of the NUV and FUV bands is important for better estimates of the SFR.

To reproduce the observing conditions and group-finding algorithm of the second Canadian Network for Observational Cosmology (CNOC2) Galaxy Redshift Survey (Yee et al., 2000), on which the GEEC group catalogue is based, McGee et al. (2011) applied the same absolute magnitude cut and then randomly removed half the remaining galaxies to match the spectroscopic completeness of the CNOC2 redshift survey (see Section 2.2). With this sample, McGee et al. (2011) calculated the local density around each galaxy by counting the number of galaxies within a cylinder of $0.33h_{75}^{-1}$ Mpc and a line-of-sight depth of $\pm 6.67h_{75}^{-1}$ Mpc. Proto-groups were then identified starting from galaxies with the highest local densities and taking all of the galaxies within the cylinder centred around the high-density galaxies as proto-group members. Next, all of the galaxies in each of the cylinders centred on the initial members were added and the process continued until no further galaxies could be added. Using these proto-groups, a preliminary geometric centre, redshift, velocity dispersion (σ) and virial radius (r_{200}: Equation 4.2) were computed. Proto-group members were then added or removed iteratively if they fell within $1.5r_{200}$ and 3σ of the group centre. Once all of the proto-groups were identified, McGee et al. (2011) then added all of the SDSS galaxies back into the sample and group membership was finalized with a methodology similar to that used to identify the GEEC groups (Carlberg et al., 2001; Wilman et al., 2005b).

4.2.2 The GEEC group catalogue

Our intermediate redshift sample is the GEEC group catalogue, which contains ∼200 groups in the range of $0.1 < z < 0.55$. The GEEC survey is based on a set of groups first identified in the CNOC2 redshift survey (Yee et al., 2000; Carlberg et al., 2001), which contained $\sim 4\times10^4$ galaxies in four patches totalling ∼1.5 deg^2. The original photometry was taken in the $UBVR_cI_c$ bands down to a limiting magnitude of $R_c = 23.0$ and spectra were obtained for more than 6000 galaxies with a completeness of 48 per cent at $R_c = 21.5$ (Yee et al., 2000).

The GEEC survey built on the CNOC2 survey by obtaining higher spectroscopic completeness to a fainter limiting magnitude with 78 per cent completeness at $R_c = 22$ for a subset of the groups (Wilman et al., 2005b; Connelly et al., 2012). The extensive follow-up spectroscopy was taken with LDSS2 (Wilman et al., 2005b) and IMACS (Connelly et al., 2012) on Magellan, as well as data from FORS2 on the Very Large Telescope (Connelly et al., 2012). Additionally, we have obtained multi-wavelength data from the X-ray to the infrared (IR) observed with the following telescopes: XMM-Newton (Finoguenov et al., 2009), Chandra X-ray Observatory (Finoguenov et al., 2009), GALEX (McGee et al., 2011), HST-ACS (Wilman et al., 2009), Spitzer-MIPS (Tyler et al., 2011), Spitzer-IRAC (Wilman et al., 2008), INGRID on the William Herschel Telescope (Balogh et al., 2009), and SOFI on the New Technology Telescope (Balogh et al., 2007). In addition, improved optical imaging was obtained in the $ugrizBVRI$ filters from the Canada-France-Hawaii Telescope's Megacam and CFH12K imagers (Balogh et al., 2009).

Group membership was defined with the friends-of-friend (FoF) algorithm outlined in Wilman et al. (2005b). Analysis of mock catalogues has shown that the contamination rate is 2.5 per cent for galaxies within $0.5h_{75}^{-1}$ Mpc of the group centroid (McGee et al., 2008).

4.2.3 The GEEC2 group catalogue

The high redshift sample contains a subset of groups identified in the GEEC2 survey. A detailed discussion of the GEEC2 survey is presented in Balogh et al. (2011) and Mok et al. (2013). The goal of the GEEC2 survey was to obtain

high spectroscopic completeness for 20 galaxy groups in the redshift range of $0.8 < z < 1.0$ that were initially identified in the Cosmic Evolution Survey (COSMOS - Scoville et al., 2007) with extended X-ray emission (Finoguenov et al., 2007; George et al., 2011). The follow-up spectroscopic survey is being conducted with the GMOS spectrograph on the GEMINI telescope and thus far, data have been collected for 11 of the 20 target groups with spectroscopic completeness between ∼0.6 and 0.75 (Balogh et al., 2011) down to $r = 24.75$.

Balogh et al. (2011) assigned group membership based on a galaxy's proximity to the measured X-ray centre. It should be noted that although the group centroid for GEEC2 is based on X-ray emission, rather than a luminosity weighted center (used in SDSS and GEEC), Connelly et al. (2012) found that the difference between these two definitions is typically small ($< 18''$) and that group membership and overall group properties did not change significantly with either centroid. For each group, the velocity dispersion (σ) was computed from all galaxies within 1.0 Mpc and 4000 km s^{-1} of the measured group X-ray centre. Next the *rms* projected radial position from the group centroid (R_{rms}) was computed and all galaxies with group-centric velocities $> C_z\sigma$ and radial position $> C_r R_{rms}$ were clipped, where the typical values for C_z and C_r were 2. Finally, σ and R_{rms} were re-computed and only galaxies with $z < 2.5\sigma_{\rm 1Mpc}$ and radial positions $< 2R_{rms}$ were defined as group members.

Ideally, all three group catalogues would be defined in the same way; however, an unbiased and highly complete spectroscopic survey at high redshifts is a difficult and expensive task. Including the GEEC2 groups allows us to probe the high redshift Universe. Additionally, GEEC2 is one of the few high redshift group catalogues with high spectroscopic completeness and more than five members per group, allowing for studies of group dynamics.

4.2.4 Spectral energy distribution fitting

In Table 4.1, we list the group catalogue, redshift range, number of groups used in this analysis and the available photometry for each sample. We see that each of the three group catalogues has multi-wavelength data (Table 4.1), which were used to measure stellar masses and SFRs via spectral energy dis-

Table 4.1: Properties of the group catalogues.

Catalogue	redshift range	# of groups	Photometry
SDSS	z < 0.1	100	FUV, NUV,
($r < 17.77$)			*u, g, r, i, z*
GEEC	0.1 < z < 0.55	37	FUV, NUV,
			u, g, r, i, z, K
($r < 23$)			Spitzer:IRAC & MIPS
GEEC2	0.8 < z < 1	8	FUV, NUV, U, B, V, G,
(r < 24.75)			R, I, Z, J, K
			Spitzer:IRAC & MIPS

tribution (SED) template-fitting. The same fitting procedure was carried out for all catalogues from all available photometric bands. A detailed discussion of the SED fitting procedure is given in McGee et al. (2011) for the SDSS and GEEC catalogues and in Balogh et al. (2011) for the GEEC2 catalogue. The observed photometry was compared to a grid of SEDs constructed with the Bruzual & Charlot (2003) stellar population synthesis code for the SDSS and GEEC catalogues and the Bruzual (2007) model for GEEC2. A Chabrier initial mass function (IMF) was assumed for all three catalogues. In both McGee et al. (2011) and Balogh et al. (2011), the SED fitting procedure followed that outlined in Salim et al. (2007), where a grid of models that uniformly sampled the allowed parameters of formation time, galaxy metallicity and a two-component dust model (Charlot & Fall, 2000) was created. An exponentially declining base SFR, with added bursts of star formation with varying duration and relative strength was used to model the star formation history of each galaxy. Probability distribution functions were created for the relevant galaxy parameters after weighing each model by its $\exp(-\chi^2/2)$ and the median value for each of the parameters was used. The SFRs have been averaged over the last 100 Myr and the 1σ uncertainties in stellar mass, when compared to both mock groups and other independent estimates, are on the order of 0.15 dex (McGee et al., 2011). For the stellar masses probed in this work ($\log_{10}(M_{\rm star}/M_{\odot}) \geq 10$) there is no systematic offset between the Bruzual & Charlot (2003) (used for SDSS and GEEC) and Bruzual (2007) (used for GEEC2) models. The observed scatter between the two models is within our quoted 1σ uncertainties. Additionally, there may be additional systematic

uncertainties due to, for example, the IMF assumed in the fitting procedure.

4.2.5 Completeness Corrections

The ability to detect faint and low mass galaxies declines with increasing redshift, which can be seen in Figure 4.1 where we plot $\log_{10}(M_{\rm star}/M_{\odot})$ versus z for all galaxies in each of the catalogues. In order to address this stellar mass incompleteness, we apply a stellar mass limit to each of the group catalogues using the methodology described in Connelly et al. (2012). Briefly, we compute the stellar mass that each galaxy would have if it was observed at the r-band magnitude limit ($r_{\rm lim}$) of the sample using

$$M_{\rm star,\ r_{lim}}(z) = M_{\rm star}(z) \times 10^{(-0.4(r_{\rm lim}-r(z)))}, \tag{4.1}$$

where $M_{\rm star}(z)$ is the stellar mass of the galaxy determined from the SED fits and $r(z)$ is the observed r-band magnitude of the galaxy.

We define a conservative stellar mass limit by only taking the passive galaxies with SSFR $< 10^{-11}$ yr^{-1} (SSFR $\equiv$ SFR/stellar mass)[1]. Since passive galaxies have on average a higher M/L ratio than actively star-forming galaxies, we obtain a higher, and therefore more conservative, stellar mass limit using this methodology. To define our limit, we compute the 90th percentile values of the mass estimates (Equation 4.1) for all passive galaxies in narrow redshift bins and then perform a linear least-squares fit to these values. For the SDSS and GEEC catalogues, we then take all galaxies that fall above this line as our stellar mass complete catalogue. To define our stellar mass completeness limit for the high redshift sample we take a different approach and apply a cut based on the GEEC2 sample selection criteria and the shape of the stellar mass function of the observed passive galaxy population (Mok et al., 2013). For groups at the high redshift end ($z \sim 1$) of the GEEC2 catalogue, Mok et al. (2013) found that the sample was complete down to $\log_{10}(M_{\rm star}/M_{\odot}) = 10.7$ for passive galaxies. We therefore take this value to be our stellar mass limit for the entire GEEC2 sample. Although a limit of $\log_{10}(M_{\rm star}/M_{\odot}) = 10.7$ is conservative, we probe galaxy evolution via the quiescent fraction (see Section

[1]It should be noted that Connelly et al. (2012) use red galaxies to define their limits

4.2.7), which requires that the population of passive galaxies is complete.

In Figure 4.1, we plot the observed stellar masses versus redshift for passive galaxies (black circles) and all galaxies (grey circles) in the SDSS (left), GEEC (middle) and GEEC2 (right) surveys. The 90th percentile stellar mass estimates for the SDSS and GEEC samples are shown as red triangles in Figure 4.1 and the linear least-squares fit to these values as the red solid line. For the GEEC2 sample (Figure 4.1: right), the red solid line indicates our stellar mass limit of $\log_{10}(M_{\rm star}/M_{\odot}) = 10.7$. The stellar mass ranges for our complete samples are; $9.5 \lesssim \log_{10}(M_{\rm star}/M_{\odot}) \lesssim 11.5$ for SDSS, $9.6 \lesssim \log_{10}(M_{\rm star}/M_{\odot}) \lesssim 11.5$ for GEEC and $10.7 \leq \log_{10}(M_{\rm star}/M_{\odot}) \lesssim 11.5$ for GEEC2.

In addition, we have applied a spectroscopic completeness correction by calculating magnitude weights for each galaxy. The weights are computed following a methodology similar to Wilman et al. (2005b), where weights are calculated in r-band magnitude bins down to the limiting magnitude of each catalogue.

4.2.6 Final group membership

To probe the effects of groups dynamics on the properties of members galaxies, we only consider the sample of group galaxies with measured stellar masses and SFRs. In addition, we only look at groups with more than five member galaxies within two virial radii (r_{200}) of the group centroid, where r_{200} is defined as Carlberg et al. (1997)

$$r_{200} = \frac{\sqrt{3}\sigma_{\rm rest}}{10H(z)}, \tag{4.2}$$

where $\sigma_{\rm rest}$ is the observed velocity dispersion ($\sigma_{\rm obs}$), computed via the Gapper Estimator (Beers et al., 1990) from all member galaxies within 1.0 Mpc of the group centroid, corrected for redshift (i.e. $\sigma_{\rm rest} = \sigma_{\rm obs}/(1+z)$) and $H(z) = H_0\sqrt{\Omega_{m,0}(1+z)^3 + \Omega_{\Lambda,0}}$.

The inclusion of galaxies out to $2r_{200}$ is motivated by previous results. In Hou et al. (2012), we found that substructure galaxies were preferentially located on the group outskirts, beyond the virial radius. Therefore, in order to better study correlations between the amount of substructure and galaxy

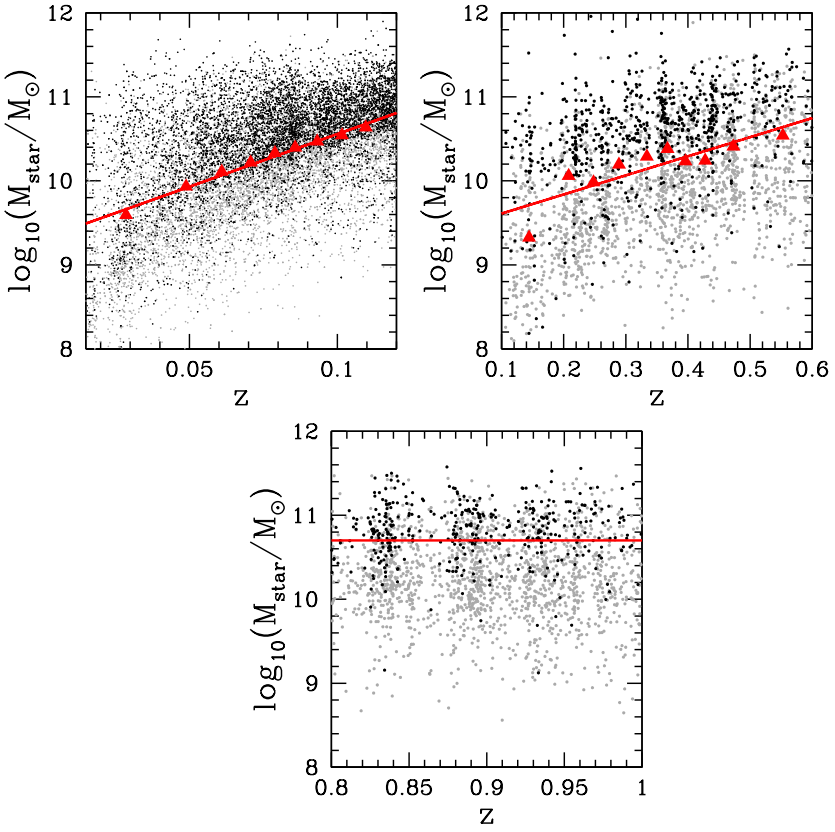

Figure 4.1: Top-left: Observed $\log_{10}(M_{\rm star}/M_{\odot})$ versus z for the quiescent galaxies (black circles) and for all galaxies (grey circles) in a sub-sample of 15 000 randomly selected galaxies in the SDSS catalogue. The red triangles indicate the 90th percentile value of the stellar mass estimates of quiescent galaxies (black circles) given by Equation 4.1 within a given redshift bin and the red solid line indicates a linear least-squares fit to these points. This line is taken to be the stellar mass completeness limit of the sample. Top-right: Same as top-left except for all galaxies in the GEEC sample. Bottom: Same as top-left except for all galaxies in the GEEC2 sample and the red solid line indicates a stellar mass cut of $\log_{10}(M_{\rm star}/M_{\odot}) = 10.7$.

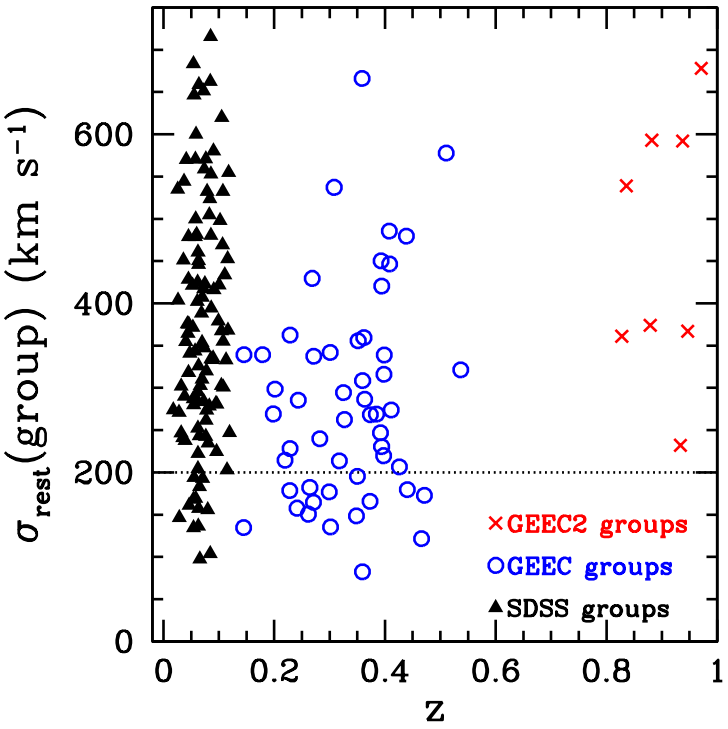

Figure 4.2: Group velocity dispersion ($\sigma_{\rm rest}$) versus redshift (z) for our sub-sample of groups with $n_{\rm members} \geq 5$ within $2r_{200}$ of the group centroid identified in SDSS (black triangles), GEEC (blue circles) and GEEC2 (red crosses). The dashed line indicates the lower limit $\sigma_{\rm rest}$ cut; we only analyze groups with $\sigma_{\rm rest} > 200$ km s^{-1}.

properties, we include galaxies out to $2r_{200}$. We discuss the effects of applying different radial cuts in Section 4.4.2.

In Figure 4.2 we plot the group velocity dispersion ($\sigma_{\rm rest}$) versus redshift (z) for our sub-sample of the three group catalogues. The SDSS, GEEC and GEEC2 groups span a wide range of velocity dispersions, and therefore masses. From Figure 4.2, we see that both the SDSS and GEEC group catalogues contain lower mass systems when compared to GEEC2; therefore, to ensure that all three catalogues span a similar mass range we only consider groups with $\sigma_{\rm rest} > 200$ km s^{-1}, which corresponds to a dynamical mass of $\sim 1.2 \times 10^{13} M_{\odot}$ at a redshift of $z = 0.25$. The minimum of five members within $2r_{200}$ requirement, and the $\sigma_{\rm rest} > 200$ km s^{-1} cut, leaves us with 100 SDSS groups, 37 GEEC groups and 8 GEEC2 groups (see Table 4.1).

4.2.7 Characterizing the properties of galaxies

In order to study the relationship between environment and galaxy evolution, we look at the specific star formation rates of the galaxies in groups. We examine both the SSFR distributions and the fraction of quiescent galaxies (hereafter $f_{\rm q}$), where $f_{\rm q}$ is defined as

$$f_{\rm q} = \frac{\#\text{ galaxies with SSFR} < 10^{-11}\text{yr}^{-1}}{\text{total }\#\text{ of galaxies}}, \tag{4.3}$$

with SSFR $= 10^{-11}$ yr^{-1} marking the division between the main sequence of star-forming galaxies from the quiescent galaxies in the SSFR-stellar mass plane (McGee et al., 2011). It should also be noted that values in Equation 4.3 are weighted to account for spectroscopic incompleteness.

4.3 Galaxy properties with galaxy stellar mass and group dynamical mass

4.3.1 Correlations with galaxy stellar mass

It is well known that the observed properties of galaxies correlate well with galaxy stellar mass. Many studies have shown that there exists a SFR-stellar mass trend, which is especially strong for star-forming galaxies (Kennicutt, 1983; Brinchmann et al., 2004; Noeske et al., 2007; Whitaker et al., 2012), and a colour-stellar mass trend (Tortora et al., 2010; Giodini et al., 2012), where massive galaxies are typically redder and have lower SFRs. Before we investigate the role of group dynamics in galaxy evolution, we must first characterize the stellar mass trend in our sample.

We look at the SSFR-stellar mass trend in each of our three group catalogues. In Figure 4.3 we plot $f_{\rm q}$ (Equation 4.3) versus stellar mass for all galaxy group members in SDSS (black triangles), GEEC (blue circles) and GEEC2 (red crosses). From Figure 4.3, we see that the quiescent fraction shows a positive correlation with stellar mass for the SDSS and GEEC samples, as previously noted by McGee et al. (2011). For all three catalogues, the f_q-stellar mass trend appears to be flat for galaxies with $\log_{10}(M_{\rm star}/M_{\odot}) > 10.5$.

An additional trend that can be seen in Figure 4.3 is that for low mass galaxies ($\log_{10}(M_{\rm star}/M_{\odot}) < 10.5$) we observe an evolution in the quiescent fraction with redshift, where galaxies at higher redshifts have lower f_q. We see a similar, though less drastic, trend for the massive galaxies ($\log_{10}(M_{\rm star}/M_{\odot}) > 10.5$) when comparing our $z \sim 0$ and $z \sim 0.4$ samples. However, we do not observe a clear evolution in the quiescent fractions of massive galaxies between $z \sim 0.4$ and $z \sim 0.9$.

In Section 4.4.2.2, we discuss how we remove this strong correlation between quiescent fraction and stellar mass so that we can examine the effects of group dynamics.

4.3.2 Correlations with group dynamical mass (M_{200})

There are a number of possible processes related to environmentally driven galaxy evolution, including: ram-pressure stripping, strangulation and galaxy-galaxy interactions. Some of these mechanisms are more directly related to the potential of the group, while others are better correlated to the local or neighbouring environment. To probe the influence of the host group, we look for correlations between the observed quiescent fraction and dynamical mass, M_{200}, of the group defined as Carlberg et al. (1997)

$$M_{200} = \frac{3 r_{200} \sigma^2_{\rm rest}}{G}, \tag{4.4}$$

where r_{200} is given by Equation 4.2. It should be noted that the mass computed in Equation 4.4 assumes that the system is in dynamical equilibrium, which we show in Section 4.4 is not always true for the groups in our catalogues. Bird (1995) showed that dynamical mass estimators, such as Equation 4.4, tend to overestimate the true mass of systems not in equilibrium, in particular those with significant substructure. However, our goal is to roughly divide our sample by mass and this methodology works well for this purpose. Alternatively, we could have used the total stellar mass of the group to characterize the host environment, though this method requires significant completeness corrections. It should be noted that we do observe similar results whether M_{200} or total stellar mass is used in the analysis.

We make a cut at $M_{200} = 6 \times 10^{13} M_{\odot}$ to distinguish between low and

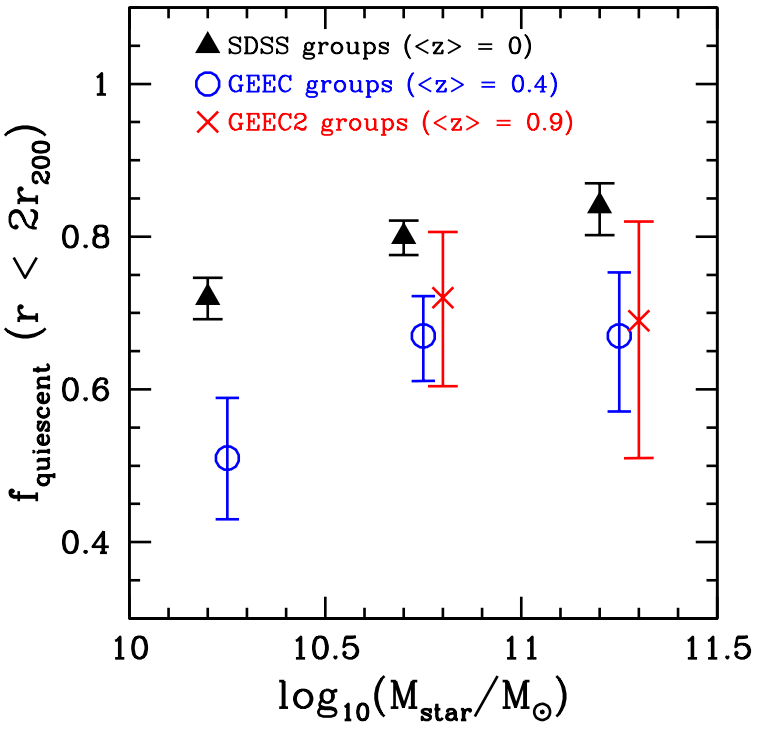

Figure 4.3: Quiescent fraction ($f_{\rm q}$) versus stellar mass for all group galaxies in SDSS (black triangles), GEEC (blue circles) and GEEC2 (red crosses). The data are divided into stellar mass bins of 0.5 dex in the range of $10 \leq \log_{10}(M_{\rm star}/M_{\odot}) \leq 11.5$ and plotted at the center of the mass range with small horizontal offsets for clarity. It should be noted that due to our stellar mass cuts, the intermediate mass galaxies in the GEEC2 sample span a stellar mass range of $10.7 \leq \log_{10}(M_{\rm star}/M_{\odot}) < 11$. Also, note that all catalogues are stellar mass complete and have been corrected for spectroscopic incompleteness. The uncertainties in the quiescent fraction are computed following the methodology of Cameron (2011).

high mass groups as this is the approximate median value for each of the three group catalogues. In Figure 4.4, we plot $f_{\rm q}$ versus z for low mass galaxies ($10 < \log_{10}(M_{\rm star}/M_{\odot}) \leq 10.5$: top left), intermediate mass galaxies ($10.5 < \log_{10}(M_{\rm star}/M_{\odot}) \leq 11$: top right) and high mass galaxies ($11 < \log_{10}(M_{\rm star}/M_{\odot}) \leq 11.5$: bottom left) in low mass ($M_{200} < 6 \times 10^{13} M_{\odot}$) groups (black circles) and in high mass ($M_{200} > 6 \times 10^{13} M_{\odot}$) groups (orange triangles). From Figure 4.4, we see that for all stellar masses the quiescent fraction of galaxies in low and high mass groups are not statistically distinct. It should be noted that if we make an additional cut at $M_{200} = 10^{14} M_{\odot}$, we still find no dependence of f_q on group halo mass. While numerous studies have found that the observed properties of galaxies do correlate with halo mass (Pasquali et al., 2010; Wetzel et al., 2012), these studies also show that the trends tend to be flatter for higher mass haloes. In particular, given the dynamical mass range of the SDSS, GEEC and GEEC2 groups ($13 \lesssim \log_{10}(M_{200}/M_{\odot}) \lesssim 14.5$) and our average errors on f_q of $\sim \pm 10$ per cent, the average quiescent fractions and ages shown in Wetzel et al. (2012) and Pasquali et al. (2010) are approximately the same for galaxies in low and high mass groups, assuming a cut at $M_{200} = 6 \times 10^{13} M_{\odot}$.

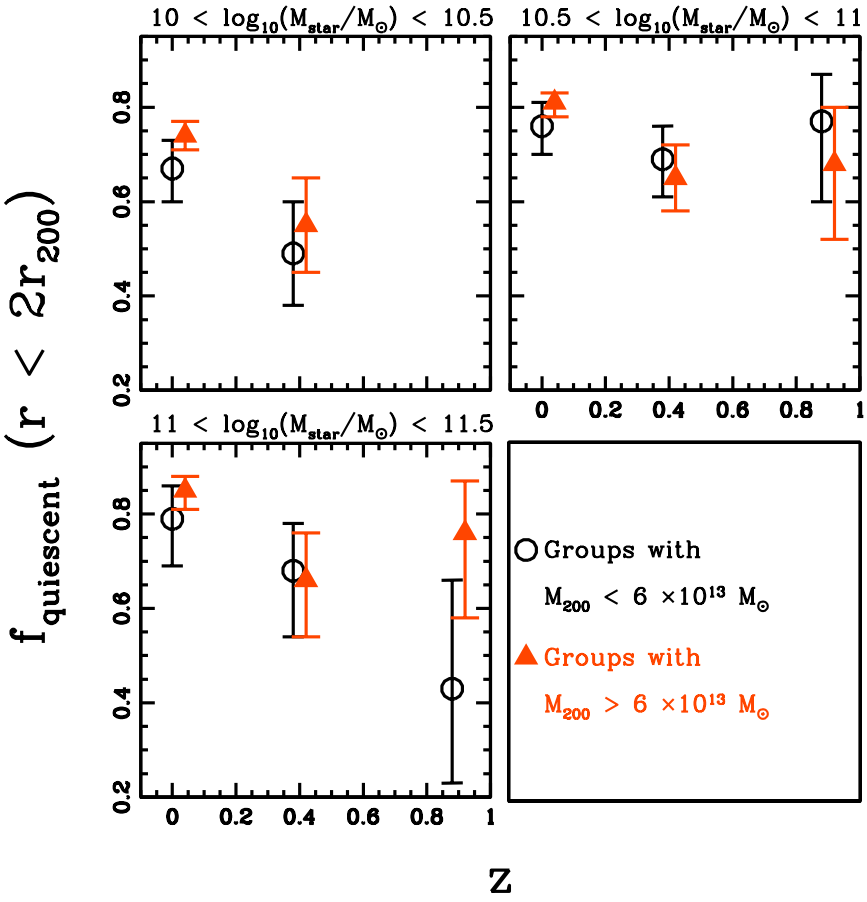

Figure 4.4: $f_{\rm q}$ versus z for low mass galaxies ($10 < \log_{10}(M_{\rm star}/M_{\odot}) \leq 10.5$: top left), intermediate mass galaxies ($10.5 < \log_{10}(M_{\rm star}/M_{\odot}) \leq 11$: top right) and high mass galaxies ($11 < \log_{10}(M_{\rm star}/M_{\odot}) \leq 11.5$: bottom left) in low mass ($M_{200} < 6 \times 10^{13} M_{\odot}$) groups (black circles) and in high mass ($M_{200} > 6 \times 10^{13} M_{\odot}$) groups (orange triangles). It should be noted that due to our stellar mass cuts, the intermediate mass galaxies in the GEEC2 sample span a stellar mass range of $10.7 \leq \log_{10}(M_{\rm star}/M_{\odot}) < 11$. We plot the data at the redshift each sample has been k-corrected to: $z = 0$ for SDSS, $z = 0.4$ for GEEC and $z = 0.9$ for GEEC2, with small horizontal offsets for clarity. We remind the reader of the redshift range for each catalogue: $0 < z < 0.12$ for SDSS, $0.15 < z < 0.55$ for GEEC and $0.8 < z < 1$ for GEEC2. The uncertainties in quiescent fraction are computed following the methodology of Cameron (2011).

4.4 Group Dynamics

Having considered how the observed quiescent fraction of galaxies in groups correlates with galaxy stellar mass and group dynamical mass, M_{200}, we now examine how the dynamical state of a group affects the properties of member galaxies. Previous studies of the local environment have been characterized by the local density (e.g., Poggianti et al., 2008) and by the number of nearest neighbours, typically 3-10 (e.g., Gómez et al., 2003; Patel et al., 2011; Sobral et al., 2011). While these methods are effective in determining the local over-density of regions within groups, they are not directly related to the dynamical state of a group. With a spectroscopic group catalogue we can directly measure the dynamical state of the group, both in terms of the local environment and the host group halo. In the following section, we describe how we classify the dynamical state of galaxy groups and present our analysis of the SDSS, GEEC and GEEC2 groups.

4.4.1 Determining the dynamical state of groups

We classify the dynamical state of a group using two methods:

1. The shape of the group velocity distribution;
2. The amount of substructure.

Theoretically, a system in dynamical equilibrium (i.e. relaxed or virialized) should have a Gaussian velocity distribution; thus, deviations from such a distribution would indicate a dynamically complex or unevolved system. In Hou et al. (2009), we showed that we can reliably and robustly identify non-Gaussian velocity distributions for systems with as few as five member galaxies using the Anderson-Darling (AD) goodness-of-fit test. A full description of the AD Test, and its application to group-sized systems, is given in Hou et al. (2009). For our analysis, we use the AD statistic to compare the cumulative distribution function (CDF) of the ordered galaxy velocities to a Gaussian distribution using the computing formula given by

$$A^2 = -n - \frac{1}{n}\sum_{i=1}^{n}(2i-1)\left(\ln\Phi\left(x_i\right) + \ln\left(1-\Phi\left(x_{n+1-i}\right)\right)\right), \qquad (4.5)$$

$$A^{2*} = A^2 \left(1 + \frac{0.75}{n} + \frac{2.25}{n^2}\right), \tag{4.6}$$

where $x_i \leq x \leq x_{i+1}$, $\Phi(x_i)$ is the CDF of a Gaussian distribution (D'Agostino & Stephens, 1986). The probabilities, or p-values, are then computed as

$$p = a \exp(-A^{2*}/b), \tag{4.7}$$

where a = 3.6789468 and b = 0.1749916, and both factors are determined via Monte Carlo methods (Nelson, 1998). We then classify groups as dynamically complex if the group velocity distribution is identified as non-Gaussian at the 95 per cent confidence level (p-value < 0.05).

We also examine the amount of substructure present in each group by applying the Dressler-Shectman (DS) Test (Dressler & Shectman, 1988) to our group samples. Substructure is indicative of the recent accretion of galaxies or smaller groups of galaxies (Lacey & Cole, 1993). In Hou et al. (2012), we showed that the DS test, originally developed for richer galaxy clusters, could robustly identify substructure for groups with $n_{\rm members} \geq 20$. Additionally, we found that the test could be applied to groups with as few as 10 members, but in this case the measured fraction of systems with substructure is underestimated. A detailed description of the test, with respect to group-sized systems can be found in Pinkney et al. (1996), Zabludoff & Mulchaey (1998a) and Hou et al. (2012). Briefly, for each group we compute the mean velocity ($\overline{\nu}$) and group velocity dispersion (σ). Then, for each member galaxy i, we compute the local mean velocity ($\overline{\nu^i_{local}}$) and local velocity dispersion (σ^i_{local}) using the ith galaxy plus a number of its nearest neighbours (N_{nn}). Using these values we then compute

$$\delta_i = \left(\frac{N_{nn}+1}{\sigma^2}\right)\left[\left(\overline{\nu^i_{local}} - \overline{\nu}\right)^2 + \left(\sigma^i_{local} - \sigma\right)^2\right], \tag{4.8}$$

where $1 \leq i \leq n_{\rm members}$ and $N_{nn} = \sqrt{n_{\rm members}}$, rounded down to the nearest integer. The DS statistic is then computed as

$$\Delta = \sum_{i=1}^{n} \delta_i. \tag{4.9}$$

Table 4.2: Fraction of dynamically complex (non-Gaussian) groups and groups with substructure using the AD and DS Tests.

Catalogue	Fraction of non-Gaussian groups	Fraction of Groups with substructure
SDSS	15/100 (15 $\pm^{6}_{4}$%)	17/71 (24 $\pm^{8}_{6}$%)
GEEC	19/37 (51±11%)	3/14 (21 $\pm^{19}_{10}$%)
GEEC2	2/8 (25 $\pm^{26}_{13}$%)	1/5 (20 $\pm^{34}_{12}$%)

We use Monte Carlo methods to determine the probability or p-value for the DS Test, which is done by comparing the observed Δ-value to 'shuffled Δ-values', which are computed by randomly shuffling the observed velocities and then re-assigning them to the observed member galaxy positions. The p-value is then calculated as

$$p = \sum(\Delta_{\rm shuffled} > \Delta_{\rm observed})/n_{\rm shuffle}, \tag{4.10}$$

where $\Delta_{\rm shuffled}$ and $\Delta_{\rm observed}$ are both computed with Equation 4.9. We compute the p-value using 100 000 shuffled Δ-values. A group is identified as having significant substructure if it has a p-value < 0.05.

Following this methodology, we classify the dynamical state of the SDSS, GEEC and GEEC2 groups using the AD Test for all groups with $n_{\rm members} \geq 5$ and the DS Test for $n_{\rm members} \geq 10$. In Table 4.2, we list the results of the tests, where we find the percentage of non-Gaussian groups in the SDSS, GEEC and GEEC2 surveys to be 15 $\pm^{6}_{4}$ per cent, 51 $\pm$11 per cent and 25 $\pm^{26}_{13}$ per cent, while the percentage of groups with detected substructure remains approximately constant at $\sim$ 20 per cent for all three group catalogues.

For completeness, we include the AD and DS Test results for the GEE2 sample, however it should be noted that with such a small sample of systems we cannot robustly determine the fraction of non-Gaussian groups and groups with substructure.

4.4.2 Dynamics and galaxy properties

Having classified the dynamical state of the groups in our sample, we now compare the SSFR distributions and quiescent fractions of the galaxies in

Table 4.3: Probabilities (p-values) from a two-sample KS Test comparing the SSFR distributions shown in Figure 4.5. Probabilities < 0.01 indicate that the systems come from different underlying parent distributions.

Catalogue	p-value comparing Gaussian versus non-Gaussian groups	p-value comparing groups with substructure vs. no substructure
SDSS	0.01099	0.4729
GEEC	~ 0	~ 0
GEEC2	0.6869	

groups that are dynamically young to those in dynamically evolved systems.

4.4.2.1 SSFR Distributions

In the top panels of Figure 4.5 we plot the SSFR distributions for galaxies in non-Gaussian (blue dashed line) and Gaussian (solid magenta line) groups identified in the SDSS (left), GEEC (middle) and GEEC2 (right) group catalogues. The bottom panels of Figure 4.5 are the same except we plot the SSFR distributions for galaxies in groups with substructure (blue dashed line) and galaxies in groups with no substructure (solid magenta line) for the SDSS (left) and GEEC (middle) samples. We do not show the SSFR distributions for the GEEC2 groups with and without substructure because the sample contains too few galaxies. For the same reason we do not include the GEEC2 groups with and without substructure in our analysis for the remainder of the paper.

In all panels of Figure 4.5, we see that the histograms are bimodal, showing a population of actively star-forming galaxies with SSFR $> 10^{-11}$ yr^{-1} and a population of passive galaxies with SSFR $< 10^{-11}$ yr^{-1}. For the SDSS groups, it appears that the SSFR distributions for dynamically complex and relaxed systems, classified with both the AD- and DS-Test, are similar with a well populated passive sequence. However, a two-sample Kolmogorov-Smirnov (KS) Test indicates that while the SSFR distributions for the SDSS galaxies in groups with and without substructure likely come from the same parent distribution, the distributions for galaxies in Gaussian and non-Gaussian groups are in fact distinct at the $\sim$99 per cent confidence level (Table 4.3). Though it should be noted that difference is small and it is easier to detect small differences given the large size of the SDSS sample.

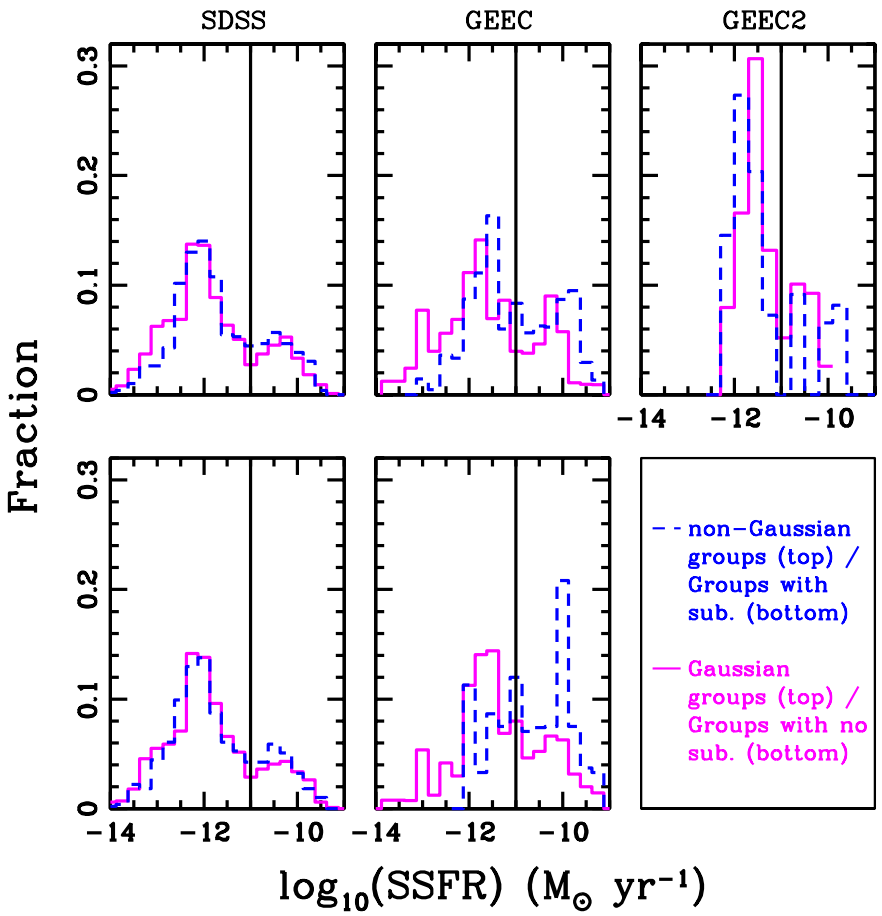

Figure 4.5: Top: SSFR distributions for galaxies in non-Gaussian groups (blue dashed line) and for galaxies in Gaussian groups (magenta solid line) in the SDSS catalogue (left), GEEC catalogue (middle) and GEEC2 catalogue (right). Note that all catalogues are stellar mass complete and spectroscopic completeness weights have been taken into account. Bottom: SSFR distributions for galaxies in groups with substructure (blue dashed line) and for galaxies in groups with no identified substructure (magenta solid line) for the SDSS (left) and GEEC (middle) sample. We do not show the SSFR distributions for the GEEC2 groups with and without substructure, as our stellar mass limit and $n \geq 10$ within $2r_{200}$ cut for the DS Test result in too few galaxies.

Looking at the $z \sim 0.4$ GEEC groups (middle panels of Figure 4.5), we see that the SSFR distributions for the dynamically complex and relaxed groups, identified with either the AD- or DS-Test, look distinct. Indeed, a two-sample KS Test indicates that both sets of SSFR distributions come from different parent distributions at a confidence level of >99 per cent (Table 4.3). For the Gaussian and non-Gaussian groups, we see that although both histograms show a bimodal distribution with a well populated passive sequence, there are more galaxies with high SSFR's ($\sim 10^{-10}$ yr^{-1}: Figure 4.5) in the non-Gaussian GEEC groups. The GEEC groups with no detected substructure show a well populated passive sequence, while the majority of galaxies in the GEEC groups with substructure appear to lie in the actively star-forming sequence. A similar result was shown in Hou et al. (2012), where we found that galaxies in groups with substructure had a significantly higher fraction of blue galaxies.

The SSFR distributions for the galaxies in Gaussian and non-Gaussian GEEC2 groups are consistent with coming from the same parent distribution (Table 4.3) and show similar features to the SDSS groups (i.e. a dominant quiescent population). The high fraction of quiescent galaxies is likely a result of our stellar mass completeness limits ($\log_{10}(M_{\rm star}/M_{\odot}) \geq 10.7$), which from Figure 4.3 would result in a more dominant quiescent population.

4.4.2.2 Quiescent Fractions

We now look at the quiescent fraction (f_q: Equation 4.3) of galaxies in dynamically complex and relaxed groups. In the left panels of Figure 4.6, we plot $f_{\rm q}$ versus z for low mass galaxies ($10 < \log_{10}(M_{\rm star}/M_{\odot}) \leq 10.5$: top left), intermediate mass galaxies ($10.5 < \log_{10}(M_{\rm star}/M_{\odot}) \leq 11$: top right) and high mass galaxies ($11 < \log_{10}(M_{\rm star}/M_{\odot}) \leq 11.5$: bottom left) in non-Gaussian groups (blue symbols) and in Gaussian groups (magenta triangles). The panels on the right are similar except we plot galaxies in groups with substructure (blue symbols) and in groups with no significant substructure (magenta triangles) but only for the SDSS and GEEC groups. The GEEC2 groups are omitted as there are too few galaxies for a robust substructure analysis. In order to isolate the effects of dynamical state on the properties of galaxies from the strong $f_{\rm q}$-stellar mass trend (Figure 4.3), we bin our data into narrow bins of stellar mass.

Looking at Figure 4.6, we find that at almost all epochs and stellar masses there is no significant difference in the quiescent fractions of galaxies in dynamically complex and relaxed groups for both dynamical classification schemes (AD and DS Tests). However, we do observe a difference in the low mass bin ($10 < \log_{10}(M_{\rm star}/M_{\odot}) \leq 10.5$) of the GEEC sample, where the groups with substructure have a lower f_q than observed in the groups with no substructure.

It should also be noted that our analysis was done using galaxies within two viral radii of the group centroid; however, if we use only galaxies with $r < r_{200}$ we find similar results. Although including galaxies beyond the virial radius (r_{200}) inherently means that we are investigating the 'unvirialized' regions of our systems, we find that while the fraction of dynamically young systems increases within each sample, the trends with redshift remain the same whether we use r_{200} or $2r_{200}$. In Hou et al. (2012), we determined that substructure galaxies were preferentially found on the group outskirts. Thus, analyzing galaxies out to two virial radii allows us to better study substructure in our groups. Additionally, studies have shown that the effects of the environment on galaxies can extend well beyond the virial radius (Feldmann et al., 2010; von der Linden et al., 2010; Bahe et al., 2012).

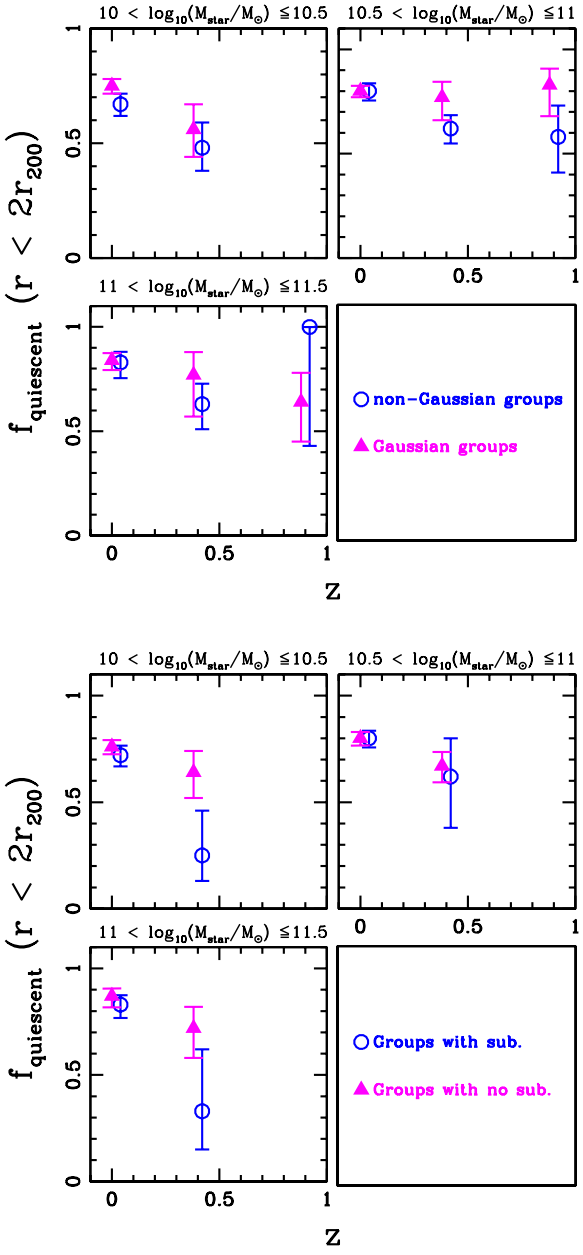

Figure 4.6: Left: $f_{\rm q}$ versus z for galaxies in groups with non-Gaussian velocity distributions (blue circles) and in groups with Gaussian velocity distributions (magenta triangles). The panels are divided into bins of stellar mass, with; $10 < \log_{10}(M_{\rm star}/M_{\odot}) \leq 10.5$ (top-left), $10.5 < \log_{10}(M_{\rm star}/M_{\odot}) \leq 11$ (top-right) and $11 < \log_{10}(M_{\rm star}/M_{\odot}) \leq 11.5$ (bottom-left). Note that all catalogues are spectroscopic and stellar mass complete. Also, due to the stellar mass limits the intermediate mass bin for the GEEC2 sample does not extend down to $\log_{10}(M_{\rm star}/M_{\odot}) \leq 10.5$, but rather covers a range of $10.7 \leq \log_{10}(M_{\rm star}/M_{\odot}) \leq 11$. We plot the data at the redshift that each sample has been k-corrected to: $z = 0$ for SDSS, $z = 0.4$ for GEEC and $z = 0.9$ for GEEC2, with small horizontal offsets for clarity. Right: Same as figure on the left except for galaxies in groups with substructure (blue circles) and in groups with no significant substructure (magenta triangles). Again, we do not show the GEEC2 groups with and without substructure, as our stellar mass limits and $n \geq 10$ within $2r_{200}$ cut for the DS Test resulted in too few galaxies in each sub-sample. The uncertainties in quiescent fraction are computed following the methodology of Cameron (2011).

4.5 Discussion

In Section 4.4 we classified the dynamical state of our group sample and then compared the SSFR distributions and quiescent fractions of galaxies in dynamically complex and relaxed groups. We now discuss the implications of our findings.

4.5.1 The evolution of group dynamics

In a ΛCDM Universe structure grows hierarchically through mergers and accretion (e.g., Springel et al., 2005). Numerous studies have shown that at a given halo mass the average accretion rate of dark matter haloes goes as $\dot{M}/M \propto (1+z)^n$, where $n \sim 1.5 - 2.5$ (Birnboim et al., 2007; McBride et al., 2009), indicating that the accretion rate increases with redshift. As a reflection of this assembly history, one might expect the fraction of dynamically unevolved systems to increase with redshift for a given mass. Although, additional factors, such as the time since infall or the mass and orbit of the accreted object, should also affect the evolution of the dynamical state. For example, continuous accretion of smaller sub-haloes could result in less obvious deviations from a relaxed state in comparison to an instantaneous major merger of larger haloes (Cohn & White, 2005). Therefore, observations that are sensitive to different forms of mass assembly may result in different dynamical evolution scenarios. However, based on a statistical study of a large sample of simulated N-body groups and clusters, identified with a FoF-algorithm, Cohn & White (2005) found that on average the virial ratio, 2KE/PE, of all clusters with $M > 10^{14}h^{-1}M_{\odot}$ increased with increasing redshift. Therefore, systems at higher redshifts are more dynamically young or complex than in the local Universe. Assuming that galaxies are a good tracer of the dark matter haloes, it should be possible to detect this predicted increase in dynamically unevolved systems.

In Section 4.4.1, we found that the fraction of groups with non-Gaussian velocity distributions, classified as dynamically young, increases significantly from ∼15 per cent at $z \sim 0$ to ∼51 per cent at $z \sim 0.4$ (Table 4.2), which is in agreement with the results of Cohn & White (2005) who found that the virial ratio increased with redshift. From $z \sim 0.4$ to $z \sim 0.9$ it appears

that the fraction of non-Gaussian groups is consistent with either being flat or decreasing with increasing redshift (Table 4.2); however, this result is based a small sample of 8 high-z groups. It is also important to note that the GEEC2 catalogue is different from the SDSS or GEEC samples in that: the groups were selected using a different methodology, all of the GEEC2 groups are X-ray bright while only some of the SDSS and GEEC groups are X-ray bright, and a different stellar mass completeness limit was applied. Thus, the results of the GEEC2 sample may be due to small number statistics or differences in the sample selection. Further investigation of a larger sample of high redshift groups is required to make any conclusive statements about the evolution of group dynamics from intermediate to high redshifts.

We now look at the evolution of substructure in groups and we find that the fraction of groups with substructure is consistent out to $z \sim 1$. These results appear to be contradictory. However, the AD and DS Tests, though both measures of dynamical state, probe different stages of dynamical complexity (Pinkney et al., 1996) and a 1-to-1 correspondence between non-Gaussian groups (identified from the AD Test) and groups with substructure (identified from the DS Test) does not necessarily hold. In Hou et al. (2012) we showed that groups with substructure that is loosely bound or spatially mixed with members of the host group can be difficult to detect. Therefore, groups with non-Gaussian profiles may have substructure that is missed by the DS test. Also, since we studied groups with as few as 10 members, the results of the DS Test can only provide a lower limit on the fraction of groups with substructure (Hou et al., 2012), so the true fraction of groups with substructure is likely higher than the values quoted in Table 4.2.

4.5.2 The effects of dynamics on galaxy properties

We first look at the quiescent fraction as a function of redshift. From Figures 4.3 and 4.6 we see that for groups only the low mass galaxies ($10 < \log_{10}(M_{\rm star}/M_{\odot}) \leq 10.5$) clearly exhibit the well known Butcher-Oemler effect (Butcher & Oemler, 1984; Poggianti et al., 1999; Wilman et al., 2005a; Urquhart et al., 2010; McGee et al., 2011; Li et al., 2012), where f_q decreases with increasing redshift. In contrast, the quiescent fraction of inter-

mediate and high mass galaxies ($10.5 < \log_{10}(M_{\rm star}/M_{\odot}) \leq 11.5$) in groups shows a marginal decrease between $z \sim 0$ to $z \sim 0.4$ and no obvious change between $z \sim 0.4$ to $z \sim 0.9$. This result is similar to those of Raichoor & Andreon (2012), who observed no increase in the fraction of high mass ($\log_{10}(M_{\rm star}/M_{\odot}) \gtrsim 11.13$) blue galaxies in clusters in the redshift range of $0 < z < 2.2$. Based on our results, we find no clear evidence for the Butcher-Oemler effect in galaxies with $\log_{10}(M_{\rm star}/M_{\odot}) \gtrsim 10.5$ in groups out to $z \sim 1$. However, we do observe decrease in the fraction of low mass ($\log_{10}(M_{\rm star}/M_{\odot}) < 10.5$) quiescent galaxies with increasing redshift.

Finally, we examine the effects of dynamical state. In general, we find that there is no correlation between dynamical state and quiescent fraction for massive galaxies ($\log_{10}(M_{\rm star}/M_{\odot}) > 10.5$); however, there may be a hint of a correlation with the presence of substructure in our lowest mass galaxies ($10 < \log_{10}(M_{\rm star}/M_{\odot}) \leq 10.5$ - Fig. 4.6: right). In our intermediate redshift GEEC sample, the groups with substructure have a lower quiescent fraction in comparison to galaxies in groups with no substructure. Our results for the SDSS sample can be compared to the Zurich Environmental Study (ZENS) sample of Carollo et al. (2012) and are in good agreement. Carollo et al. (2012) found that central galaxies and satelites with $\log_{10}(M_{\rm star}/M_{\odot}) > 10$ in dynamically relaxed and unrelaxed groups, classified via the DS Test, have similar observed galaxy properties. However, these authors did find that satellites with $\log_{10}(M_{\rm star}/M_{\odot}) < 10$ are bluer by ~ 0.1mag in unrelaxed groups. Our sample does not extend to these low masses, though we do find a similar result for slightly higer mass galaxies ($10 < \log_{10}(M_{\rm star}/M_{\odot}) \leq 10.5$) at intermediate redshifts ($z \sim 0.4$), which could indicate possible redshift evolution in the relationship between substructure and quiescent fraction.

In addition, several studies have also found that environmental effects on galaxy properties can only be observed in low mass galaxies ($\log_{10}(M_{\rm star}/M_{\odot}) \lesssim 10.5$ - Peng et al., 2010; Sobral et al., 2011). In particular, Peng et al. (2010) suggest that for low mass galaxies at $z \gtrsim 0.5$, the main mechanism responsible for star formation quenching is galaxy-galaxy interactions, which should be the dominant process in dynamically unevolved systems with significant substructure. In addition, Blanton & Berlind (2007) found that while the properties of star-forming galaxies were largely independent of environment, they did ob-

serve a correlation between colour and clustering on small scales ($< 300h^{-1}$ Mpc), which they claim indicated that substructure within groups may play a role in the evolution of galaxies. Similarly, Wilman et al. (2010) observed a correlation between the mean colour of blue galaxies and local density but only on the $\lesssim 1$ Mpc scales, further suggesting that the local, and not global or large-scale, environment may have a more dominant affect on galaxy evolution.

Although we do observe a difference in the quiescent fractions of low mass galaxies in GEEC groups with and without substructure, we note that this result is based on a small sample of groups (Table 4.2). A larger sample of intermediate and high redshift groups is required to make a more robust statement about whether quenching in low mass group galaxies is suppressed in the presence of substructure.

4.6 Conclusions

We have looked at the role of galaxy stellar mass, group dynamical mass (M_{200}) and dynamical state in the evolution of galaxies in groups out to $z \sim 1$ using the SDSS, GEEC and GEEC2 group catalogues. The dynamical state of the groups are classified with the Anderson-Darling Test to distinguish between Gaussian and non-Gaussian velocity distributions and the Dressler-Shectman Test to determine the amount of substructure within the groups. The main results of this analysis are:

1. We observe a strong trend between the quiescent fraction and galaxy stellar mass in SDSS and GEEC, where higher mass galaxies have higher $f_{\rm q}$, similar to the results of McGee et al. (2011);

2. There is no measurable difference in the quiescent fraction of galaxies in low ($10^{13} \lesssim M_{200} < 6 \times 10^{13} M_{\odot}$) and high ($6 \times 10^{13} M_{\odot} < M_{200} \lesssim 10^{14.5}$) mass groups at all stellar masses;

3. The fraction of groups with non-Gaussian velocity distributions increases from $z \sim 0$ to $z \sim 0.4$, while the fraction of groups with detected substructure is constant out to $z \sim 1$;

4. We observe the Butcher-Oemler effect in groups, where groups at higher redshifts have lower quiescent fractions, but only for low mass galaxies ($10 < \log_{10}(M_{\rm star}/M_{\odot}) \lesssim 10.5$), while galaxies with $\log_{10}(M_{\rm star}/M_{\odot}) > 10.5$ show little or no evidence of the Butcher-Oemler effect out to $z \sim 1$;

5. We do not observe a significant difference in the quiescent fractions of massive galaxies ($\log_{10}(M_{\rm star}/M_{\odot}) > 10.5$) in dynamically complex and relaxed groups, where the dynamical state is defined either by the AD or DS Test;

6. We observe a marginally lower quiescent fraction for low mass galaxies ($10 \leq \log_{10}(M_{\rm star}/M_{\odot}) < 10.5$) in groups with detected substructure at $z \sim 0.4$ when compared to groups with no significant substructure.

In conclusion, we find that there is no strong correlation between the dynamical state of a group and the observed quiescent fraction for massive galaxies; however, we do see possible signs of a correlation between f_q and substructure at $z \sim 0.4$. This result suggests that environmental effects on galaxy evolution are only evident in low mass galaxies. In order to better understand the role of group dynamics, and the environment in general, on the evolution of galaxies it is necessary to probe lower mass galaxies ($\log_{10}(M_{\rm star}/M_{\odot}) < 10.5$) where these mechanisms likely dominate.

4.7 Acknowledgments

We would like to thank the CNOC2 team for the use of unpublished redshifts. A.H, L.C.P, and W.E.H would like to thank the National Science and Engineering Research Council of Canada (NSERC) for funding.

Bibliography

Abadi, M. G., Moore, B., & Bower, R. G. 1999, MNRAS, 308, 947

Adelman-McCarthy, J. K., Agüeros, M. A., Allam, S. S., Allende Prieto, C., Anderson, K. S. J., Anderson, S. F., Annis, J., Bahcall, N. A., Bailer-Jones, C. A. L., Baldry, I. K., & et al.,. 2008, ApJS, 175, 297

Bahe, Y. M., McCarthy, I. G., Balogh, M. L., & Font, A. S. 2012, ArXiv e-prints

Baldry, I. K., Balogh, M. L., Bower, R. G., Glazebrook, K., Nichol, R. C., Bamford, S. P., & Budavari, T. 2006, MNRAS, 373, 469

Balogh, M. L., Baldry, I. K., Nichol, R., Miller, C., Bower, R., & Glazebrook, K. 2004, ApJ, 615, L101

Balogh, M. L., McGee, S. L., Wilman, D., Bower, R. G., Hau, G., Morris, S. L., Mulchaey, J. S., Oemler, Jr., A., Parker, L., & Gwyn, S. 2009, MNRAS, 398, 754

Balogh, M. L., McGee, S. L., Wilman, D. J., Finoguenov, A., Parker, L. C., Connelly, J. L., Mulchaey, J. S., Bower, R. G., Tanaka, M., & Giodini, S. 2011, MNRAS, 412, 2303

Balogh, M. L., Navarro, J. F., & Morris, S. L. 2000, ApJ, 540, 113

Balogh, M. L., Wilman, D., Henderson, R. D. E., Bower, R. G., Gilbank, D., Whitaker, R., Morris, S. L., Hau, G., Mulchaey, J. S., Oemler, A., & Carlberg, R. G. 2007, MNRAS, 374, 1169

Barnes, J. 1985, MNRAS, 215, 517

Beers, T. C., Flynn, K., & Gebhardt, K. 1990, AJ, 100, 32

Berlind, A. A., Frieman, J., Weinberg, D. H., Blanton, M. R., Warren, M. S., Abazajian, K., Scranton, R., Hogg, D. W., Scoccimarro, R., Bahcall, N. A., et al.,, J., & SDSS Collaboration. 2006, ApJS, 167, 1

Bird, C. M. 1995, ApJ, 445, L81

Birnboim, Y., Dekel, A., & Neistein, E. 2007, MNRAS, 380, 339

Blanton, M. R. & Berlind, A. A. 2007, ApJ, 664, 791

Blanton, M. R., Eisenstein, D., Hogg, D. W., Schlegel, D. J., & Brinkmann, J. 2005, ApJ, 629, 143

Blanton, M. R., Hogg, D. W., Bahcall, N. A., Baldry, I. K., Brinkmann, J., Csabai, I., Eisenstein, D., Fukugita, M., Gunn, J. E., Ivezić, Ž., & et al.,. 2003, ApJ, 594, 186

Bolzonella, M., Kovač, K., Pozzetti, L., Zucca, E., Cucciati, O., Lilly, S. J., Peng, Y., Iovino, A., Zamorani, G., Vergani, D., & et al.,. 2010, A&A, 524, A76

Brinchmann, J., Charlot, S., White, S. D. M., Tremonti, C., Kauffmann, G., Heckman, T., & Brinkmann, J. 2004, MNRAS, 351, 1151

Brough, S., Forbes, D. A., Kilborn, V. A., & Couch, W. 2006, MNRAS, 370, 1223

Bruzual, G. 2007, in Astronomical Society of the Pacific Conference Series, Vol. 374, From Stars to Galaxies: Building the Pieces to Build Up the Universe, ed. A. Vallenari, R. Tantalo, L. Portinari, & A. Moretti, 303

Bruzual, G. & Charlot, S. 2003, MNRAS, 344, 1000

Butcher, H. & Oemler, Jr., A. 1984, ApJ, 285, 426

Cameron, E. 2011, PASA, 28, 128

Carlberg, R. G., Yee, H. K. C., Ellingson, E., Morris, S. L., Abraham, R., Gravel, P., Pritchet, C. J., Smecker-Hane, T., Hartwick, F. D. A., Hesser, J. E., Hutchings, J. B., & Oke, J. B. 1997, ApJ, 485, L13

Carlberg, R. G., Yee, H. K. C., Morris, S. L., Lin, H., Hall, P. B., Patton, D. R., Sawicki, M., & Shepherd, C. W. 2001, ApJ, 552, 427

Carollo, C. M., Cibinel, A., Lilly, S. J., Miniati, F., Norberg, P., Silverman, J. D., van Gorkom, J., Cameron, E., Finoguenov, A., Pipino, A., Rudick, C. S., Lu, T., & Peng, Y. 2012, ArXiv e-prints

Charlot, S. & Fall, S. M. 2000, ApJ, 539, 718

Cohn, J. D. & White, M. 2005, Astroparticle Physics, 24, 316

Connelly, J. L., Wilman, D. J., Finoguenov, A., Hou, A., Mulchaey, J. S., McGee, S. L., Balogh, M. L., Parker, L. C., Saglia, R., Henderson, R. D. E., & Bower, R. G. 2012, ApJ, 756, 139

Cooper, M. C., Newman, J. A., Weiner, B. J., Yan, R., Willmer, C. N. A., Bundy, K., Coil, A. L., Conselice, C. J., Davis, M., Faber, S. M., Gerke, B. F., Guhathakurta, P., Koo, D. C., & Noeske, K. G. 2008, MNRAS, 383, 1058

Cox, T. J., Jonsson, P., Primack, J. R., & Somerville, R. S. 2006, MNRAS, 373, 1013

D'Agostino, R. & Stephens, M. 1986, Goodness-of-fit Techniques (Marcel Dekker Inc.)

De Lucia, G., Fontanot, F., Wilman, D., & Monaco, P. 2011, MNRAS, 414, 1439

De Lucia, G., Weinmann, S., Poggianti, B. M., Aragón-Salamanca, A., & Zaritsky, D. 2012, MNRAS, 423, 1277

Dressler, A. 1980, ApJ, 236, 351

Dressler, A. & Shectman, S. A. 1988, AJ, 95, 985

Eke, V. R., Baugh, C. M., Cole, S., Frenk, C. S., King, H. M., & Peacock, J. A. 2005, MNRAS, 362, 1233

Elbaz, D. & Cesarsky, C. J. 2003, Science, 300, 270

Feldmann, R., Carollo, C. M., Mayer, L., Renzini, A., Lake, G., Quinn, T., Stinson, G. S., & Yepes, G. 2010, ApJ, 709, 218

Finoguenov, A., Connelly, J. L., Parker, L. C., Wilman, D. J., Mulchaey, J. S., Saglia, R. P., Balogh, M. L., Bower, R. G., & McGee, S. L. 2009, ApJ, 704, 564

Finoguenov, A., Guzzo, L., Hasinger, G., Scoville, N. Z., Aussel, H., Böhringer, H., Brusa, M., Capak, P., Cappelluti, N., Comastri, A., & et al.,. 2007, ApJS, 172, 182

Geller, M. J. & Huchra, J. P. 1983, ApJS, 52, 61

George, M. R., Leauthaud, A., Bundy, K., Finoguenov, A., Tinker, J., Lin, Y.-T., Mei, S., Kneib, J.-P., Aussel, H., Behroozi, P. S., Busha, M. T., Capak, P., Coccato, L., Covone, G., Faure, C., Fiorenza, S. L., Ilbert, O., Le Floc'h, E., Koekemoer, A. M., Tanaka, M., Wechsler, R. H., & Wolk, M. 2011, ApJ, 742, 125

Giodini, S., Finoguenov, A., Pierini, D., Zamorani, G., Ilbert, O., Lilly, S., Peng, Y., Scoville, N., & Tanaka, M. 2012, A&A, 538, A104

Gómez, P. L., Nichol, R. C., Miller, C. J., Balogh, M. L., Goto, T., Zabludoff, A. I., Romer, A. K., Bernardi, M., Sheth, R., Hopkins, A. M., Castander, F. J., Connolly, A. J., Schneider, D. P., Brinkmann, J., Lamb, D. Q., SubbaRao, M., & York, D. G. 2003, ApJ, 584, 210

Gunn, J. E. & Gott, III, J. R. 1972, ApJ, 176, 1

Hogg, D. W., Blanton, M. R., Eisenstein, D. J., Gunn, J. E., Schlegel, D. J., Zehavi, I., Bahcall, N. A., Brinkmann, J., Csabai, I., Schneider, D. P., Weinberg, D. H., & York, D. G. 2003, ApJ, 585, L5

Hou, A., Parker, L. C., Harris, W. E., & Wilman, D. J. 2009, ApJ, 702, 1199

Hou, A., Parker, L. C., Wilman, D. J., McGee, S. L., Harris, W. E., Connelly, J. L., Balogh, M. L., Mulchaey, J. S., & Bower, R. G. 2012, MNRAS, 421, 3594

Kauffmann, G., White, S. D. M., Heckman, T. M., Ménard, B., Brinchmann, J., Charlot, S., Tremonti, C., & Brinkmann, J. 2004, MNRAS, 353, 713

Kawata, D. & Mulchaey, J. S. 2008, ApJ, 672, L103

Kennicutt, Jr., R. C. 1983, ApJ, 272, 54

Lacey, C. & Cole, S. 1993, MNRAS, 262, 627

Larson, R. B., Tinsley, B. M., & Caldwell, C. N. 1980, ApJ, 237, 692

Li, I. H., Yee, H. K. C., Hsieh, B. C., & Gladders, M. 2012, ApJ, 749, 150

Martin, D. C., Fanson, J., Schiminovich, D., Morrissey, P., Friedman, P. G., Barlow, T. A., Conrow, T., Grange, R., Jelinsky, P. N., Milliard, B., & et al.,. 2005, ApJ, 619, L1

McBride, J., Fakhouri, O., & Ma, C.-P. 2009, MNRAS, 398, 1858

McGee, S. L., Balogh, M. L., Bower, R. G., Font, A. S., & McCarthy, I. G. 2009, MNRAS, 400, 937

McGee, S. L., Balogh, M. L., Henderson, R. D. E., Wilman, D. J., Bower, R. G., Mulchaey, J. S., & Oemler, Jr., A. 2008, MNRAS, 387, 1605

McGee, S. L., Balogh, M. L., Wilman, D. J., Bower, R. G., Mulchaey, J. S., Parker, L. C., & Oemler, A. 2011, MNRAS, 413, 996

Mok, A., Balogh, M. L., McGee, S. L., Wilman, D. J., Finoguenov, A., Tanaka, M., Giodini, S., Bower, R. G., Connelly, J. L., Hou, A., Mulchaey, J. S., & Parker, L. C. 2013, ArXiv e-prints

Morrissey, P., Conrow, T., Barlow, T. A., Small, T., Seibert, M., Wyder, T. K., Budavári, T., Arnouts, S., Friedman, P. G., Forster, K., & et al.,. 2007, ApJS, 173, 682

Muzzin, A., Wilson, G., Yee, H. K. C., Gilbank, D., Hoekstra, H., Demarco, R., Balogh, M., van Dokkum, P., Franx, M., Ellingson, E., Hicks, A., Nantais, J., Noble, A., Lacy, M., Lidman, C., Rettura, A., Surace, J., & Webb, T. 2012, ApJ, 746, 188

Nelson, L. 1998, Journal of Quality Technology, 30, 298

Noeske, K. G., Weiner, B. J., Faber, S. M., Papovich, C., Koo, D. C., Somerville, R. S., Bundy, K., Conselice, C. J., Newman, J. A., Schiminovich, D., & et al.,. 2007, ApJ, 660, L43

Oemler, Jr., A. 1974, ApJ, 194, 1

Pasquali, A., Gallazzi, A., Fontanot, F., van den Bosch, F. C., De Lucia, G., Mo, H. J., & Yang, X. 2010, MNRAS, 407, 937

Patel, S. G., Kelson, D. D., Holden, B. P., Franx, M., & Illingworth, G. D. 2011, ApJ, 735, 53

Peng, Y.-j., Lilly, S. J., Kovač, K., Bolzonella, M., Pozzetti, L., Renzini, A., Zamorani, G., Ilbert, O., Knobel, C., Iovino, A., & et al.,. 2010, ApJ, 721, 193

Pinkney, J., Roettiger, K., Burns, J. O., & Bird, C. M. 1996, ApJS, 104, 1

Poggianti, B. M., Desai, V., Finn, R., Bamford, S., De Lucia, G., Varela, J., Aragón-Salamanca, A., Halliday, C., Noll, S., Saglia, R., Zaritsky, D., Best, P., Clowe, D., Milvang-Jensen, B., Jablonka, P., Pelló, R., Rudnick, G., Simard, L., von der Linden, A., & White, S. 2008, ApJ, 684, 888

Poggianti, B. M., Smail, I., Dressler, A., Couch, W. J., Barger, A. J., Butcher, H., Ellis, R. S., & Oemler, Jr., A. 1999, ApJ, 518, 576

Raichoor, A. & Andreon, S. 2012, A&A, 537, A88

Salim, S., Rich, R. M., Charlot, S., Brinchmann, J., Johnson, B. D., Schiminovich, D., Seibert, M., Mallery, R., Heckman, T. M., Forster, K., Friedman, P. G., Martin, D. C., Morrissey, P., Neff, S. G., Small, T., Wyder, T. K., Bianchi, L., Donas, J., Lee, Y.-W., Madore, B. F., Milliard, B., Szalay, A. S., Welsh, B. Y., & Yi, S. K. 2007, ApJS, 173, 267

Sanders, D. B., Soifer, B. T., Elias, J. H., Madore, B. F., Matthews, K., Neugebauer, G., & Scoville, N. Z. 1988, ApJ, 325, 74

Scoville, N., Abraham, R. G., Aussel, H., Barnes, J. E., Benson, A., Blain, A. W., Calzetti, D., Comastri, A., Capak, P., Carilli, C., Carlstrom, J. E., & et al.,. 2007, ApJS, 172, 38

Sobral, D., Best, P. N., Smail, I., Geach, J. E., Cirasuolo, M., Garn, T., & Dalton, G. B. 2011, MNRAS, 411, 675

Springel, V., White, S. D. M., Jenkins, A., Frenk, C. S., Yoshida, N., Gao, L., Navarro, J., Thacker, R., Croton, D., Helly, J., Peacock, J. A., Cole, S., Thomas, P., Couchman, H., Evrard, A., Colberg, J., & Pearce, F. 2005, Nature, 435, 629

Teyssier, R., Chapon, D., & Bournaud, F. 2010, ApJ, 720, L149

Tortora, C., Napolitano, N. R., Cardone, V. F., Capaccioli, M., Jetzer, P., & Molinaro, R. 2010, MNRAS, 407, 144

Tyler, K. D., Rieke, G. H., Wilman, D. J., McGee, S. L., Bower, R. G., Bai, L., Mulchaey, J. S., Parker, L. C., Shi, Y., & Pierini, D. 2011, ApJ, 738, 56

Urquhart, S. A., Willis, J. P., Hoekstra, H., & Pierre, M. 2010, MNRAS, 406, 368

von der Linden, A., Wild, V., Kauffmann, G., White, S. D. M., & Weinmann, S. 2010, MNRAS, 404, 1231

Wetzel, A. R., Tinker, J. L., & Conroy, C. 2012, MNRAS, 424, 232

Whitaker, K. E., van Dokkum, P. G., Brammer, G., & Franx, M. 2012, ApJ, 754, L29

Wilman, D. J., Balogh, M. L., Bower, R. G., Mulchaey, J. S., Oemler, A., Carlberg, R. G., Eke, V. R., Lewis, I., Morris, S. L., & Whitaker, R. J. 2005a, MNRAS, 358, 88

Wilman, D. J., Balogh, M. L., Bower, R. G., Mulchaey, J. S., Oemler, A., Carlberg, R. G., Morris, S. L., & Whitaker, R. J. 2005b, MNRAS, 358, 71

Wilman, D. J., Oemler, A., Mulchaey, J. S., McGee, S. L., Balogh, M. L., & Bower, R. G. 2009, ApJ, 692, 298

Wilman, D. J., Pierini, D., Tyler, K., McGee, S. L., Oemler, Jr., A., Morris, S. L., Balogh, M. L., Bower, R. G., & Mulchaey, J. S. 2008, in Astronomical Society of the Pacific Conference Series, Vol. 399, Panoramic Views of Galaxy Formation and Evolution, ed. T. Kodama, T. Yamada, & K. Aoki, 340

Wilman, D. J., Zibetti, S., & Budavári, T. 2010, MNRAS, 406, 1701

Yang, X., Mo, H. J., van den Bosch, F. C., Pasquali, A., Li, C., & Barden, M. 2007, ApJ, 671, 153

Yee, H. K. C., Morris, S. L., Lin, H., Carlberg, R. G., Hall, P. B., Sawicki, M., Patton, D. R., Wirth, G. D., Ellingson, E., & Shepherd, C. W. 2000, ApJS, 129, 475

Zabludoff, A. I. & Mulchaey, J. S. 1998a, ApJ, 498, L5+

—. 1998b, ApJ, 496, 39

Chapter 5

The pre-processing of subhaloes in SDSS groups and clusters

This chapter incorporates the article *"The pre-processing of subhaloes in SDSS groups and clusters"*, which has been submitted to the *Monthly Notices of the Royal Astronomical Society* and has gone through one round of revision with a referee.

Annie Hou[1], Laura C. Parker[1] & William E. Harris[1]

[1] *Department of Physics & Astronomy, McMaster University, Hamilton ON L8S 4M1, Canada*

Abstract

We investigate the importance of pre-processing in the observed quenched fraction of rich group and cluster galaxies from the SDSS-DR7 Yang et al. (2007) group catalogue in the redshift range of $0.01 < z < 0.045$. A combination of the Dressler-Shectman statistic and the group member velocity distribution is used to identify subhaloes within the group. In addition, we classify our galaxies as either virialized, infall (i.e. satellites that are infalling onto the host halo for the first time) or backsplash (i.e. galaxies that have already passed within the virial radius of the host halo and have been ejected to large radii). On average the fraction of galaxies that reside in subhaloes is a function of host halo mass where more massive systems, such as clusters, have a higher fraction of subhaloes both in the overall galaxy and infall populations. Comparison of the properties of galaxies that reside in subhaloes to those that do not shows that beyond the virial radius ($2 \lesssim r_{200} < 3$) galaxies in the subhalo population differ from the non-subhalo population. In particular, between $2 \lesssim r_{200} < 3$ we find that the quiescent fraction is higher in subhalo galaxies with respect to both the field and non-subhalo galaxies. At these large radii ($2 \lesssim r_{200} < 3$), we find that the majority of galaxies ($\sim 80\%$) belong to the infall population. Therefore, we attribute the enhanced quenching to infalling subhalo galaxies, indicating that pre-processing has occurred in the subhalo population. Based on the results presented in this paper, we conclude that pre-processing plays a significant role in the observed quiescent fraction, but only for the most massive ($M_{\rm halo} > 10^{14.5} M_{\odot}$) systems in our sample.

5.1 Introduction

Observational studies of rich galaxy clusters have shown that most of the members are red early-type galaxies with little or no on-going star formation (Oemler, 1974; Dressler, 1980; Blanton et al., 2003; Balogh et al., 2004; Baldry et al., 2006). While a high fraction of quiescent (i.e. not actively star-forming) galaxies have been observed in rich groups and clusters (Kauffmann et al., 2004; Wilman et al., 2005; Peng et al., 2010; McGee et al., 2011; Muzzin et al., 2012), recent results from observations and simulations (both numerical and semi-analytic) indicate that star formation quenching actually begins in low mass haloes with $M_{\rm halo} \sim 10^{13} M_{\odot}$ (McGee et al., 2009; Balogh & McGee, 2010; George et al., 2011; De Lucia et al., 2012; Wetzel et al., 2012). Additionally, since most galaxies reside in group-sized haloes (Geller & Huchra, 1983; Eke et al., 2005) it is likely that some cluster galaxies had their star formation quenched in groups with $M_{\rm halo} \geq 10^{13} M_{\odot}$ prior to accretion onto the more massive cluster environment, a process often referred to as pre-processing (Zabludoff & Mulchaey, 1998b; Kawata & Mulchaey, 2008; Berrier et al., 2009; McGee et al., 2009; De Lucia et al., 2012).

While quenching has been shown to occur in low mass haloes, the significance of pre-processing is still a subject of debate. Using N-body simulations Berrier et al. (2009) found that 70% of their cluster ($10^{14} < M_{\rm halo} < 10^{14.6} M_{\odot}$) galaxies fell in directly from the field, while only $\sim 10\%$ fell in as members of group-sized haloes with $M_{\rm halo} \geq 10^{13} M_{\odot}$. Based on these results, Berrier et al. (2009) concluded that pre-processing did not significantly contribute to the quenching observed in present-day clusters. In contrast, both McGee et al. (2009) and De Lucia et al. (2012) analyzed semi-analytic models (SAMs) and found that $\sim 25 - 45\%$ of their simulated cluster galaxies fell in as members of systems with $M_{\rm halo} \geq 10^{13} M_{\odot}$, where the range depends on the mass of the galaxy and the mass of the host cluster. It should be noted that according to De Lucia et al. (2012), part of the discrepancy between the results of Berrier et al. (2009) and McGee et al. (2009) arises from differing definitions of 'satellite', with the former computing fractions based on the time when a galaxy *first* becomes a satellite of any halo and the latter when a galaxy becomes a satellite of the *final or present-day* group or cluster. With the

former definition, De Lucia et al. (2012) find that their results are not inconsistent with those of Berrier et al. (2009). A similar analysis was carried out using N-body hydrodynamical simulations by Bahé et al. (2013). These authors found that $\sim 15-60\%$ of galaxies in host haloes in the mass range of $10^{13.5} < M_{\rm halo} < 10^{15.2} M_{\odot}$ had been pre-processed where the amount of pre-processing depended on halo mass. More massive haloes had a higher fraction of pre-processed galaxies (Bahé et al., 2013).

Thus, the results of some SAMs (e.g. McGee et al., 2009; De Lucia et al., 2012) and numerical simulations (e.g. Bahé et al., 2013) predict that pre-processing can play an important role in quenching star formation and producing the observed quiescent fraction, especially in massive clusters. If the simulation predictions of significant pre-processing in groups and clusters are correct then it should be possible to observe pre-processing by looking at the populations of galaxies in different environments. The aim of this paper is to investigate the significance of pre-processing in a statistical sample of observed groups and clusters. This can be achieved by studying the properties of *infalling* subhalo galaxies, where a subhalo is defined as a collection of galaxies that reside in the same halo embedded within a larger parent halo. Subhaloes can be identified by performing substructure analysis with the Dressler-Shectman (DS) Test (Dressler & Shectman, 1988), which can detect galaxies with kinematic properties that deviate from those of the host halo. It should be noted that this method of identifying subhaloes differs from those used in numerical simulations. In particular, our observational definition of subhaloes is based on identification of kinematically distinct galaxies and does not require the galaxies within the subhalo to be gravitationally bound to another, which is usually the case for subhaloes identified in numerical simulations. Subhaloes, detected via the DS Test, are preferentially found on the group or cluster outskirts (West & Bothun, 1990; Zabludoff & Mulchaey, 1998a; Hou et al., 2012; Dressler et al., 2013) and the usual assumption is that these systems are infalling. However, numerical simulations have shown that a large fraction of galaxies beyond the virial radius, and out to ~ 2.5 virial radii, have already passed through the group or cluster core (i.e. backsplash galaxies: Balogh et al., 2000; Mamon et al., 2004; Gill et al., 2005; Mahajan et al., 2011; Pimbblet, 2011; Bahé et al., 2013; Oman et al., 2013). Backsplash galaxies may have

experienced star formation quenching due to more massive group - or cluster-related processes, and it has been suggested that much of the environmental quenching beyond the virial radius (out to ~ 2.5 virial radii) is most likely due to the presence of a backsplash population (Wetzel et al., 2013b). In contrast, the infall population typically refers to galaxies that are infalling onto the host system for the first time. Thus, any observed enhanced quenching must be a results of a transformation that occurred prior to accretion onto the host halo (i.e. pre-processing).

Currently, most methods of distinguishing between the virialized, infall and backsplash populations in observed groups and clusters are based on the results of simulated systems. These classification schemes typically involve examining $|\Delta cz|/\sigma$ distributions (Gill et al., 2005; Pimbblet, 2011) or dividing the $\Delta cz/\sigma - r_{200}$ plane into regions occupied by virialized, infall and backsplash galaxies (Mahajan et al., 2011; Oman et al., 2013). Although each population resides in distinct regions in the full phase-space of simulated clusters, projection effects can distort these clear divisions and there is often contamination between the observed populations (to be discussed in more detail in Section 5.4.4). In addition to differences in their phase-space locations, infall and backsplash galaxies should also have subtle differences in their stellar mass distributions. As a result of tidal disruption, backsplash galaxies should be on average less massive than infalling galaxies at the same radius (Gill et al., 2005), and galaxies infalling in subhaloes will typically be more massive than individual infalling galaxies (McGee et al., 2009). Additionally, recent studies have suggested that environmentally driven evolution occurs in low mass galaxies ($M_{\rm star} \lesssim 10^{10} M_{\odot}$: e.g. Peng et al., 2010, 2012). Thus, in order to better probe pre-processing and environmental effects on galaxy evolution, it is important to examine the properties of virialized, infall and backsplash galaxies as a function of stellar mass and over a wide range of masses, including low mass galaxies.

Although it is well known that high-density environments, such as groups and clusters, show signs of enhanced star formation quenching with respect to the field (Kauffmann et al., 2004; Rines et al., 2005; Kimm et al., 2009; Wetzel et al., 2012; Woo et al., 2013), the processes that dominate this transformation are still debated. Comparing the properties of infalling and backsplash subhalo

galaxies allows us to probe the relative importance of rich group- and cluster-related processes, which are observable in the backsplash population, to pre-processing in lower mass haloes, which can be observed in the infalling subhalo population.

In this paper we use a well-studied SDSS group catalogue to probe the properties of subhalo galaxies in groups and clusters in order to investigate the amount of pre-processing that occurs and to study the relative importance of the lower mass group environment in the evolution of galaxies. The paper is structured as follows: in Section 5.2, we present our group and galaxy sample and in Section 5.3, we discuss how we identify subhaloes. We compare the properties of the non-subhalo and subhalo populations, as well as compare the virialized, infall and backsplash subpopulations in Section 5.4. Finally, in Section 5.5, we discuss our results and present our conclusions in Section 5.6. Throughout this paper we assume a ΛCDM cosmology with $\Omega_{m,0} = 0.31$, $\Omega_{\Lambda,0} = 0.69$ and $H_0 = 70$ km s^{-1} Mpc^{-1}.

5.2 Data

To investigate the role of pre-processing in galaxy groups, we require a large sample of group and cluster galaxies that is complete down to low stellar masses ($\log_{10}(M_{\rm star}/M_{\odot}) \sim 9.5$). These requirements can be achieved with the Yang et al. (2007) Sloan Digital Sky Survey (SDSS) group catalogue. Observational results have found correlations between the environment and galaxy properties, but only for low mass galaxies (e.g. Peng et al., 2010; Carollo et al., 2013; Hou et al., 2013). Thus, the low stellar mass completeness limit allows us to probe regimes where environmental effects are more likely to be observed.

5.2.1 The SDSS-DR7 Galaxy Catalogue

The galaxy magnitudes, extinctions, k-corrections and stellar masses are obtained from the New York University Value Added Catalogue (NYU-VAGC: Blanton et al. 2005). The k-corrections and stellar masses are computed following the methodology of Blanton & Roweis (2007), which assume a Chabrier Initial Mass Function (IMF). The star formation rates (SFRs) and specific star

formation rates (SSFR = SFR/$M_{\rm star}$) are from the most recent release of the spectral reductions of Brinchmann et al. (2004)[1]. The SSFRs are measured from either emission lines, whenever available, or determined from the 4000 Å break (D_n4000) when there are no clear emission lines or in the presence of strong contamination from active galactic nuclei (Brinchmann et al., 2004). It should be noted that SSFRs obtained from the D_n4000 value, which are typically values $< 10^{-12}$ yr^{-1} are not exact measures of SSFR but should instead be taken as an upper limit. The average 2σ errors on the SFR estimates are between 0.5 - 1.0 dex, where galaxies with higher SSFRs have lower errors (Brinchmann et al., 2004).

The effects of the environment and the importance of pre-processing are probed via the quiescent fraction (hereafter $f_{\rm q}$), where $f_{\rm q}$ is defined as

$$f_{\rm q} = \frac{\#\text{ galaxies with SSFR} < 10^{-11}\text{yr}^{-1}}{\text{total }\#\text{ of galaxies}}, \tag{5.1}$$

with SSFR = 10^{-11} yr^{-1} marking the division between the main sequence of star-forming galaxies and the quiescent galaxies in the SSFR-stellar mass plane (McGee et al., 2011; Wetzel et al., 2012). It should also be noted that values in Equation 5.1 are weighted to account for spectroscopic incompleteness using the completeness values computed in Yang et al. (2007).

To ensure that the quiescent fraction is not biased, we use a stellar mass complete sample. As a result of the magnitude limit of the SDSS survey, the stellar mass completeness limit is a function of redshift. Therefore, in order to include low mass galaxies in our analysis we restrict the redshift range to $0.01 \leq z \leq 0.045$, which provides us with a sample that is complete down to $3.16 \times 10^9 M_{\odot}$. Analysis is performed on satellite galaxies with all 'central' galaxies, taken to be the most massive galaxy as identified by Yang et al. (2007), removed from our sample.

5.2.2 The SDSS Group Catalogue

Our sample consists of groups and clusters identified in SDSS by Yang et al. (2007). These authors identify groups using all galaxies in the SDSS-DR7

[1]http://www.mpa-garching.mpg.de/SDSS/DR7

sample brighter than the survey magnitude limit of $r \leq 17.77$ and with spectroscopic completeness $> 70\%$. The groups are identified with a halo-based group finder, which uses a traditional friends-of-friends algorithm to identify potential systems and then adds or removes members iteratively based on the mass of the dark matter halo and the assumption that the distribution of galaxies follows that of dark matter haloes, which is assumed to be a projected NFW profile (Navarro et al., 1996). The mass of the halo is determined initially from the total or characteristic luminosity ($L_{19.5}$ in Yang et al. 2007) of all the potential group members with ${}^{0.1}M_{r,\rm lim} - 5\log h^{-1} \leq -19.5$, where ${}^{0.1}M_{r,\rm lim}$ is the absolute magnitude limit at the redshift of the group k-corrected to $z = 0.1$, and a constant mass-to-light (M/L) ratio of $500 M_\odot/L_\odot$. It should be noted that only for the first iteration is a constant M/L ratio used; for all subsequent iterations the $M_{\rm halo}/L_{19.5} - L_{19.5}$ relation from the previous iteration is used to determine the halo mass. In addition, an initial velocity dispersion and size are computed from the members of the potential group. Using this initial mass, size and dispersion, as well as an assumed NFW radial profile and a Gaussian distribution for the line-of-sight (LOS) velocities, the algorithm then adds or removes members until no further members can be added and the $M_{\rm halo}/L_{19.5} - L_{19.5}$ relation converges.

The Yang et al. (2007) group finder identifies systems that cover a wide range of masses, from isolated galaxies to rich clusters ($M_{\rm halo} \sim 10^{15} M_\odot$). These authors carried out performance tests of their halo-based group finder using a mock galaxy redshift survey made to mimic the SDSS-DR4 sample. The performance of the group finder was characterized by the completeness (f_c), defined as the number of members identified over the total number of true group members, and the contamination (f_i), defined as the number of interloping non-members over the total number of true members. Yang et al. (2007) found that the percentage of groups with 100% completeness ranged from $\sim 93\%$ in low-mass groups ($10^{12.5} < M_{\rm halo} \leq 10^{13.5} M_\odot$) to 60% for the most massive clusters ($10^{14.5} < M_{\rm halo} \leq 10^{15} M_\odot$). Since the majority of systems in our sample are in the low-mass halo regime, it is expected that our groups are relatively complete. The contamination from interlopers appears to be mostly independent of halo mass. On average $\sim 65\%$ of the systems had no contamination at all and $\sim 85\%$ had $f_i \leq 0.5$. Interloper galaxies

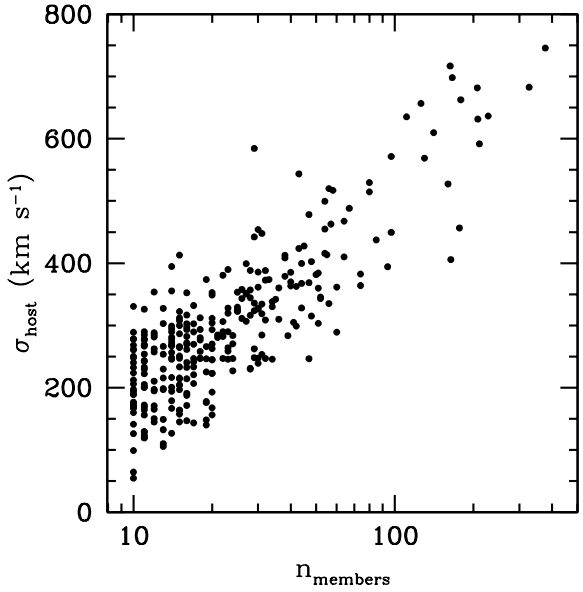

Figure 5.1: Rest-frame group velocity dispersion ($\sigma_{\rm rest}$) versus group richness ($n_{\rm members}$) for our group sample. The value of $n_{\rm members}$ is taken to be the number of group members *after* our stellar mass cut of $3.16 \times 10^9 M_\odot$ is applied.

are typically either field galaxies or members of nearby massive groups with similar projected spatial positions but offsets along the LOS. The impact of the number of interloping galaxies needs to be explored with simulations, which we reserve for future work.

In this analysis, we only study systems with $n_{\rm members} \geq 10$, which is the minimum group membership for reliable substructure analysis (Hou et al., 2012). This leaves us with a total of 306 groups and 9095 member galaxies. Additionally, while our sample contains both groups (i.e. systems with $10^{12} \lesssim M_{\rm halo} \lesssim 10^{14} M_\odot$) and clusters (i.e. systems with $M_{\rm halo} \gtrsim 10^{14} M_\odot$), we will refer to all systems as 'groups' for simplicity. In Figure 5.1, we show the main properties of the groups in our sample and plot the group velocity dispersion ($\sigma_{\rm rest}$) versus group richness ($n_{\rm members}$) for the systems in our sample. The dispersion ($\sigma_{\rm rest}$) is the observed velocity dispersion ($\sigma_{\rm obs}$) computed via the Gapper Estimator (Beers et al., 1990) from all member galaxies above our stellar mass completeness limit and then corrected for redshift (i.e. $\sigma_{\rm rest} = \sigma_{\rm obs}/(1+z)$). The group richness is taken to be the number of group members *after* our stellar mass cut of $3.16 \times 10^9 M_\odot$ is applied and is therefore the

number of members used in the dynamical analysis presented in the work. The majority of our sample resides in the group regime with $100 < \sigma_{\rm rest} < 400$ km s^{-1} and $10 \leq n_{\rm members} \lesssim 50$ (Figure 5.1). While our sample is primarily composed of group-sized haloes, there are several rich group- and cluster-sized systems with 42 out of the 306 groups having $n_{\rm members} > 50$.

5.3 Identifying Subhaloes

In order to investigate whether pre-processed galaxies contribute to the observed morphology-/colour-density relations (e.g. Dressler, 1980; Blanton et al., 2003; Balogh et al., 2004; Baldry et al., 2006; Bamford et al., 2009), we must first identify subhaloes, which we define as a collection of galaxies that occupy the same halo within a larger host group halo. One method of identifying subhaloes is to look for substructure, which is believed to be an indication of the recent accretion of galaxies or small groups of galaxies. As in our previous work (Hou et al., 2012, 2013), we identify substructure using a modified version of the DS Test on all groups with $N_{\rm members} \geq 10$ in our SDSS sample. The DS Test (Dressler & Shectman, 1988) uses both spatial and LOS information to identify substructure and searches for members or groups of members with kinematic properties that deviate from those of the host group. The DS δ_i-deviation is computed for each galaxy as

$$\delta_i = \left(\frac{N_{nn}+1}{\sigma^2}\right)\left[\left(\overline{\nu^i_{local}} - \overline{\nu}\right)^2 + \left(\sigma^i_{local} - \sigma\right)^2\right], \tag{5.2}$$

where $1 \leq i \leq n_{\rm members}$, $N_{nn} = \sqrt{n_{\rm members}}$ rounded down to the nearest integer in the modified version of the test (Pinkney et al., 1996; Zabludoff & Mulchaey, 1998a), $\overline{\nu^i_{local}}$ and σ^i_{local} are the mean velocity and velocity dispersion of the galaxy plus its N_{nn} neighbours (as projected on the sky), and $\overline{\nu}$ and σ are the mean velocity and velocity dispersion of the host group. Galaxies with large δ_i-values have large kinematic deviations and could indicate new group members that have yet to adopt the kinematic properties of the host group. To determine whether a group contains significant substructure, the sum of

DS deviations is computed as

$$\Delta = \sum_{i=1}^{n} \delta_i. \tag{5.3}$$

Monte Carlo methods are then used to determine the probability that the computed Δ value can be obtained from a random distribution of galaxy positions and velocities. The probability is computed by comparing the observed Δ-value to 'shuffled Δ-values', which are computed by randomly shuffling the observed velocities and then reassigning them to the observed member galaxy positions. Systems with probabilities below a given confidence level (typically 1 or 5 %) are identified as having significant substructure.

In our previous work, we focused on comparing groups with and without detectable substructure using the Δ statistic (Hou et al., 2012, 2013). However, the goal of this work is to investigate the role of pre-processing, which requires the identification of individual subhaloes. A simple way to identify subhaloes involves a combined analysis of the group 'bubble-plot', that is a position plot of the group members where the symbols are weighted by $\exp(\delta_i)$ and the group velocity distribution (Dressler & Shectman, 1988; Dressler et al., 2013). In the bubble-plots the size of the symbols scale with the DS δ_i-deviation, therefore larger symbols correspond to galaxies with larger kinematic deviations from the group average. Subhalo candidates are identified in the bubble-plots as regions where several galaxies have similarly large symbols. The DS δ_i-deviation does not take into account the sign of the galaxy velocity (Equation 5.2), therefore to ensure that the galaxies are also correlated in velocity-space, Dressler et al. (2013) look at the velocity distribution of the subhalo candidates. If the candidate galaxies span a small enough range in velocity ($\lesssim$ 1000km s^{-1}) then Dressler et al. (2013) identify these as a subhalo.

While the bubble-plots are effective in identifying subhaloes, it is not feasible to carry out visual inspection for a large sample of groups. Therefore, we automate this process by defining subhaloes as a collection of at least three neighbouring galaxies, as projected on the plane of the sky, with $\delta_i \geq 1.8$ that lie within a narrow range of LOS velocities of each other. The minimum value of three neighbouring galaxies in our subhaloes corresponds to the fact that the modified version of the DS Test uses $N_{nn} = \sqrt{n_{\rm members}}$ (rounded down to the

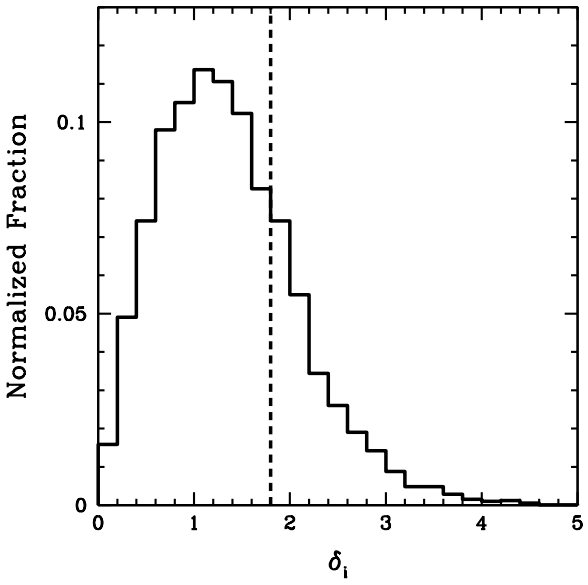

Figure 5.2: Histogram of DS δ_i-deviations (Eqn. 5.2) for all the SDSS satellite group members in our sample. The dashed vertical line represents the minimum δ_i-value required to be considered as part of a subhalo (i.e. $\delta_i \geq 1.8$. Approximately 20% of the sample lie above this value.

nearest integer) to compute δ_i (Equation 5.2). Since our smallest groups have $n_{\rm members} = 10$ then at minimum $N_{nn} = 3$. The $\delta_i \geq 1.8$ requirement results from the observation that the average δ_i-value is approximately 1, which can be seen in the δ_i-distribution shown in Figure 5.2. A minimum of $\delta_i = 1.8$ ensures that we are identifying systems with larger kinematic deviations as $\sim 75\%$ of the galaxies have $\delta_i < 1.8$. The LOS velocity cut applied around each galaxy ensures that the candidate subhalo galaxies are not only close in projection on the sky, but also correlated in redshift space. Since our sample includes groups that span a wide range in halo mass and group richness (Figure 5.1), we set our LOS velocity cut equal to $\sigma_{\rm rest}$, which allows the velocity range for subhalo galaxies to scale with the mass of the host group. Theoretically, subhaloes should also span a wide range in mass; however, massive subhaloes are likely only found in cluster-sized systems ($\gtrsim 10^{14} M_{\odot}$: McGee et al., 2009). A constant LOS velocity cut applied to all subhaloes would either be too restrictive for rich clusters or too relaxed for lower mass groups. Our methodology reflects the expected range in subhalo masses for a given group halo mass.

We now compare our automated subhalo finder to the visual inspection methodology described in Dressler et al. (2013). In Figure 5.3, we show bubble-plots for two example groups in our sample, Yang et al. (2007) SDSS Groups 138 (left) and 433 (right). Galaxies with $\delta_i < 1.8$ are indicated by black symbols, galaxies with $\delta_i \geq 1.8$ are indicated by blue symbols and the size of the symbols scale with $\exp(\delta_i)$. In addition, we also indicate the galaxies identified as subhalo members using our automated algorithm (red crosses in Figure 5.3). In both Groups 138 and 433, our subhalo finder clearly identifies the collection of galaxies with the largest DS δ_i-deviations (Figure 5.3). It appears that our automated method is able to identify the same subhaloes that a visual inspection would detect. This methodology was applied to all groups in our sample and we find similar results to those observed in the two example SDSS groups shown in Figure 5.3.

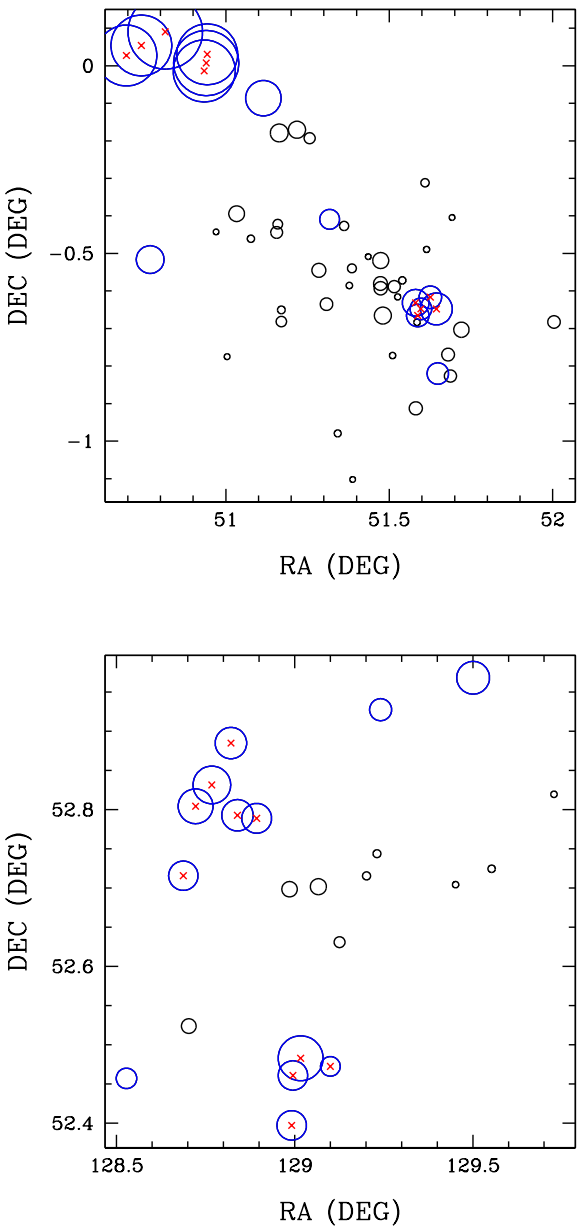

Figure 5.3: Top: Declination (DEC) versus Right Ascension (RA) for Yang et al. (2007) SDSS Group 138 where the symbols scale with $\exp(\delta_i)$ often referred to as DS 'bubble-plots', and larger symbols correspond to larger kinematic deviations from the host group properties. Black symbols represent galaxies with $\delta_i < 1.8$, blue symbols represent galaxies with $\delta_i \geq 1.8$ and the red crosses indicate galaxies that have been identified as being part of subhalo by our automated subhalo finder. Bottom: Same as top except for Yang et al. (2007) SDSS Group 433.

5.4 Comparing subhalo and non-subhalo galaxies

With our automated subhalo finder, we identify subhaloes in our group sample and find that in total $\sim 10\%$ of all group galaxies reside in subhaloes. We then stack the galaxies and divide our sample into subhalo and non-subhalo populations. In this section, we compare the the galaxy properties of these two populations.

5.4.1 Halo Mass Distribution

In Figure 5.4, we show the normalized differential (left) and cumulative (right) halo mass distribution for galaxies in groups with no identified subhaloes (black solid line) and in groups with subhaloes identified with the methodology described in Section 5.3 (red dashed line). The halo mass distributions for groups with and without subhaloes are distinct at the $> 99\%$ confidence level based on the results of a two-sample KS Test. Additionally, from Figure 5.4, it is clear that subhaloes preferentially reside in more massive systems. For groups with no identified subhaloes, we find that almost all ($\sim 95\%$) of our sample have halo masses $\leq 10^{14} M_{\odot}$, while a significantly lower fraction ($\sim 60\%$) of groups with subhaloes lie below this halo mass. These results are in agreement with results from numerical simulations and semi-analytic models (SAMs), which suggest that subhaloes are more common in more massive host groups (e.g. De Lucia et al., 2012; Bahé et al., 2013; Wetzel et al., 2013a). We discuss the relationship between subhaloes and halo mass in more detail in Section 5.5.

5.4.2 Stellar Mass Distribution

We show the normalized differential (left) and cumulative (right) stellar mass distributions for non-subhalo (black solid line) and subhalo (red dashed line) galaxies in Figure 5.5. Although the non-subhalo and subhalo stellar mass distributions appear similar, a two-sample KS Test indicates that these two distributions likely come from a distinct parent distribution at the $> 96\%$ confidence level. The main differences between the two populations is that the subhalo population appear to have fewer low mass ($\log_{10}(M_{\rm star}/M_{\odot}) \lesssim 10$)

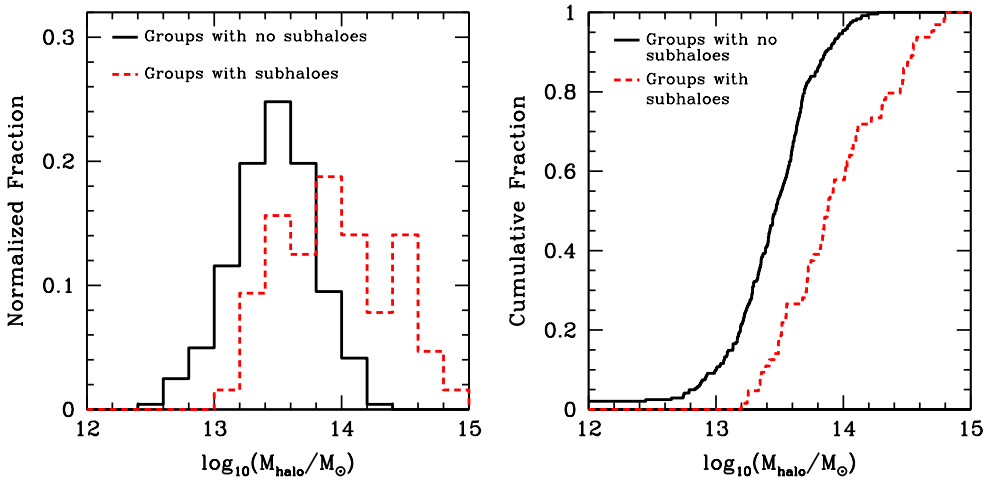

Figure 5.4: Left: Normalized differential halo mass distribution for galaxies in groups with no identified subhaloes (black solid line) and groups with subhaloes (red dashed line). Right: Same as left except we plot the cumulative halo mass distributions. It is clear that groups with subhaloes preferentially reside in more massive systems.

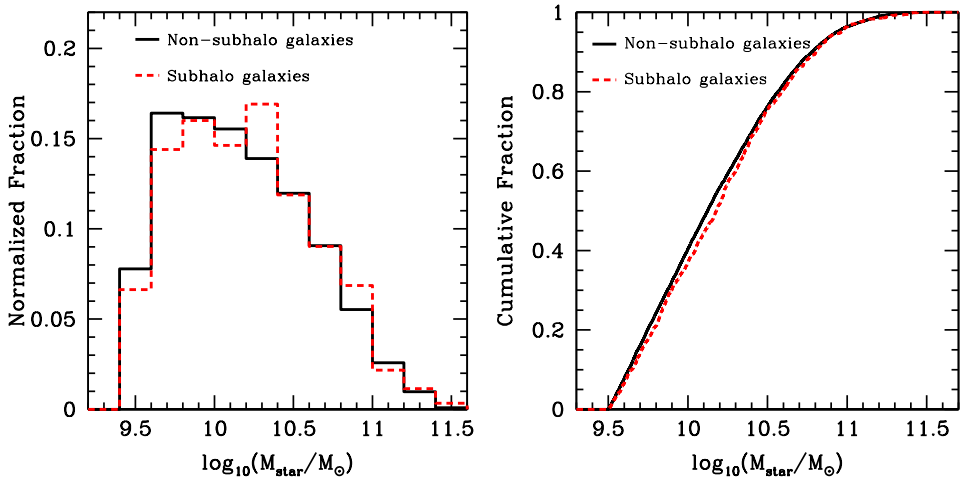

Figure 5.5: Left: Normalized differential stellar mass distribution of galaxies with $M_{\rm star} \geq 3.16 \times 10^9 M_\odot$ in the non-subhalo (black solid line) and subhalo (red dashed line) populations. Right: same as left except we plot the cumulative stellar mass distributions. The non-subhalo and subhalo stellar mass distributions appear similar; however they are distinct a the $> 96\%$ confidence level based on the results of a two-sample KS Test.

galaxies and, in some stellar mass bins, a higher fraction of more massive galaxies. However, it should be noted that the differences in the stellar mass distributions of non-subhalo and subhalo galaxies are subtle and on the order of, at most, a few percent (Figure 5.5). We discuss how these differences in the stellar mass distribution affect our results in Section 5.4.3.

5.4.3 Radial Trends

In order to obtain better statistics for our analysis, we look at the stacked group properties. Our group sample consists of groups with varying sizes and so we show radial trends as a function of $r_{\rm proj.}/r_{200}$, where $r_{\rm proj.}$ is the projected group-centric radius and r_{200} is defined as in Carlberg et al. (1997)

$$r_{200} = \frac{\sqrt{3}\sigma_{\rm rest}}{10H(z)}, \tag{5.4}$$

and $H(z) = H_0\sqrt{\Omega_{m,0}(1+z)^3 + \Omega_{\Lambda,0}}$.

5.4.3.1 Radial Distributions

In Figure 5.6, we show the normalized differential (left) and cumulative (right) group-centric radial distributions for galaxies in the non-subhalo (black solid line) and subhalo (red dashed line) populations in our stellar mass complete sample. From Figure 5.6, we see that the two distributions differ and results from a two-sample KS Test confirm that the subhalo and non-subhalo radial distributions come from different parent distributions at the $> 99\%$ confidence level (c.l.). Additionally, we find that subhalo galaxies are preferentially found at larger radii when compared to non-subhalo galaxies (Figure 5.6). The majority ($\sim 60\%$) of the galaxies in the non-subhalo population reside within the virial radius and the fraction of galaxies decreases with increasing radius. In contrast, there appears to be a dearth of subhalo galaxies close to the group core and $\sim 60\%$ of subhalo galaxies are found beyond the virial radius.

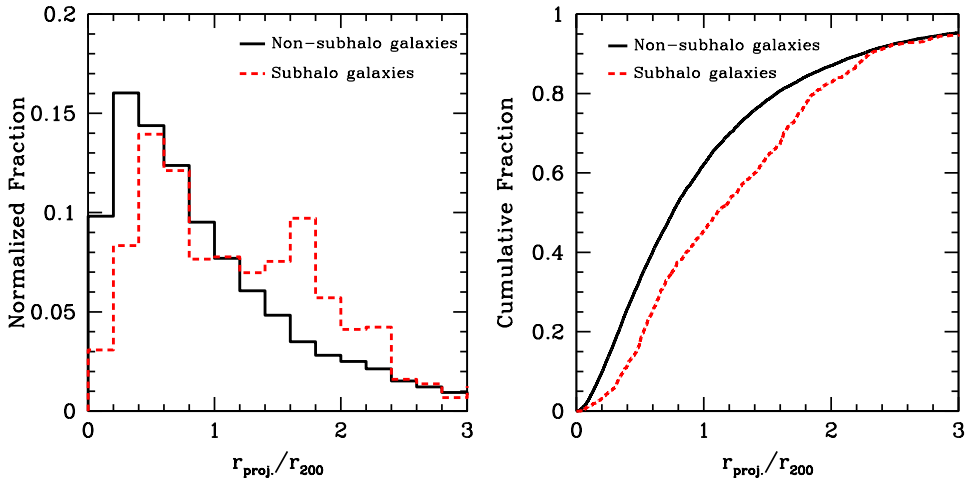

Figure 5.6: Left: Normalized differential radial distributions of galaxies with $M_{\rm star} \geq 3.16 \times 10^9 M_{\odot}$ in the non-subhalo (black solid line) and subhalo (red dashed line) populations. Right: same as left except we plot the cumulative radial distributions. Subhalo galaxies are preferentially located on the group outskirts.

5.4.3.2 Quiescent fraction versus radius

Differences between subhalo and non-subhalo galaxies can be probed by looking at their SSFRs via the quiescent fraction ($f_{\rm q}$). In Figure 5.7, we show $f_{\rm q}$ versus $r_{\rm proj.}/r_{200}$ for non-subhalo (black circles) and subhalo (red crosses) galaxies in our entire sample of satellite galaxies (top-left panel), for low mass satellites ($9.5 < \log_{10}(M_{\rm star}/M_{\odot}) < 10$: top-right panel), for intermediate mass satellites ($10 < \log_{10}(M_{\rm star}/M_{\odot}) < 10.5$: bottom-left panel) and high mass satellites ($\log_{10}(M_{\rm star}/M_{\odot}) > 10.5$: bottom-right panel). The group-centric radius covers a range between $0 < r_{\rm proj.}/r_{200} < 3$ and the data are plotted at the mean value of each bin, which have widths of 0.75 r_{200}. The dashed horizontal black line corresponds to the observed quiescent fraction in the field, where field galaxies are taken to be the isolated galaxies in the Yang et al. (2007) catalogue.

In the top-left panel of Figure 5.7 we see that for the overall group galaxy population $f_{\rm q}$ is significantly higher than in the field at all radii, indicating that group galaxies experience environmental star formation quenching out to at least three virial radii. This result is in agreement with previous observations that also find a higher quiescent fraction in groups with respect to the field as

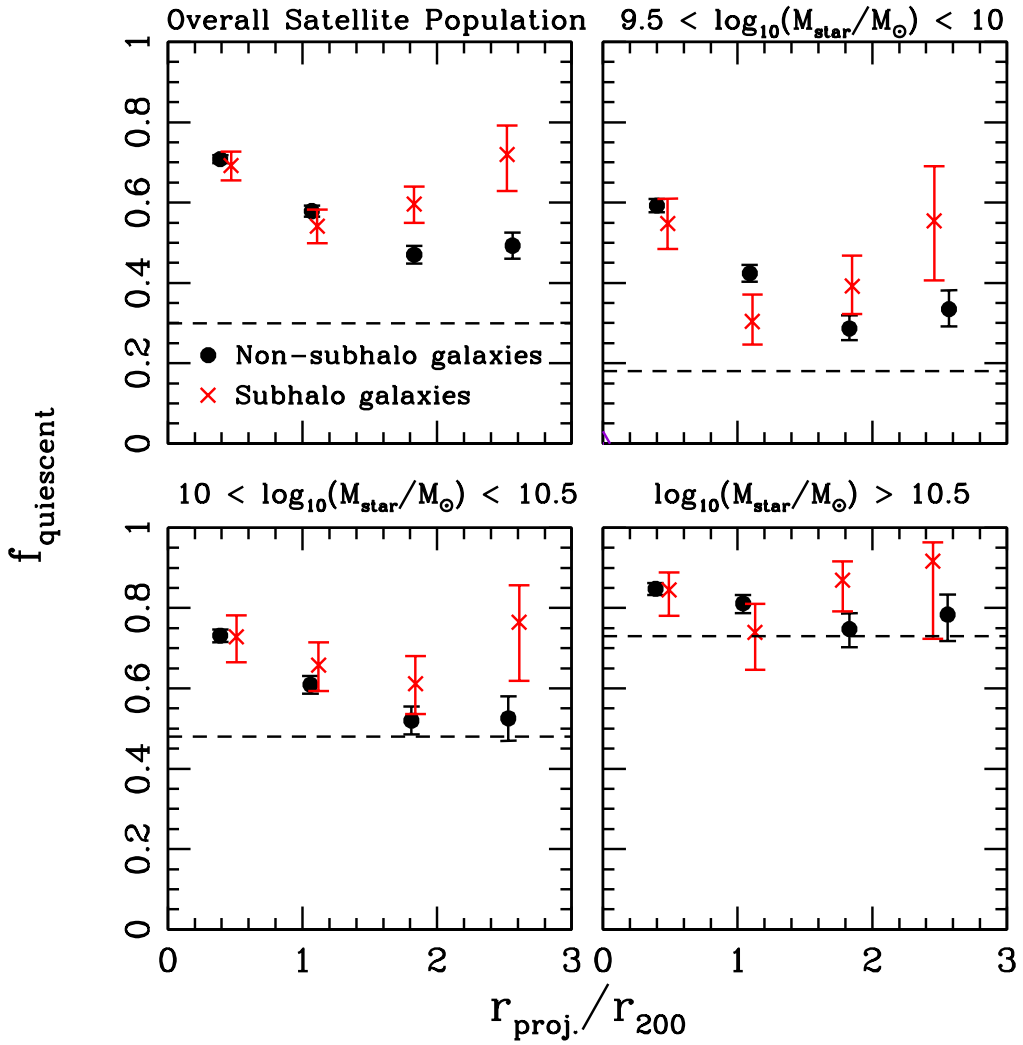

Figure 5.7: Top-left: Quiescent fraction ($f_{\rm q}$) versus $r_{\rm proj.}/r_{200}$ for all satellite non-subhalo galaxies (black circles) and all satellite subhalo galaxies (red crosses). Top-right: same as top-left except only for the low mass ($9.5 < \log_{10}(M_{\rm star}/M_{\odot}) < 10$)galaxies. Bottom-left: same as top-left except for intermediate mass ($10 < \log_{10}(M_{\rm star}/M_{\odot}) < 10.5$) galaxies. Bottom-right: same as top-left except for high mass ($\log_{10}(M_{\rm star}/M_{\odot}) > 10.5$) galaxies. The data are plotted at the mean value of each radial bin, which has a width of 0.75 r_{200}, for each subpopulation of galaxies. The dashed horizontal black line represents the quiescent fraction in isolated field galaxies in the aforementioned stellar mass bins. Errors are computed following Cameron (2011).

far out as $\sim 5r_{200}$ (e.g. von der Linden et al., 2010; Bahé et al., 2013; Wetzel et al., 2013b). Comparing group and field galaxies at a given stellar mass, we find enhanced quenching in low and intermediate mass group galaxies at almost all radii. For high mass galaxies, the non-subhalo population shows enhanced quenching at small radii ($r < 1.5r_{200}$), but have $f_{\rm q}$ values similar to field on the group outskirts (Figure 5.7: bottom-right panel). The high mass subhalo galaxies show enhanced quenching, with respect to the field, closer to the group core ($r < 0.75r_{200}$) and just beyond the virial radius ($1.5 < r < 2.25r_{200}$).

As a function of radius, we see that for non-subhalo galaxies at all stellar masses the general trend is that $f_{\rm q}$ decreases with increasing group-centric radius within $\sim 1.5r_{200}$ and then flattens on the group outskirts (Figure 5.7). The subhalo galaxy population shows a different radial trend from non-subhalo galaxies, in both the overall satellite population and at fixed stellar mass, where $f_{\rm q}$ decreases with increasing radius within $\sim 1.5r_{200}$ but then increases at large radii (Figure 5.7). This results indicates that on the group outskirts enhanced quenching, with respect to the non-subhalo population, has occurred in the subhalo population. Within the virial radius the quiescent fractions in non-subhalo and subhalo galaxies are similar; however, at large radii $f_{\rm q}$ is higher in the subhalo population at all stellar masses, although a statistically significant difference is only observed in low and intermediate mass satellites beyond two virial radii (Figure 5.7).

In Section 5.4.2 we found that the non-subhalo and subhalo stellar mass distributions differed, where more massive galaxies are preferentially found in subhaloes. The quiescent fraction has also been shown to correlate with stellar mass where more massive galaxies typically have higher values of $f_{\rm q}$ (e.g. Kimm et al., 2009; Wetzel et al., 2012; Hou et al., 2013; Woo et al., 2013). Thus, one might be worried that the higher quiescent fractions observed in the subhalo population (Figure 5.7) might be due to a higher fraction of more massive galaxies, rather than environmental star formation quenching. While this may in part be true for the overall galaxy popualtion (Figure 5.7: top-left panel), the fact that we still observe higher $f_{\rm q}$ at fixed stellar in the subhalo population (Figure 5.7) suggests that environmental effects also contribute to the enhanced quenching.

5.4.4 Separating virialized, infalling and backsplash galaxies

In Section 5.4.3, we showed that the $f_{\rm q} - r_{200}$ trend for subhalo and non-subhalo galaxies differed on the group outskirts. As a result, one might naively assume that the identified subhaloes are infalling low mass groups. However, numerous simulations have shown that backsplash galaxies can extend as far out as 2-3 virial radii (Balogh et al., 2000; Mamon et al., 2004; Gill et al., 2005; Oman et al., 2013). Additionally, results from semi-analytic models have shown that subhaloes can survive, that is maintain the kinematic properties of the subhalo, for several orbits within the host group potential (Taylor & Babul, 2004). Therefore, our goal is to distinguish between the infall and backsplash populations in order to see if our subhaloes are composed of pre-processed infalling galaxies or backsplash galaxies that have been quenched after passing through the host group core. Although it is notoriously difficult to disentangle the infall and backsplash populations, there has been significant effort in recent years using simulations and mock catalogues to develop a classification scheme from observable properties (Gill et al., 2005; Mahajan et al., 2011; Pimbblet, 2011). We make use of a combination of these schemes to identify virialized, infall and backsplash galaxies in our sample.

One way to determine if our groups contain infall and backsplash satellites is to look at the distribution of the galaxy velocities (Δcz) as a function of the group velocity dispersion (σ). Backsplash galaxies will have been slowed due to dynamical friction within the group core and will therefore have low $|\Delta cz|/\sigma$ values at fixed radius (Gill et al., 2005). In contrast, infalling galaxies can have a wide range of velocities depending on their orbital parameters; though galaxies with high velocities (i.e. $|\Delta cz|/\sigma \gtrsim 1$) are likely all infalling. Using N-body simulations, Gill et al. (2005) showed that backsplash galaxies have a narrow centrally peaked $|\Delta cz|/\sigma$ distribution, while infalling satellites have a broader distribution with a non-zero peak. While it is difficult to separate infall and backsplash galaxies from an observed, and therefore projected, $|\Delta cz|/\sigma$ distribution, Pimbblet (2011) found that by binning the $|\Delta cz|/\sigma$ histogram into narrow bins of radius, it is possible to identify regions where infalling galaxies dominate. More specifically, these authors found that bimodality

and/or a shift in the peak of the $|\Delta cz|/\sigma$ distribution to larger values indicated a large infall population.

In Figure 5.8, we show the $|\Delta cz|/\sigma_{\rm rest}$ histograms in narrow radial bins for non-subhalo (left) and subhalo (right) galaxies and also list the number of galaxies in each bin. For the non-subhalo galaxies we see that for almost all radial bins the $|\Delta cz|/\sigma_{\rm rest}$ distribution is broad and generally centrally peaked, indicating a mixed population of virialized (for galaxies with $r < r_{200}$), infall and backsplash galaxies out to $2r_{200}$ (Gill et al., 2005). Only on the outskirts ($2 \leq r_{200} \leq 3.0$) are there signs of a large infall population, indicated by the emergence of a second peak at $|\Delta cz|/\sigma_{\rm rest} \sim 0.5$. In contrast, the subhalo galaxies (Figure 5.8: right) show signs of a strong infall population just beyond the virial radius and out to $3r_{200}$. The $|\Delta cz|/\sigma_{\rm rest}$ distributions for galaxies between $1 - 2.5r_{200}$ either show bimodality or an offset peak, which are both indications of a dominant infall population (Gill et al., 2005; Pimbblet, 2011). There are too few subhalo galaxies in the $2.5 < r < 3r_{200}$ bin to comment on the shape of the $|\Delta cz|/\sigma_{\rm rest}$ distribution; however, it is clear that most of the galaxies have relatively high velocities and are likely infalling.

The $|\Delta cz|/\sigma$ distributions for the subhalo galaxies shown in Figure 5.8 indicate the presence of a dominant infall population; however, it is not possible to distinguish between infall and backsplash galaxies from these histograms alone. Using N-body simulations, both Gill et al. (2005) and Oman et al. (2013) showed that in 6-d phase-space (x, y, z, v_x, v_y and v_z), the regions occupied by each population are for the most part distinct. However, once this phase-space is collapsed into observables (i.e. x, y and v_z), projection effects tend to fill out much of the empty phase-space that separated the populations. While there is no ideal method to distinguish between infall and backsplash galaxies in observed groups, there are ways to roughly approximate regions occupied by either population. Mahajan et al. (2011) found that the fraction of virialized, infalling and backsplash galaxies occupied distinct regions in the $v_r/V_v - r/R_v$ plane, where r and v_r are the radial phase-space coordinates, V_v is the group or cluster velocity dispersion and R_v is the virial radius of the system. To distinguish between the different galaxy populations, Mahajan et al. (2011) make the following cut

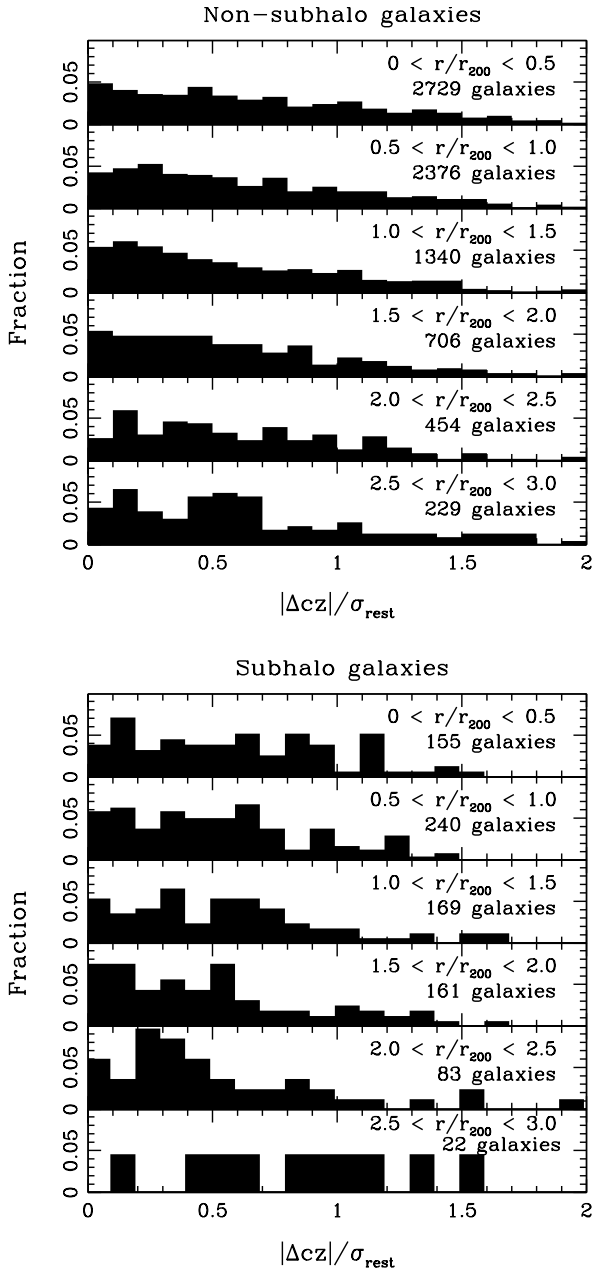

Figure 5.8: $|\Delta cz|/\sigma_{\rm rest}$ histograms for non-subhalo (left) and subhalo (right) galaxies in the $0 < r_{200} < 3$ range in bins of $0.5 r_{\rm proj}/r_{200}$. For each radial bin we list the number of galaxies in each population.

$$\frac{v_r}{V_v} = -1.8 + 1.06\left(\frac{r}{R_r}\right), \tag{5.5}$$

to separate backsplash and infall galaxies and a cut at one virial radius to separate virialized and infall galaxies. Within the viral radius there is an additional cut to separate virialized and infall galaxies, which is the mirror slope of Equation 5.5. It should be noted that while these cuts are based on the full 6-d phase-space data, the density contours for the virialized, infall and backsplash populations occupy similar regions in projected space, though with significant overlap, and therefore contamination between the populations (Mahajan et al., 2011). While the distinct regions are not as clear in projected space, the divisions made by Equation 5.5 allow us to approximately distinguish between infall and backsplash subhaloes, rather than assuming all subhaloes are infalling. Therefore, we apply a cut analogous to Equation 5.5, except v_r/V_v is replaced by the observable quantity $\Delta cz/\sigma_{\rm rest}$ and r/R_r is replaced by $r_{\rm proj.}/r_{200}$. Additionally, the aforementioned classification scheme is one of five models tested by Mahajan et al. (2011). While we elect to use the best-fitting scheme, as determined by Mahajan et al. (2011), it should be noted that the fraction of backsplash galaxies can change by as much as $\sim 20\%$ depending on the classification scheme.

In Figure 5.9, we plot $\Delta cz/\sigma_{\rm rest}$ versus $r_{\rm proj.}/r_{200}$ for our population of non-subhalo galaxies (gray crosses) and subhalo galaxies (red triangles). As in Mahajan et al. (2011), we divide the $\Delta cz/\sigma_{\rm rest} - r_{200}$ plane into regions of virialized (Region A), infalling (Regions B) and backsplash (Region C) with Equation 5.5 and a cut at $r_{\rm proj.}/r_{200} = 1.0$. Both subhalo and non-subhalo galaxies occupy all three regions of Figure 5.9, though there are some visible differences between the two populations. In particular, there are few subhalo galaxies close to the group core (also seen in Figure 5.6) and there appears to be an excess of subhalo galaxies, with respect to the non-subhalo population, in the bottom-right hand corner of Figure 5.9. This area corresponds to the region occupied by only infalling galaxies in the full 6-D phase space diagram shown in Mahajan et al. (2011).

With the divisions shown in Figure 5.9, we separate our sample into virialized, infalling and backsplash galaxies. In Figure 5.10 we show the fraction of

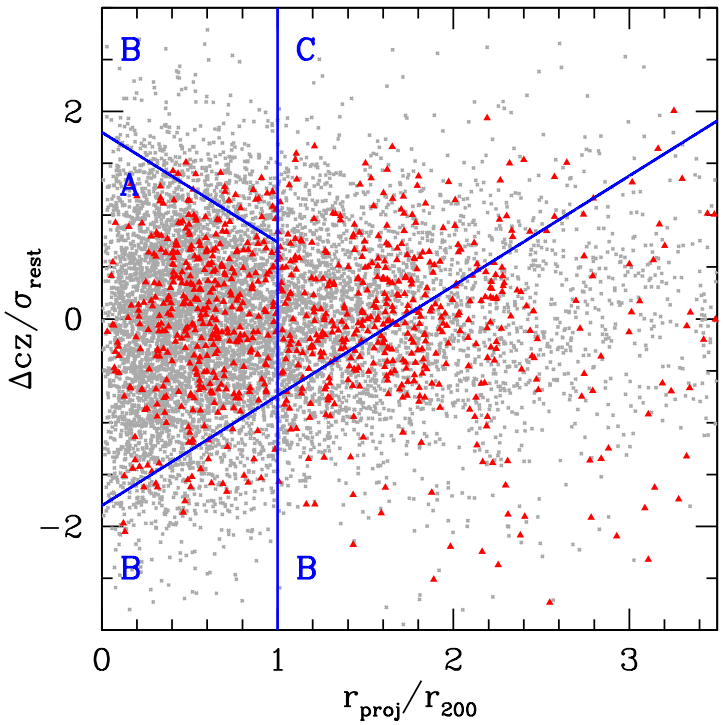

Figure 5.9: $\Delta cz/\sigma_{\rm rest}$ versus $r_{\rm proj.}/r_{200}$ for non-subhalo (grey crosses) and for subhalo (red triangles) galaxies. The blue slopes indicate the line dividing galaxy populations (Equation 5.5) as defined in Mahajan et al. (2011). Region A denotes virialized galaxies, regions B denote infalling galaxies and region C denotes backsplash galaxies.

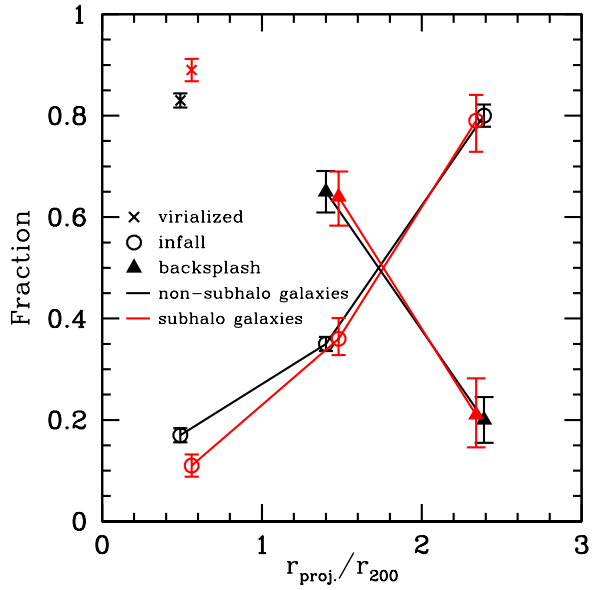

Figure 5.10: Fraction of virialized (crosses), infalling (circles) and backsplash (triangles) for the non-subhalo (black symbols and lines) and subhalo (red symbols and lines) populations as a function of projected group-centric radius. The data are plotted at the mean value of each radial bin, which has a width of 1 r_{200}, for each subpopulation of galaxies. Error include both $\sqrt{N}$ counting statistics and the uncertainty in the classification scheme given in Mahajan et al. (2011), which are typically 1% for the virialized and infall populations and 4% for the backsplash population. It should be noted that systematic errors, based on the method of classification, are not included.

virialized (crosses), infalling (circles) and backsplash (triangles) for the non-subhalo (black symbols and lines) and subhalo (red symbols and lines) populations as a function of projected group-centric radius. The data are plotted at the mean value of each radial bin, which has a width of r_{200}, for each subpopulation of galaxies. The errors quoted in Figure 5.10 include both $\sqrt{N}$ counting statistics errors and the classification scheme errors stated in Mahajan et al. (2011), which are typically 1% for the virialized and infall populations and 4% for the backsplash population. However, the aforementioned errors quoted by Mahajan et al. (2011) underestimate the true uncertainty in computing the fraction of virialized, infall and backsplash galaxies, as these authors show that the fractions can change by a significant amount ($\sim 20\%$) depending on how the galaxies are classified.

From Figure 5.10, we see that at fixed radius the non-subhalo and subhalo populations have very similar subpopulations. In particular, within the virial radius both samples are dominated by virialized galaxies; though the non-subhalo population has a slightly higher fraction of virialized galaxies. Focusing now on the infall and backsplash populations beyond the virial radius, we see that between $1 < r_{200} < 2$ roughly two-thirds of the galaxies are part of the backsplash population. However, in the $2 < r_{200} < 3.0$ regime, the majority of the satellites reside in the infall population ($\sim 80\%$). Even if we include the $\sim 20\%$ range in systematic uncertainties in classifying the infall and backsplash population fractions, we find that infall galaxies still dominate the galaxy population at large radii ($\gtrsim 2r_{200}$).

In general, our observed fractions of infall and backsplash galaxies are in relatively good agreement with values predicted from some N-body simulations (Gill et al., 2005; Bahé et al., 2013). However, we do observe a higher fraction of backsplash galaxies, at all radii, than predicted by the numerical simulations of Wetzel et al. (2013b). Although, if we take into account systematic uncertainties based on the method of classification, our observed fractions are in better agreement with those of Wetzel et al. (2013b).

The results of Figure 5.10 indicate that the enhanced quenching in subhalo galaxies seen beyond the virial radius in Figure 5.7 results from a combination of pre-processed infalling galaxies and backsplash galaxies that may have had their star formation quenched via processes related to the host group. However, the largest, and most statistically significant, difference in $f_{\rm q}$ between non-subhalo and subhalo galaxies occurs at large radii ($\gtrsim 2r_{200}$: Figure 5.7). At these radii the infall population dominates independent of the classification scheme used. Thus, the effects of pre-processing are observable and this process likely plays a significant role in observed quenching of some subhalo galaxies.

5.5 How significant is pre-processing?

To determine the importance of pre-processing in groups and clusters, we first quantify the fraction of galaxies that reside in subhaloes ($f_{\rm sub}$) defined as the number of galaxies in identified subhaloes over the total number of group members. In Figure 5.11 we plot $f_{\rm sub}$ versus host group halo mass

($M_{\rm halo}$), where $M_{\rm halo}$ is the luminosity-based halo mass from Yang et al. (2007). The data points correspond to values of $f_{\rm sub}$ computed for individual systems and the horizontal red lines represent the mean value of $f_{\rm sub}$ computed for each halo mass bin, which has a width of 0.5 dex. An immediate feature of Figure 5.11 is that for halo masses below $\sim 10^{13.2} M_{\odot}$ our automated subhalo finder does not identify any subhaloes, which can also be seen in Figure 5.4. For more massive systems, there is significant scatter in the $f_{\rm sub}$ values of individual systems, but the mean values (red lines in Figure 5.11) show a correlation with halo mass, where more massive host haloes have a higher fraction of subhaloes. In particular, while some individual groups (between $\sim 10^{13} < M_{\rm halo} < 10^{14} M_{\odot}$) may have a high value of $f_{\rm sub}$, the majority do not contain any identified subhaloes. The result is that the mean values of $f_{\rm sub}$ for group-sized systems is below 5% (Figure 5.11). In contrast, many more cluster-sized systems ($M_{\rm halo} > 10^{14} M_{\odot}$) contain subhaloes, which results in a higher mean value of $f_{\rm sub}$. The same dependence of $f_{\rm sub}$ on halo mass is also seen in both SAMs (De Lucia et al., 2012) and hydrodynamical simulations (Bahé et al., 2013).

The results of Figure 5.11 provide information about the relationship between $f_{\rm sub}$ and halo mass; however, as shown in Section 5.4.4 the subhalo population contains a mix of both infalling and backsplash galaxies. In order to better estimate the importance of pre-processing we must examine the fraction of *infalling* subhaloes ($f_{\rm sub,\ infall}$) defined as the number of infalling subhalo galaxies over the total number of infalling galaxies, where the galaxies are classified with the divisions shown in Figure 5.9. A value of $f_{\rm sub,\ infall} = 1$ indicates that all of the infalling galaxies are in subhaloes. A value of $f_{\rm sub,\ infall} = 0$ implies that all of the infalling galaxies are either accreting directly from the field or are part of a subhalo that is not identified by our algorithm (i.e. small or not very kinematically distinct subhaloes). In addition, $f_{\rm sub,\ infall} = 0$ could also indicate that either all of the subhaloes in that group are in the backsplash population *or* that the group does not contain any identified subhaloes.

In Figure 5.12, we plot $f_{\rm sub,\ infall}$ versus $\log_{10}(M_{\rm halo}/M_{\odot})$, where the data points indicate individuals systems and the red lines represents the mean value within each halo mass bin. There are many groups ($\sim 85\%$) with $f_{\rm sub,\ infall} = 0$, which indicates that for these systems the galaxies are likely infalling directly

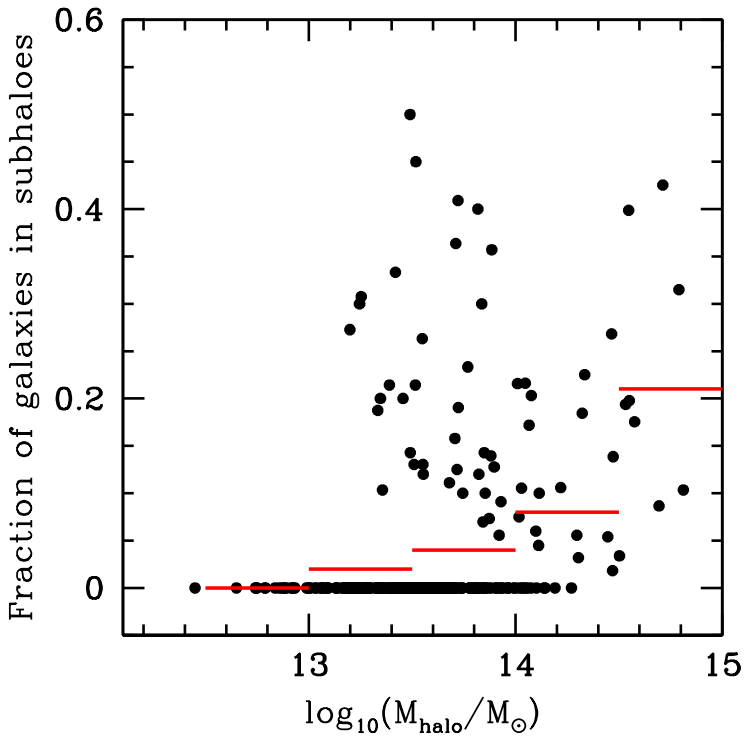

Figure 5.11: The fraction of galaxies in subhaloes ($f_{\rm sub}$) versus group halo mass in units of $\log_{10}(M_{\rm halo}/M_{\odot})$, where $M_{\rm halo}$ is taken to be the luminosity-based halo masses computed in Yang et al. (2007). The data points indicate the value of $f_{\rm sub}$ for individual systems in our sample. The horizontal red lines indicate the mean value for each halo mass bin, which has a width of 0.5 dex.

from the field rather than in lower mass groups. However, similar to the fraction of groups with subhaloes (Figure 5.11) the number of groups with *infalling* subhaloes is a function of halo mass, where $f_{\rm sub,\ infall}$ increases with increasing halo mass. For groups ($M_{\rm halo} < 10^{14} M_{\odot}$) the sample is dominated by systems with $f_{\rm sub,\ infall} = 0$, which results in mean $f_{\rm sub,\ infall}$-values $< 5\%$. For clusters with $10^{14} < M_{\rm halo} < 10^{14.5} M_{\odot}$ the mean value of $f_{\rm sub,\ infall}$ is $\sim 10\%$, which is in very good agreement with the fraction of pre-processed galaxies predicted by Berrier et al. (2009) for a similar halo mass range. Only for the most massive clusters in our sample ($M_{\rm halo} > 10^{14.5} M_{\odot}$) do we find that a significant fraction ($\sim 25\%$) of the infall population reside in subhaloes. Taking these average cluster values, we find that our results are somewhat lower than the values predicted by the SAMs of McGee et al. (2009) and De Lucia et al. (2012), who found that the the fraction of galaxies that accrete on to clusters (with $\log_{10}(M_{\rm halo}/M_{\odot}) \gtrsim 14$) as members of groups with $\log_{10}(M_{\rm halo}/M_{\odot}) \geq 10^{13}$ ranges between $\sim 25 - 45\%$. A possible explanation for the discrepancy between our observed value and values predicted by some semi-analytic models (McGee et al., 2009; De Lucia et al., 2012) is that our automated subhalo finder cannot detect smaller and/or less kinematically distinct subhaloes, and thus our fraction of subhaloes is likely a lower limit (see Hou et al., 2012, for a discussion on the limitations of the DS Test). Also, our sample of cluster-sized systems is small ($\sim 14\%$) and since there is significant scatter on the individual values of $f_{\rm sub,\ infall}$ (Figure 5.12), it is possible that our computed mean value may underestimate the true fraction of infalling subhaloes in clusters.

Based on the results shown in Figures 5.7 and 5.10, we conclude that the enhanced quenching in subhaloes observed on the group outskirts ($\gtrsim 2r_{200}$) is a result of the pre-processing of infalling subhalo galaxies. However, we find that the importance of pre-precessing appears to be a strong function of host halo mass. For group-sized systems, pre-processing does not play a significant role in star formation quenching; however, for the cluster-sized systems, and in particular clusters with $M_{\rm halo} > 10^{14.5} M_{\odot}$, a significant fraction of the member galaxies appear to have had their star formation quenched in smaller haloes prior to accretion on the final (observed) system. Unfortunately, it is not possible to further divide the results shown in Figure 5.7 by halo mass as the uncertainties become too large to draw any meaningful conclusions and

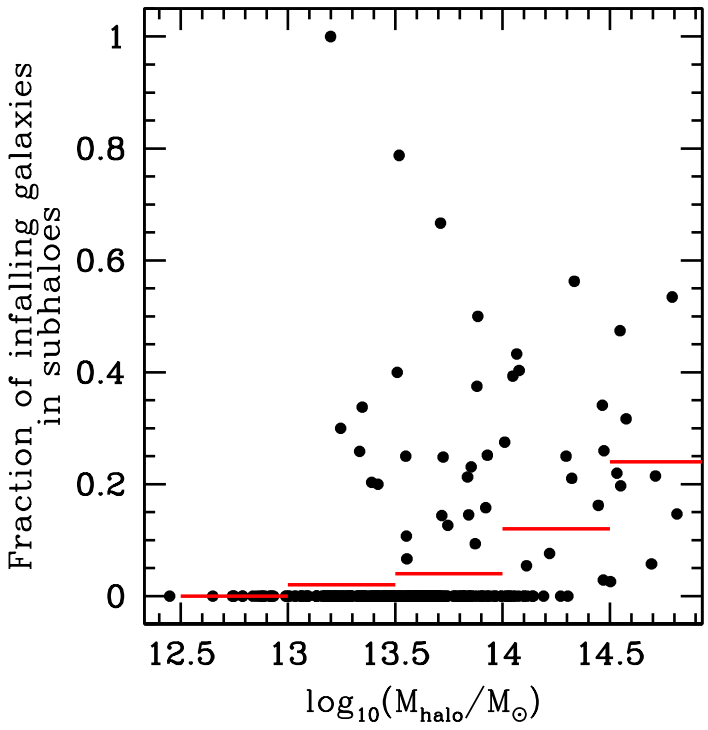

Figure 5.12: The fraction of infalling galaxies that reside in a subhalo ($f_{\rm sub,\ infall}$) versus group halo mass $M_{\rm halo}$, where $M_{\rm halo}$ is taken to be the luminosity-based halo masses computed in Yang et al. (2007). The data points indicate the value of $f_{\rm sub}$ for individual systems in our sample. The horizontal red lines indicate the mean value for each halo mass bin, which has a width of 0.5 dex.

more data, especially massive cluster data, are needed. However, in a similar analysis of rich clusters, Dressler et al. (2013) found that the fraction of passive and post-starburst galaxies was significantly higher in their identified infalling groups and they also concluded that 'substantial' pre-processing had occurred. The importance of pre-processing has also been studied using hydrodynamical simulations by Bahé et al. (2013). These authors also found a similar relationship between pre-processing and halo mass where more massive systems, such as clusters, had a much higher fraction of galaxies that had been pre-processed.

5.6 Conclusions

We have looked at the infall and backsplash subhalo populations in SDSS-DR7 groups and clusters, using a sample of satellite galaxies that is stellar mass complete to $M_{\rm star} = 3.16 \times 10^9 M_{\odot}$. The aim of this work is to investigate the importance of pre-processing in group and cluster galaxies. The Dressler-Shectman Test was used to identify subhalo galaxies and we followed the methodology of Mahajan et al. (2011) to classify virialized, infall and backsplash galaxies. The main results of this analysis are:

1. Subhaloes preferentially reside in massive systems and at large group-centric radii;

2. The stellar mass distributions of non-subhalo and subhalo galaxies are distinct, where subhaloes have, on average, slightly more massive galaxies;

3. Low and intermediate mass group galaxies out to $3r_{200}$ and high mass satellites close to the group core show enhanced SF quenching with respect to the field;

4. On the group and cluster outskirts, between $2 \lesssim r_{200} < 3.0$, $f_{\rm q}$ is higher in galaxies that reside in subhaloes than for the overall satellite galaxy population and at all stellar mass;

5. As a function of radius, the percentages of infall and backsplash galaxies do not differ between non-subhalo and subhalo galaxies;

6. The fraction of subhalo galaxies ($f_{\rm sub}$) and the fraction of infalling galaxies in subhaloes ($f_{\rm sub,\ infall}$) are both a function of halo mass, where more massive haloes have higher values of ($f_{\rm sub}$) and ($f_{\rm sub,\ infall}$);

The observed enhanced quenching in infalling subhalo galaxies, defined based as having kinematic properties distinct from the host group, suggests that pre-processing does play a role in galaxy evolution; however, it's significance depends on halo mass. Pre-processing does not appear to be important in groups and low mass clusters ($M_{\rm halo} \lesssim 10^{14.5} M_{\odot}$), but it does play a significant role in producing the observed quenched fraction of *massive cluster* galaxies with $M_{\rm halo} > 10^{14.5} M_{\odot}$.

5.7 Acknowledgements

A.H, L.C.P, and W.E.H would like to thank the National Science and Engineering Research Council of Canada (NSERC) for funding. We would like to thank X. Yang for making their SDSS-DR7 group catalogue publicly available, the NYU-VAGC team for publication of their SDSS catalogue and J. Brinchmann for publication of their SDSS SFRs. This work would not have been possible without these public catalogues.

Funding for the SDSS and SDSS-II has been provided by the Alfred P. Sloan Foundation, the Participating Institutions, the National Science Foundation, the U.S. Department of Energy, the National Aeronautics and Space Administration, the Japanese Monbukagakusho, the Max Planck Society, and the Higher Education Funding Council for England. The SDSS Web Site is http://www.sdss.org/.

The SDSS is managed by the Astrophysical Research Consortium for the Participating Institutions. The Participating Institutions are the American Museum of Natural History, Astrophysical Institute Potsdam, University of Basel, University of Cambridge, Case Western Reserve University, University of Chicago, Drexel University, Fermilab, the Institute for Advanced Study, the Japan Participation Group, Johns Hopkins University, the Joint Institute for Nuclear Astrophysics, the Kavli Institute for Particle Astrophysics and Cosmology, the Korean Scientist Group, the Chinese Academy of Sciences (LAM-

OST), Los Alamos National Laboratory, the Max-Planck-Institute for Astronomy (MPIA), the Max-Planck-Institute for Astrophysics (MPA), New Mexico State University, Ohio State University, University of Pittsburgh, University of Portsmouth, Princeton University, the United States Naval Observatory, and the University of Washington.

Bibliography

Bahé, Y. M., McCarthy, I. G., Balogh, M. L., & Font, A. S. 2013, MNRAS, 430, 3017

Baldry, I. K., Balogh, M. L., Bower, R. G., Glazebrook, K., Nichol, R. C., Bamford, S. P., & Budavari, T. 2006, MNRAS, 373, 469

Balogh, M. L., Baldry, I. K., Nichol, R., Miller, C., Bower, R., & Glazebrook, K. 2004, ApJ, 615, L101

Balogh, M. L. & McGee, S. L. 2010, MNRAS, 402, L59

Balogh, M. L., Navarro, J. F., & Morris, S. L. 2000, ApJ, 540, 113

Bamford, S. P., Nichol, R. C., Baldry, I. K., Land, K., Lintott, C. J., Schawinski, K., Slosar, A., Szalay, A. S., Thomas, D., Torki, M., & et al. 2009, MNRAS, 393, 1324

Beers, T. C., Flynn, K., & Gebhardt, K. 1990, AJ, 100, 32

Berrier, J. C., Stewart, K. R., Bullock, J. S., Purcell, C. W., Barton, E. J., & Wechsler, R. H. 2009, ApJ, 690, 1292

Blanton, M. R., Hogg, D. W., Bahcall, N. A., Baldry, I. K., Brinkmann, J., Csabai, I., Eisenstein, D., Fukugita, M., Gunn, J. E., Ivezić, Ž., & et al.,. 2003, ApJ, 594, 186

Blanton, M. R. & Roweis, S. 2007, AJ, 133, 734

Blanton, M. R., Schlegel, D. J., Strauss, M. A., Brinkmann, J., Finkbeiner, D., Fukugita, M., Gunn, J. E., Hogg, D. W., Ivezić, Ž., Knapp, G. R., Lupton, R. H., Munn, J. A., Schneider, D. P., Tegmark, M., & Zehavi, I. 2005, AJ, 129, 2562

Brinchmann, J., Charlot, S., White, S. D. M., Tremonti, C., Kauffmann, G., Heckman, T., & Brinkmann, J. 2004, MNRAS, 351, 1151

Cameron, E. 2011, PASA, 28, 128

Carlberg, R. G., Yee, H. K. C., Ellingson, E., Morris, S. L., Abraham, R., Gravel, P., Pritchet, C. J., Smecker-Hane, T., Hartwick, F. D. A., Hesser, J. E., Hutchings, J. B., & Oke, J. B. 1997, ApJ, 485, L13

Carollo, C. M., Bschorr, T. J., Renzini, A., Lilly, S. J., Capak, P., Cibinel, A., Ilbert, O., Onodera, M., Scoville, N., Cameron, E., Mobasher, B., Sanders, D., & Taniguchi, Y. 2013, ApJ, 773, 112

De Lucia, G., Weinmann, S., Poggianti, B. M., Aragón-Salamanca, A., & Zaritsky, D. 2012, MNRAS, 423, 1277

Dressler, A. 1980, ApJ, 236, 351

Dressler, A., Oemler, Jr., A., Poggianti, B. M., Gladders, M. D., Abramson, L., & Vulcani, B. 2013, ApJ, 770, 62

Dressler, A. & Shectman, S. A. 1988, AJ, 95, 985

Eke, V. R., Baugh, C. M., Cole, S., Frenk, C. S., King, H. M., & Peacock, J. A. 2005, MNRAS, 362, 1233

Geller, M. J. & Huchra, J. P. 1983, ApJS, 52, 61

George, M. R., Leauthaud, A., Bundy, K., Finoguenov, A., Tinker, J., Lin, Y.-T., Mei, S., Kneib, J.-P., Aussel, H., Behroozi, P. S., Busha, M. T., Capak, P., Coccato, L., Covone, G., Faure, C., Fiorenza, S. L., Ilbert, O., Le Floc'h, E., Koekemoer, A. M., Tanaka, M., Wechsler, R. H., & Wolk, M. 2011, ApJ, 742, 125

Gill, S. P. D., Knebe, A., & Gibson, B. K. 2005, MNRAS, 356, 1327

Hou, A., Parker, L. C., Balogh, M. L., McGee, S. L., Wilman, D. J., Connelly, J. L., Harris, W. E., Mok, A., Mulchaey, J. S., Bower, R. G., & Finoguenov, A. 2013, ArXiv e-prints

Hou, A., Parker, L. C., Wilman, D. J., McGee, S. L., Harris, W. E., Connelly, J. L., Balogh, M. L., Mulchaey, J. S., & Bower, R. G. 2012, MNRAS, 421, 3594

Kauffmann, G., White, S. D. M., Heckman, T. M., Ménard, B., Brinchmann, J., Charlot, S., Tremonti, C., & Brinkmann, J. 2004, MNRAS, 353, 713

Kawata, D. & Mulchaey, J. S. 2008, ApJ, 672, L103

Kimm, T., Somerville, R. S., Yi, S. K., van den Bosch, F. C., Salim, S., Fontanot, F., Monaco, P., Mo, H., Pasquali, A., Rich, R. M., & Yang, X. 2009, MNRAS, 394, 1131

Mahajan, S., Mamon, G. A., & Raychaudhury, S. 2011, MNRAS, 416, 2882

Mamon, G. A., Sanchis, T., Salvador-Solé, E., & Solanes, J. M. 2004, A&A, 414, 445

McGee, S. L., Balogh, M. L., Bower, R. G., Font, A. S., & McCarthy, I. G. 2009, MNRAS, 400, 937

McGee, S. L., Balogh, M. L., Wilman, D. J., Bower, R. G., Mulchaey, J. S., Parker, L. C., & Oemler, A. 2011, MNRAS, 413, 996

Muzzin, A., Wilson, G., Yee, H. K. C., Gilbank, D., Hoekstra, H., Demarco, R., Balogh, M., van Dokkum, P., Franx, M., Ellingson, E., Hicks, A., Nantais, J., Noble, A., Lacy, M., Lidman, C., Rettura, A., Surace, J., & Webb, T. 2012, ApJ, 746, 188

Navarro, J. F., Frenk, C. S., & White, S. D. M. 1996, ApJ, 462, 563

Oemler, Jr., A. 1974, ApJ, 194, 1

Oman, K. A., Hudson, M. J., & Behroozi, P. S. 2013, MNRAS, 431, 2307

Peng, Y.-j., Lilly, S. J., Kovač, K., Bolzonella, M., Pozzetti, L., Renzini, A., Zamorani, G., Ilbert, O., Knobel, C., Iovino, A., & et al.,. 2010, ApJ, 721, 193

Peng, Y.-j., Lilly, S. J., Renzini, A., & Carollo, M. 2012, ApJ, 757, 4

Pimbblet, K. A. 2011, MNRAS, 411, 2637

Pinkney, J., Roettiger, K., Burns, J. O., & Bird, C. M. 1996, ApJS, 104, 1

Rines, K., Geller, M. J., Kurtz, M. J., & Diaferio, A. 2005, AJ, 130, 1482

Taylor, J. E. & Babul, A. 2004, MNRAS, 348, 811

von der Linden, A., Wild, V., Kauffmann, G., White, S. D. M., & Weinmann, S. 2010, MNRAS, 404, 1231

West, M. J. & Bothun, G. D. 1990, ApJ, 350, 36

Wetzel, A. R., Tinker, J. L., & Conroy, C. 2012, MNRAS, 424, 232

Wetzel, A. R., Tinker, J. L., Conroy, C., & van den Bosch, F. C. 2013a, MNRAS, 432, 336

—. 2013b, ArXiv e-prints

Wilman, D. J., Balogh, M. L., Bower, R. G., Mulchaey, J. S., Oemler, A., Carlberg, R. G., Eke, V. R., Lewis, I., Morris, S. L., & Whitaker, R. J. 2005, MNRAS, 358, 88

Woo, J., Dekel, A., Faber, S. M., Noeske, K., Koo, D. C., Gerke, B. F., Cooper, M. C., Salim, S., Dutton, A. A., Newman, J., & et al. 2013, MNRAS, 428, 3306

Yang, X., Mo, H. J., van den Bosch, F. C., Pasquali, A., Li, C., & Barden, M. 2007, ApJ, 671, 153

Zabludoff, A. I. & Mulchaey, J. S. 1998a, ApJ, 498, L5+

—. 1998b, ApJ, 496, 39

Chapter 6

Summary and Future Work

Galaxy evolution is a large field of study but the key goal of current research is to understand the processes that transform actively star-forming late-type galaxies into quiescent early-type galaxies. More specifically, understanding whether internal or secular processes ('nature'), external processes related to the environment ('nurture') or a combination of the two processes are responsible for driving galaxy evolution.

The work presented in this thesis has contributed to significant advancements in understanding the role that the group environment, and in particular group dynamics, plays in galaxy evolution. With the SDSS, GEEC and GEEC2 spectroscopic group catalogues we classify the group dynamical state, examine correlations between group dynamics and observed galaxy properties and investigate the importance of pre-processing in groups and clusters. Additionally, as our groups span a redshift range of $0 < z \lesssim 1$, we are able to study the evolution of group dynamics over cosmic time.

In Chapter 3, we test the reliability of the Dressler-Shectman (DS) Test for substructure on group-sized systems and then search for substructure in 15 rich ($n \geq 20$) intermediate redshift ($z \sim 0.4$) GEEC groups. With Monte Carlo simulations we carry out performance tests of the DS statistic for groups with membership between 5 and 50 galaxies. The results of our simulations show that even for systems with as few as 5 members the false positive rates for the DS Test are low, meaning that the statistic does not incorrectly identify substructure if none exists. In contrast, the false negative rates, which in our

case represents the rate that the DS Test fails to detect substructure when it exists, varies significantly depending on the richness of the group and the properties of the input substructure. For groups with more than 20 members, the DS Test can reliably identify substructure; however, for $10 \leq n < 20$, we find that the statistic has a high rate of false negatives and can only provide a lower limit on the amount of detected substructure. Previous performance studies of the DS Test have shown that the statistic is reliable down to $n = 30$. By showing that the DS Test can be applied to groups with even fewer members, we have extended the applicability of the test to a much larger sample of systems, allowing for a more in-depth study of group dynamics.

We then apply the DS Test to our sample of rich GEEC groups and find that 4 of the 15 groups contain significant substructure that is preferentially found on the group outskirts. Additionally, with a simple analytic model we find that 2 of the 5 identified substructure subhaloes are likely gravitationally bound to the host group. The remaining subhaloes are in the nearby LSS and may be accreting onto their host groups. In addition, we find that the galaxy population in groups with substructure resembles the field population (i.e. a high fraction of blue and actively-star forming galaxies), while galaxies in groups without substructure have properties similar to cluster populations (i.e. a dominant red sequence). The location of the substructure galaxies and the properties of groups with substructure suggest that at $z \sim 0.4$, subhaloes do not feel the effects of the host group environment until well inside the group potential.

In Chapter 4, we extend the analysis of the work presented in my Master's Thesis (presented in Hou et al., 2009) and in Chapter 3 to a sample of low redshift ($z \sim 0$) SDSS groups and a sample of high redshift ($z \sim 0.9$) GEEC2 groups, allowing us to study the evolution of group dynamics. With the SDSS, GEEC and GEEC2 group catalogues we investigate how the quiescent fraction ($f_{\rm q}$) in groups depends on galaxy stellar mass, group dynamical mass and group dynamical state. We find that for the SDSS and GEEC samples $f_{\rm q}$ depends strongly on galaxy stellar mass, where higher mass galaxies have a higher value of $f_{\rm q}$. For our GEEC2 groups, we find no correlation between $f_{\rm q}$ and stellar mass; however, the GEEC2 sample is small and only contains massive galaxies ($\log_{10}(M_{\rm star}/M_{\odot}) \geq 10.7$). The SDSS and GEEC samples have significantly

more galaxies and are complete to much lower stellar masses, so the $f_{\rm q}$ - stellar mass trend is more clearly observed. With regards to group dynamical mass, which is a proxy for halo mass, we find that within our sample mass range, $f_{\rm q}$ shows no dependency on halo mass at all redshifts.

With the Anderson-Darling (AD) and DS Tests, we then study the evolution of group dynamics and find that while the fraction of non-Gaussian groups increases with redshift (to $z \sim 0.4$), the fraction of groups with substructure remains constant at $\sim 20\%$. This indicates that the increase in dynamical complexity, as probed by the AD Test, is not associated with an increased amount of accretion. Thus the AD Test could be tracing another aspect of dynamical state, such as the rate of mergers and interactions, which has been shown to increase with increasing redshift (Lotz et al., 2011). We then examine how the quiescent fraction depends on the dynamical state of the group and find that in general there is no statistically significant correlation between $f_{\rm q}$ and dynamical state, classified by either the AD or DS Tests. The only exception is that at $z \sim 0.4$, low mass galaxies in groups with substructure have a lower quiescent fraction than in groups with no substructure. The main conclusion of this chapter is that although we find some correlations between galaxy properties and group dynamical state; the trends are subtle, especially when the trend with galaxy stellar mass has been accounted for.

In Chapter 5, we take a slightly different approach and compare the properties of galaxies *in* substructure subhaloes to those not in subhaloes, which allows us to better probe the role of pre-processing in galaxy evolution. With a larger SDSS group catalogue (Yang et al., 2007), we identify subhalo galaxies using the DS Test for substructure. We find that at large radii ($r_{200} \gtrsim 1.5$), subhalo galaxies show enhanced star formation quenching with respect to both the field and non-subhalo populations. We then classify the subhalo and non-subhalo populations into virialized, infall and backsplash galaxies. The subhalo and non-subhalo galaxies have similar fractions of each subpopulation and with similar quiescent fractions at almost all radii. However, we do find that at $2 < r_{200} < 3$, $f_{\rm q}$ is higher in both the infall and backsplash subhalo populations when compared to non-subhalo galaxies. Since the infall population dominates at these radii, we conclude that the enhanced quenching observed in subhalo galaxies is a result of the higher $f_{\rm q}$ in infalling subhaloes.

Additionally, we compute the fraction of infalling galaxies that accrete as part of a subhalo and find that $\sim 20\%$ fall in as members of a subhalo. For the most massive clusters in our sample, these subhaloes have masses on the order of $\sim 10^{13} M_{\odot}$, indicating infall in group-sized haloes. Based on the observed enhanced quenching and the fraction of galaxies that accrete in subhaloes, we conclude that pre-processing contributes a significant amount to the observed quenched fraction of cluster galaxies.

While the results of the work presented in Chapters 3, 4 and 5 may appear somewhat contradictory, differences in the group samples and methods of analysis can explain the seemingly contradictory conclusions. In particular, the results of Chapter 3 and 4 suggest that at intermediate redshifts ($z \sim 0.4$), low mass galaxies in groups with substructure do not show signs of enhanced quenching and have properties similar to the field, while the results of Chapter 5 show that substructure subhalo galaxies at $z \sim 0$ have higher quiescent fractions with respect to both the field and non-subhalo galaxies. There are two possible reasons for the observed differences in the correlation between substructure and galaxy properties. The first is the redshift at which these groups are observed, and the second is that the masses of the subhaloes and groups differ between the different samples. With regards to differences in redshift, subhalo galaxies at a redshift of $z \sim 0.4$ may not have had enough time for significant star formation quenching to occur. A more likely cause is that the work presented in Chapter 5 includes numerous massive clusters ($M_{\rm halo} > 10^{14.5} M_{\odot}$), which are not included in the work presented in Chapters 3 and 4. Our results show that pre-processing, which contributes to the observed enhanced quenching, is really only significant in the most massive systems. Thus, our intermediate redshift sample does not include systems where enhanced quenching is likely to have occurred. Another set of results that appear to be contradictory involves the analysis of substructure in the SDSS groups. In Chapter 4, we found that there was no difference in the properties of SDSS groups with and without substructure, while in Chapter 5 we showed that subhalo galaxies on the outskirts of SDSS groups showed enhanced quenching. An important distinction between these two results is that the former looks at the properties of *all* galaxies in groups with substructure, and the latter focuses specifically on *subhalo* galaxies. Therefore, the analysis

presented for the SDSS groups in Chapter 4 and 5 are not analogous, and one cannot fairly compare the properties of these two populations.

Our contribution to the study of environmental effects on galaxy evolution is the development of methods to classify group dynamics for even low richness groups, allowing for in-depth studies of how dynamical state correlates with both group and galaxy properties. Additionally, the work presented in this thesis furthers our understanding of the specific aspects of environment that play a role in evolution. In particular, we find that while correlations with dynamical state are present, they are subtle. Our work further supports the argument that the local environment has a stronger affect on galaxy evolution than the larger global environment (e.g. Blanton & Berlind, 2007; Wilman et al., 2010). We also find that for $z < 1$, the environment does not appear to affect high mass galaxies ($\log_{10}(M_{\rm star}/M_{\odot}) \gtrsim 10.5$), which is also in agreement with results from recent galaxy evolution studies (e.g. Peng et al., 2010, 2012).

Thus, it appears that in order to better understand the role of groups in galaxy evolution, it is necessary to study lower mass galaxies and high redshift systems, as these are the regimes where environmental effects, and in particular mergers and interactions, are more to likely dominate. Additionally, while we observe some correlations between dynamical state and quiescent fraction, we still do not know which of the group galaxy transformation processes (i.e. interactions or strangulation) contributes most to the observed quenching. Since it currently difficult to directly observe the effects of strangulation, it will be necessary to study correlations between group dynamical state, group member properties and signatures of interactions, such as morphological or kinematic distortions and starburst or post-starburst activity, in order to determine which of the two group processes dominates. Observational evidence showing that dynamically young systems have a higher fraction of quenched galaxies and, for example, a higher fraction of morphologically distributed galaxies would strongly favour galaxy-galaxy interactions over strangulation as the dominant mechanism for galaxy transformation.

An alternative approach to studying groups is to study the proto-cluster environment and filamentary systems, which are the source of accretion material (i.e. galaxies and groups) for massive clusters. Since proto-clusters are still in the early stages of assembly, they can provide vital information about cor-

relations between dynamically young systems and observed galaxy properties. Additionally, proto-clusters have been observed at high redshifts ($z > 1$), thus environmental effects may be more easily observable than in lower redshift systems. Filaments provide an ideal environment for studying the effects of pre-processing in the group environment, as these systems have yet to accrete onto rich galaxy clusters.

Even with the largest currently available survey, the SDSS, it is difficult to disentangle all of the various factors (i.e. galaxy stellar mass, dynamical mass and dynamical state) that contribute to galaxy evolution. While the study of individual systems, such as proto-clusters, can provide some insight into galaxy evolution, much of the progress in this field will require much more ambitious surveys going both wider (for better statistics at each redshift) and deeper (to probe higher redshifts). Fortunately, there are a number of exciting imaging surveys on the horizon. Examples of such surveys include Pan-STARRS (Kaiser et al., 2002) and DES (Flaugher, 2005), both of which aim to study galaxy clustering. More specifically, one of the main science goals of Pan-STARRS is to map the three-dimensional distribution of matter in the Universe (i.e. the clustering of galaxies). This will hopefully be achieved with an ultra-deep 1200 square degree survey down to a limiting magnitude of $g = 27$. The inclusion of such faint galaxies will render it practically impossible to obtain spectroscopic redshifts for all galaxies in the proposed Pan-STARRS survey. Instead, the survey will rely on photometric redshifts obtained from measurements in four wavebands. It appears that our current reliance on spectroscopic data may not be a sustainable, if we hope to make use of these upcoming surveys. Thus, further development of photometric group-finding, including those discussed in Chapter 2.2, will be necessary to continue our study of galaxy evolution. Similar to Pan-STARRS, one of the goals of DES is to measure dark energy via galaxy cluster counts, which will be carried out in conjunction with the South Pole Telescope to study clustering via the SZ effect. Thus, DES will provide an unprecedented number of target clusters that can be studied in more detail with follow-up observations.

Additionally, complementary theoretical analysis of groups and clusters will be able to provide further insight into the underlying physical processes responsible for galaxy evolution. Current SAMs (e.g. Font et al., 2008; Somerville

et al., 2008) and hydrodynamical simulations (e.g. Bahé et al., 2013) have already provided important information about processes such as SN and AGN feedback and pre-processing. Further improvements in simulations, including better treatment of feedback processes and other sub-grid physics as well as greater computational power, will allow us to improve out understanding of the processes that dominate galaxy evolution.

Bibliography

Bahé, Y. M., McCarthy, I. G., Balogh, M. L., & Font, A. S. 2013, MNRAS, 430, 3017

Blanton, M. R. & Berlind, A. A. 2007, ApJ, 664, 791

Flaugher, B. 2005, International Journal of Modern Physics A, 20, 3121

Font, A. S., Bower, R. G., McCarthy, I. G., Benson, A. J., Frenk, C. S., Helly, J. C., Lacey, C. G., Baugh, C. M., & Cole, S. 2008, MNRAS, 389, 1619

Hou, A., Parker, L. C., Harris, W. E., & Wilman, D. J. 2009, ApJ, 702, 1199

Kaiser, N., Aussel, H., Burke, B. E., Boesgaard, H., Chambers, K., Chun, M. R., Heasley, J. N., Hodapp, K.-W., Hunt, B., Jedicke, R., & et al. 2002, in Society of Photo-Optical Instrumentation Engineers (SPIE) Conference Series, Vol. 4836, Society of Photo-Optical Instrumentation Engineers (SPIE) Conference Series, ed. J. A. Tyson & S. Wolff, 154–164

Lotz, J. M., Jonsson, P., Cox, T. J., Croton, D., Primack, J. R., Somerville, R. S., & Stewart, K. 2011, ApJ, 742, 103

Peng, Y.-j., Lilly, S. J., Kovač, K., Bolzonella, M., Pozzetti, L., Renzini, A., Zamorani, G., Ilbert, O., Knobel, C., Iovino, A., & et al.,. 2010, ApJ, 721, 193

Peng, Y.-j., Lilly, S. J., Renzini, A., & Carollo, M. 2012, ApJ, 757, 4

Somerville, R. S., Hopkins, P. F., Cox, T. J., Robertson, B. E., & Hernquist, L. 2008, MNRAS, 391, 481

Wilman, D. J., Zibetti, S., & Budavári, T. 2010, MNRAS, 406, 1701

Yang, X., Mo, H. J., van den Bosch, F. C., Pasquali, A., Li, C., & Barden, M. 2007, ApJ, 671, 153